Norwegian University of Life Sciences
Faculty of Environmental Sciences and
Natural Resource Management

Philosophiae Doctor (PhD)
Thesis 2019:42

Marine transport modeling of radionuclides using a dynamic speciation approach

Transportmodellering av radionuklider i marint miljø ved bruk av dynamisk speciering

Magne Simonsen

Marine transport modeling of radionuclides using a dynamic speciation approach

Transportmodellering av radionuklider i marint miljø ved bruk av dynamisk speciering

Philosophiae Doctor (PhD) Thesis

Magne Simonsen

Norwegian University of Life Sciences
Faculty of Environmental Sciences and Natural Resource Management
Section of Environmental chemistry

Ås 2019

Thesis number 2019:42

ISSN 1894-6402

ISBN 978-82-575-1602-4

Supervisors

Dr. Ole Christian Lind
Centre of Environmental Radioactivity (CERAD) CoE
Faculty of Environmental Sciences and Natural Resource Management
Norwegian University of Life Sciences (NMBU)
P.O. Box 5003, NO-1433 Ås, Norway
E-mail: ole-christian.lind@nmbu.no

Dr. Øyvind Sætra
Norwegian Meteorological Institute
P.O. Box 43, NO-0313 Oslo, Norway
E-mail: oyvinds@met.no

Prof. Pål Erik Isachsen
Norwegian Meteorological Institute
P.O. Box 43, NO-0313 Oslo, Norway

Department of Geosciences, University of Oslo
P.O. Box 1047, Blindern, NO-0316 Oslo, Norway
E-mail: palei@met.no

Prof. Brit Salbu
Centre of Environmental Radioactivity (CERAD) CoE
Faculty of Environmental Sciences and Natural Resource Management
Norwegian University of Life Sciences (NMBU)
P.O. Box 5003, NO-1433 Ås, Norway
E-mail: brit.salbu@nmbu.no

Dr. Per Strand
Norwegian Radiation and Nuclear Safety Authority
P.O. Box 329 Skøyen, NO-0213 Oslo, Norway
E-mail: per.strand@dsa.no

Evaluation committee

Dr. Raúl Periáñez
Applied Physics I
University of Seville
ETSIA, Ctra Utrera km 1,
41013-Sevilla, Spain
E-mail: rperianez@us.es

Dr. Céline Duffa
Institut de Radioprotection et de Sûreté Nucléaire (IRSN), PSE/SRTE/LRTA
Laboratory of Radionuclide Transfers in Aquatic Ecosystems
BP 3- 13115 Saint-Paul-Lez-Durance, France
E-mail: celine.duffa@irsn.fr

Prof. Helen K. French
Faculty of Environmental Sciences and Natural Resource Management, NMBU
P.O. Box 5003 NMBU, 1432 Ås, Norway
E-mail: helen.french@nmbu.no

Acknowledgements

Financial support for the work was provided by The Research Council of Norway through its Centre of Excellence (CoE) funding scheme (Project No. 223268/F50) and by the Norwegian Meteorological Institute (MET). The research work was carried out at the facilities at MET and Norwegian University of Life Sciences (NMBU).

First, I would like to express my gratitude towards my main supervisor, Ole Christian Lind (NMBU) for patiently guiding and supporting me through this long journey. I would also like to thank my co-supervisors: Brit Salbu (NMBU), Pål Erik Isachsen (MET and University of Oslo), Øyvind Sætra (MET) and Per Strand (Norwegian Radiation and Nuclear Safety Authority, DSA). Your scientific support and guidance, good advices, criticism and sharing of your knowledge has been highly appreciated!

I will express my greatest gratitude to Jon Albretsen (Institute for Marine Research, IMR) for very kindly setting up and running the ocean model simulations that were utilized in the Boknafjorden (^{137}Cs) and Sandnesfjorden (Al) papers. Thanks to Nils M. Kristensen (MET) for providing model data used in the Sellafield (^{99}Tc) case. Thanks to Hans-Christian Teien (NMBU) for providing observational data and sharing your knowledge of radionuclide and metal behavior in water systems through numerous discussions. Your help and effort is highly appreciated! Thanks to Hilde Kristin Skjerdal (DSA), Justin Gwynn (DSA) and Hilde Elise Heldal (IMR) for providing observational ^{99}Tc data from open ocean surveys and coastal stations in the Sellafield paper.

I would also like to thank all my friends and colleagues at MET as well as at NMBU and everyone involved in CERAD for interesting and fruitful discussions, help and advice. Thanks to Yan Lin (Norwegian Institute for Water Research) and Astrid Liland for interesting discussions through the Western Norway and Boknafjorden cases.

Finally, this work would not have been possible without the support from my family. Thanks to Marianne for supporting and standing with me all the way and patiently taking care of all the family stuff these years, and to my dear kids Thomas and Selma for everyday reminding me of what the most important things in life really are about.

Ås, March 29, 2019
Magne Simonsen

Contents

Summary

Anthropogenic radionuclides are introduced to the marine environment from many sources, such as atmospheric fallout, direct releases from nuclear installations (either via operational or accidental discharges) and indirectly via river run-off through estuaries. In the marine environment, the transport is affected by a number of processes, such as hydrodynamic advection and diffusion, turbulent mixing, sedimentation and resuspension. As the environmental transport and toxicity depend on the distribution of physico-chemical forms (species), numerical models should include relevant species and dynamic transformation processes to properly predict marine transport and environmental impact of radionuclides.

The present PhD project is addressing topics in the crossing point between physical oceanography and radioecology. Aiming to investigate the impact of numerical model representation of biogeochemical and geophysical processes, a numerical model system for marine radionuclide transport was developed and utilized. A set of case studies was performed, including historical and hypothetical radionuclide discharges as well as estuarine transport of a trace metal. When available, the model results were compared to observational data.

Focusing on hydrodynamic processes, the impact of including mesoscale eddies and tides was investigated in a long-term (12 years) simulation of historical discharges of technetium (^{99}Tc) radionuclides from Sellafield, UK (Paper I). Comparison with observational data showed that due to better resolution of mesoscale eddy fluxes, increasing the horizontal model grid resolution from $\sim$14 km to 4 km improved the model skill. The importance of tidal advection was investigated by comparing transport in the eddy-permitting model when this was run either with tides included (1 hour temporal resolution) or with tides filtered out (24 hour mean). The results pointed to systematic Lagrangian tidal drift in the Irish Sea and the North Sea that eventually impacted the ^{99}Tc activity concentration levels also far downstream. Therefore, to avoid systematic errors due to sub-grid scale processes, it was concluded that mesoscale eddies and tides should be included also in long-range transport simulations.

A new numerical code describing the distribution and transformation of radionuclide species was implemented in the transport model. These processes have commonly been neglected in previous studies, but including them was assumed to reduce the overall model uncertainty as the model became more in line with reality. However, these implementations also introduced new uncertainties, due to relatively large uncertainties associated with the descriptions (parameterizations) of the transformation processes.

Investigating the impact of key processes on the transport estimates in the hypothetical case involving coastal dispersion of river-discharged ^{137}Cs (Paper II), the effects of including in-

teractions with solid matter were found to be considerable, locally affecting the results with orders of magnitude. The predicted transport was found to be sensitive to factors affecting the particle affinity, especially the fraction slowly reversibly bound to particles, but also regarding the particle size distributions, as increased settling reduced the transport away from the discharge points and increased the total exposure near the river mouths with up to a factor 10. However, these parameterizations are typically associated to relatively large uncertainties.

To address the effects of changing environmental conditions on the elemental speciation, a more complex speciation scheme was implemented (Paper III), where the transfer rates were dependent on the local salinity to fit the observed behavior of aluminium (Al) in River Storelva and Sandnesfjorden estuary (south-eastern Norway). The general patterns of observational total Al concentrations and speciation data were well reproduced by the model.

The results from this set of case studies showed that due to knowledge gaps related to descriptions of transformation processes and difficulties in transferring locally observed features to generic algorithms, there are still considerable uncertainty involved in the predictions. The present study has identified some of the key factors contributing to such uncertainties and their impacts on the transport estimates. By including these key factors and processes (tides, mesoscale eddies, element speciation and transformations) the model skill improves and in general, the observed concentration levels were sufficiently well reproduced as shown in the case studies. The model system developed in the present PhD project may be further developed and utilized as a tool for environmental impact assessments in emergency situations and for research purposes.

Sammendrag

Det finnes mange kilder til antropogent utslipp av radionuklider til havet, slik som atmosfærisk nedfall, direkte utslipp fra atomkraftverk (enten via operasjonelle eller utilsiktede utslipp) og indirekte utslipp via elveavrenning gjennom estuarier. Videre blir radionuklidetransporten i havet påvirket av en rekke prosesser, som hydrodynamisk adveksjon, spredning og diffusjon, turbulent blanding, sedimentasjon og resuspensjon. Både transporten og toksisteten avhenger av fordelingen mellom de forskjellige tilstandsformene (speciene), og numeriske modeller bør derfor kunne beskrive de relevante formene og dynamiske overganger mellom disse for å forutsi hvordan radionuklider transporteres og hvordan de vil påvirke miljøet.

Dette PhD-prosjektet tar opp temaer i krysningspunktet mellom fysisk oseanografi og radioøkologi. For å undersøke hvordan modellresultatene påvirkes av biogeokjemiske og geofysiske prosesser, ble et numerisk modellsystem utviklet og tatt i bruk. Et sett med casestudier ble gjennomført, både et historisk og et hypotetisk radionuklide-scenario og i tillegg et tilfelle med transport av et spormetall i et estuarie. Der det var mulig, ble modellresultatene sammenlignet med observasjonsdata.

I Paper I ble det fokusert på hydrodynamiske prosesser, og det ble undersøkt hvordan inkludering av mesoskala virvler og tidevann påvirket modellens resultater i en langtids-simulering over 12 år av historiske utslipp av technetium-radionuklider fra Sellafield i Storbritannia. Sammenligning med observasjonsdata viste at økt horisontal oppløsning ga en klar forbedring av modellresultatene på grunn av at virvelfelt på mesoskala ble bedre oppløst. Påvirkningen fra tidevannsdrevne transportflukser ble undersøkt ved å sammenligne simuleringer hvor tidevannet var inkludert (1 times tidsoppløsning) med simuleringer der tidevannet var filtrert ut (døgnmidler). Sammenligningen viste en systematisk tidevannsdrevet drift av vannmassene i Irskesjøen, som også påvirket technetiumkonsentrasjonene over større avstander. Derfor ble det konkludert med at for å unngå systematiske feil, bør mesoskala virvler og tidevann også inkluderes i modellsimuleringer som skal beregne langtransport av radionuklider.

Transportmodellen ble utvidet med modellkode som beskriver fordelingen og transformasjoner mellom radionuklidenes forskjellige tilstandsformer. Disse prosessene har vanligvis blitt neglisjert i tidligere modellstuder, men ved å inkludere disse ble det antatt at den totale usikkerheten ble redusert siden det gjorde modellen mer virkelighetsnær. Likevel vil slik modellutvikling også introdusere nye usikkerheter som er forbundet med nye parametere og algoritmer som trengs for å beskrive transformasjonsprosessene.

Virkningen av sentrale prosesser ble undersøkt i et hypotetisk tilfelle med utslipp av ^{137}Cs

fra elver og spredning langs kysten (Paper II). Effekten av å inkludere interaksjoner med faste stoffer var betydelig, da forurensningsnivåene lokalt økte med opp mot en faktor 10. Transportberegningene viste seg å være sensitive overfor faktorer som påvirker partikkel-affiniteten, særlig fraksjonen som var 'sakte-reversibelt' bundet til partikler men også til den antatte fordelingen av partikkelstørrelse, siden økt sedimentering også ga redusert transport vekk fra kildene og økt totaleksponering nær elvemunningene (opp til en faktor 10). Men i de fleste tilfeller er parameteriseringen av disse faktorene forbundet med stor usikkerhet.

For å undersøke hvordan endrede eksterne miljøforhold påvirket specieringen, ble det utviklet et mer komplekst specieringsoppsett i Paper III. Her var overføringshastighetene avhengig av lokal salinitet i det omkringliggende vannet, kalibrert mot observert oppførsel av Al i Storelva og Sandnesfjorden. Modellen klarte fint å reprodusere de observerte trendene, både for totalkonsentrasjon av Al og for hver av de forskjellige tilstandsformene.

Resultatene fra dette settet av casestudier viste at det fortsatt er stor usikkerhet knyttet til modellprognoser av radionuklidetransport. Dette skyldes blant annet manglende kunnskap om hvordan transformasjonsprosessene bør beskrives og vanskeligheter med å overføre målte verdier mellom forskjellige lokasjoner. Dette studiet har identifisert noen av de faktorene som bidrar mest til slike usikkerheter og hvordan disse påvirker transportestimatene. Ved å inkludere disse nøkkelfaktorene og -prosessene (tidevann, mesoskala virvler, speciering og transformasjoner) blir modellen forbedret. I de aktuelle tilfellene klarte modellen i all hovedsak å gjenskape de observerte konsentrasjonsnivåene. Videre kan dette modellsystemet videreutvikles og benyttes som et verktøy som vil være nyttig både til konsekvensutredninger, i nødsituasjoner og til forskningsformål.

List of papers

I. Simonsen, M., Ø. Saetra, P. E. Isachsen, O. C. Lind, H. K. Skjerdal, B. Salbu, H. E. Heldal, and J. P. Gwynn (2017), *The impact of tidal and mesoscale eddy advection on the long term dispersion of ^{99}Tc from Sellafield*, Journal of Environmental Radioactivity, **177**, 100 – 112, doi:10.1016/j.jenvrad.2017.06.002.

II. Simonsen, M, O. C. Lind, Ø. Saetra, P. E. Isachsen, H.-C.. Teien, J. Albretsen, B. Salbu (2019), *Coastal transport of river-discharged radionuclides: Impact of speciation and transformation processes in numerical model simulations*, Science of the Total Environment, **669**, 856–871 doi:10.1016/j.scitotenv.2019.01.434

III. Simonsen, M, H.-C.. Teien, O. C. Lind, Ø. Saetra, J. Albretsen, B. Salbu, *Modeling key processes affecting Al speciation and transport in estuaries*, Submitted to Science of the Total Environment (2019-03-25)

1 Introduction

The major sources of anthropogenic radioactive contamination to the marine environment are related to nuclear weapon and fuel cycles, in particular global fallout from atmospheric test detonations, accidental and authorized discharges from nuclear installations and leakages from nuclear waste dumped in or near the oceans (*AMAP*, 2016; *OSPAR*, 2018). Offshore industry also contributes considerably through releases of naturally occurring radionuclides as by-products from petroleum production (*Betti et al.*, 2004; *NRPA*, 2004; *Hosseini et al.*, 2012). As seen from historical cases, and also likely in future accidental discharge scenarios, radionuclides can enter the marine environment either directly from releases of radioactive material from permanent, mobile or decommissioned installations, and as surface deposition from the atmosphere. In addition, parts of the terrestrial atmospheric fallout in river catchments will subsequently end up in the marine environment via river runoff. Even though nuclear power is considered to be relatively safe, historical cases such as the Fukushima and Chernobyl accidents have shown that even incidents with low probability might happen and lead to accidents with severe consequences. Since the nuclear industry involves handling and storage of hazardous substances, there will always be a risk of accidental or intentional discharges. Potential sources of radionuclides causing ionizing radiation to the environment include permanent installations as well as reactor-driven vessels (e.g., submarines, ice breakers, airplanes, satellites and missiles) and ships or barges loaded with radioactive cargo.

Numerical models have proven to be useful in understanding and predicting the transport and fate of radionuclides in the marine environment (e.g., *Periáñez et al.*, 2016b; *Vives i Batlle et al.*, 2018). Being able to interpolate between the scattered observations in a dynamically consistent way and predict future transport pathways, such models can provide important support for impact assessments. Typically, this is important for decision-makers considering interventions or counter-measures in the acute phase after a nuclear accident (*Duffa et al.*, 2016), as well as for long-term assessments of historical or hypothetical discharges (*Karcher et al.*, 2004; *Kauker et al.*, 2016). For research purposes, models are also useful for the investigation of processes and hypotheses related to the fate of the released radionuclides (*Orre et al.*, 2007, 2008; *Karcher et al.*, 2012).

In principal, the transport behavior of radionuclides in the marine environment is similar to that of other trace elements such as metals. Although the present work is primarily focusing on radionuclides, the conclusions obtained here are valid for and can be applied to stable elements as well. Due to available fractionated aluminium concentration data from the Sandnesfjorden estuary, a case study of riverine Al discharges was considered in Paper III to

develop a more complex speciation scheme that can also be modified and utilized to simulate radionuclide behavior in the estuarine mixing zone.

In the oceans, radionuclides can appear in a broad range of different physico-chemical forms (*species*), varying in size, structure and morphology, density, oxidation states and charge properties (*Salbu*, 2000). Typically reactive species are easily taken up in specific tissues and organs through adsorption on external body surface or internal absorption through food or water intake (*Carvalho*, 2018). The size can range from ions and low molecular mass (LMM) species (defined as entities smaller than 10 kDa or approximately 1 nm) to radionuclides chemically or physically associated with suspended colloids (10 kDa – 0.45 µm) and particles ($>$ 0.45 µm) such as clay or humic substances and with seabed sediments (*Salbu*, 2009). The distribution of species (the *speciation*) and subsequently the potential for biological uptake is affected by a number of complex dynamic and biogeochemical processes, initiated by shifting environmental conditions such as pH, salinity and temperature (*Rosseland et al.*, 1992; *Teien et al.*, 2004, 2006; *Salbu*, 2009). As natural dynamic environmental systems generally are in non-equilibrium conditions, transformation processes will lead to changes in the speciation over time (*Periáñez et al.*, 2018). LMM and colloidal species are commonly referred to as *dissolved species* and are assumed to be transported passively by the water masses. The LMM species are assumed to be mobile and potentially bioavailable and may give rise to significant uptake, especially in pelagic biota (*Teien et al.*, 2006). On the other hand, radionuclides associated with suspended particles will sink towards the seabed and can accumulate in the sediments, being less available for pelagic uptake, but potentially more available for filtering benthic organisms (*Børretzen and Salbu*, 2009). As seen in the Irish Sea, contaminated seabed sediments may act as a secondary source, as the radionuclides over time may resuspend and migrate due to mechanical bottom stress or remobilize to the water column (*Mitchell et al.*, 1999; *McCubbin et al.*, 2006; *Hunt et al.*, 2013). The radionuclide speciation is therefore essential for the transport properties, as well as for biological uptake and impacts/response of the radionuclides. Proper estimates of doses and exposure from ionizing radiation on ecosystems rely on detailed predictions of dispersion and transformation processes (*Caffrey et al.*, 2014). Information on bioavailable forms of radionuclides is, however, still scarce (*Salbu*, 2016), and there are large data gaps in parameters for biological uptake (*Caffrey et al.*, 2014).

Therefore, for safety reasons as well as for scientific purpose, there is a need for model systems predicting accurately the spatio-temporal dispersion of radionuclide species in the marine environment (*Vives i Batlle et al.*, 2018). Ideally, such predictive models should be generic and include an appropriate set of species, where the transformations of elemental species are de-

scribed as dynamic processes dependent on external environmental factors (*Machado et al.*, 2016). However, many of the key environmental factors affecting the transfer rates (such as suspended particle content, hydrolysis, aggregation, sedimentation and resuspension, redox conditions) are non-homogeneously distributed, with large gradients shifting rapidly over small temporal and spatial scales. Typically, these gradients are large in or near strong fronts, such as in the mixing zones near river outlets. To resolve these processes properly, the models must have very high resolution. Otherwise, if these processes are not sufficiently resolved by the model, well-defined parameterizations of the small scale processes, based on general or empirical descriptions, are required. Unfortunately, the transformation processes are still not sufficiently known to be described by generic parameterizations which easily can be transferred between different ecosystems. Due to the large uncertainties involved, speciation and transformation processes are often neglected or scarcely described in impact assessments. In addition, as hydrodynamic simulations are computationally expensive, radionuclide transport modeling is generally suffering from low spatial and temporal resolution.

Objectives and hypotheses: The overall aim of the current PhD project was to improve the quality of impact assessments in marine radionuclide transport modeling in the intersection point between numerical oceanography and radioecology. The more specific objectives of the project were:

O1. To investigate the impact of including tides and mesoscale eddies in large-scale radionuclide transport simulations

O2. To investigate the structural uncertainty associated to negligence of radionuclide speciation and transformation processes which in previous literature either are neglected or suffering from relatively large uncertainty, and to investigate the uncertainty associated to parameterization of key processes controlling the distribution of species

O3. To develop, implement and validate model code describing key processes influencing the trace metal specie distribution through shifting environmental conditions in estuaries

Three hypotheses were set up:

H1. More realistic estimates are obtained in simulations where tides and mesoscale eddies are resolved than in simulations where such physical processes are ignored or based on parameterizations

H2. Inclusion of elemental speciation and transformation processes in a model will change the estimated radionuclide inventory in a fjord system

H3. Inclusion of interactions with colloidal species and salinity-dependent transformation processes in an estuarine mixing zone enables a high resolution transport model to reproduce the general patterns of observed levels of Al specie distributions

To investigate these objectives and hypotheses, a numerical model system for marine radionuclide transport simulations was established and developed. The model system consisted of a hydrodynamic model and a Lagrangian transport model in which radionuclide speciation and transformation processes were included. A set of case studies were performed and where applicable, the model results were compared with available observation datasets.

To test hypothesis H1, eddy and tide-resolving simulations of transport and dispersion of radionuclides discharged from the Sellafield reprocessing plant were performed. The model skill was assessed by comparison with available observations and related to results from a model simulation at coarser resolution where these processes were parameterized.

To test hypothesis H2, a hypothetical case study of river runoff to a fjord system in south-western Norway (Boknafjorden) was performed. Results from simulations of non-reactive radionuclide species were compared with results from simulations of reactive species undergoing dynamic transformation processes. The relative and absolute impact on the activity concentration levels was investigated by comparing model output from a number of simulations where selected key processes were changed one by one.

To test hypothesis H3, new model code describing key processes influencing the trace metal specie distribution through shifting environmental conditions in estuaries, including the role of colloidal species, was developed and implemented. The new model developments were utilized in a case study of aluminium in the Sandnesfjorden estuary, south-eastern Norway, where modeled Al specie distribution was validated against observational data including LMM, colloidal and particle fractions.

2 Background

2.1 Sources of anthropogenic radionuclides to the marine environment

Since the development of nuclear power and weapons, the major sources of anthropogenic radionuclides to the marine environment are related to different steps in the nuclear weapon and power production. More than 500 atmospheric test detonations of atom bombs between 1945 and 1980 have given a considerable nuclear legacy with widespread deposition on the entire Earth's surface, known as *global fallout* (*UNSCEAR*, 2000). These atmospheric test detonations were at the most intense in the Northern Hemisphere during 1950–1960s. Although the major contamination was deposited locally and regionally around the test sites, a considerable amount of radioactive gases, dust and particles consisting of a range of radionuclides were elevated into the stratosphere from the explosions (*UNSCEAR*, 2000). At high altitudes, these radionuclides were distributed globally by the large-scale weather systems and subsequently deposited at the surface. The deposition was highest in the Northern Hemisphere and relatively evenly distributed zonally for each latitude band (*AMAP*, 2016). Today, ^{90}Sr and ^{137}Cs are of the highest concern (*Wright et al.*, 1999). A brief list of contaminants relevant for the present study can be seen in Table 1.

Considerable amounts of nuclear waste have also been regularly or occasionally released to the environment at all stages in the nuclear weapon and fuel production cycles, from the mining, enrichment, conversion to fuel elements, power production, storage and reprocessing of spent fuel to the handling of nuclear waste (*UNSCEAR*, 2000). In the North Atlantic region, the most dominant sources from the nuclear cycles are direct discharges of low-level radioactive liquids from the reprocessing plants at Sellafield in the UK and Cap La Hague in France (*Povinec et al.*, 2003). These two sites have since 1952 and 1962, respectively, contributed mostly to local contamination near the sources, but the contaminants have also been transported to remote locations. The dominating radionuclides discharged from these reprocessing plants are ^{3}H, ^{137}Cs, ^{99}Tc, ^{106}Ru, ^{125}Sb, ^{239,240}Pb, ^{129}I and ^{14}C. The releases peaked in the 1970s, and since the 1990s, the discharges from nuclear installations have decreased (*OSPAR*, 2018). An exception is the ^{99}Tc discharges from Sellafield, which, after a long period of low discharges, peaked in 1995 due to changes in the treatment of stored waste (*AMAP*, 2016). Due to extensive remobilization of sediment-bound radionuclides, contaminated sediments, such as the mud patches in the Irish Sea, have also become significant sources of radionuclides which have been transported out of the Irish Sea and further downstream into the North Sea and the Nordic Seas (*Mitchell et al.*, 1999; *McCubbin et al.*, 2006; *Hunt et al.*, 2013). Due

to the presence of nuclear sites in and near the river catchments, particularly the rivers Ob and Yenisey are recognized as historical and potential sources of radioactive contamination to the Arctic Ocean (*AMAP*, 2016).

Discharges from the Chernobyl accident in 1986 have affected and still affect the environment locally and regionally, with surface deposition and river discharges to the Atlantic and Arctic Oceans and the Baltic Sea. The major source to Pu and Am contamination in sediments from Swedish coastal areas was found to be global fallout, while the Chernobyl accident was the main contributor to ^{137}Cs contaminants (*Olszewski et al.*, 2018). More recently, direct liquid releases as well as surface deposition to the oceans, caused by the Fukushima accident in 2011, have elevated the ^{137}Cs activity concentration levels in the western North Pacific Ocean surface waters with three orders of magnitude compared to pre-accident values (*Aoyama et al.*, 2016; *Povinec et al.*, 2017). But the impact of discharges from the Fukushima accident on the North Atlantic and Arctic waters is low (*AMAP*, 2016).

Table 1: Radionuclides and contaminants in the North Atlantic and their origin, which are relevant for the present work. $T_{1/2}$ is the half-life time due to radioactive disintegration. K_d values are open ocean distribution coefficients recommended by *IAEA* (2004). Contaminants above the dashed line have been applied to numerical simulations in the present study.

Radionuclide/ contaminant	Element	$T_{1/2}$	K_d (L kg^{-1})	Major sources
^{99}Tc	Technetium	2×10^5 y	10^2	Sellafield
^{137}Cs	Cesium	30 y	2×10^3	Global fallout, Chernobyl
Al	Aluminium	stable	-	River run-off
^{129}I	Iodine	1.57×10^7 y	2×10^2	Cap La Hague
^{131}I	Iodine	8 days	2×10^2	Cap La Hague
^{90}Sr	Strontium	29 y	2×10^2	Global fallout
^{3}H	Tritium (hydrogen)	12.3 y	1	Reprocessing facilities
^{226}Ra	Radium	1600 y	4×10^3	Produced water
^{228}Ra	Radium	5.75 y	4×10^3	Produced water
^{210}Pb	Lead	22 y	10^7	Produced water
^{238}Pu	Plutonium	87.74 y	10^5	Global fallout, reprocessing facilities
^{239}Pu	Plutonium	2.4×10^4 y	10^5	Global fallout, reprocessing facilities
^{240}Pu	Plutonium	6500 y	10^5	Global fallout, reprocessing facilities
^{241}Am	Americium	432 y	2×10^6	Global fallout, reprocessing facilities

Produced water from the petroleum production contribute significantly to discharges of a number of naturally occurring radionuclides to the North Sea, where the radium isotopes ^{226}Ra and ^{228}Ra are of highest concern (*Hosseini et al.*, 2012). A sampling campaign performed by *NRPA* (2004) showed enhanced activity concentrations around the oil platforms,

with discharged levels being three orders of magnitude higher than the background. It was concluded by *Hosseini et al.* (2012) that although uncertainties are large, the environmental impact from the current releases of radionuclides in produced water from oil platforms are negligible.

From 1946 until 1993, there was extensive dumping of radioactive contaminants to the deep oceans. This included deposition of spent fuel and waste from the nuclear production, used reactors, vessels and buildings as well as contaminated clothes and equipment, tailings from uranium mining and other radioactive by-products. In total, approximately 85 000 TBq were disposed by European countries, the United States and the former Soviet Union into the Pacific, Arctic and North Atlantic Oceans (*IAEA*, 2015). The disposals were spread over large dumping zones with limited possibilities for monitoring and maintenance. More than 50 % of the total disposals was low level solid waste, dumped at the internationally approved sites in the North Atlantic, while reactors with spent nuclear fuel dumped in the Arctic Ocean contributed to 42 % (*IAEA*, 2015).

Following these accidental and authorized discharges to the oceans, the scientific and public concern about ionizing radiation in the environment was growing through the second half of the 20th century. Observed radionuclide accumulation in marine organisms highlighted the need for improved knowledge of underlying mechanisms for radionuclide concentration and transfer in the marine environment (*Carvalho*, 2018). Different international forums such as the CRESP research program, the OSPAR Convention, AMAP and the UNSCEAR committee were initiated, aiming to improve the scientific knowledge on behavior and effects of radioactive elements in the environment. These programs consider both dynamic dispersion by ocean currents as well as uptake and transfer in living organisms (ecosystem transfer). Extensive systematic monitoring has been performed both through short-time monitoring surveys and long-term time series from monitoring stations (e.g., *Herrmann et al.*, 1995; *Salbu et al.*, 1997; *UNSCEAR*, 2000; *RPII*, 2012; *RIFE*, 2013; *Skjerdal et al.*, 2015; *AMAP*, 2016; *Jensen et al.*, 2017; *Gwynn et al.*, 2018; *OSPAR*, 2018). Clear signals from increased discharges have been identified at observation stations downstream of the sources, such as observed increase in Sellafield-derived ^{99}Tc in Northern Norway (*Brown et al.*, 2002). This increasing scientific knowledge revealed that the deep oceans are not isolated from the rest of the environment, but host a large variety of organic species which are connected to the rest of the ecosystem via transfer pathways such as hydrodynamic transport and ecosystem transfer.

2.2 Radionuclide modeling

In the context of the present work, we define hydrodynamic ocean models as digital, discretized representations of the real, continuous ocean state. These are numerical programs that solve prognostic equations describing the hydrodynamics in a defined domain divided into a number of grid cells. Thus, during a chosen time period after the initialization time, such models are able to predict the full ocean state at discretized time intervals. Transport models make use of such current estimates, which may be obtained from a hydrodynamic ocean model, to predict the transport of a discharged matter such as radionuclides, particles or trace elements. For the purpose of providing transport estimates of existing radionuclide contaminants, source identification and a variety of process studies in the marine environment, model systems combining hydrodynamic ocean models with numerical transport models have been adapted into the radioecology research. The development of such predictive ocean transport model systems has thus introduced new valuable insight into radioecological processes (*Caffrey et al.*, 2014; *Carvalho*, 2018). However, the model estimates are influenced by uncertainties at a number of levels (e.g., *Salbu*, 2016), and therefore, there are currently international research projects going on, aiming to develop models that are fit for purpose and quantify and reduce uncertainties (e.g., *Raskob et al.*, 2018).

Although extensive monitoring and laboratory experiments are important for assessments and scientific understanding of the behavior of radionuclides in the marine environment, the use of transport model systems can also provide substantial additional information in the understanding of the fate of radioactive contaminants in the oceans. Generally, compared to observational data, model simulations have three primary benefits:

- They can provide comprehensive and dynamically consistent estimates for locations and times in which observational data are not available
- They can predict future transport and hypothetical cases
- They open up for process investigation

First, due to heterogeneity, observation samples can only be representative for a limited geographic area or time period. In contrast, model simulations can provide results covering large areas far more efficient than expensive sampling campaigns. Within the model limitations, the model output can practically provide results in any location and time. Generally, the computational costs increase with increasing spatial and temporal resolution, so large-scale or long-term simulations have typically coarser resolution than simulations covering smaller

scales and shorter time periods. Hence, the range and resolution in time and space has to be selected according to the relevant dynamical scales involved in the considered case. Increasing complexity is also typically more resource demanding. Secondly, numerical models can be used for future predictions of existing discharges and for testing of hypothetical scenarios. Utilizing a well-defined input source, the models can predict the dispersion of the contaminants, identify regions with elevated activity, transit times to certain regions and magnitudes of activity concentrations. Another practical model application can be to distinguish the relative contribution from different sources and thus to refine source term estimates (*Kobayashi et al.*, 2013). Reverse simulations (running the models backwards in time) can also be used in back-tracking of measured activity concentration levels to estimate the location, magnitude and relative contribution of different sources. Finally, models are well suited tools to investigate the impact of key factors and processes affecting the activity concentration levels. In such sensitivity studies, selected processes can easily be enabled or disabled and parameters can be adjusted for the purpose of quantifying the impact of each factor by comparing results from simulations with slightly different configurations. For validation of the model results during such process investigation, available measurements of contamination levels at different locations and stages after real radionuclide discharge events, as well as controlled laboratory experiments, are highly valuable. Furthermore, accurate source term estimates as well as comprehensive and consistent monitoring surveys including time series from established stations and densely distributed ocean campaigns are also important for the purpose of model validation.

Another aspect of the radionuclide discharges was their ability for model assessment for oceanographic purposes. In general, the radionuclide discharges are relatively well documented, and radioactive contamination can be recognized at trace level (*Dahlgaard*, 1995). Since anthropogenic radionuclides originally were absent in marine waters, such observations can be related to human activity. For example, since ^{3}H has been introduced to surface water by atmospheric deposition or direct releases, observations of ^{3}H traces in deep ocean water masses indicate ventilation and exchange of surface water masses beneath the mixed layer (*Orre*, 2008). Therefore, when applied in model studies, the anthropogenic radionuclide discharges have become valuable resources to understand and investigate oceanographic processes (*Casacuberta et al.*, 2018).

In case of accidental discharges from nuclear installations, and particularly in the acute phase of emergency situations, models predicting dynamic transport of radionuclides as well as ecosystem transfer are important to protect man and the environment from harmful effects of ionizing radiation. Results from such models can serve as a basis when decisions about

evacuation or counter-measures are taken. Therefore, generic and operationally available preparedness models for marine radionuclide contamination are necessary for fast-response in emergency situations (e.g., *Duffa et al.*, 2016). With only two research reactors, the nuclear industry in Norway is limited. However, with numerous nuclear facilities in neighboring and overseas countries, the possibilities of impacts in Norwegian territories from potential accidents abroad are non-negligible. For example, due to prevailing wind directions, there is 40 % probability of deposition at the western coast of Norway in the case of an accidental atmospheric release of radionuclides from Sellafield (*Klein and Bartnicki*, 2018). In addition, with the long and heavily trafficked Norwegian coastline, the possibilities of accidents involving vessels that are nuclear powered or loaded with nuclear cargo or nuclear weapon near the coast need to be taken into account. Such cases may lead to significant consequences for aquaculture, fishing industry and populated places and a fast response preparedness system for ocean dispersion of radionuclides are needed to minimize the impacts. Also during planning of new nuclear facility installations, models can be used to reveal and investigate the potential pathways for contaminants in different relevant release scenarios, to obtain the best practical solutions and to identify and reduce risks for accidental contamination and environmental impact.

For the purpose of predicting the transport of radionuclides in the marine environment, a number of different approaches have been utilized, with variable accuracy and prediction skill (e.g., *Prandle and Charnock*, 1984; *Periáñez et al.*, 1996; *Margvelashvily et al.*, 1997; *Iosjpe et al.*, 2002; *Aldridge et al.*, 2003; *Goshawk et al.*, 2003; *Karcher et al.*, 2004; *Kobayashi et al.*, 2006). The work in the present PhD project has been conducted with applications of three-dimensional hydrodynamic models. Therefore, in the following, such models, predicting the dispersion of tracers such as radionuclides are described. Basically, tracer transport in the oceans can be described by the advection-diffusion equation (e.g., *Periáñez*, 2005):

$$\frac{\partial C}{\partial t} + \frac{\partial uC}{\partial x} + \frac{\partial vC}{\partial y} + \frac{\partial wC}{\partial z} = A_h \left(\frac{\partial^2 C}{\partial x^2} + \frac{\partial^2 C}{\partial y^2} \right) + A_v \frac{\partial^2 C}{\partial z^2} \tag{1}$$

where C is the concentration of the tracer, t is time, u, v and w are the flow components in x, y and z directions, respectively. The first term on the left-hand side is the temporal change of tracer concentration, the remaining terms on the left hand side are advection terms, while the terms on the right hand side describe the diffusion where A_h and A_v are horizontal and vertical tracer diffusion coefficients, respectively. Sources and sinks can also be included as additional terms. In numerical models, this equation can be integrated over time in a three-dimensional grid, providing concentration levels in any position and time covered by the simulation. Similar equations are also solved for momentum, salinity and temperature.

Numerical integration of these equations with hydrodynamical models involves three major fundamental issues, which cannot be solved exactly, but has to be accounted for, namely *initial conditions*, *boundary conditions* and *unresolved turbulent motion*.

Integration of Eq (1) forward in time implies that the full ocean state at the time of initialization ($t = 0$) is known. With generally sparse observation datasets, the full ocean state cannot be extracted from observations and the initial ocean state has to be estimated. Such estimates are typically fields from a stationary solution, fields from a previous simulation or climatology at the same grid or an interpolation/downscaling of fields from a coarser grid, eventually combined with observational data. Therefore, since these initial fields normally are based on smoothed or low resolution fields, some of the high-energetic flow features are lacking. In any case, before the results can be considered realistic and reliable, the model should be run for a sufficiently long spin-up period. The duration of this spin-up period depends on how well the initial fields represent the real ocean state including tracer distribution. Realistic forcing on the domain boundaries, such as currents, tracer concentration, winds, tides and river flow, and eventually data assimilation of measured variables within the model domain, contributes to keeping the model dynamics close to the real ocean state. However, after the spin-up period, the skill of the model predictions relies on the quality of the forcing data.

Even though the advection by large scale oceanic motions can be described relatively precisely by equations of motions, all hydrodynamic flows are fundamentally chaotic and affected by turbulence (*Griffies*, 2004). Such turbulent flows are unpredictable, and being nature's way of reducing strong gradients, they contribute significantly to fluxes of tracers and momentum. Parameterizations of diffusive transport (i.e., molecular diffusion and turbulent mixing) are commonly done with diffusion parameters, which can be assumed constant or described by the properties of the mean flow (*Zilitinkevich et al.*, 2007). Hence, while the advective flow becomes more precisely described by increasing the resolution, the unresolved turbulent motions still needs to be parameterized. This remains today a large source of errors to model transport estimates.

2.3 Physico-chemical forms and transformation of element species

Radionuclides present in sea water can appear in a broad range of physico-chemical forms, varying in size, structure and morphology, density, oxidation states and charge properties (*Salbu*, 2000). The effective size of the species can range from simple atoms and ions to colloids, particles and fragments, as shown in Fig 1. In the marine environment, the specie distribution is affected by a number of complex biogeochemical processes (Fig 1). Processes

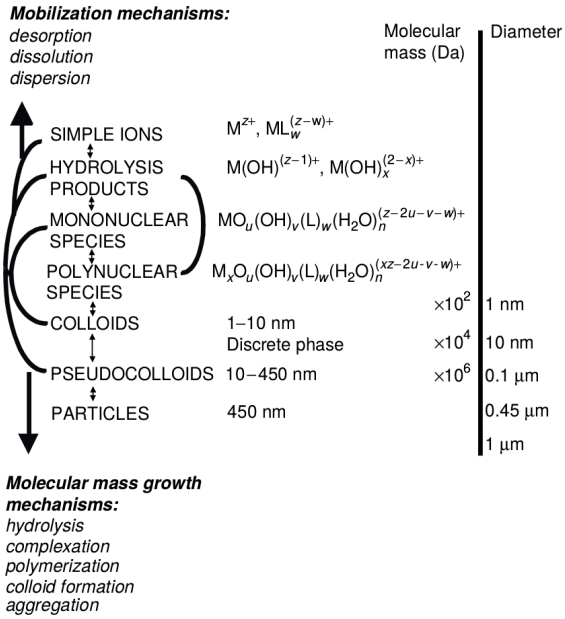

Figure 1: Radionuclides can be present in a number of different physico-chemical forms and sizes, and undergo continuous transformation processes. Reprint from (*Salbu*, 2000).

affecting the radionuclide activity concentration of the different species include advection and dispersion with the water masses, sorption and desorption, hydrolysis and aggregation, complexation and sedimentation. Low molecular mass (LMM) species (<10 kDa) can interact with clay minerals either suspended in the water column or embedded in seabed through reversible and irreversible sorption (physical, electrostatic and chemisorption) processes. On the other hand, LMM species can remobilize from colloids, particles or seabed sediments through desorption due to increased ionic strength and mechanical dispersion (weathering) processes. Colloidal species are defined as entities between 10 kDa and 0.45 µm, while particle species are larger than 0.45 µm. Colloids act as transporting agents in natural water systems (*Kersting et al.*, 1999; *Salbu*, 2000; *Novikov et al.*, 2006), especially in the fresh water end member of rivers (*Eyrolle and Charmasson*, 2004; *Lind et al.*, 2006). In estuaries, however, aggregation of river transported colloids can take place upon mixing with high ionic strength sea water, and associated radionuclides are removed from the water column through particle sedimentation. In addition, at sufficiently high concentration levels, hydrolysis and polymerization of scavenging elements such as Al due to increasing pH may give formation of highly reactive polymer colloids in estuarine mixing zones. Processes controlled by the macrochemistry of such stable elements may therefore affect the concentration levels of ra-

dionuclides being present at trace levels (*Salbu*, 2000). In sum, the physico-chemical forms of the radionuclides undergo continuous transformations due to these mobilization and molecular growth mechanisms. The transformations typically take place in highly dynamic regions with large gradients and rapidly shifting environmental conditions such as in frontal zones and in estuarine mixing zones where fresh river water meets and mixes with high-saline coastal water.

The distribution of species in turn affects the hydrodynamic transport behavior of radionuclides and trace metals as well as the uptake and responses in living organisms (*Salbu*, 2000, 2009). Generally, as illustrated in Fig 2, the processes affecting the transport behavior are different for the different species. Dissolved species (the blue circles in Fig 2), including LMM and colloidal species, are typically assumed to be mobile, following the water masses with the ocean currents. Particle species, i.e., radionuclides associated to suspended particulate matter (SPM) in the water column (green circles) are assumed to be sufficiently large to be affected by gravity and small enough to stay suspended in the water column for significant time. Hence, due to gravitational acceleration, these particle-bound species will be affected by an additional settling velocity and contribute to sedimentation, i.e., accumulation of radionuclides in the seabed sediments (red circles). The sedimentation rates depend on the particle size, shape and density as well as the water flow. Particle species can be separated in clay (0.45 µm to 2 µm) and silt (2 µm to 63 µm) classes, while larger sand and gravel particles are assumed to remain settled in the seabed sediments.

While the particle transport can be large in rivers, especially under high flow conditions, the currents and the vertical exchange are more moderate when river water enter estuaries and mix with marine water masses. Hence, particles following the river water will generally be subject to gravitational settling and accumulate in the seabed sediments in the estuaries outside the river outlets. As strong winds, large surface waves and high river flow rates typically increase the seabed stress, extensive resuspension and displacement of contaminated sediments and particles can be observed during such events. The particle size distribution also affects the transport of suspended particles, since larger particles generally are exposed to faster and more extensive settling than smaller particles, which are more easily resuspended and transported by turbulent water flow.

Thus, since the different elements and radionuclides have variable particle-affinity and the different species behave differently in the marine environment, the water-particle distribution should be considered in models aiming to simulate radionuclide transport. A widely used indicator of the specific particle-reactivity is the *sediment-water distribution coefficient* K_d, defined as the relationship between radionuclide activity concentrations in SPM or bottom

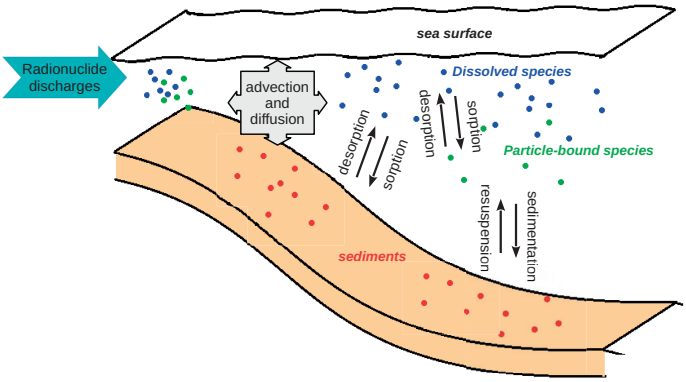

Figure 2: Sketch of the relevant processes affecting the transport of the different radionuclide species in the marine environment.

sediments and water under equilibrium conditions (*IAEA*, 2004):

$$K_d = \frac{C_p}{C_w} \tag{2}$$

Here, assuming wholly reversible exchanges, C_p is the activity concentration of particle or sediment species (Bq kg^{-1}) and C_w is the activity concentration of dissolved species (Bq L^{-1}), giving K_d the unit L kg^{-1}. Based on measured data, the range of the distribution coefficients cover several orders of magnitude, from calcium (1 L kg^{-1}), chlorine (1 L kg^{-1}) and technetium (10^2 L kg^{-1}) to americium (2×10^6 L kg^{-1}) and lead (10^7 L kg^{-1}) (*IAEA*, 2004). Elements with low K_d are usually referred to as *mobile*, *conservative* or *non-reactive* radionuclides, while elements with high K_d are called *particle-reactive* or *non-conservative*. As there are many local environmental factors controlling the K_d, such as pH, salinity and temperature, the values recommended by *IAEA* (2004) are given with large uncertainties, where the K_d values may span a range up to 2–3 orders of magnitude for a single element (*Abril and Fraga*, 1996; *Salbu*, 2000). Therefore, *Periáñez et al.* (2018) emphasizes the need of documenting the conditions under which the K_d measurements are taken, as the results are greatly affected by whether equilibrium conditions are reached or not. The fraction which is not reversibly bound to the solid matter, i.e., slowly reversibly or irreversibly bound, also affects the K_d

measurements.

For transport estimates of radionuclides with low affinity to particles (low K_d), non-reactive behavior has been a common assumption which has been shown to provide acceptable results in many cases (e.g., *Karcher et al.*, 2004; *Orre et al.*, 2010; *Tsumune et al.*, 2013; *Simonsen et al.*, 2017). However, for more particle-reactive elements with higher K_d, the fraction bound to particles and sediments cannot be neglected. Even though using the K_d value to estimate the distribution may be a good first approach, it may in reality take long time to reach equilibrium conditions. Therefore, in practice, such conditions are hardly ever obtained, and the equilibrium distribution is not very useful in model applications (*Periáñez et al.*, 2018). Laboratory experiments by *Børretzen and Salbu* (2000, 2002) show time dependency of the distribution between dissolved and particle-bound radionuclides. Thus, not only the equilibrium distribution itself, but the time it takes to reach equilibrium conditions is essential for speciation predictions. A *dynamic approach* has been shown to improve the transport estimates regarding radionuclide modeling (e.g., *Periáñez*, 2005). In such models, a certain amount of the activity in a specie is transferred to each of the other species during a time step, described by *dynamic transfer rates*. Rapid transfer processes have high transfer rates, while slower processes are characterized by lower transfer rates. These rates are interpreted as the fraction of a concentration that is transferred to another specie during a certain time period. A simplified system consisting of two model compartments is illustrated in Fig 3, where sorption and desorption processes continuously rearrange the radionuclides between dissolved and particle-bound species.

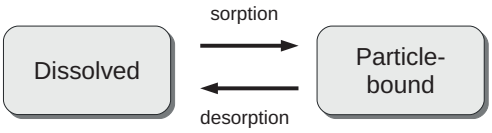

Figure 3: Sketch of a simplified system including dissolved and particle-bound species.

When such dynamic approach is applied, and reversible processes are assumed, the tracer equation (Eq (1)) can be split into one equation for the concentration of the reactive fraction of the dissolved species (C_w) and one for the concentration of the reactive part of the particle-

bound species (C_p):

$$\frac{\partial C_w}{\partial t} = \mathrm{adv}_w + \mathrm{diff}_w - k_{12}C_w + k_{21}mC_p \tag{3}$$

$$\frac{\partial (mC_p)}{\partial t} = \mathrm{adv}_p + \mathrm{diff}_p + k_{12}C_w - k_{21}mC_p \tag{4}$$

Here, $\mathrm{adv}_{w,p}$ and $\mathrm{diff}_{w,p}$ are the convergence of advective and diffusive terms for each of the dissolved and the particle-bound fractions, respectively. In the interaction terms, k_{12} and k_{21} are the transfer rates for sorption and desorption, respectively, while m is the mass density of available SPM in the water column.

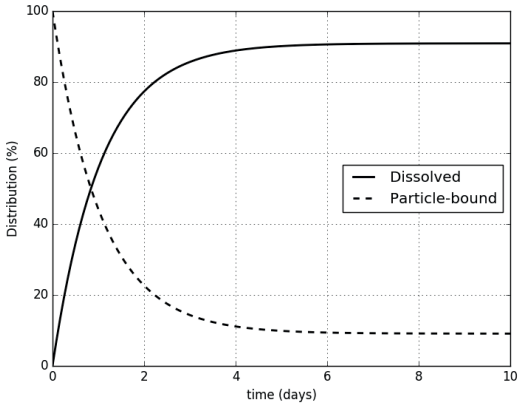

Figure 4: Illustration of time evolution of dynamic distribution of reactive dissolved (solid line) and particle-bound (dashed line) fractions in a closed system, assuming fully reversible exchange processes. The transfer rates were set to $k_{12} = 1 \times 10^{-6}\,\mathrm{s}^{-1}$ and $k_{21} = 1 \times 10^{-5}\,\mathrm{s}^{-1}$. The initial distribution was 100 % particle-bound species.

Assuming a closed system (setting $\mathrm{adv}_{w,p} = \mathrm{diff}_{w,p} = 0$), the time evolution of the distribution can be illustrated as in Fig 4, where all radionuclides initially were reversibly particle-bound and the transfer rates were set to $k_{12} = 1 \times 10^{-6}\,\mathrm{s}^{-1}$ and $k_{21} = 1 \times 10^{-5}\,\mathrm{s}^{-1}$. During each time step, a fraction of the dissolved radionuclides will sorb to the particles while a fraction of the particle-bound radionuclides will desorb to dissolved species. Hence, in a closed system, as illustrated here, the distribution converged towards equilibrium which was reached after approximately 5 days, and thereafter the distributions were unchanged. In a natural marine environment, however, such equilibrium conditions would practically never be reached, due to continuously shifting advective and diffusive transport processes (*Periáñez et al.*, 2018). In the simplified system illustrated here, only dissolved and particle-bound species were considered. But such a system could easily be extended to contain numer-

ous species and interaction pathways to be suitable for any purpose, e.g., include fractions with lower reactivity and colloidal species. Such extension would require one additional differential equation for each new specie and interaction terms for the relevant transformation pathways.

Characterization of radionuclide species is normally done by utilization of size fractionation techniques such as filtration, ultracentrifugation, dialysis and ultrafiltration (*Salbu*, 2000). The exact borderlines between the specie categories are difficult to distinguish as fractionation techniques are needed to separate species according to size, and thereby the categories are operationally defined. However, size fractionation will in many cases be insufficient for a proper description of the real speciation, as species with completely different properties may be present in the same size interval. Different speciation schemes have been tested and compared/optimized to observations (e.g., *Børretzen and Salbu*, 2002; *Periáñez*, 2004). For LMM species, such as dissolved ions or molecules, the charge is essential for the reactivity, and hence the most reactive LMM species will rapidly transform to colloidal, particle and sediment species, while the less reactive species may behave practically inert. Particle- and sediment-associated species can appear with several types of physical and chemical bindings. Reversibly bound LMM species are easily remobilized by small perturbations in environmental conditions (such as increasing salinity in estuaries), slowly reversibly bound radionuclides are stronger bound, while irreversibly bound radionuclides are fixed and can only be dissolved by using reagents with high dissolution power. For redox sensitive elements, the oxidation state may affect the speciation and may therefore strongly influence the mobility (e.g, *McKay and Pattenden*, 1993; *Skipperud et al.*, 2000). Especially in estuaries and in coastal regions, where rivers provide suspended mineral and organic matter to the marine environment, the colloidal fraction is evidently important for the geochemical cycling of trace metals (*Sañudo-Wilhelmy et al.*, 1996). However, previous model studies of radionuclides involving colloidal species are scarce.

During the transport through the marine environment, many external environmental factors as well as elemental properties affect the radionuclide speciation and transformations. Generally, surface sorption of LMM species to colloids and SPM in the water column depends on the chemical properties of the radionuclide, the available surface area of SPM (denoted as m in Eq (3) and (4), which usually is highest near the river outlets and in high turbidity regions) and the concentration of competing elements (*Machado et al.*, 2016). In general, due to competing effects from ions present in saline water, the sorption of radionuclides to suspended matter is reduced as salinity increases, while the desorption increases with higher salinity. For highly particle-reactive elements, this process may change the speciation signif-

icantly. On the other hand, desorption of radionuclides from river transported colloids and particles or accumulated in the sediments may locally increase the total concentration and especially the fraction of LMM species despite high dilution effects present in estuaries (*Teien et al.*, 2006; *Machado et al.*, 2016; *Sanial et al.*, 2017). Similarly, sorption of LMM species to seabed sediments can change the speciation considerably, dependent on the specific element's affinity to solid matter, environmental conditions, as well as the available amount of sorption surface in the sediments. The latter factor depends again on a number of local sediment properties, such as the porosity, the thickness of the active seabed layer and the fraction of small (available) particles in the sediments.

Therefore, to summarize, since the transfer rates can be dependent on both the elemental properties of the radionuclides as well as on external environmental conditions, the impact of environmental factors, such as salinity, pH, SPM and seabed properties on the transfer rates should ideally be taken into account when applied in a model. This is most relevant for particle-reactive radionuclides in cases where these environmental conditions change over relatively short distances and time scales such as in estuaries, near river outlets and in frontal zones (*Machado et al.*, 2016). However, a dynamic approach using kinetic transfer rates should always be preferred compared to equilibrium assumption.

2.4 Properties of Tc, Cs and Al

Technetium is an artificial radioactive element, whose predominant isotope is the fission product ^{99}Tc ($T_{1/2} = 2 \times 10^5$ y). The major source of ^{99}Tc contamination in the North Atlantic region is the Sellafield reprocessing plant. In addition, a small background radiation level originates from the global fallout (*Dahlgaard et al.*, 1995). In the marine environment, Tc is presumably present as the highly mobile pertechnetate TcO_4^-, having low reactivity to SPM and colloidal matter (*Salbu et al.*, 1993). The recommended K_d value in the marine environment is relatively low (10^2 L kg^{-1}) (*AMAP*, 2004). However, under anoxic environmental conditions, as can be found in coastal areas, Tc may be more particle-reactive and the sediment distribution coefficient being orders of magnitude higher (*Keith-Roach et al.*, 2003; *Salbu and Holm*, 2005).

Radioactive cesium isotopes are also products of nuclear fission. From an environmental concern, ^{137}Cs is the most relevant isotope, with a moderately long half-life ($T_{1/2} = 30$ y), originating mainly from nuclear reprocessing facilities as well as global fallout and the Chernobyl accident. Other relevant radionuclides of cesium are ^{134}Cs ($T_{1/2} = 2$ y) and ^{135}Cs ($T_{1/2} = 2.3 \times 10^6$ y). In freshwater, the particle reactivity of Cs is relatively high

($K_d = 2.9 \times 10^4\,\mathrm{L\,kg^{-1}}$, (*IAEA*, 2010)), but due to increasing competing effects in salt water, the particle reactivity decreases with increasing salinity (recommended open ocean K_d: $2 \times 10^3\,\mathrm{L\,kg^{-1}}$, (*IAEA*, 2004)). Hence, in marine environments, Cs is usually present as simple cations (Cs^+), with high solubility and mobility and with relatively low sorption to SPM and sediment surfaces. According to *Børretzen and Salbu* (2002), Cs binds to particles and sediments in three ways (Fig 5): Reversibly bound to planar sites, slowly reversibly bound to wedge sites and irreversibly bound to interlayer sites.

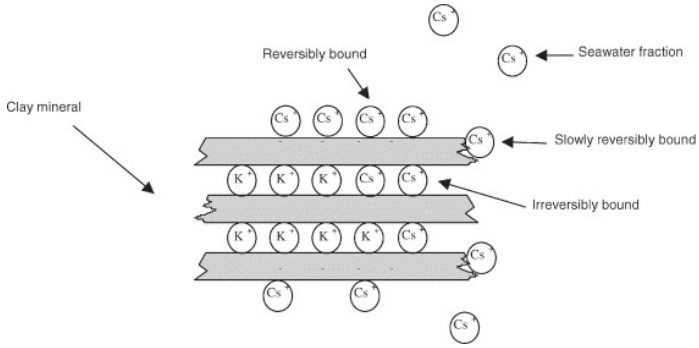

Figure 5: Illustration of binding sites for Cs on clay minerals. Reprint from *Børretzen and Salbu* (2002).

The major source of Al contamination to Norwegian marine waters is river run-off. Therefore, Al undergo extensive speciation changes initiated by a number of processes caused by the shifting environmental conditions during transport through the estuary from the river outlet to the open ocean. In addition to the processes described in section 2.3, as fresh river water comes into contact with sea water, pH increases and LMM cationic species of Al will hydrolyze, polymerize and form positively charged transient colloidal polymer species being highly reactive towards available surfaces (*Lydersen et al.*, 1992; *Teien et al.*, 2004). Alternatively, when pH increases, LMM Al species can hydrolyze and transform to aluminate, i.e., LMM anions which is the predominant form of Al in alkaline water (pH $>$7.5) such as sea water (*Lydersen et al.*, 1990). Furthermore, these processes and the following speciation are also of major relevance for organisms living in the estuarine zone, as transient Al polymers formed are toxic to fish (*Teien et al.*, 2006).

3 Tools and methods

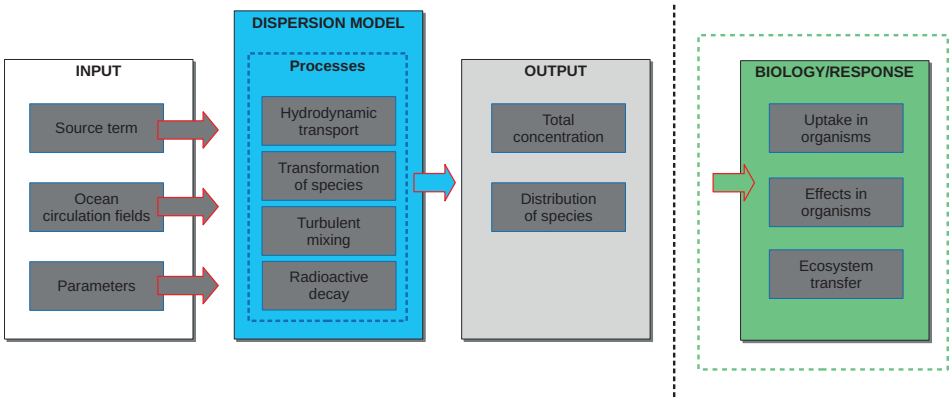

Figure 6: Sketch of the model system utilized in the present PhD project. The white, blue and gray boxes illustrate the model system covered by the present project, while the green box illustrates potential extended applications.

In the present work, to compute radionuclide activity concentration levels and transport in the marine environment, the main component of the model system was the dispersion model (blue box in Fig 6). We used TRACMASS (`www.tracmass.org`, *Döös et al.* (2017)), a Lagrangian (particle-tracking) trajectory model, to compute the pathways of a finite number of synthetic numerical units, here called *trajectories*. The TRACMASS model has previously been applied to simulations at global (*Döös et al.*, 2011; *Nilsson et al.*, 2013), regional (*Kjellsson and Döös*, 2012) and local (*Döös and Engqvist*, 2007; *Jönsson et al.*, 2011; *Viikmäe et al.*, 2013) scale, and it has also been used to simulate nuclear contaminants in the Baltic Sea (*Döös and Engqvist*, 2007; *Corell and Döös*, 2013). In such Lagrangian simulations, a large number of trajectories are released according to the source term where each trajectory represents a certain amount of radioactivity or a mass of a trace metal. In *off-line* simulations, as were performed here, the trajectory transport is computed using three-dimensional time-varying currents taken from a pre-computed external circulation model. In this study, the three dimensional ocean circulation fields were primarily provided by the Regional Ocean Model System (ROMS, `http://myroms.org`, *Shchepetkin and McWilliams* (2005)), the main model in the operational ocean forecast system at the Norwegian Meteorological Institute. ROMS is a generic hydrodynamic ocean model, based on discretized formulations of the Boussinesq and hydrostatic approximations of the Navier-Stokes equations. It computes ocean variables (such as sea surface elevation, three dimensional velocity components, salinity, temperature and density) in a three dimensional pre-defined grid. The vertical s-coordinates are stretched

and terrain-following with a constant number of levels, hence the vertical resolution depends on the depth.

An example of a snap-shot of a surface current field is illustrated in Fig 7a. For illustration, four trajectories were simultaneously released in slightly different positions, marked with a red circle in Fig 7b. Moving forward in time, the movement of each individual trajectory was estimated based on the ocean currents interpolated in time and space to the trajectory's location at propagating discretized time steps. Details of the TRACMASS model are described in *Döös et al.* (2017). During the simulation period, the pathways of the individual trajectories may be illustrated as trajectory lines, shown as black lines in Fig 7b. As explained in Section 2, physico-chemical processes will also affect the transport properties, for example by additional settling velocity for particle species. To account for unresolved dynamics such as unpredictable turbulence and eddy diffusion, small random perturbations are normally added to the deterministically computed drift (*Christensen et al.*, 2018).

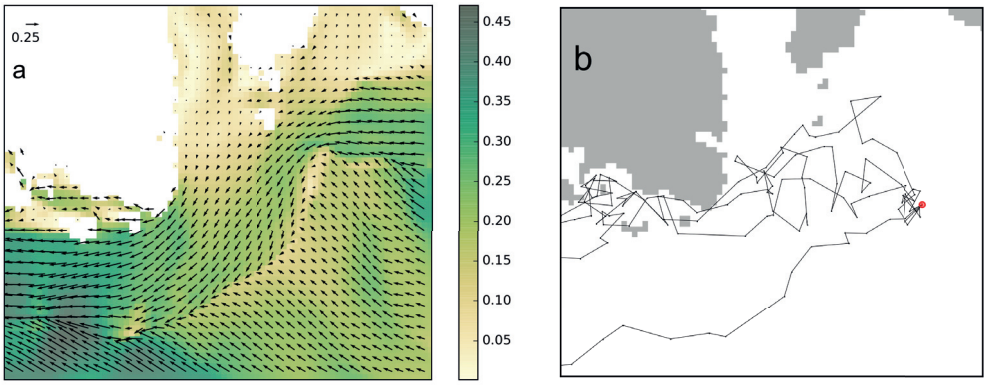

Figure 7: a: Example of a snap-shot of surface current direction (arrows) and speed (in $m\,s^{-1}$, color shading) from the hydrodynamic model (ROMS). The arrow in the upper left corner indicate the length of a $0.25\,m\,s^{-1}$ arrow. b: Pathways of four trajectories computed by the Lagrangian transport model (TRACMASS), using time-varying current fields from ROMS. Red point indicate the arbitrarily chosen release position of the trajectories.

Applying a sufficiently large number of trajectories, the number of trajectories present within a certain volume and time interval can during the post-processing be used to compute the radionuclide activity concentration levels. The results may then be visualized as maps valid at a limited time period or as time series from a given location.

In the present PhD study, three case studies were performed, involving transport of radionuclides in Paper I and II and using stable Al in Paper III. The required input (white box in Fig 6) for the dispersion simulations in these case studies were specifically chosen and optimized

for each of the three scenarios. They all included appropriate case-specific source terms, ocean circulation fields from a hydrodynamic model and a set of appropriate input parameters. Output from the dispersion model was the three dimensional position and the speciation of each trajectory at the output time steps, which was the basis for computing concentration levels and distribution of species in the post-processing step (gray box in Fig 6). In this PhD project, focusing on the hydrodynamic marine transport of radionuclides, the final output has been the radioactivity concentration levels, visualized as time series from target locations and maps showing the spatial distribution at given times. However, a very relevant future perspective is to utilize the concentration levels in biological impact and dose assessments (green box in Fig 6), estimating the ecological impact of the predicted activity concentrations.

In the scenarios that were investigated in this PhD thesis, the input of trajectories were time-dependent point sources. The simulations in Paper I covered large scale dispersion of ^{99}Tc discharges from Sellafield Nuclear Reprocessing Plant, UK, from 1994 to 2012. For investigation of the impact of spatial and temporal resolution, monthly-mean fields from the global FOAM model (*Blockley et al.*, 2014) at 0.25 ° horizontal resolution were compared to hourly 4 km $\times$ 4 km fields from ROMS. In the Boknafjorden case in Paper II, coastal dispersion of ^{137}Cs released as runoff from the 18 largest rivers in Boknafjorden in Western Norway was computed. The discharges considered originated from a hypothetical accident scenario (*Ytre-Eide et al.*, 2009; *Lin et al.*, In press), and hence no observational data were available for validation. The simulation period covered 7 months, with hourly fields at 160 m $\times$ 160 m horizontal resolution. The simulation of aluminium released from River Storelva in Paper III covered a 6 week period, and the target area was Sandnesfjorden, an 8 km long fjord at the Norwegian Skagerrak coast. Hourly circulation fields from ROMS at 32 m $\times$ 32 m horizontal resolution were applied.

While the dispersion of ^{99}Tc radionuclides was considered non-reactive in Paper I, model code describing element speciation and transformation processes was implemented in TRACMASS and applied to the cases in Papers II and III. Such speciation and transformation processes for radionuclides and trace metals have to the best of our knowledge not previously been included in TRACMASS. Since TRACMASS is a Lagrangian model, the specie distribution was obtained using a stochastic approach as described by *Periáñez and Elliott* (2002), equivalent to solving the specie interaction terms in the general tracer equations (Eq (3) and (4)) in Eulerian models. Here, each trajectory is associated with one of the pre-defined species, and during each time step, there is a certain probability of transformation to each of the other species, determined by the transfer rates. At each update (the model time step), a random number is drawn, and the value of this number is used to decide whether the trans-

formation shall take place or not for each individual trajectory. Statistically, this method will provide a specie distribution similar to the Eulerian approach (*Periáñez and Elliott*, 2002).

In the Boknafjorden case (Paper II), all transfer rates were constant, except for the sorption to suspended particles, which depended on a horizontally variable SPM concentration field, computed in advance of the simulations. In Paper III, where the behavior of trace metals in the Sandnesfjorden estuary was investigated, the transfer rates changed with respect to salinity, based on empirical estimates from field speciation data.

4 Summary of the papers

4.1 Paper I

"The impact of tidal and mesoscale eddy advection on the long term dispersion of ^{99}Tc from Sellafield"

Simonsen, M., Ø. Saetra, P. E. Isachsen, O. C. Lind, H. K. Skjerdal, B. Salbu, H. E. Heldal, and J. P. Gwynn

https://doi.org/10.1016/j.jenvrad.2017.06.002

In Paper I, the role of mesoscale eddy and tidal advection on transport and dispersion was investigated by model simulations of ^{99}Tc released from Sellafield. The simulations covered the years from 1994 through 2012, when relatively high ^{99}Tc discharges were resumed after a 13 years long period with relatively low discharges. Due to the low particle affinity of ^{99}Tc, only the dissolved species were considered, assuming no significant interactions with suspended particles or sediments. Transport estimates in the North Atlantic, Barents Sea and Arctic Ocean were performed with an ocean model at 4 km horizontal resolution resolving a large part of the ocean mesoscale eddy field and also including tides. Equivalent estimates were also computed with a model at coarser resolution in which these processes were either absent or parametrized.

Compared with field observations, the general features of the ^{99}Tc dispersion were well reproduced by the coarse scale model if the diffusivity in its eddy parametrization scheme was suitably chosen. However, the eddy-permitting simulations captured regional details better and showed an overall higher prediction skill, with the model predictions agreeing with the observations within a factor of two to four. The importance of tidal advection was investigated by comparing transport in the eddy-permitting model when this was run either with tides included or with tides filtered out. The results pointed to systematic Lagrangian tidal drift in the Irish Sea and the North Sea that eventually impacted the ^{99}Tc activity concentration levels also far downstream.

4.2 Paper II

"Coastal transport of river-discharged radionuclides: Impact of speciation and transformation processes in numerical model simulations"

Simonsen, M, O. C. Lind, Ø. Saetra, P. E. Isachsen, H.-C.. Teien, J. Albretsen and B. Salbu

https://doi.org/10.1016/j.scitotenv.2019.01.434

In Paper II, the effect of radionuclide river runoff on the total exposure in a fjord system was investigated. A case study was performed, considering a hypothetical accident scenario including river discharges of ^{137}Cs to the coastal marine environment in Boknafjorden i Western Norway. The model system utilized ocean circulation fields at relatively high spatial (160 m $\times$ 160 m in horizontal direction) and temporal resolution (1 hour). Code for radionuclide speciation and dynamic transformation of radionuclides between the different species was implemented in the dispersion model to estimate the distribution of the LMM, suspended particulate and sediment-bound species as well as radionuclides slowly reversibly bound to suspended particles and sediments. Results from a number of simulations were compared to identify how factors associated with radionuclide speciation and transfer between the model compartments could affect the predicted radiocesium activity concentrations.

The results showed that by including dynamic transformation of radionuclides between the model compartments, the total activity concentrations at far-field sites could vary with more than two orders of magnitude, demonstrating that this model configuration enables prediction of potential local hot-spots. However, the total activity concentrations near the river outlets were less affected ($<$ factor 10). Changing the radionuclide speciation in the river discharges (releasing radionuclides as slowly reversibly bound and changing particle size) and the parameterization of ^{137}Cs particle affinity (varying the coefficients) greatly affected the specie distribution ($>$ factor 10^3 increase in fraction of ^{137}Cs associated with SPM). The settling of radionuclides towards the seabed was also increased by increasing the particle affinity and increasing the particle size (up to factor 10^2 increase in ^{137}Cs sediment concentrations). These factors were therefore identified as important contributors to the overall uncertainty.

4.3 Paper III

"Modeling key processes affecting Al speciation and transport in estuaries"
Simonsen, M, H.-C.. Teien, O. C. Lind, Ø. Saetra, J. Albretsen and B. Salbu

In Paper III, transport of river-discharged aluminium (Al) through changing estuarine environmental conditions was simulated. Since the Al toxicity is largely dependent on the element speciation, new model code predicting speciation and transformation processes of LMM, colloidal, particle and sediment associated species was implemented. Dynamic, salinity-dependent transfer rates were based on *in situ* measurements from several Norwegian estuaries as well as experimental data. Predicted total Al concentrations as well as fractions of LMM, colloidal and particle species were compared to observational data from Sandnesfjorden estuary in south-eastern Norway collected in May 2008.

Good agreement was obtained between the model results and the observed total and fractionated Al concentration levels at several stations along the fjord transect. Without including background contribution of Al from the coastal water, the predicted Al concentrations were underestimated in the outer part of the fjord, where mixing with coastal water was considerable. In addition, the near-surface Al concentrations were also underestimated due to overestimated vertical mixing in the hydrodynamic model. In general, the hydrodynamic model overestimated the near-surface salinity (with 7 psu in average) and the transport model underestimated the Al concentration levels by up to a factor 4. The observed correlation between salinity and total Al concentration was well reproduced by the model in situations with low upper layer volume flux, typical under low river flow conditions. In contrast, the predicted surface salinity and total Al concentration were less correlated in high-flux situations. As the general trends of Al concentrations and speciation were well reproduced, this study demonstrated that by including carefully chosen transfer rates, the model can be used to predict spatio-temporal distribution of total contamination as well as concentration levels of the elemental species.

5 Discussion

5.1 Major sources of uncertainty

At all stages of the present work, the overarching aim has been to identify and quantify the major sources of variability and uncertainty involved in numerical dispersion simulations at various scales. During the three case studies considered in the present project, the complexity related to the speciation increased progressively, and simulations with such a complex model system introduce uncertainties at many levels. As described by *Salbu* (2016), the overall uncertainty in environmental risk assessments can be associated with a number of categories:

1. Input uncertainty
2. Interpolation and extrapolation uncertainty
3. Parameter uncertainty and variability
4. Algorithmic uncertainty
5. Structural uncertainty

In the context of the present work, *input uncertainty* include errors associated with observational data, such as typically small errors introduced by the sampling instruments, but also larger errors associated with representativity of samples and with algorithms converting the measured signal to model input variables. *Interpolation and extrapolation uncertainty* is introduced when input data are interpolated e.g., by using statistical methods to obtain values between noncontinuous samples in time series or in heterogeneously distributed variables. *Parameter uncertainty* is assigned to uncertainty in model parameters. Both *algorithmic* and *structural uncertainties* are assigned to mismatch between model and reality and may be caused by insufficient understanding or approximations of natural processes in the model. The *algorithmic uncertainty* comes from model approximations and assumptions, giving rise to deviations between the model's descriptions of phenomena and processes and the real world. The *structural uncertainty* is assigned to exclusion of relevant processes or misinterpreted conceptual understanding in the model due to lack of knowledge or excessive simplifications.

Within each of these uncertainty categories, a number of factors can be relevant to various degrees. To perform a proper sensitivity analysis of a complex model system such as the ROMS-TRACMASS system, a huge number of total simulations would be required to cover

all combinations of all likely values of each factor. The computational costs would escalate, especially if uncertainties in the ocean circulation fields are taken into account. We can assume that the impact of the variability and uncertainty associated with the circulation fields is considerable, and for practical reasons, no real sensitivity analyses were performed in the present work. Instead, selected key factors were varied within reasonable ranges and the model response to these variations were investigated. With focus on process investigation in Papers I and II, results from a number of simulations with slightly different configuration were compared, aiming to identify and quantify the impact of each process on the model output. Although only one simulation was performed in Paper III, uncertainties arising from many processes were involved and discussed at many levels also in that paper.

In all papers, the source term estimates involved input, interpolation and extrapolation uncertainties, as well as structural and algorithmic uncertainty. In this work, the phrase 'source term' refers to the input source in the model, i.e., the input of radionuclides or trace metal contaminants, either directly from the conventional sources as nuclear installations in Paper I, or secondary via environmental compartments such as atmosphere, catchments, rivers and estuaries in Papers II and III. Issues regarding the source terms are further discussed in subsection 5.2.

The Sellafield (Paper I) and Sandnesfjorden (Paper III) case studies involved historical releases that have been subject to long-term and periodic monitoring. The model results in those papers could therefore be validated against observations. The radionuclide discharges from Sellafield appear to be relatively well monitored, both regarding the local contamination in the Irish Sea and the far-field transport to remote regions such as the North Atlantic and Nordic Seas. Despite this, determining an objective skill performance for comparison of the different model simulations in Paper I was not straight-forward. Historically, the purpose of most radionuclide data sampling campaigns has been to monitor the general contamination levels with respect to protection limits, which does not necessarily make them well suited for model validation. Direct one-to-one comparison of model results and sampling data may be mis-leading for several reasons, since the observed and computed activity concentrations do not exactly represent the same thing. By definition, the model results cover an average in time and space, affected by assumptions and limitations, while the observations normally are snap-shot values. In areas with highly energetic flow patterns, the contaminants will most likely be inhomogeneously distributed and characterized by large fluctuations, either in time or space, or as a combination of both. Since such variability cannot be determined by a single (or very few) snap-shot observations, the representation error of a single sample may be large in areas with high natural variability (*Sandvik et al.*, 2016; *Janjić et al.*, 2018). Due to

relatively high costs and human efforts involved in collecting each data sample, especially the ones collected during open ocean cruises, the number of samples are kept at a minimum to maintain sufficient monitoring (*Dowdall et al.*, 2005). Hence, the coarser the observation sample density (either in time or space), the higher is the representation error associated with the samples. Therefore, in practice, mainly the general trends and large-scale distributions can be assessed when comparing model results with observations.

Accurately modeled ocean circulation fields are essential for proper transport estimates. Errors and uncertainties in the flow field might in worst case potentially predict the transport of contaminants in wrong direction or over- or underestimate the radionuclide fluxes. Further, correct placement of dynamic features such as depth of the mixed layer, vertical stratification, horizontal fronts and eddies are essential for correct transport predictions. Hence, the impact of uncertainties in the circulation fields on the total model outcome may be high. With some exceptions, all the hydrodynamic fields used in the present work were provided from the ROMS model. ROMS is widely used in numerous applications all over the world, and is considered reliable at basin scale and also at coastal scale (e.g., *Shchepetkin and McWilliams*, 2005; *Wilkin et al.*, 2005). The variability between different realizations of the hydrodynamic ocean currents was found to be the largest contributor to discrepancies between transport estimates of the Fukushima discharges (*Periáñez et al.*, 2016a). Therefore, some discrepancies could be expected if circulation data from other hydrodynamic models had been utilized. However, we considered the applied ROMS data to be of high quality and to be the best choice for our purpose. Results from the hydrodynamic simulations utilized in Paper I were validated by *Røed et al.* (2015), while in the simulations used in Papers II and III, hydrography data were validated against available CTD casts taken within the model domain in the simulation period. A well-known method to quantify the variability in the circulation fields is to conduct ensembles of a number of equivalent realizations of the same case, but with small perturbations in the initial conditions, attributed to the dynamics or in the external forcing. The simulations performed in the present PhD, were performed with circulation fields at relatively high resolution. Although it would have been preferred, for practical reasons, it was not feasible to conduct ensemble simulations in our scenarios.

5.2 Source term

Uncertainties and inaccuracies in the description of the source term will obviously affect the downstream predictions of activity concentration levels. This can be categorized as input uncertainty, i.e., the errors directly associated with the estimated discharges (category 1), but

also as interpolation and extrapolation uncertainties due to non-continuous or inconsistent time series (category 2) as well as algorithmic uncertainty in cases where the source term estimates are dependent on some other variables (category 4), such as the river flow in Papers II and III. These aspects become typically more relevant when the estimated source term is distributed over a number of element species (*Salbu*, 2016). In such cases, the uncertainty associated with the time series of each specie is typically larger than that of the total activity concentration.

Nuclear facilities are in many cases owned by commercial companies or are military properties, which may contribute to difficulties in accurate determination of nuclear inventories and source terms for scientific purposes, since these numbers commonly are confidential. In addition, in many cases, the discharge details are actually unknown or badly documented even for the operators, especially for the major nuclear accidents. Since the source term is considered to be one of the major contributors to uncertainty in radionuclide modeling, a well-defined source term should be highly prioritized by modelers. Combined with dense and detailed monitoring of the fate of the discharges, reducing the uncertainties related to the source term will increase the benefits from environmental modeling. Thus, precise determination of the source terms is important, not only the magnitudes of the total activity concentrations for series of radionuclides (e.g., *Kobayashi et al.*, 2013; *Aoyama et al.*, 2016), but also regarding temporal distribution as well as radionuclide speciation (*Salbu et al.*, 1993, 2003).

In the Sellafield case (Paper I), the source term itself appeared to be relatively certain and reliable, with total monthly discharges provided by the operators (Sellafield Ltd). What was missing, though, was information about how the discharge batches were distributed within each month. Thus, in our simulation, we assumed the monthly discharges to be released in a single batch on the last day in each month. For the purpose of our long-term simulation, this uncertainty was considered to be acceptable. However, in case of studies at shorter time scales, this issue would probably affect the results considerably. In addition, it was assumed that the concentration of ^{99}Tc in the model domain was zero when the simulation started. Since Sellafield is the primary source of ^{99}Tc to the North Atlantic, having low releases between 1980 and 1994, the background levels were assumed to be negligible. In reality, there was a low background concentration in the years before 1994 (*Dahlgaard et al.*, 1995). However, as reported by *Brown et al.* (2002), the activity concentration levels in Northern Norway increased with a factor of 4–8 in the first years after the Sellafield discharges increased in 1994, supporting our assumption of negligible background levels. The background concentration could have been accounted for by adding a uniformly distributed small amount to the model results, but that would not have affected the main results and conclusions of Paper I.

The hypothetical releases of ^{137}Cs in the Boknafjorden case (Paper II) were assumed to be distributed between the 18 largest rivers contributing to 80 % of the total river input to Boknafjorden. Here, the major concern was to obtain a realistic relative distribution between the rivers, which was done by scaling the discharge from each river according to its daily flow rate. Also here, the background contamination was neglected, and the initial activity concentration was set to zero. We considered this as a reasonable assumption, as the study primarily was aiming to investigate the contribution from the river discharges. But in case of a real deposition scenario, such assumption should be reconsidered, as other significant sources also may be present and should be taken into account. This can be atmospheric deposition on sea surface and radionuclides transported with ocean currents from other regions, e.g., by the Norwegian Coastal Current. In contrast to Papers I and II, the uncertainties associated with the background Al concentration in the Skagerrak water were considerable in the Sandnesfjorden case (Paper III). Due to large variability, correcting for this background term appeared to not be straight-forward, and negligence gave too low modeled Al concentration levels near the fjord mouth in our simulations.

An issue considered both in Papers II and III was the relationship between the source term (concentration levels of the contaminant) and the river flow. As increasing flow also increases the erosion of particles from the river banks and river beds (*Teien et al.*, 2006) with subsequent remobilization of mobile species, the total concentration levels were assumed to increase as a power function of the flow rate. Such a relationship agrees with measurements in River Suldalslågen (*Bogen and Bønsnes*, 2004). Although empirical correlations are found in one river, development of such an algorithm for discharges as function of river flow will introduce algorithmic uncertainty (category 4). Further, as these relationships probably depend on local conditions, such dependency observed in one river cannot directly be transfered to other locations without introducing extrapolation uncertainty (category 2). However, being aware of these uncertainties, we considered the structural uncertainty (category 5) of *not* including such relationship between river flow and total concentration to be unacceptably large.

In a real scenario, the radionuclides are most likely present as a mixture of different species, and the most realistic release scenario would include several species, as we did in Paper III. But since the aim of the Boknafjorden study (Paper II) was to investigate the variability, only the extremes were presented in that paper. In those simulations, all radionuclides were assumed to have equal physico-chemical form in the moment of discharge, either LMM species or slowly reversibly bound to particles. Due to rapid remobilization, releasing all radionuclides as reversibly bound to particles did only impact the results slightly compared to releasing them as LMM species.

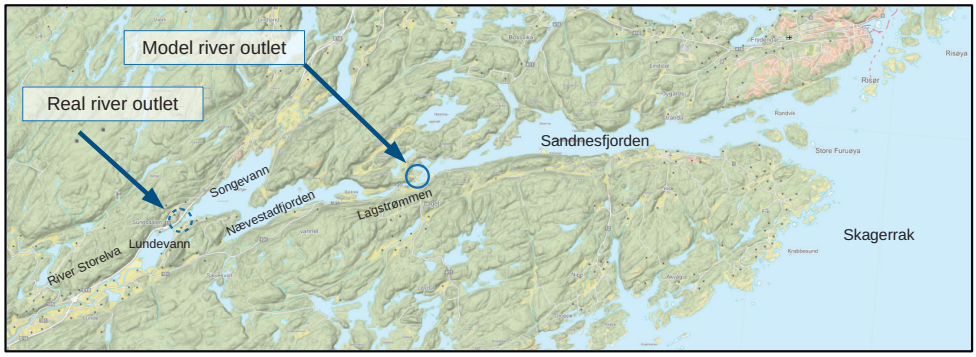

Figure 8: Map of the simulation area in Paper III. Map from `www.norgeskart.no`

In Paper III, the estimated total Al concentration and specie distribution in the discharges were based on observation samples from River Storelva collected during the simulation period. For technical reasons, the river outlet was placed outside the narrow Lagstrømmen Canal, while in reality, the river outlet is located at Lundevann upstream of the two basins Songevann and Nævestadfjorden (Fig 8). Thus, these basins were omitted in the simulations. On the way through these basins, many processes such as sedimentation and transformation of species can be expected to take place to some extent. Hence, neglecting these estuary basins might have contributed to inaccuracies in the model results due to structural uncertainty (category 5, discrepancy between model and reality) as well as input uncertainty (category 1). It can also be expected to have affected the circulation fields.

When starting a model simulation, the initial fields are most likely not in agreement with the real world, and they are most likely unbalanced with respect to hydrography and flow pattern of the water masses. Turning on the external forcing in the initial time step may give an unphysical shock (i.e., unrealistic dynamic features) to the model fields, from which it takes significant time to recover. The so-called 'spin-up time' is the time it takes for key variables to obtain realistically balanced conditions after initialization. While the barotropic signals are balanced relatively fast, the baroclinic features and deep mixing of water masses may require longer time until a realistic physical balance is obtained. Such model spin-up may also be relevant for the dispersion of contaminants. The discharges in the Sellafield and Boknafjorden scenarios (Papers I and II) were based on sudden releases into initially clean conditions. In these cases, the evolution of activity concentration levels in different regions, as well as the time scales of the increments and the transport times were relevant when the results were interpreted. In the Sandnesfjorden case (Paper III) in contrast, we considered continuous discharges of aluminium from the river, and thus the issues related to

the spin-up should be considered. In our case, however, the Al in the surface water masses had a residence time in Sandnesfjorden of only a few days, and hence only a short spin-up period was required. However, a considerable and increasing amount of the Al discharges became associated with bottom sediments, which in reality probably was accumulated over years. With such a long resistance time and assuming initially uncontaminated sediments in the model simulations, the concentration levels in the seabed interior as well as in the water masses close to the bottom could be expected to be underestimated in the model results. However, testing showed that this only affected the seabed and the near-bottom water masses. In contrast, the surface layer (upper 1 m), which was evaluated in the paper, was practically not impacted after the first few days of the simulation.

5.3 Numerical description of physical processes

Although there are many advantages of numerical models and their applications, such models are always based on mathematical descriptions of the real environment and hence they will always be constrained by simplifications and assumptions. Therefore, model results should always be interpreted as one out of many possible realizations of the actual scenario with a given overall uncertainty, only valid within the model limitations (*Salbu*, 2016). Such limitations can be related to validity in time and space and processes that are either accounted for or not. To describe a real phenomena, the model should ideally include all relevant processes, and at the same time be as simple as possible to avoid unnecessary use of computational resources. Therefore, when numerical models are designed, compromises have to be made regarding inclusion of relevant processes and required complexity for the actual cases in question. Hence, there will always be discrepancies between models and the real world, introducing structural and/or algorithmic uncertainties (categories 4 and 5).

As described in Section 3, all the simulations presented in the present study were performed using the TRACMASS dispersion model, and with a few exceptions, hydrodynamic fields from the ROMS ocean model were used. Since off-line Lagrangian models normally are fast, these models are the most common approach for ocean drift simulations (*Christensen et al.*, 2018). The spatial and temporal detail level of the dispersion simulation depends on the resolution and output frequency of the hydrodynamical model. However, by using interpolation routines, most Lagrangian dispersion models are able to compute transport also at intermittent times and locations between the output from the circulation model. In contrast, in on-line simulations, the radionuclides are computed internally in the hydrodynamical model either as Eulerian (grid-based) tracer fields or Lagrangian particles. The update time intervals would

then typically be similar to the internal time steps in the hydrodynamic model and much shorter than the time intervals in the output fields. The advantages of an on-line approach are obviously having higher temporal resolution and being less storage-demanding. But the major disadvantage is the high computational cost (and/or time consumption) for each simulation, as the whole hydrodynamical model has to be run simultaneously. An advantage of Lagrangian models is that they keep track of each individual trajectory, enabling extraction of statistics such as trajectory age (relative time since the trajectory was released), transit times and transport routes. This is typically computed in the post-processing after the model simulations are finished. In addition, artificial numerical down-gradient diffusion is non-existent in Lagrangian models, which may cause erroneous results in Eulerian models, especially in frontal zones where large gradients are present.

In Eulerian models, the concentration levels are computed in each individual grid cell and the *detection level* is limited by numerical truncation, which for most practical purposes means 'infinitely small'. In Lagrangian models, in contrast, each trajectory is normally not representing one physical particle or radionuclide, but is instead implemented as a discrete 'super-particle', attributed to a certain amount of activity in becquerel for radionuclides, or a certain mass for stable trace elements. Each trajectory can then be interpreted as a possible pathway of a water parcel or a bulk mass of particles initiated in a given position and time. Since each trajectory behave independently of all other trajectories, such models are not automatically calculating the concentration levels. Instead, the density of trajectories present in a given volume during a time interval can be used to compute the activity concentration at that location and time. This can be extracted to and presented as time series for a chosen water volume, or as gridded maps. For highest detail level in the concentration estimates, it would be preferred to use short time intervals and small volumes. However, in regions with few trajectories, the results will become noisy as the presence of each single trajectory will have relatively high impact. The uncertainty associated with this 'detection threshold' may therefore be high in Lagrangian simulations, as the difference between zero and one particle may be significant. This undersampling can be solved by applying more trajectories in the simulation, but this will increase the computational costs and will only transfer the problem to some other more remote regions. Therefore, while the resolution in Eulerian models is typically similar to that of the hydrodynamic model, the detail levels in Lagrangian models also depends on the number of individual, independent synthetic particles, and the total number of trajectories used in a simulation must be a trade-off between the need for detailed results in target regions and the computational costs.

Due to the 'cascade of energy' continuously transforming kinetic energy from large scales to

smaller scales in dynamic systems (*Griffies*, 2004), there will always be unresolved turbulent processes at scales below the model grid scale which may contribute significantly to the total transport (Fig 9). To take care of this problem in circulation models, these unresolved fluxes of momentum and tracers are commonly parameterized as diffusive processes, where the diffusion coefficients often are described with dependence to the resolved flow components. Such parameterizations are usually introducing algorithmic uncertainty. To directly resolve the small scale dynamic features and obtain more detailed flow fields, the model resolution can be increased, however, at the expense of higher computational costs, which usually turn out to be one of the major limiting factors in ocean modeling. In high resolution models, a larger part of the turbulent flow field is resolved directly, while in low resolution model, these processes have to be parameterized. In Paper I, the impact of model resolution on the

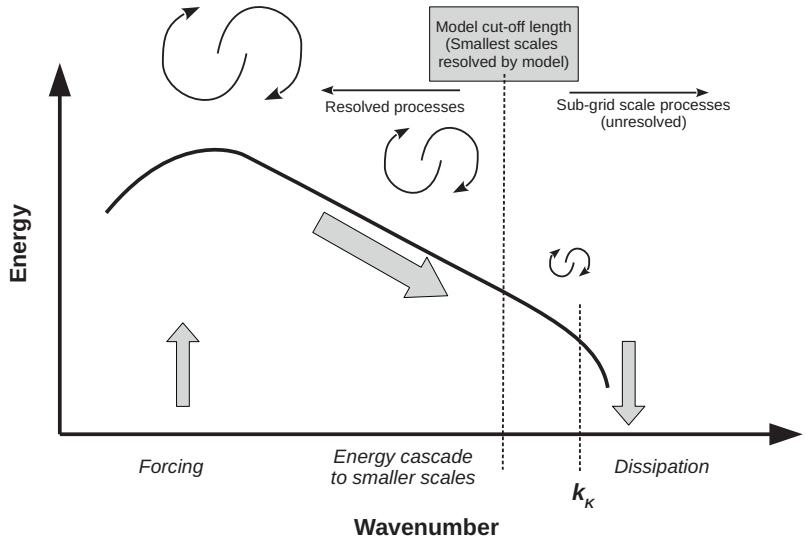

Figure 9: Sketch of the energy distribution at the different wave numbers. Energy is introduced to the model system by external forcing, typically at small wavenumbers (large scales). The energy is transferred to smaller scales due to turbulent processes. At some point, the model resolution is too coarse to resolve the turbulent flow. For small scale processes at wavenumbers above the Kolmogorov-scale wavenumber (k_K), the energy is transferred to heat due to viscous friction (dissipation).

results was investigated. As a coarse scale model, we used monthly-mean fields from the global FOAM model (*Blockley et al.*, 2014), at 0.25 ° horizontal resolution, corresponding to around 14 km at 60 °N. For comparison, daily-mean ROMS fields at 4 km horizontal resolution were used. In these waters, the ROMS setup was considered to be eddy-permitting, while the FOAM setup was non-eddy-permitting with higher need of eddy parameterizations.

Although many other factors than the resolution contribute to discrepancies in such a model comparison, we saw clear effects of the increased resolution. Therefore, based on the results from Paper I, the model resolution in Papers II and III was as high as practically feasible, for the purpose of resolving small scale dynamic processes directly in the model, and not by parameterizations.

The turbulent water flow has a fundamentally chaotic turbulent mixing behavior which affects the flow by breaking down unstable gradients to smaller scales. In dispersion models, the unresolved turbulent transport and mixing, including unresolved eddies and chaotic mixing, are assumed to behave analogous to diffusive viscous friction and are commonly parameterized as 'turbulent diffusion'. Although these are unpredictable processes, they commonly become more statistically correctly described by increasing the model resolution, rather than by parameterizations.

From our model comparisons in Paper I, it was clear that diffusion should be added to the mean flow in the coarse scale simulations (Fig 10). Increasing the diffusion coefficient in

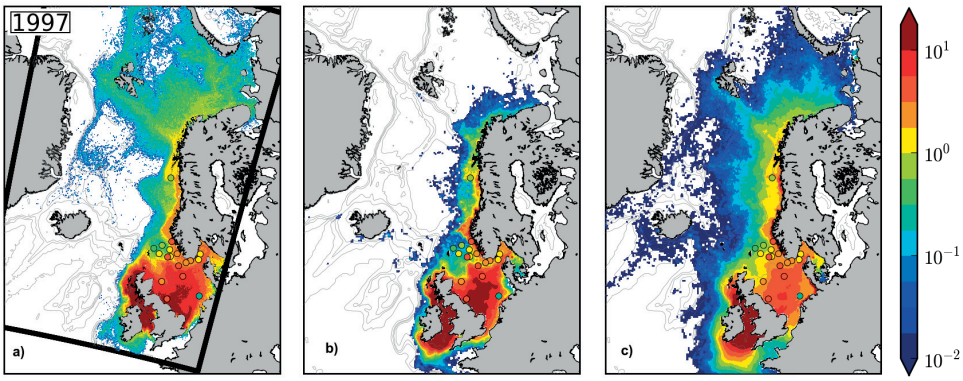

Figure 10: Surface (top 50 m) ^{99}Tc activity concentration averaged over 1997 including observational data from a: ROMS 4 km resolution with no additional diffusion b: FOAM with eddy diffusion of $A_h = 50\,\mathrm{m^2\,s^{-1}}$ and c: FOAM with eddy diffusion of $A_h = 500\,\mathrm{m^2\,s^{-1}}$. (Reprint from Paper I.)

the simulations using coarse scale flow fields improved the results considerably. However, the diffusion parameterization in TRACMASS assumes isotropic lateral distribution, which is not always the case in reality. In many cases, the horizontal diffusion is flow-dependent and mostly directed along the mean flow. As discussed in Paper I, the mean currents in the Nordic Seas are strongly steered by the topographic contours of the continental shelf, while the across-slope eddy transport is suppressed (*Blumsack and Gierasch*, 1972; *Isachsen and Nøst*, 2012; *Isachsen*, 2015). Adding isotropic turbulent eddy diffusion to the flow field ap-

peared to overestimate the radionuclide transport across the topographic contours, especially above the continental slopes (Fig 10). For improved results using ocean circulation fields from the coarse scale model, a more sophisticated parameterization of the diffusion would be preferred.

Another commonly parameterized process in dispersion models is the settling of particles, introducing algorithmic and structural uncertainties as well as parameter uncertainty (categories 3, 4 and 5). While the particle size distribution in the real environment is expected to be continuous, all particles in the TRACMASS model are assumed to be of equal size and density. However, to investigate the impact of size distribution on the transport estimates, results from simulations with small (1 µm), intermediate (5 µm) and large (10 µm) particles were compared in Paper II. Although no measurements of suspended particle size distribu-

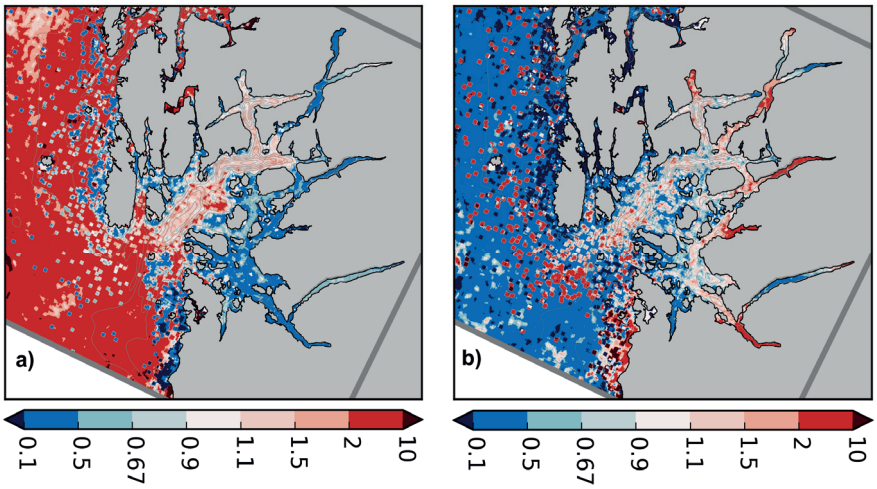

Figure 11: a: Ratio of May 2016 total depth-integrated activity concentration between simulation with ^{137}Cs radionuclides discharged as slowly reversibly bound to small particles and simulation with discharges as intermediate size particles. b: Ratio of predicted total depth-integrated activity concentration between simulation with ^{137}Cs radionuclides discharged as slowly reversibly bound to large particles and simulation with discharges as intermediate size particles. (Reprint from Paper II.)

tion were available, these sizes were considered to be representative for the distribution in Boknafjorden. The sensitivity to the particle size was found to be small in simulations where the radionuclides were discharged as reversibly bound to particles or as LMM species. In contrast, the impact was much higher when the radionuclides were slowly reversibly bound to particles when released from the rivers. This can be explained by the residence time, the aver-

age time for radionuclides being bound to particles, which was much longer in case of slowly reversible binding. In the simulation with large particles, the settling of radionuclides close to the river outlets increased, with increased radionuclide inventory in the fjord system in the end of the simulation (Fig 11b). In contrast, smaller particles were transported much faster in the upper water layer, with lower sedimentation rates and increased long-range transport of radionuclides (Fig 11a).

When analyzing the results from our simulations, we mainly looked at concentration levels in the surface waters, using the upper 50 m as a representation of the surface mixed layer in Papers I and II. In the Sandnesfjorden case (Paper III), where the length scales involved were much smaller than in the two other cases and we expected stronger vertical gradients, a representative surface layer thickness of 1 m was used for comparison with observations taken at 1 m depth. Indeed, the mixing layer depth varies in time and space, but with this approach, we assumed the results to represent the mean value of the surface layer. Under circumstances with strong vertical gradients, our assumption will obviously affect the results. However, as explained above, a thinner layer would increase the uncertainty due to sampling error as less trajectories would be included in the concentration estimates.

5.4 Speciation and transformation processes

Including speciation and transformation processes in numerical models requires several choices, assumptions and approximations regarding the numerical description of processes in the real world. Complex systems involving radionuclide speciation and transformation processes require a number of transfer rates describing the kinetics. These processes may be impacted by local environmental conditions, which still contain substantial knowledge gaps and are in general relatively insufficiently described (*Machado et al.*, 2016). Throughout the present study, the model complexity increased progressively from assuming non-reactive behavior in Paper I, including LMM, particle and seabed species in Paper II and introducing colloidal species and response to environmental changes in Paper III. The speciation and transformation processes were utilized by two different schemes for ^{137}Cs and Al, respectively, as sketched in Fig 12.

The ^{99}Tc case study in Paper I was simulated without transformation processes, assuming all radionuclides were present as non-reactive dissolved species. As explained earlier, this was due to the low particle-affinity of technetium ($K_d = 10^2\,\mathrm{L\,kg^{-1}}$, *IAEA* (2004)), giving low interaction with sediments and suspended particles (*Leonard et al.*, 2004). Assuming non-reactive behavior is rather common in simulations with radionuclides with low K_d, and

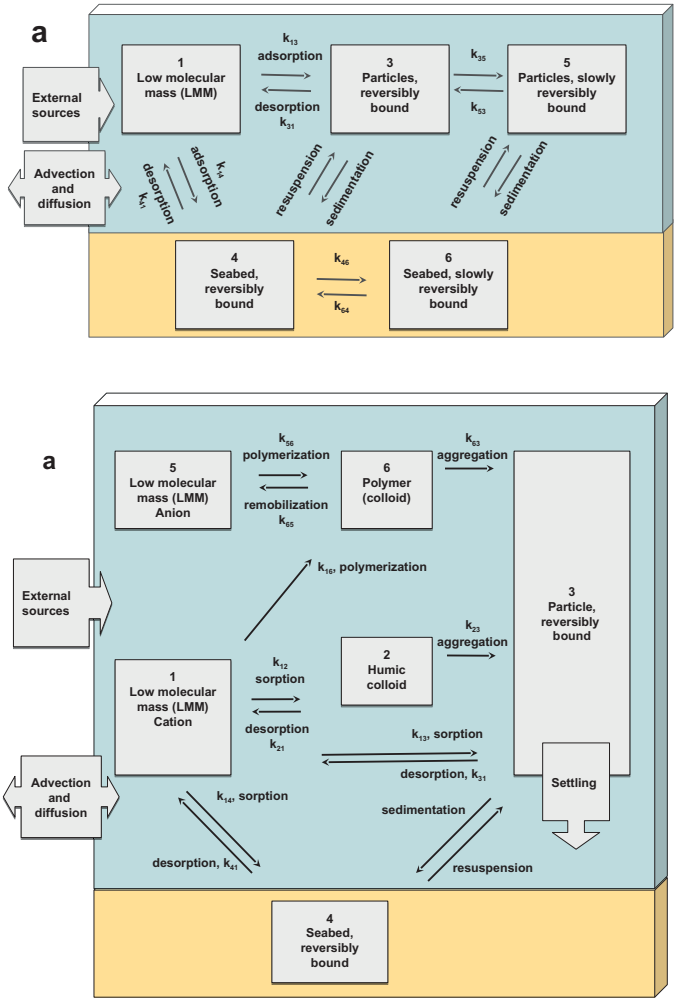

Figure 12: Speciation, transformation pathways and physical processes utilized for ^{137}Cs in Paper II (a) and for Al in Paper III (b). In both schemes, the external sources can introduce radionuclides or trace metals into any of the model compartments and may vary in time and space. Interaction between LMM and seabed is limited to the seabed interaction layer. Advection and diffusion determine the horizontal and vertical transport of ^{137}Cs and Al in the water column. It was not included any threshold limit for aluminate (LMM anion).

appears to be an acceptable approximation, at least in periods with high and/or increasing discharges to the water phase, as was the case for ^{99}Tc in the Irish Sea in our simulation period. Although anoxic conditions have been shown to increase the particle-affinity for technetium (*Keith-Roach et al.*, 2003; *Salbu and Holm*, 2005), the sediment-bound fraction in the Irish Sea is still low (*Jenkinson et al.*, 2014), and no effects of sustained remobilization of ^{99}Tc from the seabed are evident in the Irish Sea (*Hunt et al.*, 2013).

For Papers II and III, we implemented a dynamic, stochastic approach for the transformation processes in the TRACMASS model, using transfer rates as described by *Periáñez and Elliott* (2002). Here, a number of radionuclide and Al species with specified properties were defined (Fig 12a and b, respectively). The possible transformation pathways were parameterized by transfer rates, which assign the probability for transformation to each of the other species during a time step. Although the transfer rates are uncertain, they must be parameterized in some way. An approach based on physical and chemical processes should be preferred, however, such an approach will typically introduce another new parameters for which both the parameter and algorithmic uncertainty (categories 3 and 4) may be substantial. Hence, another approach would be to utilize empirical transfer rates based on field measurements or laboratory experiments of elemental kinetics. The applicability of such data depends on how much they are affected by local environmental conditions, or if they can be considered universal. Even though implementation of such new code involves a new set of parameters with their own uncertainty, we concluded that simulations in which speciation is neglected are less accurate, due to systematic errors caused by structural uncertainty (category 5). This is based on the idea that models should ideally be processes based and as similar as possible to the real environment they are representing. And yet, our implementation of the transformation processes depends on a set of algorithms and parameters which are difficult or occasionally not even possible to measure directly (introducing input, parameter and/or algorithmic uncertainty, category 1, 3 and 4).

The radionuclide speciation scheme utilized in Paper II included LMM, particle and sediment species (Fig 12a). The solid forms (particles and sediments) included reversible (compartment 3 and 4) as well as slowly reversible bindings (compartment 5 and 6). The purpose of the slowly reversibly bound species was to represent radionuclides which were chemically strongly or irreversibly bound to the particle sites as well as radionuclides trapped in the deep sediment layers having relatively long residence time, e.g., clay particles. The parameters for the reversible transfer rates were based on literature data (*Periáñez*, 2008). The rates of interactions with the slowly reversibly bound species were also obtained from available literature (*Børretzen and Salbu*, 2002; *Periáñez*, 2004; *Periáñez et al.*, 2013), and testing revealed

relatively high sensitivity to these rates when the discharges were slowly reversibly bound to the particles. As the default values allowed relatively slow remobilization of the slowly reversibly bound radionuclides, an alternative and higher value of the slowly reversible interaction parameter increased the fraction of remobilized LMM species, affecting the transport properties (higher transport away from the sources) and the total exposure of radionuclides (decreased exposure in the fjord system).

The sorption to suspended particles ($k_{13} = K_d D_C m$, can be derived from Eq (2), (3) and (4)) was parameterized by the distribution coefficient K_d, the desorption rate D_C, and the local area of surface available for adsorption. Using a geometric approach, where the particles were assumed to be spherical, the available surface was dependent on an estimate of the mass density of SPM in the water column, denoted by m. Since m in reality is highly variable in time and space, such estimates may introduce considerable uncertainty to the model predictions. In general, the content of SPM is high near river outlets during high flow event and in shallow water during strong winds when seabed sediments are resuspended into the water column due to surface waves. In stratified waters, these suspended particles are often accumulated in thin high turbidity layers. Oppositely, the SPM content is generally low in the open ocean. Aiming to estimate the large scale distribution field of suspended matter, we therefore performed a simulation of particles in advance of the radionuclide simulations, using the same domain and time period as in the radionuclide simulation, and releasing particles from the same 18 rivers. From this simulation, a horizontally smoothed, vertically integrated time average of the particle concentration was computed, with individual values of m in each grid cell. Thus, the small scale temporal and vertical variations were filtered out. However, as these small-scale processes were not expected to be resolved properly by our model, we considered the horizontal variability, being present at larger scales, to be the most important factor to be estimated at the time scales involved in this study.

The sorption to seabed sediments was parameterized as $k_{14} = K_d D_C L \rho (1-p) f \phi \delta / H$, where L is the thickness of the sediment layer interacting with LMM species, ρ is the density of the sediments, p is the porosity, H is the thickness of the deepest water layer interacting with seabed species, f is the fraction of small particles in the sediments and ϕ is a correction factor that takes into account that a fraction of sediment particle surfaces may be unavailable for sorption/desorption interactions due to neighboring sediment particles. The logical variable δ ensures that only the radionuclides in the seabed interaction layer were able to sorb to sediments. We can expect these parameters describing the seabed conditions to vary considerably in nature, but in the model simulations, they were assumed to be uniformly distributed, due to insufficient or non-existing local measurements. Although more advanced sedimentation

models exist and have been applied to radionuclide simulations (e.g., *Aldridge et al.*, 2003; *Maderich et al.*, 2017), the description of the sedimentation and resuspension processes in TRACMASS are relatively simple, and they were not further developed in the present work. The settling velocity of the suspended particles was determined by Stokes' law (*Stokes*, 1851), $w_s = (\rho_s - \rho_w)gd^2/18\nu$ where ρ_s is the particle's density, ρ_w is the density of the water, g is the gravitational acceleration, and ν is the water viscosity, assuming one representative diameter d for all particles. Sedimentation occurred when the particles reached the bottom, and resuspension occurred when the current speed in the deepest model layer exceeded a critical threshold value. This are simplifications of reality, where the environmental properties such as lithology, grain size, porosity and mixing depth can be expected to change both spatially and temporally and affect the sediment distribution. Without local measurements, the parameters used in the present study were taken from available literature data, and were assumed to be uniform in the model domain. Hence, our representation of the seabed involves both parameter and structural uncertainties (categories 3 and 5). A refined description of these properties would improve the model predictions regarding the distribution of the sediment-bound radionuclides, however, obtaining applicable measurements at sufficient detail level would require considerable effort. In addition, we considered the errors associated with the seabed properties to be minor compared to the variability in other factors (such as D_R, D_C and K_d) for which we actually tested the impact.

Combined with increased resolution in the hydrodynamics, a more complex speciation scheme was considered in the estuary case for Al (Paper III), as shown in Fig 12b. This included two LMM species (anions and cations), two colloidal species (humic colloids and polymer) as well as particles and sediments. Bi-, tri- and multivalent elements such as aluminium, iron and manganese are present in several physico-chemical forms, and due to changing environmental conditions, the different forms dominate at variable degree during the transport from the river outlet to the open ocean. It has been shown that the toxicity depends on the speciation, such as the clogging of Al polymers on salmon gills causing increasing mortality (*Teien et al.*, 2006). Therefore, reliable predictions of the spatial and temporal distribution of the species are highly relevant for management purposes. Since the transformation processes are affected by changes in pH and salinity, the most toxic species are only present under certain environmental conditions. Therefore, the model transfer rates should depend on the water chemistry, here expressed by the salinity obtained from the ocean model. Based on observational data of Al, distributed between LMM, colloidal and particle species from River Storelva and Sandnesfjorden, the transfer rates were estimated in a set of salinity intervals, aiming to obtain reasonable specie distributions after short time ($<$ 1 day) of mixing and when equilibrium conditions were assumed to be reached after $\sim$10 days. The different

rates were evaluated and adjusted against each other to obtain reasonable time scales for each process, based on the current understanding of estuarine transfer kinetics obtained from experience from numerous field studies and experimental work (e.g., *Teien et al.*, 2004, 2006). As the results from the model simulation of the Sandnesfjorden estuary generally were in good agreement with the observed concentration levels, we concluded that the applied method was working well in that case. However, as long as these transfer rates were based on locally sampled empirical data, it is difficult to quantify the uncertainties that are introduced by transferring them between different sites. However, technically, the configuration used for Al predictions in Sandnesfjorden can easily be applied to other metals and radionuclides by changing the parameters to suitable values. As mentioned above, in such case, the key issue will be to find parameters applicable for the element and site in question.

6 Conclusions and future perspectives

6.1 Conclusions

Modeling of radionuclides in the marine environment touches a range of different disciplines, such as oceanography, radioecology, biogeochemistry, environmental chemistry and geophysics. Hence, such models may include a wide range of different processes, and to avoid systematic errors and unacceptable mismatch between model and reality, model complexity must be fit for purpose of the case to be investigated. Depending on the purpose of the considered application, the most relevant key processes should ideally be accurately described by the model, while less important processes can be more generally described or even neglected.

According to the objectives of the present work, a model system for marine radionuclide and trace metal transport was established for investigation of a set of three case studies. These cases involved different sites, contaminants and release scenarios, as well as varying spatio-temporal scales, optimized to test each of the three hypotheses.

To investigate the impact of including tides and mesoscale eddies in large-scale radionuclide transport simulations, model estimated activity concentration levels of Sellafield-discharged ^{99}Tc radionuclides were compared with open ocean observations, as well as with time series from coastal stations (Paper I). The model-observation comparisons showed that by increasing the horizontal resolution from $\sim$14 km to 4 km, the model skill was improved due to better resolution of mesoscale eddies and thus being less reliant on parameterization of sub-grid scale turbulent eddy fluxes. Thus, hypothesis H1 (p. 3) could not be refuted. However, with well-tuned parameterization of eddy diffusivity, the coarse scale model was also able to provide acceptable results. By including tidal components in the flow field, the outflow from the Irish Sea, as well as the downstream activity concentration levels in more remote areas were affected by the high-frequent tidal fluctuations, and the model results showed better agreement with observations. Therefore, to avoid systematic errors due to sub-grid scale fluxes also in long-term simulations, model resolution should ideally be high enough to explicitly resolve mesoscale eddies and tidal flow.

Aiming for a more physical consistent description and to reduce the structural uncertainties, code for element speciation and transformation processes was developed and implemented. The model complexity increased progressively through the present work. Speciation and transformation processes involving LMM, suspended particles and sediment species were implemented in the case study of ^{137}Cs (Paper II), while the system was extended with colloidal species responding to environmental changes in the case of estuarine transport of Al

(Paper III).

The effects of including interactions with seabed species were found to be considerable, affecting the results with orders of magnitude, even for ^{137}Cs (Paper II), for which particle- and sediment interactions commonly have been neglected in previous model studies. Thus, hypothesis H2 (p. 4) could not be refuted. Using the default set of parameters, the main response in the estimated activity concentration fields was increased sorption to seabed sediments. Hence, at intermediate temporal scales, from several months to years, the solid species should not be ignored, also for the relatively easily soluble elements. Important factors affecting the radionuclide exposure of the fjord system were found to be sorption coefficients, speciation in the discharges and particle size distribution. These factors were found to affect the affinity to suspended matter in the water column considerably, subsequently affecting the vertical settling and sedimentation and eventually increasing the activity concentration with up to a factor 10. Thus, for these factors, the parameterization schemes need to be carefully considered.

Since the toxicity and potential biological effects of Al are largely dependent on the speciation, proper predictions of the specie distribution are of major concern for environmental impact assessments. In the case of estuarine transport of river-discharged Al (Paper III), the transfer rates, controlling the transformation processes of Al species, were calibrated for changing environmental conditions to fit the observed behavior of Al species. The model results showed good agreement with available fractionated observational data, and despite some relatively large uncertainties related to background concentration levels and mixing in the surface layers, the general patterns of the observed concentration levels were well reproduced by the model. Hence, hypothesis H3 (p. 4) could not be refuted.

6.2 Future perspectives

In the model system utilized in the present study, the input variables and parameters related to element speciation and transformation of species are characterized by large uncertainties, especially the transfer rates. Being based on relatively uncertain or limited site-specific data, there are still knowledge gaps associated with the transformation parameters which need to be filled. So far, it appeared to be difficult to develop generic expressions for transfer rates that can be utilized in other similar scenarios. Therefore, for further improvement of the model system, field sampling campaigns aiming to achieve parameters optimized for modeling purposes are needed. A comprehensive database containing recommended transfer rates would be useful. These rates should ideally be element-specific and based on measurements

taken under changing environmental conditions. For modeling purposes, using dynamic approaches, measurements of the rates of the transformations are more useful than total concentration levels and distribution coefficients. These are, however, valuable for evaluation of the integrated effects on the model system and for parameter calibration. Hence, ideally, controlled measurements of the time evolution of each isolated process should be performed. Since factors such as salinity, particle size and surface area available for sorption are known to affect the speciation, experiments should ideally be repeated over a broad range of environmental conditions.

For preparedness in time-critical circumstances, such as in a nuclear accident, model systems predicting pathways and concentration levels for radioactive contaminants should be operationally available for rapid response. For best possible predictions, speciation and transformation processes should preferably be included in such models. Considerations of the conclusions from the present work will therefore be useful when deciding the level of complexity in the development of preparedness models.

As the impact of radionuclide contamination on man and the environment may depend on the radionuclide speciation, high resolution models providing detailed and reliable predictions of specie distributions will be superior compared to present model systems. Output from such models should therefore feed into future decision support systems for dose assessments within radioecology.

References

Abril, J., and E. Fraga (1996), Some physical and chemical features of the variability of k(d) distribution coefficients for radionuclides, *Journal of Environmental Radioactivity*, *30*(3), 253–270, doi:10.1016/0265-931X(95)00010-8.

Aldridge, J., P. Kershaw, J. Brown, D. McCubbin, K. Leonard, and E. Young (2003), Transport of plutonium (239/240Pu) and caesium (137Cs) in the Irish Sea: comparison between observations and results from sediment and contaminant transport modelling, *Continental Shelf Research*, *23*(9), 869 – 899, doi:http://dx.doi.org/10.1016/S0278-4343(03)00047-5.

AMAP (2004), AMAP Assessment 2002. Radioactivity in the Arctic, *Arctic Monitoring and Assessment Programme. Oslo. Norway.*

AMAP (2016), AMAP Assessment 2015: Radioactivity in the Arctic, *Tech. rep.*, Arctic Monitoring and Assessment Programme (AMAP), Oslo, Norway.

Aoyama, M., M. Kajino, T. Y. Tanaka, T. T. Sekiyama, D. Tsumune, T. Tsubono, Y. Hamajima, Y. Inomata, and T. Gamo (2016), 134Cs and 137Cs in the North Pacific Ocean derived from the March 2011 TEPCO Fukushima Dai-ichi Nuclear Power Plant accident, Japan. Part two: estimation of 134Cs and 137Cs inventories in the North Pacific Ocean, *Journal of Oceanography*, *72*(1), 67–76, doi:10.1007/s10872-015-0332-2.

Betti, M., L. A. de las Heras, A. Janssens, E. Henrich, G. Hunter, M. Gerchikov, M. Dutton, A. van Weers, S. Nielsen, J. Simmonds, A. Bexon, and T. Sazykina (2004), Results of the European Commission Marina II Study Part II—effects of discharges of naturally occurring radioactive material, *Journal of Environmental Radioactivity*, *74*(1), 255 – 277, doi:10.1016/j.jenvrad.2004.01.021.

Blockley, E. W., M. J. Martin, A. J. McLaren, A. G. Ryan, J. Waters, D. J. Lea, I. Mirouze, K. A. Peterson, A. Sellar, and D. Storkey (2014), Recent development of the Met Office operational ocean forecasting system: an overview and assessment of the new Global FOAM forecasts, *Geoscientific Model Development*, *7*(6), 2613–2638, doi:10.5194/gmd-7-2613-2014.

Blumsack, S. L., and P. J. Gierasch (1972), Mars: The effects of topography on baroclinic instability, *Journal of the Atmospheric Sciences*, *29*, 1081–1089, doi:http://dx.doi.org/10.1175/1520-0469(1972)029<1081:MTEOTO>2.0.CO;2.

Bogen, J., and T. Bønsnes (2004), Sedimenttransport og substratforhold i Suldalslågen, sluttrapport, 1998-2003, *Suldalslågen - miljørapport nr 39*, Norges vassdrags- og energidirektorat.

Brown, J., M. Iospje, K. Kolstad, B. Lind, A. Rudjord, and P. Strand (2002), Temporal trends for 99Tc in Norwegian coastal environments and spatial distribution in the Barents Sea,

Journal of Environmental Radioactivity, *60*(1–2), 49 – 60, doi:http://dx.doi.org/10.1016/S0265-931X(01)00095-9.

Børretzen, P., and B. Salbu (2000), Estimation of apparent rate coefficients for radionuclides interacting with marine sediments from Novaya Zemlya, *Science of The Total Environment*, *262*(1), 91 – 102, doi:https://doi.org/10.1016/S0048-9697(00)00575-1.

Børretzen, P., and B. Salbu (2002), Fixation of Cs to marine sediments estimated by a stochastic modelling approach, *Journal of Environmental Radioactivity*, *61*(1), 1 – 20, doi:https://doi.org/10.1016/S0265-931X(01)00107-2.

Børretzen, P., and B. Salbu (2009), Bioavailability of sediment-associated and low-molecular-mass species of radionuclides/trace metals to the mussel Mytilus edulis, *Journal of Environmental Radioactivity*, *100*(4), 333 – 341, doi:10.1016/j.jenvrad.2008.12.020.

Caffrey, E., M. Leonard, J. Napier, D. Neville, and K. Higley (2014), Radioecology: Why bother?, *Journal of Environmental Protection*, *5*, 181–192, doi:10.4236/jep.2014.53022.

Carvalho, F. P. (2018), Radionuclide concentration processes in marine organisms: A comprehensive review, *Journal of Environmental Radioactivity*, *186*, 124 – 130, doi:10.1016/j.jenvrad.2017.11.002.

Casacuberta, N., M. Christl, C. Vockenhuber, A.-M. Wefing, L. Wacker, P. Masqué, H.-A. Synal, and M. Rutgers van der Loeff (2018), Tracing the Three Atlantic Branches Entering the Arctic Ocean With 129I and 236U, *Journal of Geophysical Research: Oceans*, *123*(9), 6909–6921, doi:10.1029/2018JC014168.

Christensen, K. H., Øyvind Breivik, K.-F. Dagestad, J. Röhrs, and B. Ward (2018), Short-term predictions of oceanic drift, *Oceanography*, *31*, doi:doi.org/10.5670/oceanog.2018.310.

Corell, H., and K. Döös (2013), Difference in particle transport between two coastal areas in the Baltic Sea investigated with high-resolution trajectory modeling, *Ambio*, *42*(4), 455–463, doi:10.1007/s13280-013-0397-3.

Dahlgaard, H. (1995), Transfer of European coastal pollution to the arctic: Radioactive tracers, *Marine Pollution Bulletin*, *31*(1), 3 – 7, doi:10.1016/0025-326X(95)00003-6.

Dahlgaard, H., Q. Chen, J. Herrmann, H. Nies, R. Ibbett, and P. Kershaw (1995), On the background level of 99Tc, 90Sr and 137Cs in the North Atlantic, *Journal of Marine Systems*, *6*(5–6), 571 – 578, doi:http://dx.doi.org/10.1016/0924-7963(95)00025-K.

Dowdall, M., S. Gerland, M. Karcher, J. P. Gwynn, A. L. Rudjord, and A. K. Kolstad (2005), Optimisation of sampling for the temporal monitoring of technetium-99 in the Arctic marine environment, *Journal of Environmental Radioactivity*, *84*(1), 111 – 130, doi:https://doi.org/10.1016/j.jenvrad.2005.04.010.

Duffa, C., P. B. du Bois, M. Caillaud, S. Charmasson, C. Couvez, D. Didier, F. Dumas, B. Fievet, M. Morillon, P. Renaud, and H. Thébault (2016), Development of emergency response tools for accidental radiological contamination of French coastal areas, *Journal of Environmental Radioactivity*, *151*, 487 – 494, doi:10.1016/j.jenvrad.2015.04.019.

Döös, K., and A. Engqvist (2007), Assessment of water exchange between a discharge region and the open sea – A comparison of different methodological concepts, *Estuarine, Coastal and Shelf Science*, *74*(4), 709 – 721, doi:10.1016/j.ecss.2007.05.022.

Döös, K., V. Rupolo, and L. Brodeau (2011), Dispersion of surface drifters and model-simulated trajectories, *Ocean Modelling*, *39*(3–4), 301 – 310, doi:10.1016/j.ocemod.2011.05.005.

Döös, K., B. Jönsson, and J. Kjellsson (2017), Evaluation of oceanic and atmospheric trajectory schemes in the TRACMASS trajectory model v6.0, *Geoscientific Model Development*, *10*(4), 1733–1749, doi:10.5194/gmd-10-1733-2017.

Eyrolle, F., and S. Charmasson (2004), Importance of colloids in the transport within the dissolved phase (< 450 nm) of artificial radionuclides from the Rhône river towards the Gulf of Lions (Mediterranean Sea), *Journal of Environmental Radioactivity*, *72*(3), 273 – 286, doi:https://doi.org/10.1016/S0265-931X(03)00178-4.

Goshawk, J., S. Clarke, C. Smith, and P. McDonald (2003), MEAD (part I)—a mathematical model of the long-term dispersion of radioactivity in shelf sea environments, *Journal of Environmental Radioactivity*, *68*(2), 115 – 135, doi:10.1016/S0265-931X(03)00040-7.

Griffies, S. (2004), *Fundamentals of ocean climate models*, Princeton university press, ISBN:9780691118925.

Gwynn, J. P., H. E. Heldal, J. K. Flo, I. Sværen, T. Gäfvert, H. Haanes, L. Føyn, and A. L. Rudjord (2018), Norwegian monitoring (1990–2015) of the marine environment around the sunken nuclear submarine Komsomolets, *Journal of Environmental Radioactivity*, *182*, 52 – 62, doi:10.1016/j.jenvrad.2017.11.015.

Herrmann, J., P. Kershaw, P. du Bois, and P. Guegueniat (1995), The distribution of artificial radionuclides in the English Channel, southern North Sea, Skagerrak and Kattegat, 1990–1993, *Journal of Marine Systems*, *6*(5), 427 – 456, doi:https://doi.org/10.1016/0924-7963(95)00026-L.

Hosseini, A., J. E. Brown, J. P. Gwynn, and M. Dowdall (2012), Review of research on impacts to biota of discharges of naturally occurring radionuclides in produced water to the marine environment, *Science of The Total Environment*, *438*, 325 – 333, doi:10.1016/j.scitotenv.2012.08.047.

Hunt, J., K. Leonard, and L. Hughes (2013), Artificial radionuclides in the Irish Sea from Sellafield: remobilisation revisited, *Journal of Radiological Protection*, *33*(2), 261, doi:10.1088/0952-4746/33/2/261.

IAEA (2004), *Sediment Distribution Coefficients and Concentration Factors for Biota in the Marine Environment*, Technical report series, No. 422, International Atomic Energy Agency.

IAEA (2010), *Handbook of parameter values for the prediction of radionuclide transfer in terrestrial and freshwater environments*, Technical report series, No. 472, International Atomic Energy Agency.

IAEA (2015), *Inventory of Radioactive Material Resulting from Historical Dumping, Accidents and Losses at Sea - IAEA-Tecdoc-1776*, Technical report series, No. 1776, International Atomic Energy Agency.

Iosjpe, M., J. Brown, and P. Strand (2002), Modified approach to modelling radiological consequences from releases into the marine environment, *Journal of Environmental Radioactivity*, *60*(1), 91 – 103, doi:10.1016/S0265-931X(01)00098-4.

Isachsen, P. E. (2015), Baroclinic instability and the mesoscale eddy field around the Lofoten Basin, *J. Geophy. Res. Oceans*, *120*, doi:10.1002/2014JC010448.

Isachsen, P. E., and O. A. Nøst (2012), The air-sea transformation and residual overturning circulation within the Nordic Seas, *J. Mar. Res.*, *70*, 31–68.

Janjić, T., N. Bormann, M. Bocquet, J. A. Carton, S. E. Cohn, S. L. Dance, S. N. Losa, N. K. Nichols, R. Potthast, J. A. Waller, and P. Weston (2018), On the representation error in data assimilation, *Quarterly Journal of the Royal Meteorological Society*, *144*(713), 1257–1278, doi:10.1002/qj.3130.

Jenkinson, S. B., D. McCubbin, P. H. Kennedy, A. Dewar, R. Bonfield, and K. S. Leonard (2014), An estimate of the inventory of technetium-99 in the sub-tidal sediments of the Irish Sea, *Journal of Environmental Radioactivity*, *133*(0), 40 – 47, doi:http://dx.doi.org/10.1016/j.jenvrad.2013.05.004.

Jensen, L. K., V. Shpinkov, H. E. Heldal, J. P. Gwynn, B. Møller, V. Bulgakov, M. Katkova, and G. Artemyev (2017), 10 years of joint monitoring of radioactive substances in the Barents Sea, 2006-2015, https://www.dsa.no/publikasjon/10-years-of-joint-monitoring-of-radioactive-substances-in-the-barents-sea.pdf.

Jönsson, B. F., K. Döös, K. Myrberg, and P. A. Lundberg (2011), A Lagrangian-trajectory study of a gradually mixed estuary, *Continental Shelf Research*, *31*(17), 1811 – 1817, doi:10.1016/j.csr.2011.07.007.

Karcher, M., J. N. Smith, F. Kauker, R. Gerdes, and W. M. Smethie Jr. (2012), Recent changes in Arctic Ocean circulation revealed by iodine-129 observations and modeling, *Journal of Geophysical Research: Oceans*, *117*(C8), doi:10.1029/2011JC007513.

Karcher, M. J., S. Gerland, I. H. Harms, M. Iosjpe, H. E. Heldal, P. J. Kershaw, and M. Sickel (2004), The dispersion of 99Tc in the Nordic Seas and the Arctic Ocean: a comparison of model results and observations, *Journal of Environmental Radioactivity*, *74*(1–3), 185 – 198, doi:10.1016/j.jenvrad.2004.01.026.

Kauker, F., T. Kaminski, M. Karcher, M. Dowdall, J. Brown, A. Hosseini, and P. Strand (2016), Model analysis of worst place scenarios for nuclear accidents in the northern marine environment, *Environmental Modelling & Software*, *77*, 13 – 18, doi:10.1016/j.envsoft.2015.11.021.

Keith-Roach, M. J., K. Morris, and H. Dahlgaard (2003), An investigation into technetium binding in sediments, *Marine Chemistry*, *81*(3–4), 149 – 162, doi:http://dx.doi.org/10.1016/S0304-4203(03)00014-8.

Kersting, A. B., D. W. Efurd, D. L. Finnegan, D. J. Rokop, D. K. Smith, and J. L. Thompson (1999), Migration of plutonium in ground water at the Nevada Test Site, *Nature*, *397*, 56–59, doi:http://dx.doi.org/10.1038/16231.

Kjellsson, J., and K. Döös (2012), Surface drifters and model trajectories in the Baltic Sea, *Boreal Environment Research*, *17*(6), 447–459.

Klein, H., and J. Bartnicki (2018), Worst case meteorological scenario for Norway in case of an accident in Sellafield Nuclear Site, in *Air Pollution Modeling and its Application XXV*, edited by C. Mensink and G. Kallos, pp. 457–462, Springer International Publishing, Cham.

Kobayashi, T., M. Chino, and O. Togawa (2006), Numerical simulations of short-term migration processes of dissolved cesium-137 due to a hypothetical accident of a nuclear submarine in the Japan Sea, *Journal of Nuclear Science and Technology*, *43*(5), 569–575, doi:10.1080/18811248.2006.9711135.

Kobayashi, T., H. Nagai, M. Chino, and H. Kawamura (2013), Source term estimation of atmospheric release due to the Fukushima Dai-ichi Nuclear Power Plant accident by atmospheric and oceanic dispersion simulations, *Journal of Nuclear Science and Technology*, *50*(3), 255–264, doi:10.1080/00223131.2013.772449.

Leonard, K. S., D. McCubbin, P. McDonald, M. Service, R. Bonfield, and S. Conney (2004), Accumulation of technetium-99 in the Irish Sea?, *Science of The Total Environment*, *322*(1–3), 255 – 270, doi:http://dx.doi.org/10.1016/j.scitotenv.2003.09.023.

Lin, Y., R.-M. Couture, H. Klein, M. A. Ytre-Eide, J. E. Dyve, O. C. Lind, J. Bartnicki, L. Nizzetto, D. Butterfield, T. Larssen, and B. Salbu (In press), Modelling Environmental Impacts of Cesium-137 under a Hypothetical Release of Radioactive Waste, *Accepted by Bulletin of Environmental Contamination and Toxicology*.

Lind, O. C., D. H. Oughton, B. Salbu, L. Skipperud, M. A. Sickel, J. E. Brown, L. K. Fifield, and S. G. Tims (2006), Transport of low 240Pu/239Pu atom ratio plutonium-species in the Ob and Yenisey Rivers to the Kara Sea, *Earth and Planetary Science Letters*, *251*(1), 33 – 43, doi:https://doi.org/10.1016/j.epsl.2006.08.023.

Lydersen, E., B. Salbu, A. B. Poleo, and W. P. Muniz (1990), The influences of temperature on aqueous aluminium chemistry, *Water, Air, and Soil Pollution*, *51*(3-4), 203–215.

Lydersen, E., B. Salbu, and A. B. S. Polèo (1992), Size and charge fractionation of aqueous aluminium in dilute acidic waters: effects of changes in pH and temperature, *Analyst*, *117*, 613–617, doi:10.1039/AN9921700613.

Machado, A. A. d. S., K. Spencer, W. Kloas, M. Toffolon, and C. Zarfl (2016), Metal fate and effects in estuaries: A review and conceptual model for better understanding of toxicity, *Science of The Total Environment*, *541*, 268 – 281, doi:https://doi.org/10.1016/j.scitotenv.2015.09.045.

Maderich, V., K. T. Jung, I. Brovchenko, and K. O. Kim (2017), Migration of radioactivity in multi-fraction sediments, *Environmental Fluid Mechanics*, *17*(6), 1207–1231, doi:10.1007/s10652-017-9545-9.

Margvelashvily, N., V. Maderich, and M. Zheleznyak (1997), THREETOX - A computer code to simulate three-dimensional dispersion of radionuclides in stratified water bodies, *Radiation Protection Dosimetry*, *73*(1-4), 177–180, doi:10.1093/oxfordjournals.rpd.a032128.

McCubbin, D., K. S. Leonard, P. McDonald, R. Bonfield, and D. Boust (2006), Distribution of Technetium-99 in sub-tidal sediments of the Irish Sea, *Continental Shelf Research*, *26*(4), 458 – 473, doi:http://dx.doi.org/10.1016/j.csr.2005.12.010.

McKay, W., and N. Pattenden (1993), The behaviour of plutonium and americium in the shoreline waters of the Irish Sea: A review of Harwell studies in the 1990s, *Journal of Environmental Radioactivity*, *18*(2), 99 – 132, doi:10.1016/0265-931X(93)90075-I.

Mitchell, P., O. Condren, L. Vintró, and C. McMahon (1999), Trends in plutonium, americium and radiocaesium accumulation and long-term bioavailability in the western Irish Sea mud basin, *Journal of Environmental Radioactivity*, *44*(2–3), 223 – 251, doi:http://dx.doi.org/10.1016/S0265-931X(98)00135-0.

Nilsson, J. A. U., K. Döös, P. M. Ruti, V. Artale, A. Coward, and L. Brodeau (2013), Observed and modeled global ocean turbulence regimes as deduced from surface trajectory data, *Journal of Physical Oceanography*, *43*(11), 2249–2269, doi:10.1175/JPO-D-12-0193.1.

Novikov, A. P., S. N. Kalmykov, S. Utsunomiya, R. C. Ewing, F. Horreard, A. Merkulov, S. B. Clark, V. V. Tkachev, and B. F. Myasoedov (2006), Colloid transport of Plutonium in the Far-Field of the Mayak Production Association, Russia, *Science*, *314*(5799), 638–641, doi:10.1126/science.1131307.

NRPA (2004), Natural Radioactivity in Produced Water from the Norwegian Oil and Gas Industry in 2003, *Tech. Rep. StrålevernRapport 2005:2*, Østerås: Norwegian Radiation Protection Authority.

Olszewski, G., P. Andersson, P. Lindahl, and M. Eriksson (2018), On the distribution and inventories of radionuclides in dated sediments around the Swedish coast, *Journal of Environmental Radioactivity*, *186*, 142 – 151, doi:10.1016/j.jenvrad.2017.09.025.

Orre, S. (2008), Circulation features in the northern North Atlantic Ocean inferred from simulated radioactive tracers, Dissertation for the Degree of Philosophiae Doctor (PhD), Geophysical Institute, University of Bergen.

Orre, S., Y. Gao, H. Drange, and J. E. O. Nilsen (2007), A reassessment of the dispersion properties of 99Tc in the North Sea and the Norwegian Sea, *Journal of Marine Systems*, *68*(1–2), 24 – 38, doi:http://dx.doi.org/10.1016/j.jmarsys.2006.10.009.

Orre, S., Y. Gao, H. Drange, and E. Deleersnijder (2008), Diagnosing ocean tracer transport from Sellafield and Dounreay by equivalent diffusion and age, *Advances in Atmospheric Sciences*, *25*(5), 805–814, doi:10.1007/s00376-008-0805-y.

Orre, S., J. N. Smith, V. Alfimov, and M. Bentsen (2010), Simulating transport of 129I and idealized tracers in the northern North Atlantic Ocean, *Environmental Fluid Mechanics*, *10*(1), 213–233, doi:10.1007/s10652-009-9138-3.

OSPAR (2018), Liquid Discharges from Nuclear Installations in 2016, *Tech. Rep. 720/2018*, OSPAR Commission, London, Radioactive Substances Series.

Periáñez, R. (2004), Testing the behaviour of different kinetic models for uptake/release of radionuclides between water and sediments when implemented in a marine dispersion model, *Journal of Environmental Radioactivity*, *71*(3), 243 – 259, doi:10.1016/S0265-931X(03)00172-3.

Periáñez, R. (2005), *Modelling the Dispersion of Radionuclides in the Marine Environment*, Springer Verlag Berlin Heidelberg, ISBN:978-3-540-24875-0.

Periáñez, R. (2008), A modelling study on 137Cs and 239,240Pu behaviour in the Alborán Sea, western Mediterranean, *Journal of Environmental Radioactivity*, *99*(4), 694 – 715, doi:http://dx.doi.org/10.1016/j.jenvrad.2007.09.011.

Periáñez, R., and A. Elliott (2002), A particle-tracking method for simulating the dispersion of non-conservative radionuclides in coastal waters, *Journal of Environmental Radioactivity*, *58*(1), 13 – 33, doi:http://dx.doi.org/10.1016/S0265-931X(01)00028-5.

Periáñez, R., J. Abril, and M. García-Léon (1996), Modelling the dispersion of non-conservative radionuclides in tidal waters—Part 1: Conceptual and mathematical model, *Journal of Environmental Radioactivity*, *31*(2), 127 – 141, doi:https://doi.org/10.1016/0265-931X(95)00050-K.

Periáñez, R., A. Hierro, J. P. Bolívar, and F. Vaca (2013), The geochemical behavior of natural radionuclides in coastal waters: A modeling study for the Huelva estuary, *Journal of Marine Systems*, *126*(Supplement C), 82 – 93, doi:https://doi.org/10.1016/j.jmarsys.2012.08.001.

Periáñez, R., R. Bezhenar, I. Brovchenko, C. Duffa, M. Iosjpe, K. Jung, T. Kobayashi, F. Lamego, V. Maderich, B. Min, H. Nies, I. Osvath, I. Outola, M. Psaltaki, K. Suh, and G. de With (2016a), Modelling of marine radionuclide dispersion in IAEA MODARIA program: Lessons learnt from the Baltic Sea and Fukushima scenarios, *Science of The Total Environment*, *569-570*(Supplement C), 594 – 602, doi:https://doi.org/10.1016/j.scitotenv.2016.06.131.

Periáñez, R., K.-S. Suh, and B.-I. Min (2016b), The behaviour of 137Cs in the North Atlantic Ocean assessed from numerical modelling: Releases from nuclear fuel reprocessing factories, redissolution from contaminated sediments and leakage from dumped nuclear wastes, *Marine Pollution Bulletin*, *113*(1), 343 – 361, doi:http://dx.doi.org/10.1016/j.marpolbul.2016.10.021.

Periáñez, R., I. Brovchenko, K. Jung, K. Kim, and V. Maderich (2018), The marine kd and water/sediment interaction problem, *Journal of Environmental Radioactivity*, *192*, 635 – 647, doi:https://doi.org/10.1016/j.jenvrad.2018.02.014.

Povinec, P., L. L. W. Kwong, J. Kaizer, M. Molnár, H. Nies, L. Palcsu, L. Papp, M. Pham, and P. Jean-Baptiste (2017), Impact of the Fukushima accident on tritium, radiocarbon and radiocesium levels in seawater of the western North Pacific Ocean: A comparison with pre-Fukushima situation, *Journal of Environmental Radioactivity*, *166*, 56 – 66, doi: https://doi.org/10.1016/j.jenvrad.2016.02.027.

Povinec, P. P., P. B. du Bois, P. J. Kershaw, H. Nies, and P. Scotto (2003), Temporal and spatial trends in the distribution of 137Cs in surface waters of Northern European Seas — a record of 40 years of investigations, *Deep Sea Research Part II: Topical Studies in Oceanography*, *50*(17–21), 2785 – 2801, doi:http://dx.doi.org/10.1016/S0967-0645(03)00148-6, worldwide Marine Radioactivity Studies (WOMARS).

Prandle, D., and H. Charnock (1984), A modelling study of the mixing of 137Cs in the seas of the European Continental Shelf, *Philosophical Transactions of the Royal Society of London. Series A, Mathematical and Physical Sciences*, *310*(1513), 407–436, doi: 10.1098/rsta.1984.0002.

Raskob, W., T. Almahayni, and N. A. Beresford (2018), Radioecology in CONFIDENCE: Dealing with uncertainties relevant for decision making, *Journal of Environmental Radioactivity*, *192*, 399 – 404, doi:10.1016/j.jenvrad.2018.07.017.

RIFE (2013), Radioactivity in Food and the Environment, 2012, RIFE-18, *Tech. rep.*, Environment Agency.

Rosseland, B., I. Blakar, A. Bulger, F. Kroglund, A. Kvellstad, E. Lydersen, D. Oughton, B. Salbu, M. Staurnes, and R. Vogt (1992), The mixing zone between limed and acidic river waters: Complex aluminium chemistry and extreme toxicity for salmonids, *Environmental Pollution*, *78*(1), 3 – 8, doi:https://doi.org/10.1016/0269-7491(92)90003-S.

RPII (2012), Radioactivity Monitoring of the Irish Environment 2010-2011, *Tech. rep.*, Radiological Protection Institute of Ireland.

Røed, L. P., V. S. Lien, A. Melsom, N. M. Kristensen, Y. Gusdal, B. Ådlandsvik, and J. Albretsen (2015), BaSIC Technical Report 4. Part I: Evaluation of the BaSIC4 long term hindcast results, *Tech. Rep. 5/2015*, Norwegian Meteorological Institute Oslo.

Salbu, B. (2000), Speciation of Radionuclides in the Environment, in *Encyclopedia of Analytical Chemistry*, edited by R. A. Meyers, pp. 12,993–13,016, John Wiley & Sons Ltd, Chichester, doi:10.1002/9780470027318.a6308.

Salbu, B. (2009), Fractionation of radionuclide species in the environment, *Journal of Environmental Radioactivity*, *100*(4), 283 – 289, doi:https://doi.org/10.1016/j.jenvrad.2008.12.013.

Salbu, B. (2016), Environmental impact and risk assessments and key factors contributing to the overall uncertainties, *Journal of Environmental Radioactivity*, *151*, 352 – 360, doi: 10.1016/j.jenvrad.2015.09.001.

Salbu, B., and E. Holm (2005), RADIOCHEMICAL METHODS | Technetium, in *Encyclopedia of Analytical Science (Second Edition)*, edited by P. Worsfold, A. Townshend, and C. Poole, second edition ed., pp. 24 – 32, Elsevier, Oxford, doi:10.1016/B0-12-369397-7/00519-7.

Salbu, B., H. Bjørnstad, I. Svaren, S. Prosser, R. Bulman, B. Harvey, and M. Lovett (1993), Size distribution of radionuclides in nuclear fuel reprocessing liquids after mixing with seawater, *Science of The Total Environment*, *130–131*, 51 – 63, doi:10.1016/0048-9697(93)90059-F.

Salbu, B., A. Nikitin, P. Strand, G. Christensen, V. Chumichev, B. Lind, H. Fjelldal, T. Bergan, A. Rudjord, M. Sickel, N. Valetova, and L. Føyn (1997), Radioactive contamination from dumped nuclear waste in the Kara Sea — results from the joint Russian-Norwegian expeditions in 1992–1994, *Science of The Total Environment*, *202*(1), 185 – 198, doi:10.1016/S0048-9697(97)00115-0.

Salbu, B., L. Skipperud, P. Germain, P. Guéguéniat, P. Strand, O. Lind, and G. Christensen (2003), Radionuclide speciation in effluent from La Hague reprocessing plant in France, *Health Physics*, *85*(3), 311–322, doi:10.1097/00004032-200309000-00007.

Sandvik, A. D., Øystein Skagseth, and M. D. Skogen (2016), Model validation: Issues regarding comparisons of point measurements and high-resolution modeling results, *Ocean Modelling*, *106*, 68 – 73, doi:https://doi.org/10.1016/j.ocemod.2016.09.007.

Sanial, V., K. O. Buesseler, M. A. Charette, and S. Nagao (2017), Unexpected source of Fukushima-derived radiocesium to the coastal ocean of Japan, *Proceedings of the National Academy of Sciences*, *114*(42), 11,092–11,096, doi:10.1073/pnas.1708659114.

Sañudo-Wilhelmy, S. A., I. Rivera-Duarte, and A. R. Flegal (1996), Distribution of colloidal trace metals in the San Francisco Bay estuary, *Geochimica et Cosmochimica Acta*, *60*(24), 4933 – 4944.

Shchepetkin, A. F., and J. C. McWilliams (2005), The regional oceanic modeling system (ROMS): a split-explicit, free-surface, topography-following-coordinate oceanic model, *Ocean Modelling*, *9*(4), 347 – 404, doi:https://doi.org/10.1016/j.ocemod.2004.08.002.

Simonsen, M., Øyvind Saetra, P. E. Isachsen, O. C. Lind, H. K. Skjerdal, B. Salbu, H. E. Heldal, and J. P. Gwynn (2017), The impact of tidal and mesoscale eddy advection on the long term dispersion of 99Tc from Sellafield, *Journal of Environmental Radioactivity*, *177*, 100 – 112, doi:https://doi.org/10.1016/j.jenvrad.2017.06.002.

Skipperud, L., D. H. Oughton, and B. Salbu (2000), The impact of plutonium speciation on the distribution coefficients in a sediment-sea water system, and radiological assessment of doses to humans, *Health Physics*, *79*(2), 174–153.

Skjerdal, H., T. Gäfvert, H. E. Heldal, J. Gwynn, E. Strålberg, I. Sværen, P. L. Liebig, A. K. Kolstad, B. Møller, M. Komperød, B. Lind, and A. L. Rudjord (2015), Radioactivity in the marine environment 2011. Results from the Norwegian National Monitoring Programme (RAME), *Tech. Rep. StrålevernRapport2015:3*, Statens Straalevern.

Stokes, G. G. (1851), On the Effect of the Internal Friction of Fluids on the Motion of Pendulums, *Transactions of the Cambridge Philosophical Society*, *9*, 8.

Teien, H. C., B. Salbu, F. Kroglund, and B. O. Rosseland (2004), Transformation of positively charged aluminium-species in unstable mixing zones following liming, *Science of The Total Environment*, *330*(1), 217 – 232, doi:https://doi.org/10.1016/j.scitotenv.2004.03.040.

Teien, H.-C., W. J. Standring, and B. Salbu (2006), Mobilization of river transported colloidal aluminium upon mixing with seawater and subsequent deposition in fish gills, *Science of The Total Environment*, *364*(1), 149 – 164, doi:https://doi.org/10.1016/j.scitotenv.2006.01.005.

Tsumune, D., T. Tsubono, M. Aoyama, M. Uematsu, K. Misumi, Y. Maeda, Y. Yoshida, and H. Hayami (2013), One-year, regional-scale simulation of ^{137}Cs radioactivity in the ocean following the Fukushima Dai-ichi Nuclear Power Plant accident, *Biogeosciences*, *10*(8), 5601–5617, doi:10.5194/bg-10-5601-2013.

UNSCEAR (2000), *Sources and effects of ionizing radiation: sources*, vol. 1, United Nations Publications, United Nations. Scientific Committee on the Effects of Atomic Radiation.

Viikmäe, B., T. Torsvik, and T. Soomere (2013), Impact of horizontal eddy diffusivity on Lagrangian statistics for coastal pollution from a major marine fairway, *Ocean Dynamics*, *63*(5), 589–597, doi:10.1007/s10236-013-0615-3.

Vives i Batlle, J., M. Aoyama, C. Bradshaw, J. Brown, K. Buesseler, N. Casacuberta, M. Christl, C. Duffa, N. Impens, M. Iosjpe, P. Masqué, and J. Nishikawa (2018), Marine radioecology after the Fukushima Dai-ichi nuclear accident: Are we better positioned to understand the impact of radionuclides in marine ecosystems?, *Science of The Total Environment*, *618*(Supplement C), 80 – 92, doi:https://doi.org/10.1016/j.scitotenv.2017.11.005.

Wilkin, J. L., H. G. Arango, D. B. Haidvogel, C. S. Lichtenwalner, S. M. Glenn, and K. S. Hedström (2005), A regional ocean modeling system for the Long-term Ecosystem Observatory, *Journal of Geophysical Research: Oceans*, *110*(C6), doi:10.1029/2003JC002218.

Wright, S., B. Howard, P. Strand, T. Nylén, and M. Sickel (1999), Prediction of 137Cs deposition from atmospheric nuclear weapons tests within the Arctic, *Environmental Pollution*, *104*(1), 131 – 143, doi:10.1016/S0269-7491(98)00140-7.

Ytre-Eide, M. A., W. J. Standring, I. Amundsen, M. Sickel, A. Liland, J. Saltbones, J. Bartnicki, H. Haakenstad, and B. Salbu (2009), Consequences in Norway of a hypothetical accident at Sellafield: Potential release–transport and fallout, *Tech. Rep. StrålevernRapport2009:7*, Statens Straalevern.

Zilitinkevich, S. S., T. Elperin, N. Kleeorin, and I. Rogachevskii (2007), Energy- and flux-budget (EFB) turbulence closure model for stably stratified flows. Part I: steady-state, homogeneous regimes, *Boundary-Layer Meteorology*, *125*(2), 167–191, doi:10.1007/s10546-007-9189-2.

7 Scientific papers

Paper I

Journal of Environmental Radioactivity 177 (2017) 100–112

Contents lists available at ScienceDirect

Journal of Environmental Radioactivity

journal homepage: www.elsevier.com/locate/jenvrad

The impact of tidal and mesoscale eddy advection on the long term dispersion of ^{99}Tc from Sellafield

Magne Simonsen [a, b, *], Øyvind Saetra [a], Pål Erik Isachsen [a, c], Ole Christian Lind [b], Hilde Kristin Skjerdal [d], Brit Salbu [b], Hilde Elise Heldal [e], Justin P. Gwynn [f]

[a] Norwegian Meteorological Institute, P.O. Box 43, Blindern, NO-0313 Oslo, Norway
[b] Centre of Environmental Radioactivity CoE, Faculty of Environmental Sciences and Natural Resource Management, Norwegian University of Life Sciences (NMBU), P.O. Box 5003, N-1432 Ås, Norway
[c] Department of Geosciences, University of Oslo, P.O. Box 1047, Blindern, NO-0316 Oslo, Norway
[d] Norwegian Radiation Protection Authority, P.O. Box 55, NO-1332 Østerås, Norway
[e] Institute of Marine Research, P.O. Box 1870 Nordnes, NO-5817 Bergen, Norway
[f] Norwegian Radiation Protection Authority, The Fram Centre, NO-9296 Tromsø, Norway

ARTICLE INFO

Article history:
Received 22 December 2016
Received in revised form
30 May 2017
Accepted 2 June 2017

Keywords:
Technetium-99
Sellafield
Lagrangian ocean dispersion model
North East Atlantic
Nordic Seas
Model resolution

ABSTRACT

In the present work, numerical models are used to study the fate of the ^{99}Tc discharges from Sellafield with a specific focus on the role of mesoscale eddy and tidal advection on the transport and dispersion of this radionuclide. Transport estimates are made with an ocean model that resolves a large part of the ocean mesoscale eddy field and also includes tides. Equivalent estimates are also computed with another model in which these processes are either absent or parametrized. Comparison with field observations shows that the coarse-resolution model can reproduce the general features of the observed time-space ^{99}Tc distribution if the diffusivity in its eddy parametrization scheme is suitably chosen. However, the eddy-permitting simulations capture regional details better and show an overall higher prediction skill, with the model predictions agreeing with the observations within a factor of two to four. The importance of tidal advection is investigated by comparing transport in the eddy-permitting model when this is run either with tides included or with tides filtered out. The results point to systematic Lagrangian tidal drift in the Irish Sea and the North Sea that eventually impacts the ^{99}Tc activity concentration levels also far downstream.

1. Introduction

The dominant sources of the artificial radionuclide ^{99}Tc to the North Atlantic marine environment are authorized discharges from nuclear reprocessing facilities at Sellafield in the UK and La Hague in France (Fig. 1). In addition, a small background radiation level of about 5×10^{-3} Bqm^{-3} originates from the global fallout from nuclear weapon testing (Dahlgaard et al., 1995). After 1994, the ^{99}Tc contamination of the seawater in these areas have almost exclusively originated from Sellafield nuclear reprocessing plant, especially due to clean-up of legacy waste with resulting elevated discharges into the Irish Sea between 1994 and 2004 (Fig. 2). Discharged ^{99}Tc from Sellafield is transported with ocean currents out of the Irish Sea and further into the North Atlantic marine environment and beyond, so in order to follow the evolution of these releases a number of observational campaigns and fixed observation sites have been established. Thus, elevated ^{99}Tc activity concentration levels have been observed as far away as in the Barents Sea and the Arctic Ocean (Brown et al., 2002; Gerland et al., 2003; Kershaw et al., 2004).

The long-term transport of radionuclides from both Sellafield and La Hague have also been estimated by various numerical ocean transport models. Models are useful tools for interpolating between the scattered observations in a dynamically consistent way and they are also useful for the investigation of processes and hypotheses related to the fate of the released matter. Karcher et al. (2004) simulated the transport and dispersion of ^{99}Tc from Sellafield for the period 1979–1999. They found indications of a shorter transport time (2.5–3.5 years) to the northern regions (Barents Sea and

* Corresponding author. Norwegian Meteorological Institute, P.O. Box 43, Blindern, NO-0313 Oslo, Norway.
E-mail address: magnes@met.no (M. Simonsen).

http://dx.doi.org/10.1016/j.jenvrad.2017.06.002
0265-931X/

Fram Strait) than previously estimated from ^{137}Cs field observations (4–5 years, Kershaw and Baxter (1995)). The study also found large seasonal and interannual variations in the activity concentration levels in the Fram Strait. Orre et al. (2007) simulated the transport of ^{99}Tc during the period from 1975 to 2003, and found that different environmental forcing regimes, such as the North Atlantic Oscillation and winds in the northern Irish Sea, are important for the transport of radionuclides between Sellafield and Northern Norway. Finally, Villa et al. (2015) simulated the transport of the ^{129}I releases from both Sellafield and La Hague between 1966 and 2012. According to this study, a significant fraction of the Sellafield discharges is transported through the southern opening of the Irish Sea and into the Celtic Sea.

Common for all the above-mentioned model studies is their use of circulation fields having spatial resolutions of a few tens of kilometers. At such coarse resolution transport and dispersion of radionuclides by the ocean's *mesoscale eddy field*, stemming in large part from baroclinic instability of hydrographic fronts and having dynamic length scales of about 5–50 km, will practically not be resolved. Thus, in all the aforementioned studies the unresolved eddy mixing has been parametrized as lateral downgradient diffusion. The sensitivity of the model predictions to the details of these parametrizations, i.e. the size of 'eddy diffusivities' used, was not, however, discussed.

Furthermore, the previous model studies have used circulation fields with temporal resolutions longer than a day, and hence they did not include tidal advection of radionuclides. This is not an uncommon simplification since one intuitively expects the net transport by oscillating tides to be very small, leading only to some enhanced mixing or diffusion (which may be taken care of by the eddy diffusion scheme). However, where tidal currents are particularly strong, non-linear effects may also cause systematic *rectified*

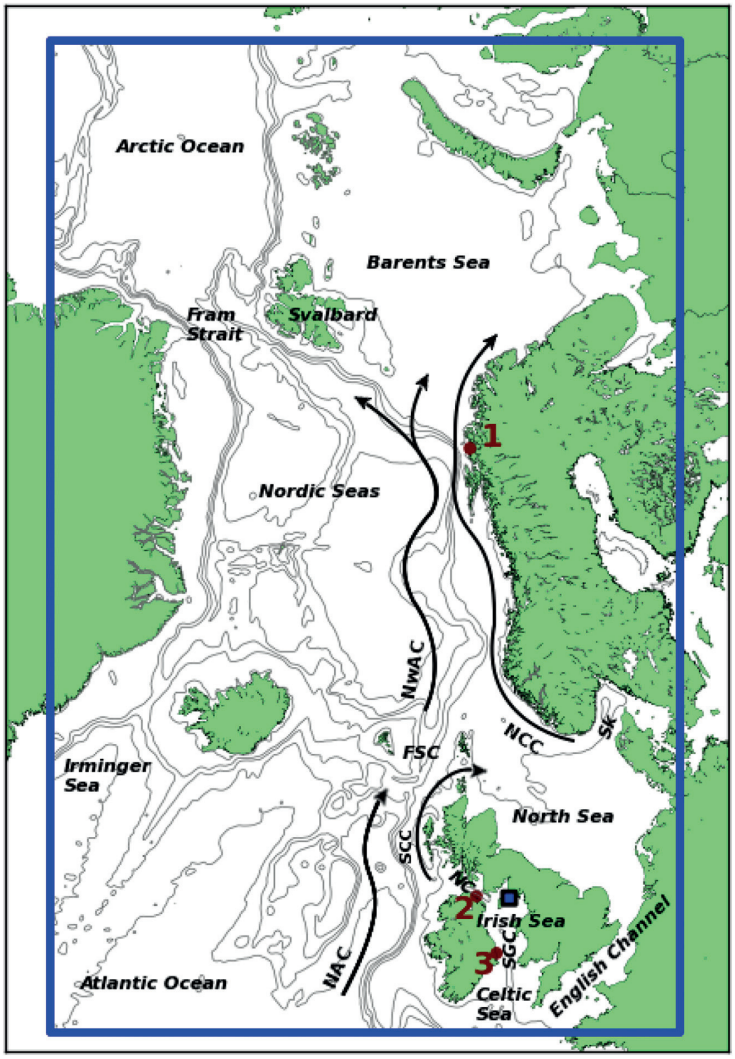

Fig. 1. Overview of the region. Blue lines are the ROMS 4 km model domain boundaries. Positions of the Norwegian, British and Irish observation sites (red dots) 1: Hillesøy (Norway), 2: Larne (UK), 3: Cahore (Ireland). Position of the seeding point in TRACMASS (blue square). Sk: Skagerrak, SGC: St George's Channel, NC: North Channel, FSC: Faroe-Shetland Channel NAC: North Atlantic Current, NwAC: Norwegian Atlantic Current, NCC: Norwegian Coastal Current, SCC: Scottish Coastal Current. Gray lines are the 100, 500, 1000, 1500, 2500 m depth contour lines from the model. (For interpretation of the references to colour in this figure legend, the reader is referred to the web version of this article.)

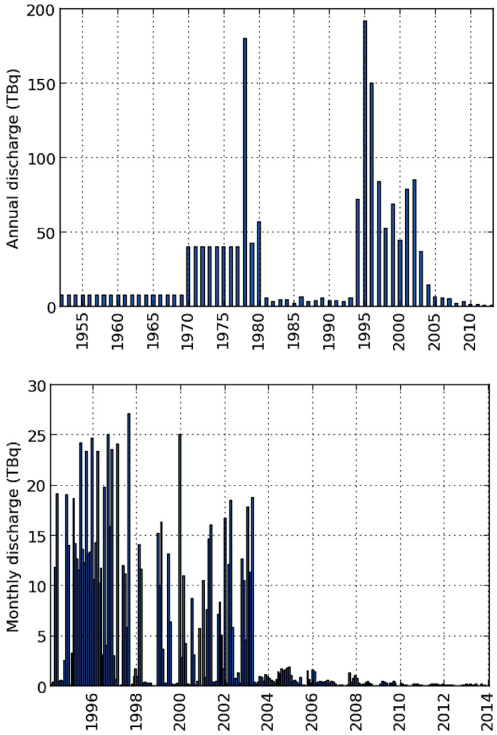

Fig. 2. Upper: Annual discharges from Sellafield. Lower: Monthly discharges from Sellafield (Sellafield Ltd.).

transports of radionuclides. Such non-linear interactions may result in non-zero time-mean Eulerian currents (currents at fixed position), or they may even give zero net Eulerian currents and a non-zero Lagrangian drift of water mass due to correlations between the currents and the ocean depth (Wei et al., 2004). In either case, the aforementioned model studies would not be able to pick up such transport of ^{99}Tc.

Motivated by these potential shortcomings of previous model studies, we here re-examine the transport and dispersion of ^{99}Tc discharges from Sellafield using an ocean model with higher resolution that contains both a vigorous mesoscale eddy field and tidal currents. To our knowledge, no simulation with comparable temporal and spatial resolution has been conducted previously. To assess the benefit of the added model resolution—in light of the substantially increased computational cost—a comparison has been carried out with a coarse-resolution model where eddy transport has been parametrized and tidal advection is entirely absent. The simulated upper-ocean ^{99}Tc activity concentration levels from both relatively high and lower resolution models have then been validated against an extended set of radionuclide measurements of samples collected from various open ocean surveys and from three long-time coastal monitoring stations.

2. Models and observations

2.1. The Sellafield ^{99}Tc discharges

2.1.1. Release scenario

The highly soluble ^{99}Tc is traditionally assumed to behave as a conservative radionuclide in oxic seawater, with low interactions with seabed sediments and suspended particles (Leonard et al., 2004). The recommended distribution coefficient (defined as the ratio between particle-bound and dissolved radioactivity) is low, in the order of 10^2 Lkg^{-1} (IAEA, 2004). Under anoxic environmental conditions, as can be found in some coastal areas, sediment distribution coefficients for ^{99}Tc can be orders of magnitude higher (e.g. Keith-Roach et al., 2003; Salbu and Holm, 2005). Still, Jenkinson et al. (2014) estimated that the inventory of ^{99}Tc in Irish Sea sediments was only about 2% of the total cumulative discharges. Salbu et al. (1993) showed that ^{99}Tc was present in the low molecular mass fraction in discharge waters from the reprocessing facility at Sellafield, presumably as the highly mobile pertechnetate TcO_4^-. In our study, ^{99}Tc was therefore assumed to be totally dissolved in sea water and transported with neutral buoyancy relative to the surrounding water masses. Only ^{99}Tc discharges from Sellafield was considered in this study due to the relatively lower contributions from other sources prior to and during the simulation period. Due to the long half-life of ^{99}Tc ($T_{1/2} = 2.13 \times 10^5$ years) relative to the length of the simulation period, radioactive decay has been ignored.

2.1.2. Observations

In what follows we compare model simulations with measurements of sea water ^{99}Tc activity concentration collected both from the open ocean and from coastal sites. Open ocean surface ^{99}Tc activity concentrations have been measured and compiled by the Norwegian Institute of Marine Research (IMR) and the Norwegian Radiation Protection Authority (NRPA) during annual ocean surveys between 1997 and 2012. The samples were collected at different locations and the spatial coverage varied from year to year, alternating between the North Sea and Skagerrak, the Norwegian Sea and the Barents Sea. At IMR, the samples were analyzed using a modified version of the method described by Harvey et al. (1992) and a low-background anticoincidence gas flow beta counter. The sample sizes varied from 50 to 100 L and the count times were of the order of 48 h. The theoretical analytical detection limit for a 100 L sample was 0.05 Bqm^{-3} and the total uncertainty was estimated to be below 10%.

A continuous time series of sea water ^{99}Tc activity concentration at Hillesøy in Northern Norway (see Fig. 1 for location) reaches back to July 1997. The data set consists of approximately monthly samples and has been collected by NRPA as part of the Norwegian Marine Monitoring Programme. At NRPA, the samples were analyzed using a modified version of the method described by Chen et al. (1991) and a low-background anticoincidence beta counter. Sample sizes varied from 50 to 100 L. The analytical detection limit was calculated to be approximately 0.10 Bqm^{-3} and the total uncertainty was normally around 10%.

Two shorter coastal time series also exist from sites near Sellafield (see Fig. 1). First, activity concentration levels representing conditions in the North Channel have been collected at Larne in Northern Ireland. Data used in our study have been extracted from the annual Radioactivity in Food and Environment (RIFE) reports (e.g. RIFE, 2013), where annual values are based on 12 (occasionally 11) monthly samples. Second, sea water activity concentrations in the southern Irish Sea have been collected at Cahore in south-eastern Ireland, and the data used here have been obtained from the annual reports from the Radiological Protection Institute of Ireland (RPII) (e.g. RPII, 2012). As for Larne, the observations have been collected from a shore-based site in Cahore, but at more variable temporal intervals.

2.2. Modeling tools

Trajectories of a finite number of synthetic radionuclides have

been integrated with a Lagrangian transport model, using pre-computed three-dimensional and time-dependent velocity fields from ocean general circulation models. The activity concentration can be estimated at any position and time from the number of particles present within a representative volume and time interval. Since long-term hydrodynamical simulations are resource-demanding, the three dimensional ocean current fields applied to the dispersion model in this study have been obtained from two existing ocean circulation datasets, one with relatively high spatial and temporal resolution and another with lower resolution.

2.2.1. The regional ROMS ocean circulation model

A regional hindcast of the ocean dynamics has been computed with the Regional Ocean Model System (ROMS) (Haidvogel et al., 2008) at the Norwegian Meteorological Institute (Røed et al., 2015). The model domain (Fig. 1) covers the northern part of the Atlantic Ocean, including the Irish Sea, North Sea, Nordic Seas, Barents Sea and parts of the Arctic Ocean. The grid is polar stereographic with horizontal resolution of 4 km, which is considered to be 'eddy-permitting' in these ocean regions where the internal deformation radius is 10–50 km. Thus, the model has a vigorous mesoscale eddy field even if it fails to resolve all dynamically active mesoscale features. The model had 42 terrain-following vertical layers, with increasing resolution near the surface. The atmospheric forcing was taken from the NORA10 (Reistad et al., 2011) hindcast archive (a regional 10 km downscaling of the ERA40 reanalysis (Uppala et al., 2005)) and daily fields from a ROMS hindcast with lower spatial resolution were used at the open lateral boundaries. The available period from the full hindcast is from January 1st, 1982 to December 31st, 2012. From this dataset, output files at two different temporal intervals were used in the dispersion simulations, namely hourly instantaneous fields and 24-h daily averaged fields.

2.2.2. The global FOAM ocean circulation model

The global Forecast Ocean Assimilation Model (FOAM) reanalysis (Blockley et al., 2014) has been made with the Nucleus for European Modeling of the Oceans (NEMO) ocean model (Madec, 2008) on the 'Orca025' grid, a three-polar grid with 0.25° resolution (Drévillon et al., 2008). The number of vertical layers is 75, at fixed depths, with layer thickness increasing from the surface to the bottom. The reanalysis covers the time period from January 1993 to December 2010 and is forced by atmospheric fields from the ERA-Interim reanalysis (Dee et al., 2011). The 0.25° model grid is most coarse near the equator (28 km) but gets refined at higher latitudes, giving a horizontal resolution of approximately 14 km at 60°N. This spatial resolution must be considered nearly eddy-permitting in our region of interest, but the outputs available to us, collected from the Copernicus web catalogue (www.marine.copernicus.eu), are monthly averages. So any energy at the mesoscale has been smoothed out and all mesoscale transport thus needs to be parametrized.

2.2.3. The TRACMASS Lagrangian trajectory model

The transport estimates for the ^{99}Tc discharges have been made with TRACMASS, a Lagrangian trajectory model described by Döös (1995). The transport model has been used in a number of previous studies at varying scales (e.g. Döös and Engqvist, 2007; Döös et al., 2011; Nilsson et al., 2013; Viikmäe et al., 2013). Using pre-computed velocity fields from the circulation models, the three-dimensional particle trajectories have been computed off-line, where the vertical velocity component was computed from the divergence of the horizontal velocities, assuming conservation of mass.

In our model simulations, each synthetic particle was assigned a fixed value of radioactivity. The seeding of the synthetic particles was hence determined from the reported monthly discharges from Sellafield (shown in Fig. 2) with a constant conversion factor. At Sellafield, the radionuclides were not discharged continuously, but on different dates during the month. The exact information on how and when this happened is classified information, and the only data released are monthly estimates. For simplicity, the trajectories in the model were therefore seeded on the last day in each month from January 1994 to December 2012, according to the available monthly discharge data (Fig. 2).

In total, 120 000 particle trajectories were computed for each simulation. This particular number was a trade-off between computational cost and resolution (detection limits) in the computed activity concentration levels.

The seeding of radioactive particles was done at a single model grid cell near Sellafield in the eastern Irish Sea (54.25°N, 3.83°W), marked with a blue square in Fig. 1. To avoid artificial effects near the shore, this seeding point was located around 25 km from the coast. Particles were released at different depths, but testing showed low sensitivity in far-field activity concentrations to the actual seeding depth, an indication that water masses in the eastern Irish Sea are vertically well-mixed.

In TRACMASS, the number of iterations between each updated time step from the circulation model will vary as the position is updated when a trajectory crosses a cell wall (Vries and Döös, 2001). However, the maximum time step was 3 min for the ROMS model at hourly resolution, roughly an hour for the ROMS simulation at daily resolution and 2 h for the FOAM simulations.

Sub-grid scale turbulent mixing in TRACMASS is parametrized as an isotropic diffusion process with a random displacement, as described in detail by Döös et al. (2011). For each time step, a horizontal random walk perturbation, limited by a maximum value determined by the diffusion coefficient and the length of the time step, is added to the end position from the advective motion. Döös et al. (2011) showed that even such a simple diffusion scheme can give results in good agreement with actual drifter trajectories by proper tuning of the diffusivity. In the present study, the transport simulations were performed with different values for the horizontal eddy diffusivity, including one run with zero diffusion.

No vertical diffusion were added to the trajectories. Neither was the contribution to the transport from wind-driven surface gravity waves considered in this study. This is because the wind-driven surface Stokes drift is confined to a shallow upper layer of the ocean, down to approximately half a wave length, whereas the simulated radionuclides will be distributed over a much larger part of the water column.

The dispersion simulations were conducted at local post-processing infrastructure at the Norwegian Meteorological Institute. The simulation time was about 9 days for the hourly ROMS simulations, approximately 5 h for the FOAM simulations, and 9 h for the daily ROMS simulations.

3. Results and discussion

3.1. The role of eddy diffusion in a coarse-resolution model

We begin by looking at transport of ^{99}Tc using velocity fields from the FOAM model, a model that have spatial and temporal resolutions in line with earlier studies. Fig. 3 shows this model's near-surface (top 50 m) activity concentration averaged over the year 1997, or three years after the initial release in the model. The four panels show results from simulations using four different levels of parametrized eddy diffusion.

The first panel shows the activity concentration field when eddy diffusion has been turned off and ^{99}Tc has been advected exclusively with the monthly-mean currents of the model. Transport

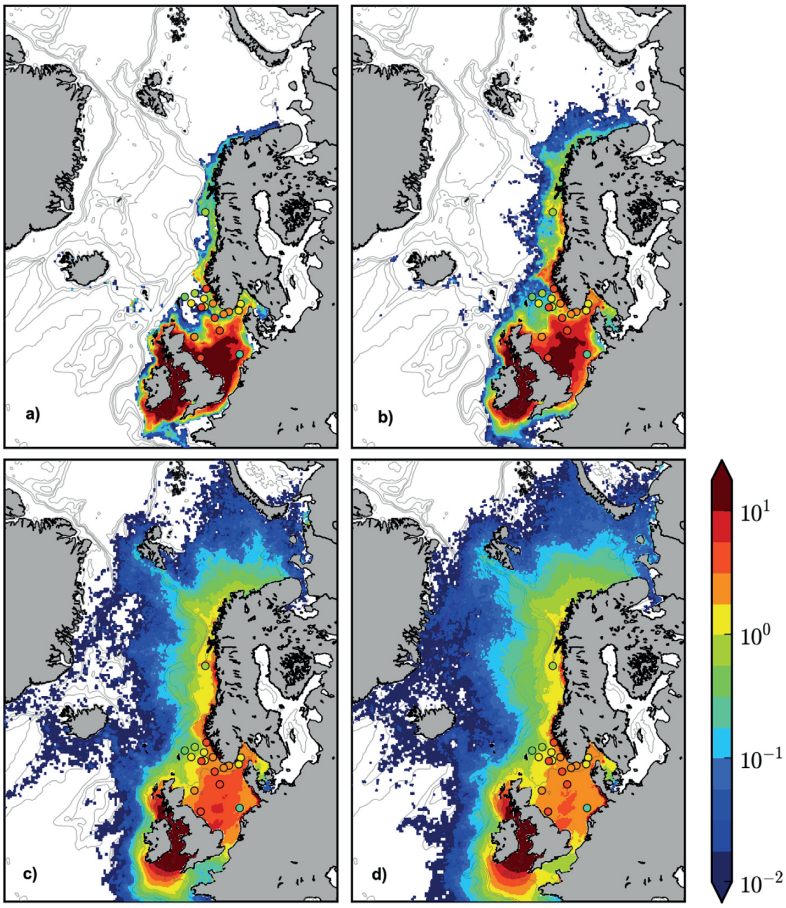

Fig. 3. Surface (top 50 m) activity concentration distribution from FOAM, averaged over 1997, with different values of horizontal diffusivity. a): $A_h = 0\ m^2s^{-1}$ (i.e. no diffusion), b): $A_h = 50\ m^2s^{-1}$, c): $A_h = 500\ m^2s^{-1}$, d): $A_h = 1000\ m^2s^{-1}$. Colored points show surface ^{99}Tc observations. Unit is Bqm^{-3}. Thin gray lines are contour lines for 100, 500, 1000, 1500 and 2500 m depths.

paths, even with no eddy diffusion, are in general agreement with earlier estimates (e.g. Davies and Hall, 2000; McCubbin et al., 2002; Povinec et al., 2003; Orre et al., 2007). The majority of the discharged radionuclide exits the Irish Sea through the North Channel and follows the Scottish Coastal Current around the north coast of Scotland into the North Sea. Along the outer edges of the North Sea Basin, there is a prevailing cyclonic (counter-clockwise) circulation, clearly traced out in the activity concentration field. Stirring of the water masses in the central North Sea is considerable due to complex wind-driven currents (Sündermann and Pohlmann, 2011), but a large fraction of the dispersed ^{99}Tc end up in Skagerrak in the north-east corner where it enters the Norwegian Coastal Current (NCC). This currents then transports ^{99}Tc swiftly northward along the Norwegian coast and up to the Barents Sea. The radionuclide remains on the Norwegian continental shelf as the dynamical constraint of the steep continental slope inhibits westward flow into the deep basins of the Nordic Seas. A smaller part of the discharged ^{99}Tc from the Sellafield plant is transported southwards through the Irish Sea and enters the Celtic Sea via the St. George's Channel. From the Celtic Sea, the discharges either flow eastward into the English Channel to enter the North Sea or turn clockwise around the western coast of Ireland to eventually rejoin with ^{99}Tc that have exited the Irish Sea via the North Channel.

The remaining three panels of Fig. 3 show the equivalent estimates of surface activity concentrations when lateral eddy fluxes have been parameterized as downgradient diffusion with diffusivities A_h of 50, 500 and 1000 m^2s^{-1}. A noticeable broadening of the activity concentration fields is as expected from the diffusive process. But a more interesting feature is the increased activity concentration levels along the Norwegian coast at this early stage, and importantly, the clear evidence of a more efficient, i.e. faster, transport to the Barents Sea and to the Fram Strait west of Svalbard. That eddy diffusion would have such an impact on transport to these remote regions is not immediately obvious since most of the route follows currents that are also included in the model that has no diffusion added. The faster transport can in fact be explained by eddy dispersion (diffusion in these models) of ^{99}Tc north of Scotland. North-westward eddy transport here brings part of the discharges into the North Atlantic Current (NAC) and later the Norwegian Atlantic Current (NwAC) which flows swiftly northward along the Norwegian continental slope, thus bypassing the cyclonic route around the North Sea. The result is a shorter transit time to the Barents Sea and Fram Strait. Similarly, the parametrized eddy diffusion appears to allow a direct route to Iceland and the Irminger

Sea by westward-flowing currents south of the Greenland-Scotland Ridge system.

Included in Fig. 3 are also actual surface observations of ^{99}Tc activity concentration levels collected in 1997. The scattered observations show a general fall-off in activity concentration with advective distance from the Irish Sea, an expected trend which is also seen in the simulations. Comparison of the various panels of the figure illustrate how sensitive the model estimates are to the choice of lateral eddy diffusivity and, as discussed above, how this diffusive eddy transport can have a fundamental impact on transport paths and transit times. Essentially, the eddy diffusion can cause bifurcation points in the trajectories experienced by ^{99}Tc, guiding the radionuclide between different main advection paths.

3.2. Transport in an eddy-permitting model

We proceed here to see what transport of ^{99}Tc from Sellafield looks like in a model in which much of the nonlinear mesoscale flow field is actually resolved. Fig. 4 shows the average near-surface activity concentration of ^{99}Tc estimated using the regional ROMS model—with no parametrization of eddy transport added. The activity concentrations for four different periods are shown: a year from the early transport period (1997), a period when the activity concentration levels were at the highest (2000–2001), a year from the period with reduced discharges (2007) and a year when the majority of the released ^{99}Tc was diluted or advected out of the model domain (2010).

As in Fig. 3, real surface observations are also shown, now for all four time periods. The eddy-permitting model appears to capture correctly both the observed increase of ^{99}Tc activity concentrations following the start of the period of enhanced Sellafield discharges in 1994 and an observed decrease following the reduction in discharges after about 2003. Throughout this entire period, the simulated activity concentration fields are generally in agreement with the available open-ocean observations within an order of magnitude.

Before we look into the quantitative assessment of the model simulations, it is worth pointing to at least one systematic discrepancy between the coarse-resolution and eddy-permitting model predictions. In contrast to the FOAM simulations (Fig. 3), the ROMS field from 1997 (Fig. 4a) shows very little transport of ^{99}Tc across the continental slope and into the deep basins of the Nordic Seas. This indicates that the model with higher resolution captures a well-known feature of high-latitude ocean dynamics,

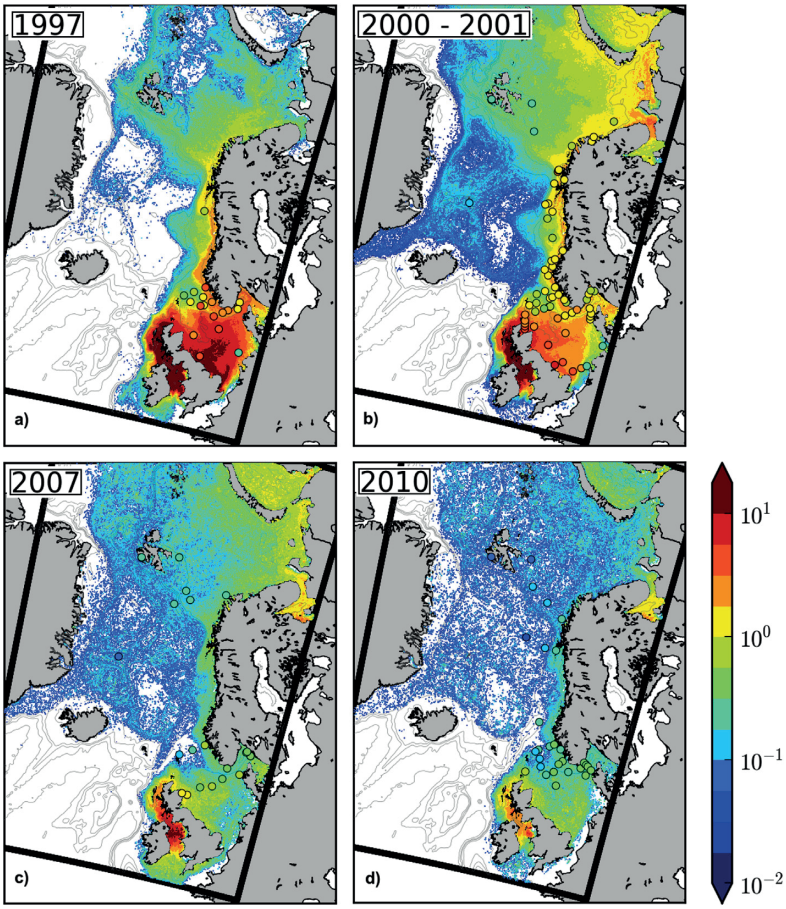

Fig. 4. Surface (top 50 m) activity concentration distribution from ROMS averaged over a): 1997, b): 2000–2001, c): 2007 and d): 2010. Colored points show surface ^{99}Tc observations. Black lines show the model boundaries. Unit is Bqm^{-3}. Thin gray lines are contour lines for 100, 500, 1000, 1500 and 2500 m depths. (For interpretation of the references to colour in this figure legend, the reader is referred to the web version of this article.)

namely a topographic suppression of all flows, including mesoscale eddy diffusion, across steep topography (Blumsack and Gierasch, 1972; Isachsen and Nøst, 2012; Isachsen, 2015). This dynamical constraint is entirely missed by the constant and isotropic diffusivity added to the FOAM fields (Fig. 3). There is reason to believe that the ROMS model, which uses a terrain-following vertical coordinate system, may actually overestimate the topographic suppression (Isachsen et al., 2012) somewhat. But the dynamical effect is real and is clearly missed by the eddy parametrization scheme. Finally, we note that the ROMS simulations show no indication of a westward transport along the southern flanks of the Greenland-Scotland Ridge, a transport route suggested by FOAM with parametrized eddy diffusion. The observational datasets at hand are insufficient to determine what happens in the real ocean, but again we see lowest-order qualitative features of the transport paths that clearly depend on how eddy advection is represented in the models.

3.3. Assessing the added value of increased resolution

Running long-term simulations with an eddy-permitting model is computationally expensive, so it is reasonable to consider whether the added value is worth the cost. In addition, regional models bring with them their own inherent problems, like inconsistent flow fields near open lateral boundaries. So it is not entirely obvious that the high-resolution model effort is worth the additional cost. Here, we therefore look more closely into the relative skill of the simulations based on ROMS and FOAM flow fields.

Comparing the 1997 activity concentration fields in Figs. 3 and 4 suggests that the FOAM simulations with an eddy diffusivity of $A_h = 500\ \mathrm{m^2 s^{-1}}$ produce relatively realistic transport estimates. We take this value as our best guess for the analysis below but also, for comparison, assess the skill for $A_h = 50\ \mathrm{m^2 s^{-1}}$.

It also worth noting that the regional ROMS model is only *eddy-permitting*, not fully *eddy-resolving*. With a grid resolution of 4 km, the model can be expected to start resolving flow features having scales larger than about 8–12 km (allowing for the effect of some scale-dependent dissipation in the model's advection scheme). Given that the internal deformation radius in the northern North Atlantic and Nordic Seas is as low as 10 km (Chelton et al., 1998; Nurser and Bacon, 2014), we can expect some eddy transport to be missed also by this relatively high-resolution model. Allowing

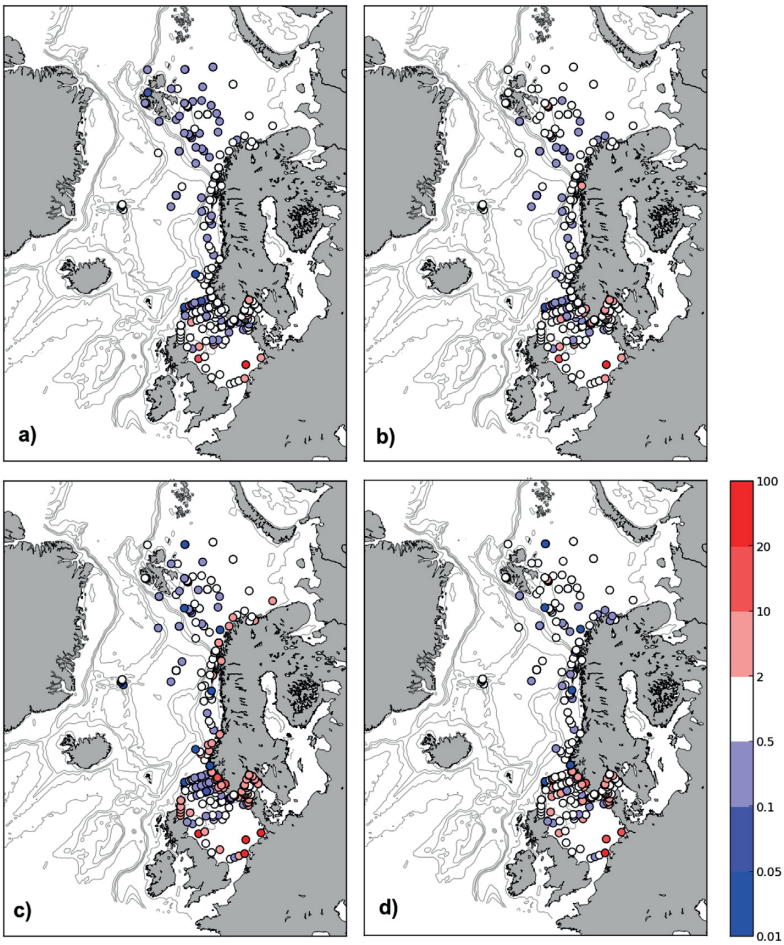

Fig. 5. Ratio of model to ocean observations values, for the period 1996–2012. From ROMS with a): no diffusion and b): $A_h = 100\ \mathrm{m^2 s^{-1}}$ and from FOAM with eddy diffusivity c): $A_h = 50\ \mathrm{m^2 s^{-1}}$ and d): $A_h = 500\ \mathrm{m^2 s^{-1}}$. Thin gray lines are contour lines for 100, 500, 1000, 1500 and 2500 m depths.

for this possibility we therefore tested the skill of two separate simulations based on ROMS, one without parametrized diffusion and another employing weak diffusion, with $A_h = 100\ m^2s^{-1}$. To test the models' performance against the observations the root-mean-square error (RMSE) and model bias was calculated. Since neither the observations or the model results were normally distributed, Wilcoxon signed-rank test has been used for significance testing. This is a non-parametric test that does not impose any pre-assumption on the shape of the distributions (Wilks, 2011). A confidence level of 95% was used as a requirement for significance.

3.3.1. Comparison with open-ocean observations

To compare model predictions with open-ocean observations between 1996 and 2012, the model fields were interpolated (in space and time) to the observations. Specifically, model surface activity concentrations were computed by summing up the number of trajectories present within 45 km× 45 km wide and 50 m deep boxes centered in the observation position. To reduce noise levels, such summations were made over 365 days centered on the observation time.

The results are shown in Fig. 5 as ratios of model to observed activity concentrations. Summary statistics and the outcomes of Wilcoxon signed-rank tests (for agreement with observations) are given in Table 1. Four different model simulations are studied: ROMS with A_h values of 0 and 100 m^2s^{-1} and FOAM with A_h values of 50 and 500 m^2s^{-1}. The direct comparison again illustrates how transport with the eddy-permitting ROMS model produces fairly good overall estimates (Table 1), but with a slight tendency for regional underestimation, especially in western and northern regions. The addition of weak diffusion to these model fields has a relatively minor impact with a small improvement in the RMSE but a slight worsening of the bias. In Skagerrak and the northern North Sea the simulation without added diffusion shows best agreement with the observations, whereas further north, in the Barents Sea and around Svalbard, the simulation with added diffusion is notably better.

The FOAM simulation with a low eddy diffusivity, $A_h = 50\ m^2s^{-1}$, performs worst of all. It overestimates activity concentrations in the boundary currents along the coastal margins all the way from the North Sea to the Barents Sea. At the same time the simulation underestimates activity concentrations in the central and northern North Sea. In the simulation using $A_h = 500\ m^2s^{-1}$ these biases are reduced, but there is still an indication of overestimation in Skagerrak and along the southwestern coast of Norway. As with ROMS, the underestimation near Svalbard and in the Barents Sea has improved slightly in the simulation with higher diffusion. For both FOAM simulations, the overall bias and RMSE is somewhat larger than for the two ROMS simulations (Table 1).

Results from the Wilcoxon signed-rank tests indicate that data from the FOAM simulations and the ROMS simulation without diffusion are significantly different from the observations, while the ROMS model with weak diffusion added produces fields that are not significantly different from the observations. Interestingly, the FOAM simulation with a low diffusivity has the largest RMSE of all model simulations. Increasing the diffusivity applied to the FOAM simulations improved the agreement with observations slightly. However, the RMSE is still larger than for both ROMS simulations.

Table 1
The table shows the statistical scores for the different model simulations when compared with the observations. The significance have been tested with the Wilcoxon signed-rank test using a 95% confidence level. Note that the time series from Larne and Cahore are shorter than 20 data points recommended for reliable results.

Circulation model	ROMS	ROMS	ROMS	FOAM	FOAM
Added diffusion (m^2s^{-1})	$A_h = 0$	$A_h = 100$	$A_h = 100$	$A_h = 50$	$A_h = 500$
Temporal resolution	1 h	1 h	1 day	1 month	1 month
Open ocean					
Bias	0.0355	0.0462	–	0.8596	0.2514
RMSE	1.1747	1.0232	–	2.4845	1.4712
Significant	No	Yes	–	No	No
Hillesøy					
Bias	0.2772	0.1032	–	2.2137	0.0125
RMSE	0.6044	0.4724	–	2.7445	0.4375
Significant	No	Yes	–	No	Yes
Larne					
Bias	–	5.2582	1.2613	–	15.4215
RMSE	–	11.1776	7.0004	–	21.4446
Significant	–	Yes	Yes	–	No
Cahore					
Bias	–	−0.5856	4.5774	–	10.5346
RMSE	–	2.3584	7.0492	–	13.1308
Significant	–	Yes	No	–	No

3.3.2. Comparison with the Hillesøy coastal time series

Further comparisons were done using the long time series of sea water observations collected at Hillesøy in Northern Norway (see Fig. 1). Time series from observations and from model activity concentrations averaged over the upper 50 m in 45 km× 45 km wide boxes around Hillesøy island are shown in Fig. 6. For this comparison, model values that fall below the detection threshold (due to a finite number of synthetic particles) have been set to one half of the value of that threshold.

In general, both ROMS simulations show good agreement with the observational trends. At early stages, from 1997 to about 2000, the simulations overestimate the activity concentration levels somewhat and also put the timing of the concentration peak about one year too early. In the period between 2000 and 2006 there is excellent agreement between simulations and observations, but after 2006 the modeled activity concentration levels appear to decrease too rapidly. Note however, that except for during the earliest stages, the observations largely all fall within the envelope of day-to-day model variability. The main impact of the added diffusion in the ROMS simulations is a smoothing of the time series. Nevertheless, the simulation with added diffusion shows slightly better agreement with the observations, especially for the magnitude of the peak and the rate of decrease after 2006. Over the full period (1994–2010) the diffusive simulation has a slightly lower bias and RMSE than the non-diffusive simulation (Table 1). According to the Wilcoxon signed-rank test, the samples from the non-diffusive simulation are significantly different from the observations, while the samples from the diffusive simulation are not.

The predicted time series obtained from the two FOAM simulations are highly correlated with each other, but the simulation with weak eddy diffusivity systematically overestimates the activity concentrations throughout the entire period, in some cases by up to an order of magnitude. Bias and RMSE are both higher than for the ROMS simulations (Table 1). This is in agreement with too high activity concentration levels near the coasts for this simulation, as seen in Fig. 5. The statistics in Table 1 shows that the simulation with a more realistic diffusivity shows better agreement with the magnitudes obtained with the ROMS simulations and with the observations. This is to be expected, as the eddy diffusion should transport ^{99}Tc away from the coastal boundary current (NCC). Both for the ROMS and FOAM simulations, the choice of eddy diffusivity also affect the transit times, with earlier initial enhancement of activity concentration at Hillesøy in the simulations with high diffusivity. As discussed above, this is likely due to eddy diffusion feeding ^{99}Tc into the North Atlantic Current off

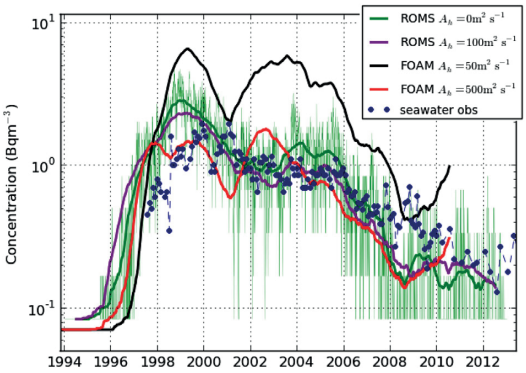

Fig. 6. Time series of modeled activity concentration at Hillesøy, compared with sea water observations. Black line: FOAM global model $A_h = 50\ m^2 s^{-1}$, red line: FOAM global model $A_h = 500\ m^2 s^{-1}$, green line: ROMS $A_h = 0\ m^2 s^{-1}$, purple line: ROMS $A_h = 100\ m^2 s^{-1}$. Thick lines are one-year running mean values, while the thin green line is daily values from the ROMS simulation without parametrized diffusion. (For interpretation of the references to colour in this figure legend, the reader is referred to the web version of this article.)

Scotland, thus reducing the length of the transport pathway to Northern Norway.

From the comparison with observations above, we have seen that both the coarse and the eddy-permitting models are able to reproduce the observed activity concentrations for the large scale dispersion with sufficiently good overall statistics. Since much of the eddy transport is actually resolved by the eddy-permitting model, it can provide good results even without added diffusion. In contrast, the skill of the non-eddy-permitting model depends on the magnitude of the diffusivity, which has to be tuned somewhat to achieve good results. In the next section we will see how increased temporal resolution will impact the results at regional scale by comparing results from simulations where circulation fields with different temporal resolution have been used. As we will see, the impacts from processes at tidal scales can not be accounted for simply by adding diffusion, and they might even affect the concentration levels far away from the source.

3.4. The role of tidal advection

Tidal currents oscillate in ellipses which are almost circular in the open ocean but can have high eccentricity where ocean geometry impose anisotropy, e.g. near the coast. Spatial variations in the shape of these ellipses can cause a net dispersion of substances floating in the ocean. A model that not resolves the tides may have the net effect parametrized as some form of enhanced lateral diffusion. But where currents are large nonlinear effects in the momentum budget can produce non-zero Eulerian mean currents that transport substances in a non-diffusive way. And even where the tidal currents themselves are linear, correlations between these currents and water depth can cause a net Lagrangian transport which again is non-diffusive. In this section we look into the importance of such effects on the fate of Sellafield-released ^{99}Tc.

Estimates of the maximum tidal current speeds of the dominant tidal constituent in the study region, M2, are shown in Fig. 7. The estimates come from the TPXO global data set for ocean tides, where TOPEX/POSEIDON satellite altimeter data have been used to constrain a global inverse tidal model (Egbert et al., 1994). The plot reveals that tidal currents are strong in the Irish Sea, around Scotland, in the English Channel and the southern North Sea, as well as outside the Norwegian and Russian coastlines in the southern

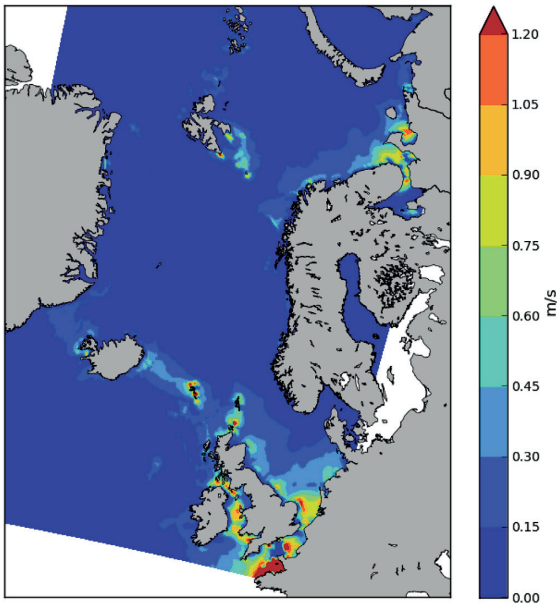

Fig. 7. Maximum tidal current speed from the M2 constituent from TPXO (Egbert et al., 1994).

Barents Sea.

We assessed the net effect of tides on the transport of ^{99}Tc near the British Isles by comparing activity concentration fields from the tide-resolving ROMS simulation with fields produced from the same model but using currents that had been averaged over 24 h. Such averaging removes almost all tidal energy in diurnal and semi-diurnal tides. For consistency the comparison was also done against fields produced by the monthly-mean FOAM fields. Fig. 8 shows the results as modeled activity concentration in the Irish Sea and the Celtic Sea averaged over the entire simulation period (1994–2010). In light of the model performances assessed above, the ROMS simulations use $A_h = 100\ m^2 s^{-1}$ and FOAM simulations use $A_h = 500\ m^2 s^{-1}$.

The figure shows clear discrepancies between the ROMS simulation that include tides and the other two simulations. The detided ROMS and FOAM fields both indicate an extensive southward drift of radionuclides through the St. George's Channel into the Celtic Sea. As a result of this southward transport, activity concentration levels are also elevated in the English Channel and off the west coast of Ireland. The fields from ROMS with tides included show activity concentrations that are more than one order of magnitude lower in the same waters. Intuitively one might expect that strong oscillating tidal currents in this region would contribute to an increased mixing of radionuclides out of the Irish Sea and into the Celtic Sea. However, the inclusion of tides instead reduces the southward transport of ^{99}Tc.

Measurements of sea water ^{99}Tc activity concentrations from two observation sites in each end of the Irish Sea, Larne in Northern Ireland and Cahore in south-western Ireland (see Fig. 1 for positions), can be used to assess the various model predictions. Fig. 9 shows activity concentration time series from both observations and model simulations. The observed activity concentration levels at Larne are about one order of magnitude higher than the levels at Cahore. This is as expected due to a closer proximity to Sellafield and a predominantly northward ocean flow through the Irish Sea

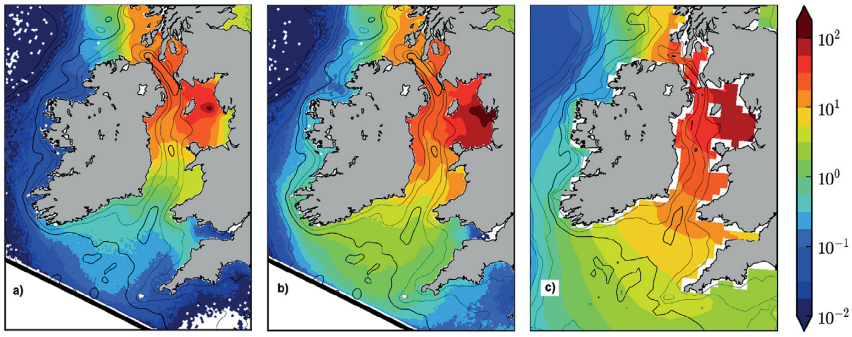

Fig. 8. Surface activity concentration averaged over Feb 1994–Dec 2010 from a:) ROMS including tides, b:) ROMS without tides and c:) FOAM $A_h = 500\ \mathrm{m^2 s^{-1}}$. Unit is $\mathrm{Bqm^{-3}}$. Thick black lines are model domain boundaries. Thin black lines are contour lines for 50, 75, 100, 150, 250 and 500 m depths. Contour lines for 100 m and 500 m are emphasized.

(Davies and Hall, 2000). Not unexpectedly, the observed pattern at Larne closely reflects the discharge history (see Fig. 2). In general, all three model simulations show good agreement with the observations, with a slightly better performance for the two ROMS simulations than for the FOAM simulation (Table 1). Here, close to the release site, both ROMS simulations are statistically indistinguishable from the observations (by the Wilcoxon signed-rank test) whereas the FOAM simulation is not (Table 1). The observation time series at Cahore is shorter and generally has a lower time resolution than that at Larne. However, the general time evolution is similar to that observed in the north. The model predictions here are characterized by large fluctuations while still being in rough agreement with the observations. But here the ROMS simulation that includes the effects of tides clearly does better, especially in the latter half of the simulation period. The other two simulations that ignore tidal advection consistently overestimate the activity concentrations in this period and, as a result, fail to be statistically indistinguishable from the observations by the Wilcoxon signed-rank test.

We take these results as strong indication that there is a real and non-trivial tidal drift of ^{99}Tc in the southern Irish Sea. To further illustrate this, a 'net Lagrangian velocity field' was computed as the mean particle displacements (divided by time increment) in each model grid cell over the time period from 1994 to 2012. The difference between this mean Lagrangian velocity field from the tidal and the detided ROMS simulations for the Irish Sea can be seen in Fig. 10. The overall direction is quite unstructured in the northern Irish Sea and in the North Channel, but a northward net drift pattern is clearly seen in the south and in the St. George's Channel. Hence, in this region, the tides induce a northward residual which is not resolved in the detided fields.

It is worth noting that the net tidal drift of ^{99}Tc observed here does not necessarily imply net northward Eulerian mean currents. In other words, this drift would not be picked up by a moored current meter deployed in the region. Such residual Eulerian currents may indeed exist, but they would also be present in the detided ROMS model fields. What we observe here is instead evidence for what can be termed the 'tide-induced Lagrangian residual' (Wei et al., 2004), i.e. the difference between the Lagrangian and the Eulerian mean. This is sometimes referred to as 'the tidal Stokes drift' due to its clear analogy with the classical solution of Stoke (1847) for particle drift under inviscid surface gravity waves.

So the drift studied here is purely Lagrangian and is caused by systematic correlations between tidal currents and water depth from variations in bottom topography. As mentioned above, tidal currents trace out ellipses. To conserve volume, flow speeds are higher in shallow water compared to deep water. Over a sloping bottom a water parcel advected in such a tidal ellipse will be

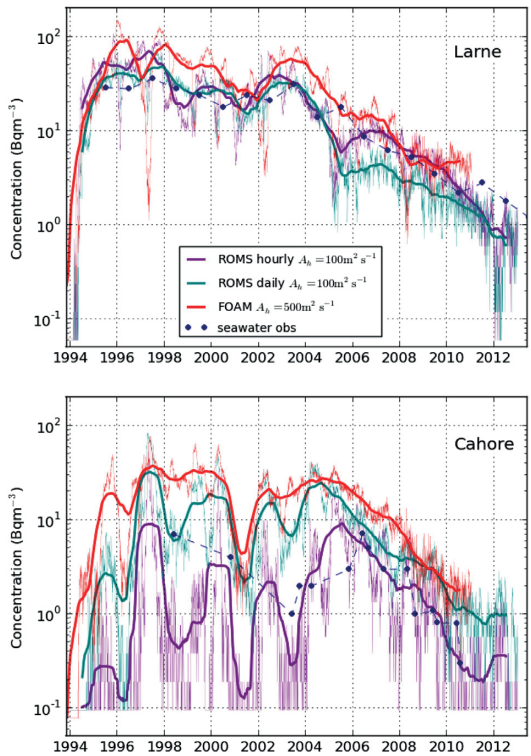

Fig. 9. Time series of modeled activity concentration at Larne observation site, compared with sea water observations (upper panel) and at Cahore (lower panel). Thin lines are daily values, thick lines are one-year running mean.

transported over a longer distance on the shallower side and a shorter distance on the deeper side. The result is movement along open ellipses or spirals—and a net translation. The direction of the translation depends on whether the tidal currents are rotating clockwise or counterclockwise with respect to the topographic slope. In the Irish Sea this result in net Lagrangian drift velocities as shown in Fig. 10 and the differences in ^{99}Tc activity concentration as shown in Fig. 8.

Residual tidal advection is of course not limited to the Irish Sea. The difference between the mean Lagrangian velocity fields from the tidal and detided simulations in the southern North Sea is

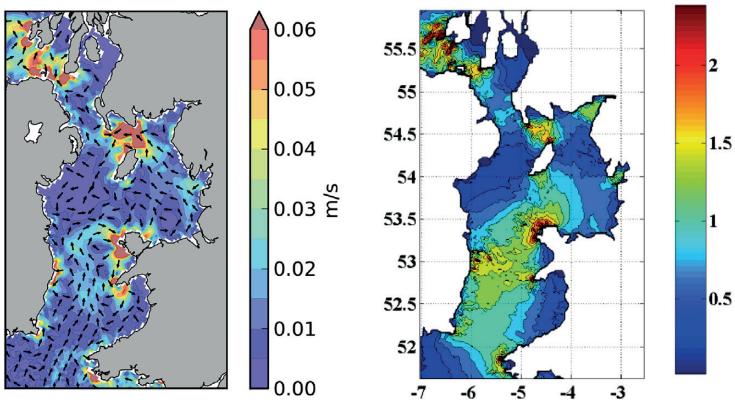

Fig. 10. Left panel: Time-averaged difference between particle velocity from ROMS simulations with and without tides in the Irish Sea. The arrows show the direction and the color shading shows the magnitude of the difference in drift. Right panel: Maximum amplitude of the depth-averaged current for a mean spring tide (ms^{-1}) (reproduced with permission from Howarth (2005)).

shown in Fig. 11. We can see that the southward drift along the eastern UK coast was strengthened by the tide-induced Lagrangian residual, resulting in greater transport of ^{99}Tc to the southern part of the North Sea in the simulation where tides were included. In fact, there was an additional near-coastal Lagrangian drift of ^{99}Tc from the eastern UK coast all the way to the western Danish coast.

So tides can cause an additional Lagrangian drift of ^{99}Tc, at least in the Irish Sea, Celtic Sea and the southern North Sea. And as Fig. 12 illustrates, the net impact on activity concentrations can also extend far beyond these regions. The figure shows the ratio between the activity concentrations from the ROMS simulations without and with tidal currents, averaged over the entire simulation period. In the detided simulation, the activity concentrations are increased by about one order of magnitude in the southern Irish Sea and in the Celtic Sea, as discussed above. But the activity concentrations are also enhanced further downstream, e.g. in the English Channel and along the western Irish Coast. And the enhanced transport along the Irish coast has consequences much further north, resulting in enhanced activity concentrations in the entire Norwegian Sea and all the way up to the Fram Strait. Conversely, the simulation without tides underestimated the ^{99}Tc activity concentration in the southern North Sea and in the coastal currents up to the Barents Sea. Clearly, the net impact of not including tides in model predictions is systematic and can, as illustrated, be far-reaching.

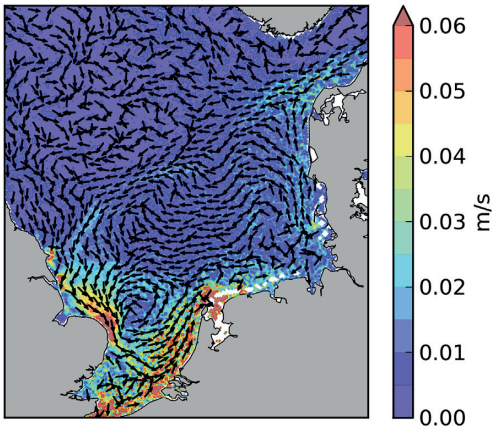

Fig. 11. Time-averaged difference between particle velocity in ROMS simulations with and without tides in central and southern North Sea.

4. Summary and conclusions

We have re-examined the transport and dispersion of ^{99}Tc discharges from the Sellafield nuclear reprocessing facility using circulation fields from numerical ocean models at two different spatial resolutions; the global coarse-resolution FOAM model and the regional eddy-permitting ROMS model which also includes tides. Although there are many more discrepancies between the two models, such as the choice of vertical coordinate system and mixing and advection schemes, we consider the difference in resolution to be most relevant for net transport. Essentially, one model resolves a large part of the mesoscale eddy transport in the ocean whereas the other model either lacks eddy transport completely or has it entirely parametrized.

By comparing concentration fields from simulations using the FOAM model with and without an eddy parametrization it was shown that eddy transport has qualitative impacts beyond a simple diffusive spreading of the activity concentration field. By connecting ^{99}Tc outflow from the Irish Sea with the North Atlantic Current, north of Scotland, eddy transport significantly shortened travel times to e.g. the Barents Sea and the Fram Strait.

A comparison of model results against open ocean and coastal time-series observations showed that the coarse-resolution model, with eddies parametrized, is able to reproduce the gross features of the actual spreading of ^{99}Tc, both close to and far from the Sellafield releases. But the skill here is strongly dependent on the choice of diffusion coefficient. Not unexpected, the eddy-permitting model does better when compared to observations, but the improvement appeared to be relatively modest in light of the considerable additional computational cost. And since this model is also just eddy-permitting and not fully eddy-resolving, a best skill was obtained after weak lateral diffusion was added here too. Nevertheless, an example of added value in eddy-permitting simulations was seen in the transport across steep continental slopes. As the ROMS simulations clearly indicated, mesoscale eddy transport across such topographic features is reduced in an eddy-permitting model. But current eddy parametrization schemes, like the down-gradient scheme used in the coarse-resolution simulations here, fail to account for this effect.

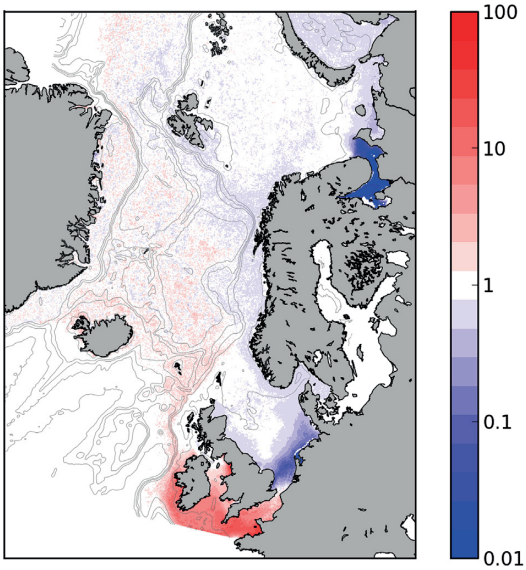

Fig. 12. Ratio of modeled activity concentration from ROMS simulations without and with tides, 1994–2012. Thin gray lines are contour lines for 100, 500, 1000, 1500, 2500 m depths.

A second focus of the study was the net effect of tidal advection on the fate of ^{99}Tc from Sellafield. Transport estimates using velocity fields from the ROMS model which also included tides was compared with similar estimates based on daily-mean currents, i.e. with tides filtered out. The comparison showed that transport out of the Irish Sea is greatly affected by the inclusion of tides as these cause a net northward tide-induced Lagrangian drift in the southern Irish Sea. This additional northward drift causes a reduced transport of ^{99}Tc into the Celtic Sea via St. George's Channel (compared to simulations in which tides are not included). Earlier studies, where this tidal drift not is taken into account (such as Villa et al. (2015)), might thus have overestimated the drift into the Celtic Sea. Importantly, this additional Lagrangian tidal drift turns out to impact activity concentration levels as far away as the Barents Sea and the Arctic Ocean.

When comparing model predictions and observations, as done here, there are a number of caveats that should be considered. Fundamental issues are the *representation errors* that arise as observations are typically snapshot measurements while model fields represent some form of averages (e.g. over the volume of grid cells). In this study we have tried to see the model-observation comparisons in some kind of averaged sense, but sampling issues related to the observations can still introduce biases that make a perfect match between observations and model fields wishful thinking even after extensive averaging. A measure of the root-mean-square error (RMSE) can even penalized a high-resolution model over a lower-resolution model because of the higher energy and variability in the former.

In summary, the model-observation comparisons performed here confirmed that both higher and lower resolution model simulations were able to give descriptions of the dispersion of the Sellafield ^{99}Tc discharges that were largely consistent with the available observations. But the high-resolution simulations have shed light on the role of the mesoscale eddy field and tidal currents for the transport of this radionuclide. The residual transport from tides and their apparent impact further downstream as seen in the model simulations were particularly unexpected. Future studies of transport through shallow seas should consider the additional computation cost involved in resolving tides—or have the net tide-induced Lagrangian residual parametrized.

Acknowledgements

We gratefully acknowledge M.J. Howarth at the National Oceanography Centre for kindly giving us permission to reproduce the plot of the tidal currents in the Irish Sea (right panel in Fig. 10). We also would like to thank Anne Liv Rudjord at the Norwegian Radiation Protection Authority for helpful discussions, and co-workers at the Norwegian Meteorological Institute for providing the datasets from the BaSIC hindcast. This study has been funded by the Norwegian Research Council through its Centre of Excellence (CoE) funding scheme (Project No. 223268/F50).

References

Blockley, E.W., Martin, M.J., McLaren, A.J., Ryan, A.G., Waters, J., Lea, D.J., Mirouze, I., Peterson, K.A., Sellar, A., Storkey, D., 2014. Recent development of the Met Office operational ocean forecasting system: an overview and assessment of the new Global FOAM forecasts. Geosci. Model Dev. 7 (6), 2613–2638. http://www.geosci-model-dev.net/7/2613/2014/.

Blumsack, S.L., Gierasch, P.J., 1972. Mars: the effects of topography on baroclinic instability. J. Atmos. Sci. 29, 1081–1089 http://dx.doi.org/10.1175/1520-0469(1972)029<1081:MTEOTO>2.0.CO;2.

Brown, J., Iospje, M., Kolstad, K., Lind, B., Rudjord, A., Strand, P., 2002. Temporal trends for 99Tc in Norwegian coastal environments and spatial distribution in the Barents Sea. J. Environ. Radioact. 60 (1–2), 49–60. http://www.sciencedirect.com/science/article/pii/S0265931X01000959.

Chelton, D.B., deSzoeke, R.A., Schlax, M.G., Naggar, K.E., Siwertz, N., 1998. Geographical variability of the first baroclinic rossby radius of deformation. J. Phys. Oceanogr. 28 (3), 433–460 http://dx.doi.org/10.1175/1520-0485(1998)028<0433:GVOTFB>2.0.CO;2.

Chen, Q., Aarkrog, A., Nielsen, S., Dahlgaard, H., Nies, H., Yu, Y., Mandrup, K., 1991. Determination of Plutonium in Environmental Samples by Controlled Valence in Anion Exchange. Tech. Rep. RISO-M–2856, Risoe National Lab.

Dahlgaard, H., Chen, Q., Herrmann, J., Nies, H., Ibbett, R., Kershaw, P., 1995. On the background level of 99Tc, 90Sr and 137Cs in the North Atlantic. J. Mar. Syst. 6 (5–6), 571–578. http://www.sciencedirect.com/science/article/pii/092479639500025K.

Davies, A.M., Hall, P., 2000. The response of the North channel of the Irish Sea and clyde Sea to wind forcing. Cont. Shelf Res. 20 (8), 897–940. http://www.ingentaconnect.com/content/els/02784343/2000/00000020/00000008/art00009.

Dee, D.P., Uppala, S.M., Simmons, A.J., Berrisford, P., Poli, P., Kobayashi, S., Andrae, U., Balmaseda, M.A., Balsamo, G., Bauer, P., Bechtold, P., Beljaars, A.C.M., van de Berg, L., Bidlot, J., Bormann, N., Delsol, C., Dragani, R., Fuentes, M., Geer, A.J., Haimberger, L., Healy, S.B., Hersbach, H., Hólm, E.V., Isaksen, L., Kållberg, P., Köhler, M., Matricardi, M., McNally, A.P., Monge-Sanz, B.M., Morcrette, J.-J., Park, B.-K., Peubey, C., de Rosnay, P., Tavolato, C., Thépaut, J.-N., Vitart, F., 2011. The ERA-Interim reanalysis: configuration and performance of the data assimilation system. Q. J. R. Meteorol. Soc. 137 (656), 553–597. http://dx.doi.org/10.1002/qj.828.

Drévillon, M., Bourdallé-Badie, R., Derval, C., Lellouche, J.M., Rémy, E., Tranchant, B., Benkiran, M., Greiner, E., Guinehut, S., Verbrugge, N., Garric, G., Testut, C.E., Laborie, M., Nouel, L., Bahurel, P., Bricaud, C., Crosnier, L., Dombrowsky, E., Durand, E., Ferry, N., Hernandez, F., Galloudec, O.L., Messal, F., Parent, L., 2008. The GODAE/Mercator-Ocean global ocean forecasting system: results, applications and prospects. J. Oper. Oceanogr. 1 (1), 51–57. http://dx.doi.org/10.1080/1755876X.2008.11020095.

Döös, K., 1995. Interocean exchange of water masses. J. Geophys. Res. Oceans 100 (C7), 13499–13514. http://dx.doi.org/10.1029/95JC00337.

Döös, K., Engqvist, A., 2007. Assessment of water exchange between a discharge region and the open sea – a comparison of different methodological concepts. Estuarine, Coast. Shelf Sci. 74 (4), 709–721. http://www.sciencedirect.com/science/article/pii/S027277140700159X.

Döös, K., Rupolo, V., Brodeau, L., 2011. Dispersion of surface drifters and model-simulated trajectories. Ocean. Model. 39 (3–4), 301–310. http://www.sciencedirect.com/science/article/pii/S1463500311000989.

Egbert, G.D., Bennett, A.F., Foreman, M.G.G., 1994. TOPEX/POSEIDON tides estimated using a global inverse model. J. Geophys. Res. Oceans 99 (C12), 2156–2202. http://dx.doi.org/10.1029/94JC01894.

Gerland, S., Lind, B., Dowdall, M., Karcher, M., Kolstad, A.K., 2003. 99Tc in seawater in the West Spitsbergen Current and adjacent areas. J. Environ. Radioact. 69 (1–2), 119–127. http://www.sciencedirect.com/science/article/pii/S0265931X03000900.

Haidvogel, D., Arango, H., Budgell, W., Cornuelle, B., Curchitser, E., Lorenzo, E.D.,

Fennel, K., Geyer, W., Hermann, A., Lanerolle, L., Levin, J., McWilliams, J., Miller, A., Moore, A., Powell, T., Shchepetkin, A., Sherwood, C., Signell, R., Warner, J., Wilkin, J., 2008. Ocean forecasting in terrain-following coordinates: formulation and skill assessment of the Regional Ocean modeling system. J. Comput. Phys. 227 (7), 3595–3624 predicting weather, climate and extreme events. http://www.sciencedirect.com/science/article/pii/S0021999107002549.

Harvey, B.R., Williams, K.J., Lovett, M.B., Ibbett, R.D., 1992. Determination of technetium-99 in environmental material with rhenium as a yield monitor. J. Radioanal. Nucl. Chem. 158 (2), 417–436. http://dx.doi.org/10.1007/BF02047127.

Howarth, M.J., 2005. Hydrography of the Irish Sea. SEA6 Technical Report. Tech. Rep. POL Internal Document 174. POL.

IAEA, 2004. Sediment Distribution Coefficients and Concentration Factors for Biota in the Marine Environment. Technical report series, No. 422. International Atomic Energy Agency.

Isachsen, P.E., 2015. Baroclinic instability and the mesoscale eddy field around the Lofoten Basin. J. Geophy. Res. Oceans 120.

Isachsen, P.E., Koszalka, I., Lacasce, J.H., 2012. Observed and modeled surface eddy heat fluxes in the eastern Nordic Seas. J. Geophys. Res. 117, C08020.

Isachsen, P.E., Nøst, O.A., 2012. The air-sea transformation and residual overturning circulation within the Nordic Seas. J. Mar. Res. 70, 31–68.

Jenkinson, S.B., McCubbin, D., Kennedy, P.H., Dewar, A., Bonfield, R., Leonard, K.S., 2014. An estimate of the inventory of technetium-99 in the sub-tidal sediments of the Irish Sea. J. Environ. Radioact. 133 (0), 40–47. http://www.sciencedirect.com/science/article/pii/S0265931X1300129X.

Karcher, M.J., Gerland, S., Harms, I.H., Iosjpe, M., Heldal, H.E., Kershaw, P.J., Sickel, M., 2004. The dispersion of 99Tc in the Nordic Seas and the Arctic Ocean: a comparison of model results and observations. J. Environ. Radioact. 74 (1–3), 185–198 papers from the International Conference on Radioactivity in the Environment, Monaco, 1-5 September 2002. http://www.sciencedirect.com/science/article/pii/S0265931X04000311.

Keith-Roach, M.J., Morris, K., Dahlgaard, H., 2003. An investigation into technetium binding in sediments. Mar. Chem. 81 (3–4), 149–162. http://dx.doi.org/10.1016/S0304-4203(03)00014-8.

Kershaw, P., Baxter, A., 1995. The transfer of reprocessing wastes from north-west Europe to the Arctic. Deep Sea Res. Part II 42 (6), 1413–1448. http://dx.doi.org/10.1016/0967-0645(95)00048-8.

Kershaw, P.J., Heldal, H.E., Mork, K.A., Rudjord, A.L., 2004. Variability in the supply, distribution and transport of the transient tracer 99Tc in the NE Atlantic. J. Mar. Syst. 44 (1–2), 55–81. http://www.sciencedirect.com/science/article/pii/S092479630300126X.

Leonard, K.S., McCubbin, D., McDonald, P., Service, M., Bonfield, R., Conney, S., 2004. Accumulation of technetium-99 in the Irish Sea? Sci. Total Environ. 322 (1–3), 255–270. http://www.sciencedirect.com/science/article/pii/S0048969703005710.

Madec, G., 2008. NEMO ocean engine. Note du Pôle de modélisation. Tech. Rep. 27. Institut Pierre-Simon Laplace (IPSL), France. ISSN No 1288–1619.

McCubbin, D., Leonard, K.S., Brown, J., Kershaw, P.J., Bonfield, R.A., Peak, T., Jun. 2002. Further studies of the distribution of technetium-99 and caesium-137 in UK and European coastal waters. Cont. Shelf Res. 22, 1417–1445.

Nilsson, J.A.U., Döös, K., Ruti, P.M., Artale, V., Coward, A., Brodeau, L., 2013. Observed and modeled global ocean turbulence regimes as deduced from surface trajectory data. J. Phys. Oceanogr. 43 (11), 2249–2269. http://dx.doi.org/10.1175/JPO-D-12-0193.1.

Nurser, A.J.G., Bacon, S., 2014. The rossby radius in the Arctic Ocean. Ocean Sci. 10 (6), 967–975. http://www.ocean-sci.net/10/967/2014/.

Orre, S., Gao, Y., Drange, H., Nilsen, J.E.O., 2007. A reassessment of the dispersion properties of 99Tc in the North Sea and the Norwegian Sea. J. Mar. Syst. 68 (1–2), 24–38. http://www.sciencedirect.com/science/article/pii/S0924796306003253.

Povinec, P.P., du Bois, P.B., Kershaw, P.J., Nies, H., Scotto, P., 2003. Temporal and spatial trends in the distribution of 137Cs in surface waters of Northern European Seas — a record of 40 years of investigations. Deep Sea Res. Part II Top. Stud. Oceanogr. 50 (17–21), 2785–2801 worldwide Marine Radioactivity Studies (WOMARS). http://www.sciencedirect.com/science/article/pii/S0967064503001486.

Røed, L.P., Lien, V.S., Melsom, A., Kristensen, N.M., Gausdal, Y., Ådlandsvik, B., Albretsen, J., 2015. BaSIC Technical Report 4. Part I: Evaluation of the BaSIC4 Long Term Hindcast Results. Tech. Rep. 5/2015. Norwegian Meteorological Institute Oslo.

Reistad, M., Breivik, Ø., Haakenstad, H., Aarnes, O.J., Furevik, B.R., Bidlot, J.-R., 2011. A high-resolution hindcast of wind and waves for the North Sea, the Norwegian Sea, and the Barents Sea. J. Geophys. Res. Oceans 116 (C5) n/a–n/a, c05019. http://dx.doi.org/10.1029/2010JC006402.

RIFE, 2013. Radioactivity in Food and the Environment, 2012, RIFE-18. Tech. rep.. Environment Agency.

RPII, 2012. Radioactivity Monitoring of the Irish Environment 2010-2011. Tech. rep.. Radiological Protection Institute of Ireland.

Salbu, B., Bjørnstad, H., Svaren, I., Prosser, S., Bulman, R., Harvey, B., Lovett, M., 1993. Size distribution of radionuclides in nuclear fuel reprocessing liquids after mixing with seawater. Sci. Total Environ. 130–131, 51–63, 6th International Symposium on Environmental Radiochemical Analysis. http://dx.doi.org/10.1016/0048-9697(93)90059-F.

Salbu, B., Holm, E., 2005. RADIOCHEMICAL METHODS — technetium. In: Worsfold, P., Townshend, A., Poole, C. (Eds.), Encyclopedia of Analytical Science, second ed. Elsevier, Oxford, pp. 24–32. second edition Edition. http://www.sciencedirect.com/science/article/pii/B0123693977005197.

Sündermann, J., Pohlmann, T., 2011. A brief analysis of North Sea physics. Oceanologia 53 (3), 663–689. http://dx.doi.org/10.5697/oc.53-3.663.

Stoke, G.G., 1847. On the theory of oscillatory waves. Trans. Camb. Philos. Soc. 8, 441–455.

Uppala, S.M., Kållberg, P.W., Simmons, A.J., Andrae, U., Bechtold, V.D.C., Fiorino, M., Gibson, J.K., Haseler, J., Hernandez, A., Kelly, G.A., Li, X., Onogi, K., Saarinen, S., Sokka, N., Allan, R.P., Andersson, E., Arpe, K., Balmaseda, M.A., Beljaars, A.C.M., Berg, L.V.D., Bidlot, J., Bormann, N., Caires, S., Chevallier, F., Dethof, A., Dragosavac, M., Fisher, M., Fuentes, M., Hagemann, S., Hólm, E., Hoskins, B.J., Isaksen, L., Janssen, P.A.E.M., Jenne, R., Mcnally, A.P., Mahfouf, J.-F., Morcrette, J.-J., Rayner, N.A., Saunders, R.W., Simon, P., Sterl, A., Trenberth, K.E., Untch, A., Vasiljevic, D., Viterbo, P., Woollen, J., 2005. The ERA-40 re-analysis. Q. J. R. Meteorol. Soc. 131 (612), 2961–3012. http://dx.doi.org/10.1256/qj.04.176.

Viikmäe, B., Torsvik, T., Soomere, T., 2013. Impact of horizontal eddy diffusivity on Lagrangian statistics for coastal pollution from a major marine fairway. Ocean. Dyn. 63 (5), 589–597. http://dx.doi.org/10.1007/s10236-013-0615-3.

Villa, M., López-Gutiérrez, J., Suh, K.-S., Min, B.-I., Periáñez, R., 2015. The behaviour of 129I released from nuclear fuel reprocessing factories in the North Atlantic Ocean and transport to the Arctic assessed from numerical modelling. Mar. Pollut. Bull. 90 (1–2), 15–24. http://www.sciencedirect.com/science/article/pii/S0025326X14007929.

Vries, P., Döös, K., 2001. Calculating Lagrangian trajectories using time-dependent velocity fields. J. Atmos. Ocean. Technol. 18 (6), 1092–1101 http://dx.doi.org/10.1175/1520 0426(2001)018<1092:CLTUTD>2.0.CO;2.

Wei, H., Hainbucher, D., Pohlmann, T., Feng, S., Suendermann, J., 2004. Tidal-induced Lagrangian and Eulerian mean circulation in the Bohai Sea. J. Mar. Syst. 44, 141–151. http://dx.doi.org/10.1016/j.jmarsys.2003.09.007.

Wilks, D., 2011. International Geophysics Series Volume 100. Statistical Methods in the Atmospheric Sciences. Academic Press.

Paper II

Science of the Total Environment 669 (2019) 856–871

Contents lists available at ScienceDirect

Science of the Total Environment

journal homepage: www.elsevier.com/locate/scitotenv

Coastal transport of river-discharged radionuclides: Impact of speciation and transformation processes in numerical model simulations

Magne Simonsen [a,b,*], Ole Christian Lind [b], Øyvind Saetra [a], Pål Erik Isachsen [a,c], Hans-Christian Teien [b], Jon Albretsen [d], Brit Salbu [b]

[a] Norwegian Meteorological Institute, P.O. Box 43, Blindern, Oslo NO-0313, Norway
[b] Centre of Environmental Radioactivity CoE, Faculty of Environmental Sciences and Natural Resource Management, Norwegian University of Life Sciences (NMBU), P.O. Box 5003, NO-1433 Ås, Norway
[c] Department of Geosciences, University of Oslo, P.O. Box 1047, Blindern, NO-0316 Oslo, Norway
[d] Institute of Marine Research, P.O. Box 1870 Nordnes, Bergen NO-5817, Norway

HIGHLIGHTS

- Coastal 137Cs transport simulated with high spatial and temporal resolution model
- The model includes speciation and dynamic transformation processes
- Key factors influencing the overall uncertainty of model output were identified
- Implementing transformation processes enables identifying far field hot spots
- Transformation kinetics simulations recommended also for conservative radionuclides

GRAPHICAL ABSTRACT

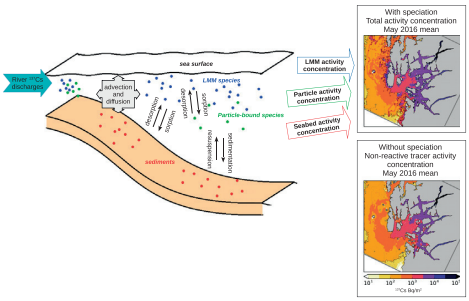

ARTICLE INFO

Article history:
Received 12 October 2018
Received in revised form 15 January 2019
Accepted 16 January 2019
Available online 7 March 2019

Editor: Kevin V. Thomas

Keywords:
Cesium-137 speciation
Hypothetic nuclear accident scenario
River discharges
Lagrangian coastal dispersion model
Dynamic phase interactions

ABSTRACT

Following a potential nuclear accident, river run-off may potentially become a significant source of radionuclide contamination to the coastal marine environment. In the present work, code for radionuclide speciation and dynamic transfer of radionuclides between the different species was implemented in a Lagrangian marine dispersion model. A case study was performed where the model system utilized ocean circulation fields at relatively high spatial (160 m × 160 m in horizontal direction) and temporal resolution (1 hour), considering a hypothetical accident scenario including river discharges of ^{137}Cs to the marine environment. Results from a number of simulations were compared to identify how factors associated with radionuclide speciation and transfer between the model compartments could affect the predicted radiocesium activity concentrations.

The results showed that by including dynamic transfer of radionuclides between the model compartments, the total activity concentrations at far-field sites could vary with more than two orders of magnitude, demonstrating that this model configuration enables prediction of potential local hot-spots. However, the total activity concentration near the river outlets was less affected (< factor 10). The radionuclide speciation in the river discharges and the parameterization of ^{137}Cs particle affinity greatly affected the specie distribution (> factor 10^3 increase in concentration of particle-associated ^{137}Cs) as well as the settling of radionuclides towards the seabed (up to factor 10^2 increase in ^{137}Cs sediment concentrations). These factors were therefore identified as important contributors to the overall uncertainty.

* Corresponding author at: Norwegian Meteorological Institute, P.O. Box 43, Blindern, Oslo NO-0313, Norway.
E-mail address: magnes@met.no (M. Simonsen).

https://doi.org/10.1016/j.scitotenv.2019.01.434
0048-9697/

1. Introduction

A series of sources associated with nuclear weapon and fuel cycles have contributed to radioactive contamination of the marine environment. Examples are fallout from nuclear weapon testing, discharges from reprocessing and power plants, as well as contamination from nuclear accidents. For coastal waters in particular, a significant source is river run-off of radionuclides originating from terrestrially deposited fallout within catchments (Yamagata et al., 1963; Aarkrog, 2003). Such concentrated river sources may cause high contamination levels in estuaries and the coastal zone with potentially harmful consequences for local ecosystems and aquaculture infrastructure.

Radionuclides in the aquatic environment can appear in a broad range of physico-chemical forms (species), ranging from single ions and low molecular mass (LMM) species to species associated with colloids, particles, suspended matter and seabed sediments. The physico-chemical form and transformations of species can have significant impact on the hydrodynamic transport and dispersion which in turn affect the spatial distribution and temporal evolution of the activity concentration levels, as well as on the biological uptake and transfer in the marine ecosystems (Salbu, 2009). Generally, the LMM and colloid-associated radionuclide species are believed to be easily advected by water flow (mobile) and are assumed to be potentially bioavailable. Particle-associated radionuclides are, in contrast, relatively quickly removed from the water column by gravitational settling and less available for pelagic biological uptake (Børretzen and Salbu, 2009).

The distribution of radionuclide species (i.e. speciation) will change over time due to transformation processes or interactions with other components in the system. Such changes are particularly common in the estuarine mixing zone where fresh river water mix with high-saline coastal water, but they can also take place throughout the entire coastal zone. Processes affecting the radionuclide activity concentration of the different species include advection and dispersion with the water masses, sorption and remobilization, hydrolysis and aggregation and sedimentation. LMM species can interact with clay minerals either suspended in the water column or embedded in seabed through reversible and irreversible sorption (physical, electrostatic and chemisorption) processes. On the other hand, LMM species can remobilize from colloids, particles or seabed sediments through desorption due to increased ionic strength and mechanical weathering processes. Colloids act as transporting agents in natural water systems (Kersting et al., 1999; Salbu, 2000; Novikov et al., 2006), especially in the fresh water end member of rivers (Eyrolle and Charmasson, 2004; Lind et al., 2006). In estuaries, however, aggregation of river transported colloids can take place upon mixing with high ionic strength sea water, and associated radionuclides are removed from the water column through particle sedimentation.

Numerical models have proven to be useful in understanding and predicting the transport and fate of radionuclides in the marine environment (e.g., Periáñez et al., 2016a; Simonsen et al., 2017; Vives i Batlle et al., 2018). Clearly, such models can provide important support for impact assessment, e.g. in the acute phase after a severe nuclear accident with atmospheric transport of radionuclides and subsequent deposition in river catchments or directly to the sea water. In model predictions, elements with low affinity to marine sediments, such as tritium, technetium, iodine and cesium, have commonly been assumed to behave conservatively (i.e., non-reactive) and thus interactions between LMM species and solid matter have often been ignored (e.g., Karcher et al., 2004; Orre et al., 2010; Tsumune et al., 2013; Simonsen et al., 2017). As shown by the references above, this might be a reasonable simplification in some long-term studies, but it can also be applied for the purpose of saving computational resources in accident cases when fast response is required (Duffa et al., 2016).

However, especially in cases with long-term contamination, particle processes and especially the role of seabed sediments as temporary reservoirs for radioactive contamination has been found to be significant also for relatively mobile elements (Mitchell et al., 1999; McCubbin et al., 2006; Hunt et al., 2013; Periáñez et al., 2016a). Hence, dynamic water-solid phase interactions seems essential in order to predict the fate of elements interacting with sediments under non-equilibrium conditions (Periáñez et al., 2012; Choi et al., 2013; Min et al., 2013; Vives i Batlle et al., 2018). Particle dynamics also affect the uptake in living organisms since remobilization of radionuclides from sediments contributes to slower reduction in activity concentrations in benthic biota than what has been predicted from only considering the surrounding seawater (Vives i Batlle et al., 2018). Therefore, in recent years, such interactions have more frequently been included in models (Aldridge et al., 2003; Smith et al., 2003; Kobayashi et al., 2007; Choi et al., 2013).

As mentioned, sediment interactions typically take place in the dynamically active coastal zone and in estuaries, and the skill of transport models depends on accurate representation of the ocean currents. For example, Periáñez et al. (2016a) found the variability between different realizations of the hydrodynamic ocean currents to be the largest contributor to discrepancies between transport estimates of the Fukushima discharges. But it is clear that the mechanisms of transfer processes (physico-chemical and biogeochemical processes at interfaces between solid matter, living organisms and groundwater/seawater) are not fully understood and therefore not sufficiently well represented in models (Sanial et al., 2017; Vives i Batlle et al., 2018). Although implementing dynamic sorption kinetics has shown to improve the predictions in particular cases (Choi et al., 2013; Min et al., 2013), it is not clear to what extent inaccuracies in the parameterization of these processes affect the overall uncertainty.

Motivated by these knowledge gaps, the objective of the present study was to investigate the impact of the parameterization of selected key speciation processes on the overall outcome of model predictions of marine radionuclide transport. The present paper deals with coastal dispersion of radionuclides in a complex fjord environment in Boknafjorden, a fjord system in Rogaland county in south-western Norway (Fig. 1), consisting of a number of small and large islands and fjord arms. The extent of the fjord system is around 90 km from the inlet between Karmøy (one of the largest islands in the region) in north-west and Tungeneset in south-west to the deepest fjord arms in the east. The largest depths are around 700 m. The dominating dynamic forces are attributed to wind, tides and density differences between freshwater run-off from rivers and more saline coastal water (Aure and Rey, 1992; Staalstrøm et al., 2013). The tides are relatively weak (maximum spring amplitude is around 50 cm, http://www.sehavniva.no). We considered a hypothetical accident scenario, in which ^{137}Cs originating from Sellafield Nuclear Reprocessing Plant, UK, enters the fjord via river run-off following atmospheric transport from UK and subsequent deposition in catchments. A number of simulations were performed in which the configuration was varied with respect to; 1) either assuming conservative behavior (non-reactive species) or assuming reactive species undergoing dynamic transformation processes, 2) the initial distribution of radionuclide species (physico-chemical form and particle size) in the river discharges and 3) key parameters affecting the transformation of species. By studying the variation in activity concentration fields in the fjord system we aim for an improved intuitive understanding of the interaction between the various physico-chemical and dynamic processes at play.

2. Methods

2.1. Case and source description

Atmospheric transport simulations of a hypothetical accident scenario involving HAL-tanks (Highly Active Liquor) at Sellafield during a storm situation in October 2008 predicted significant atmospheric transport and deposition of radionuclides to south-western parts of

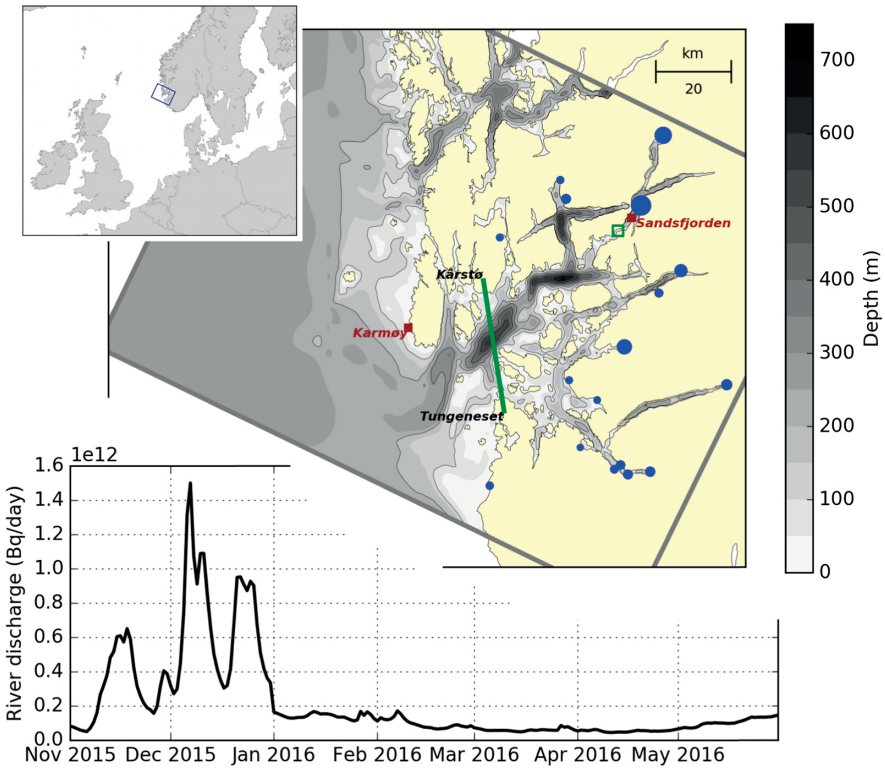

Fig. 1. Overview of the region and time series of the daily total radionuclide discharges from all rivers (inserted). The boundaries of the model domain are shown with grey solid lines. Grey shading is the model depth in meters, where each 100 m is highlighted with a solid line. Blue points are the positions of the rivers, where the area illustrate the relative magnitude of the discharge. For better visualization in this plot, two of the rivers (Åbøelva and Saudavassdraget) are added since their locations appear equal. The red squares indicate the locations where the timeseries are taken and the green square indicate the location of the vertical current profile (Fig. S.4). The green line is the section of which the transport time is computed. (For interpretation of the references to color in this figure legend, the reader is referred to the web version of this article.)

Norway, especially in Rogaland county (Ytre-Eide et al., 2009). Total deposition in this area exceeded 100 kBq m^2. Due to prevailing wind directions, similar situations might occur relatively often, with 40 % probability of deposition at the western coast of Norway in case of accidental atmospheric releases of radionuclides from Sellafield (Klein and Bartnicki, 2018). Much of the deposited ^{137}Cs will be transported by rivers towards the ocean due to hydrological and biogeochemichal processes (such as erosion and snow melting).

Based on the above-mentioned studies, the present paper considers numerical Lagrangian coastal transport simulations of riverine ^{137}Cs discharges in Boknafjorden. The simulations covered a 7 months time period from November 1, 2015 to May 31, 2016 for which the model input of radionuclides was computed from the daily water flow in each of the 18 largest rivers (Fig. 1), contributing to ~ 80 % of the river input to Boknafjorden. Based on regression analysis of suspended matter and water flow rate data in Suldalslågen, the largest of these rivers, (Bogen and Bønsnes, 2004), the daily flux of radionuclides G_s in each individual river was assumed to follow a power function of its daily water flow rate Q:

$$G_s = 0.002172 \times Q^{1.3376593} \quad (1)$$

assuming that the increased erosion and higher particle content at high flow rates increase the total radionuclide concentration in the river water. Thus, the daily total ^{137}Cs concentration in each river changes with the flow rate. Focusing on the extreme situations, the speciation in the river flow was not considered. Instead all radionuclides were assumed to have the same physico-chemical form at initialization. This is a generalized assumption, and in reality, other factors such as tides, wind, waves, snow melt and soil conditions in the catchment area should be expected to affect the discharged radionuclide concentration in each river. According to river transport simulations, activity concentrations ranging from 2000 Bq m^{-3} to 9000 Bq m^{-3} can be expected (Lin et al. Unpublished results) and to account for retention of radiocesium in the upstream catchment area the radionuclide flux was assumed to decay exponentially with 50 % reduction each year (Lin et al. Unpublished results) Time series of the daily sum of the total radionuclide discharge from all rivers is plotted in Fig. 1. The total time-integrated sum of all river discharges was 44 Tbq.

Since the focus in the present study was on the marine transport of riverine ^{137}Cs, radionuclides that potentially could be directly deposited on the ocean surface or originate from any other source were omitted. Furthermore, the activity concentration of ^{137}Cs in the ocean was initially set to zero in the model simulations. Finally, as the interactions involving colloids take place at short time scales in a narrow mixing zone with increasing salinity near the river outlets, these processes were assumed to be exhausted at the time the radionuclides were released into the model. Hence, the colloidal fraction of radiocesium was not included in the simulations, assuming that it is relatively small (Eyrolle and Charmasson, 2004) and exhibits relatively little interaction with the other radionuclide species in the marine environment beyond the mixing zone.

2.2. Model description

2.2.1. Hydrodynamic model

Dynamic ocean circulation fields of the full ocean state were simulated with the open-source Regional Ocean Modeling System (ROMS, see e.g., Shchepetkin and McWilliams (2005), Haidvogel et al. (2008), http://myroms.org) which is a state-of-the-art, three-dimensional, free-surface, hydrostatic, primitive equation ocean model that uses generalized terrain-following s-coordinates in the vertical. The model grid used in the present work covers Boknafjorden and surrounding areas (Fig. 1) with 160 m × 160 m resolution in the horizontal and applies 35 vertical levels. Tides from TPXO7.2 global tidal analysis (Egbert and Erofeeva, 2002) were included. Initial fields were obtained from the 800 m × 800 m resolution model NorKyst-800 (Albretsen et al., 2011) run operationally at the Norwegian Meteorological Institute (http://thredds.met.no). From the 160 m model, a spin-up period of 2 months was performed in advance of the simulation period from November 1, 2015 to May 31, 2016. Daily river flow rates were computed by the HBV model provided by the Norwegian Water Resources and Energy Directorate (Beldring et al., 2003). Atmospheric forcing was provided from AROME MetCoOp (Meteorological Co-operation on Operational Numerical Weather Prediction) 2.5 km, the main forecasting system at the Norwegian Meteorological Institute (Müller et al., 2017). Hydrodynamic forcing on the open boundaries was taken from hourly fields from the NorKyst-800 simulation. ROMS comes with a variety of lateral boundary conditions, including open, closed, and periodic (Marchesiello et al., 2001). The Chapman boundary condition (Chapman, 1985) was used for the free-surface boundary condition and the Flather boundary condition (Flather, 1976) was applied for the barotropic velocity. As described by Marchesiello et al. (2001) and as applied in our model set-up, ROMS has an option for providing radiation conditions on outflow and nudging to a known exterior value on inflow for 3D momentum and tracers. This is implemented as a variation on the radiation condition, requiring two timescales, namely the inflow nudging timescale and the outflow nudging timescale. Here, the nudging on inflow was 120 times larger than on the outflow. For vertical turbulence, the local closure scheme was based on the Generic Length Scale (GLS) parameterization (Umlauf and Burchard, 2003).

Validation of the hydrographical data from the model against available CTD casts taken within the model domain in the simulation period showed good agreement with measured temperature while the model was slightly too saline (Supp. mat. 1).

2.2.2. Lagrangian dispersion model

The dispersion of radionuclides was computed with the Lagrangian trajectory model TRACMASS (Döös et al., 2017), which has been used in a number of previous studies at varying scale (e.g., Döös and Engqvist, 2007; Döös et al., 2011; Nilsson et al., 2013; Viikmäe et al., 2013) and recently in an application with transport of ^{99}Tc radionuclides from the Irish Sea (Simonsen et al., 2017). Using pre-computed velocity fields at 1 hour resolution from the ROMS model, the three-dimensional pathways of the discrete numerical units (hereafter called trajectories) were computed off-line, where the vertical velocity component was computed from the divergence of the horizontal velocities, assuming conservation of mass. Additional vertical turbulent diffusivity was parameterized as a random-walk displacement of the trajectory position as described in detail by Döös et al. (2011). The magnitudes of the displacements were computed applying three dimensional, time dependent fields of the vertical diffusion coefficient from ROMS output. It was assumed no diffusive flux of trajectories through the boundaries (ocean surface and bottom). Except for numerical diffusion in the advection scheme (third-order upstream), no horizontal diffusion was added in the hydrodynamic model. Thus, for lateral transport and dispersion, we relied on the turbulent flow field in the ROMS model and no horizontal diffusion was added in the TRACMASS simulations. The total number of Lagrangian trajectories in each simulation was 88,970.

As a part of the present work, new model code was adapted to TRACMASS for predictions of particle-reactive radionuclide transport. In the present set-up, each trajectory represents a certain amount of radioactivity and is at any time present in one of the five defined model compartments, as illustrated by Fig. 2, representing different physicochemical forms of radionuclides. The low molecular mass (LMM; Fig. 2, compartment 1) species are assumed to be transported passively with the surrounding water masses. Assuming representative particle sizes between 0.45 μm and 63 μm, the radionuclides associated to suspended particles (either reversibly or slowly reversibly bound, Fig. 2, compartments 3 and 5) will sink towards the bottom with a settling velocity w_s determined from Stoke's law (Stokes, 1851);

$$w_s = -\frac{(\rho_s - \rho_w) g d^2}{18\nu} \tag{2}$$

where ρ_s is the particle's density, ρ_w is the density of the water, g is the gravitational acceleration, d is the particle's diameter and ν is the water viscosity. Flocculation effects are assumed to be limited to the freshwater-saltwater interfaces near the river outlets and are therefore not considered in the present study. When particle-associated radionuclides reach the bottom of the deepest water layer due to gravitational settling, they transfer to the sediments (Fig. 2, compartments 4 and 6) where they are preliminary deactivated from further advection. But due to mechanical stress from near-bottom currents, radionuclides associated with sediments will resuspend given that the current speed in the deepest model layer exceed a critical threshold value, v_{crit}. In such cases, the trajectories are reactivated as particle-associated species located in the deepest model layer of the water column. Impact of surface waves on the resuspension was ignored.

The radionuclide transfer between the model compartments was computed with a stochastic approach with probabilistic transfer rates as described by Periáñez and Elliott (2002). For transformation between several possible phases, the stochastic method showed good agreement with finite difference solution (Periáñez and Elliott, 2002). The parameterization of the transfer rates were based on Periáñez (2008), assuming that adsorption of LMM species takes place on a thin surface layer of spherical particles. Although the radioactive half-life for ^{137}Cs ($t_{1/2}$ = 30.17y) is long compared to the simulation time, radioactive decay was adapted similarly to the transformation of species, where the probability for each trajectory to be removed from the simulation during each time step was determined by $t_{1/2}$.

The transfer rate for reversible sorption of LMM species to surfaces of suspended material in the water column was parameterized with

$$k_{13} = D_C K_d m \tag{3}$$

where D_C (s^{-1}) is the desorption coefficient and K_d (m^3 kg^{-1}) is the distribution coefficient, (i.e. the ratio between activity concentration of reversibly particle-bound and dissolved radionuclides under equilibrium conditions). A stationary two dimensional field of the concentration of the fraction of suspended matter available for adsorption (m) was estimated in advance of the radionuclide transport simulations, shown in Fig. S.2. Using TRACMASS, the particles were discharged from the 18 largest rivers as a function of the daily river flow (based on Bogen and Bønsnes (2004) analogous to Eq. (1)), and values in each grid cell was computed as the horizontally smoothed sum of the vertically integrated time-averaged (over a 5-months period) concentration fields from each of three size classes. The particle sizes (diameter 1, 5 and 15 μm, respectively) were assumed to be representative for a realistic range of size classes, with the smallest particles being transported farther away from the sources than the larger particles before settling. A similar approach has been used by Periáñez (2004a, 2005, 2008, 2009, 2012) and Periáñez et al. (2016b). With a minimum value set to 1×10^{-5} kg m^{-3}, the highest particle concentrations exceeded 1×10^{-2} kg m^{-3} in the inner parts of the fjord, while the particle

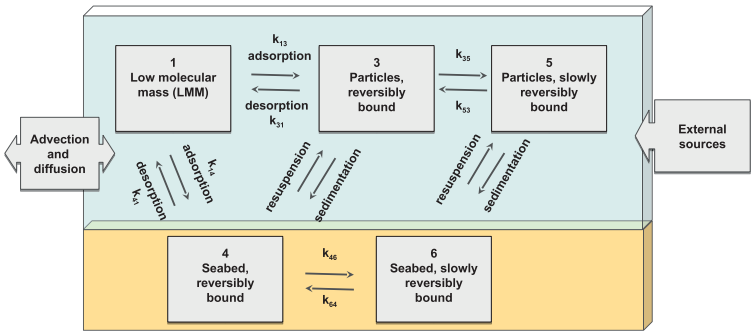

Fig. 2. Model compartments based on radionuclide species categories and interaction pathways. The external sources may vary in time and space and can introduce radionuclides into any of the model compartments. Transformation of LMM species to the seabed is limited to the seabed interaction layer. Advection and diffusion determine the horizontal and vertical transport of radionuclides in the water column.

concentration in the central part of Boknafjorden ranged from 1×10^{-4} kg m^{-3} to 1×10^{-3} kg m^{-3}, generally in agreement with available observed values from Boknafjorden (Johnsen and Dale, 2009) as well as from nearby Norwegian fjords (Brekke and Johnsen, 2006; Sundfjord and Bjerkeng, 2008). Changes in K_d due to salinity changes (Periáñez et al., 2018) was considered to be most relevant at the interface between freshwater and saltwater close to the river outlets. Since smaller changes in salinity were expected further away from the rivers and the uncertainty in such parameterizations are considerable, the K_d dependence on salinity was therefore neglected here.

The transfer rate for sorption of LMM radionuclides to seabed sediments was parameterized as

$$k_{14} = D_C K_d \frac{L\rho(1-p)f\phi}{H}\delta \tag{4}$$

where L is the thickness of the sediment layer which interact with dissolved radionuclides (m), ρ is the density of the sediments (kg m^{-3}), p is the porosity (dimensionless) and H is the thickness of the seabed interaction layer (m). The two dimensionless parameters f and ϕ were included to estimate the available surface for adsorption of radionuclides (Periáñez, 2008), where f is the fraction of small particles in the sediments (diameter 0.45 μm to 63 μm) and ϕ is a correction factor that takes into account that a fraction of sediment particle surfaces may be unavailable for sorption/desorption interactions due to neighboring sediment particles. The logical variable δ ensures that only the radionuclides in the seabed interaction layer were able to sorb to sediments and was set to 1 when the distance to seabed was less than H, and 0 elsewhere.

The desorption rates control the remobilization of LMM species from radionuclides reversibly bound to seabed and suspended particles. Due to the high ionic strength in sea water, the variation between observed desorption rates is small (less than one order of magnitude) compared to the variation in adsorption (Nyffeler et al., 1984). Hence the desorption rate for particle-associated species (k_{31}) was assumed to be a constant (D_C), while the desorption from seabed (k_{41}) was scaled with the correction factor ϕ (Periáñez, 2008):

$$k_{31} = D_C \tag{5}$$

$$k_{41} = \phi D_C. \tag{6}$$

Interactions between the LMM and solid matter species were implemented as two-step functions, with sequentially reversible and slowly reversible/irreversible interactions (Periáñez, 2003, 2004b). The model compartments with slowly reversibly bound species represent radionuclides which were chemically strongly or irreversibly bound to the particle sites as well as radionuclides trapped in the deep sediment layers (Fig. 2, compartments 5 and 6) having relatively long residence time, e.g., clay particles. The rates for transfer to the slowly reversible bound fractions (k_{35} and k_{46}) were set to a constant coefficient D_R (Periáñez, 2004b):

$$k_{35} = D_R \tag{7}$$

$$k_{46} = D_R, \tag{8}$$

while the rates for the reverse transformations (k_{53} and k_{64}) were assumed to be ten times slower (Børretzen and Salbu, 2000, 2002; Periáñez, 2004b):

$$k_{53} = D_R/10 \tag{9}$$

$$k_{64} = D_R/10. \tag{10}$$

In reality, the parameters in Eq. (2)–(10) can be expected to be heterogeneously distributed, and sediment properties such as layering and physical and chemical features might affect the results (Maderich et al., 2017). Without local measurements, the parameters used in the present study were taken from available literature data, assumed to be uniform in the model domain, as listed in Table 1.

2.3. Model simulations

A number of simulations with slightly different configurations (physico-chemical form in the river input and parameterization of the interactions between the species) were performed, as summarized in Table 2. Then, to quantify the impact of each key factor, results from the simulations were compared to each other, one by one, as listed in Table 3. First, a simplified base-line simulation was performed where all radionuclides were released as neutral non-reactive LMM species and no interactions with suspended particles and seabed sediments took place (ph1-nr). To investigate the impact of including speciation and particle interactions, another simulation (ph1) was performed, in which interactions were enabled, the default parameters (Table 1) were applied and all ^{137}Cs radionuclides were released as reactive (positively charged) LMM species. The results from simulation ph1 was compared with the simplified simulation (ph1-nr).

To investigate the impact of the variations in the initial specie distribution, two simulations were performed; one where all radionuclides were released as reversibly bound to particles (ph3) and one where the radionuclides were released as slowly reversibly or irreversibly bound to particles (ph5). Results from each of the two simulations were compared to the results from simulation ph1.

Table 1
Default parameters.

Parameter	Value	Reference
Desorption rate	$D_C = 1.16 \times 10^{-5}\ s^{-1}$	Nyffeler et al. (1984)
Slowly reversible/irreversible interaction coefficient	$D_R = 1.2 \times 10^{-7}\ s^{-1}$	Periáñez (2004b), Periáñez et al. (2013)
Distribution coefficient for Cs	$K_d = 2.0\ m^3\ kg^{-1}$	IAEA (2004)
Particle density	$\rho_s = 2600\ kg\ m^{-3}$	e.g., Periáñez (2004a), Periáñez (2008)
Particle diameter	$d = 5\ \mu m$	
Sediment mixing depth	$L = 0.1\ m$	Periáñez (2008)
Fraction of effective sorbents	$f = 0.90$	Periáñez (2008)
Sediment correction factor	$\phi = 0.1$	Periáñez et al. (2013)
Sediment porosity	$p = 0.6$	Periáñez (2008)
Thickness of seabed interaction layer	$H = 1\ m$	Kobayashi et al. (2007), Periáñez and Elliott (2002)
Horizontal diffusivity	$A_h = 0\ m^2\ s^{-1}$	
Critical current speed for resuspension	$v_{crit} = 0.1\ m\ s^{-1}$	

The effect of variable particle size was investigated using results from two simulations in which the particle size was decreased to 1 μm (ph5-S) and increased to 10 μm (ph5-L), respectively. Results from each of these two simulations were compared to the results from simulation ph5, in which the default particle size (5 μm) was used. In all of these three simulations, the radionuclides were initially slowly reversibly bound to particles.

The impact of the slowly reversible interaction parameter D_R was investigated by performing another simulation (ph5-iDR) where the radionuclides were released as slowly reversibly bound species but the value of D_R was increased. Results from this simulation were compared to simulation ph5.

Finally, the sensitivity to the sorption parameters was studied by performing a simulation in which K_d was increased and D_C was decreased (ph1-Sorp). This simulation was compared to the simulation using default sorption parameters (ph1). In addition, one simulation with only increased K_d (ph1-iKd) and another simulation with only reduced D_C (ph1-rDc) were individually compared to the simulation using default parameters (ph1).

3. Results and discussion

3.1. Impacts of speciation changes

To illustrate traditional simulations of non-reactive radionuclides with low affinity to solid matter, a simplified simulation was performed

Table 2
Configuration of the simulations.

Simulation name	Physico-chemical form of ^{137}Cs from external sources (river discharge)	Deviation from default parameters (Table 1)
ph1-nr	LMM	Speciation and interactions neglected
ph1	LMM	None
ph3	Reversibly bound to particles	None
ph5	Slowly reversibly bound to particles	None
ph5-S	Slowly reversibly bound to particles	Particle diameter decreased to 1 μm
ph5-L	Slowly reversibly bound to particles	Particle diameter increased to 10 μm
ph5-iDR	Slowly reversibly bound to particles	D_R increased to $3.5 \times 10^{-6}\ s^{-1}$
ph1-Sorp	LMM	K_d increased to $150\ m^3\ kg^{-1}$, D_C decreased to $5.8 \times 10^{-7}\ s^{-1}$
ph1-iKd	LMM	K_d increased to $150\ m^3\ kg^{-1}$
ph1-rDc	LMM	D_C decreased to $2.3 \times 10^{-6}\ s^{-1}$

Table 3
Simulation comparisons.

Investigated key factor	Simulations	Deviating configurations
Enabling transformation processes	ph1, ph1-nr	Reactive and non-reactive
Speciation in river discharges	ph3, ph1	Initially reversibly bound species and initially LMM species
Speciation in river discharges	ph5, ph1	Initially slowly reversibly bound species and initially LMM species
Particle size	ph5-S, ph5	Small particles and default particle size
Particle size	ph5-L, ph5	Large particles and default particle size
Slowly reversible interaction coefficient	ph5-iDR, ph5	Increased D_R and default D_R
Sorption coefficients	ph1-Sorp, ph1	Increased K_d and decreased D_C and default sorption parameters
Sorption coefficients	ph1-iKd, ph1	Increased K_d and default sorption parameters
Sorption coefficients	ph1-rDc, ph1	Decreased D_C and default sorption parameters

(ph1-nr, Table 2) where non-reactive radionuclide properties were applied to the river discharges in Boknafjorden. In the present work, we contend that even though colloidal interactions were neglected, this simulation can also be interpreted as a simulation of colloids behaving conservatively, assuming that the changes in the colloidal fraction were small beyond the mixing zone near the river outlets (Eyrolle and Charmasson, 2004).

Fig. 3a–c shows the time evolution of horizontal distribution of surface activity concentration from this simulation (ph1-nr, non-reactive). In our hypothetical discharge scenario, the highest river discharges of ^{137}Cs were in November and December 2015, with relatively low and steady discharges from January to May 2016 (Fig. 1). Since the water masses were considered to be uncontaminated at the beginning of the simulation, the inventory of radionuclides in Boknafjorden increased rapidly the first months, whereas it generally decreased slowly in the rest of the simulation. The highest activity concentration levels were predicted near the largest river outlets in Sandsfjorden and reached 2500 Bq m^{-3} in the February mean (Fig. 3b), with generally lower activity concentrations in November (Fig. 3a) and May (Fig. 3c).

In general, and partly due to the Coriolis acceleration, the radionuclides followed the major transport route out of Boknafjorden on the northern side of the bay (as indicated by the surface currents plotted in Fig. S.2). However, since the variability in the flow pattern is large and the mobile radionuclides were spread over the entire fjord system by the flow fluctuations, there was in general a gradually decrease in the activity concentration levels with distance from the river outlets in all time periods. Most of the radionuclides that left Boknafjorden were entrained into the Norwegian Coastal Current, which flows northward along the western coast of Norway. Hence, the activity concentration was higher around Karmøy and in the coastal area north of Boknafjorden than in the southern area in all time periods shown in Fig. 3.

To investigate the impact of including solid matter interactions in the transport simulations, we compared results from the simulation where transformation of species was enabled (ph1, Table 2) with the results from the simplified simulation of non-reactive species (ph1-nr). In both simulations, all radionuclides were released as LMM species. Fig. 3d–f shows that simulation ph1 in general predicted lower activity concentration of the LMM fraction than the simulation of non-reactive species in all time periods. But the activity concentration was only slightly lower, mostly a factor 2 or less. Thus, in agreement with Periáñez et al. (2016a), the activity concentration of the LMM fraction was not much affected by including interactions between species.

The effect of enabling transformation of species was small also for the fraction associated with suspended particles (figure not shown). This can largely be attributed to the time scales of the transfer rates achieved when utilizing the default parameters (Table 1), which were

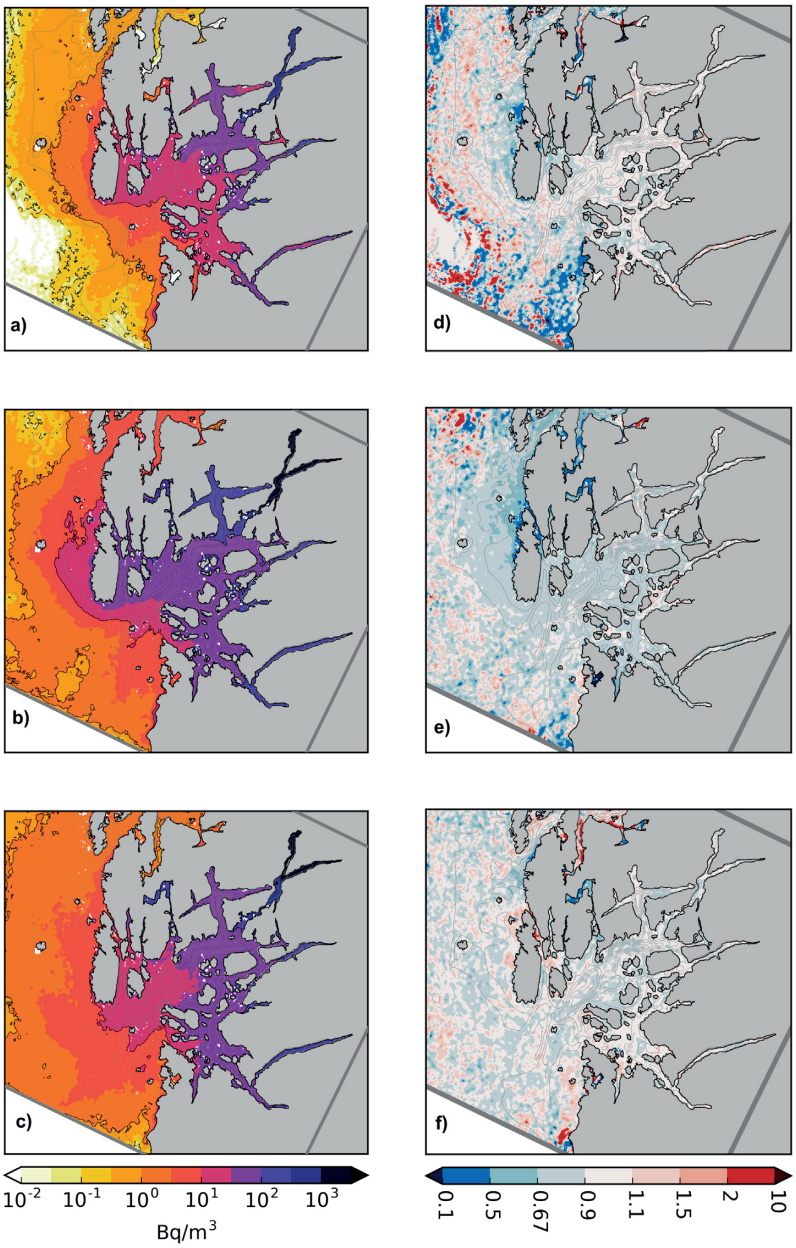

Fig. 3. Activity concentration of ^{137}Cs from the simulation of non-reactive LMM species (ph1-nr, panels a–c) and ratio of activity concentration between reactive LMM species from simulation ph1 and non-reactive LMM species from simulation ph1-nr (panels d–f). Average values for November 2015 (top), February 2016 (middle) and May 2016 (bottom) were integrated over the upper 50 m of the water column, horizontally smoothed over six grid points in each direction, assumed to represent the surface mixed layer.

much shorter for desorption (1 day, Table S.1) than for adsorption (typically 500 days). Only 1 % of the total activity was associated to the particles at the end of simulation ph1, in agreement with Periáñez et al. (2016b), which estimated less than 2 % of ^{137}Cs to be adsorbed on suspended particle surfaces in the open North Atlantic Ocean.

From Eq. (3), the sorption, and hence the results of the particle-associated fraction, were affected by our assumptions regarding the suspended matter concentration *m*, being stationary and vertically uniform. In reality, *m* will certainly vary both in time and in the vertical. As these small-scale processes were not expected to be resolved properly by our model, we considered the horizontal variations to be most important at the time scales involved.

Although the fractions of radionuclides associated with LMM and particle species were only slightly affected, the total activity concentration of ^{137}Cs as the sum of all species changed dramatically when including speciation and interactions in the simulations. While the fraction of ^{137}Cs in the seabed sediments was neglected in simulation ph1-nr, Fig. 4 reveals that a considerable part of the radionuclides in simulation ph1

was bound to seabed sediments in May 2016. With a heterogeneously distributed pattern, the activity concentration in the sediments locally exceeded 10^4 Bq m^{-2} in some hot-spots (Fig. 4a). Since the sorption of LMM species to the sediments was restricted to the seabed interaction layer (by δ in Eq. (4)), and the sorption (0.05 days, Table S.1) had a shorter time scale than the desorption (10 days), the accumulation of radionuclides in the sediments was predominant in shallow waters and areas where the radionuclides were efficiently mixed down into the deepest water layers. Hence, the highest activity concentrations in the sediments were found near river outlets and in shallow areas along the main transport paths where the LMM activity concentration was high. This difference is illustrated by the time series of the depth-integrated activity concentration from Sandnesfjorden and Karmøy (Fig. S.3). At Sandsfjorden where the water is relatively deep (Fig. S.3a), the majority (>90 %) of the ^{137}Cs was present as LMM species in simulation ph1 and the differences between the simulations were small. At the far-field location close to Karmøy, however, where the water is shallower and a higher fraction (>90 %) of the radionuclides was associated with sediments in simulation ph1, the sum of activity concentration in all species was around a factor 20 higher than in the simplified simulation (Fig. S.3b). Obviously, the radionuclides accumulated in the sediments did also impact the overall fjord inventory as well as the total activity concentration, which in May 2016 (Fig. 4b) was more than two orders of magnitude higher in simulation ph1 than in ph1-nr in the most contaminated areas.

Considerations of the sediment-bound radionuclide fraction which was neglected in the simplified simulation (ph1-nr) is important mainly for two reasons. First, the capability of the model used in the present work to predict uneven distributions of ^{137}Cs in sediment inventory is largely attributed to the relatively high resolution in the hydrodynamic model. Although more complex sedimentation models exist (e.g., Maderich et al., 2017), in the present simulations, we have used a relative simple approach with a single sediment layer. The seabed property parameters in Eq. (4) were assumed to be uniformly distributed and were chosen according to available literature (Table 1). In reality, the environmental properties such as lithology, grain size, porosity and mixing depth change both spatially and temporally. In addition, variable roughness in the ocean bottom terrain may cause large variations in the activity concentrations over short distance (Thornton et al., 2013; Black and Buesseler, 2014). However, we consider the errors associated with the seabed properties to be minor compared to the variability in other factors. The largest variability is expected to appear in D_R, D_C and K_d, for which we have tested the impact. Smaller variations can be expected also in ρ_s, L, f, ϕ, p and H, which in total probably might impact the results with less than a factor 2–10. A refined description of these parameters should improve the model predictions regarding the distribution of the sediment-bound radionuclides, however applicable measurements would require considerable effort. This will in turn have implications for dose assessment, especially for benthic organisms, which can be sensitive to high radioactive exposure in the seabed (Salbu et al., 2004; Vives i Batlle et al., 2018).

Secondly, remobilization of radionuclides from the sediments can potentially impact the activity concentration of LMM species on longer term. The sediments are expected to act as a temporary reservoir and subsequently as a diffuse source for the radionuclides, effectively delaying the dispersion (Mitchell et al., 1999; AMAP, 2004; Choi et al., 2013; Hunt et al., 2013; Sanial et al., 2017). Therefore, although the impact on the LMM species was small over the time scales considered in the present simulation, in extended simulations (years to decades), we can expect larger impacts by including transformation processes also for the radionuclides present as LMM species. At shorter time scales, however, as in this study, the dominating effect obtained by enabling the speciation and specie interactions in simulations of elements such as cesium is sorption to the sediments giving rise to increased total activity concentration.

3.2. Impact of speciation in the river discharge

The simulations compared in Section 3.1 were based on scenarios in which ^{137}Cs was discharged entirely as LMM species, interacting with particles with a fixed particle size. However, radionuclides in the real environment are typically present in a variety of physicochemical forms, where the particle-bound species are associated with suspended matter covering a continuous size distribution. In the present section, we therefore investigate how some other possible discharge scenarios (Table 2) would affect the predicted activity concentration levels. Although it is not likely that all radionuclides are bound to particles in a real discharge, a considerable fraction of the radionuclides may be strongly associated with particles, e.g., clay particles (Yamasaki et al., 2016). Such scenarios are therefore relevant for investigation of the behavior of the fraction of radionuclides which is bound to particles.

3.2.1. Reversible and slowly reversible particle binding

Utilizing the default set of parameters (Table 1), the reversibly particle-bound radionuclides desorb rapidly to LMM species (time

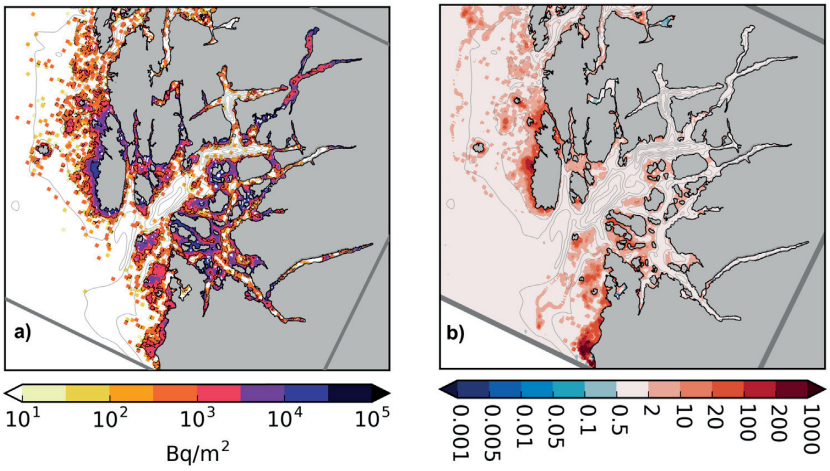

Fig. 4. Activity concentration of sediment-bound ^{137}Cs (sum of reversibly and slowly reversibly bound) from simulation ph1 (reactive), averaged over May 2016 (a). Ratio between total activity concentration from simulation ph1 (reactive) and the simplified simulation (ph1-nr, non-reactive), averaged over May 2016 (b).

scale 1 day). Hence, the only notable differences between the results from the simulation with discharges as LMM species (ph1) and the simulation with discharges as reversibly particle-bound species (ph3) were slightly higher activity concentrations for the particle-bound fraction and correspondingly reduced activity concentrations for the LMM fraction near the river outlets shortly after the largest discharges. But further away from the sources, and when the discharges were low, the results from these two simulations were hardly distinguishable (figure not shown).

In contrast to the rapid remobilization of radionuclides reversibly bound to particles, the time scales of the remobilization from the slowly reversibly bound species was long (965 days) and therefore had strong impact on the speciation throughout the whole simulation. This can be seen in the time series of the total volume-integrated activity in each specie in the whole domain from simulation ph1 (Fig. 5a) and simulation ph5 (Fig. 5b). While the LMM fraction was dominating through the whole time period in simulation ph1, most ^{137}Cs was slowly reversibly bound to particles in the early part of simulation ph5, until the particles reached bottom and the activity was transferred to sediments. At the end of simulation ph5, the major part (around 70 %) of the radionuclides were slowly reversibly bound to sediments, while only a minor part were associated with the LMM phase.

Comparison of the surface activity concentration of LMM species (Fig. 6b) shows that the activity concentration in simulation ph5 was around one order of magnitude lower than in simulation ph1, relatively evenly distributed over the domain. In contrast, while the surface particle-associated fraction was minor in simulation ph1, the major part of the radionuclides in simulation ph5 were associated with particles. The activity concentration of the particle-associated species was more than three orders of magnitude higher in simulation ph5 than in

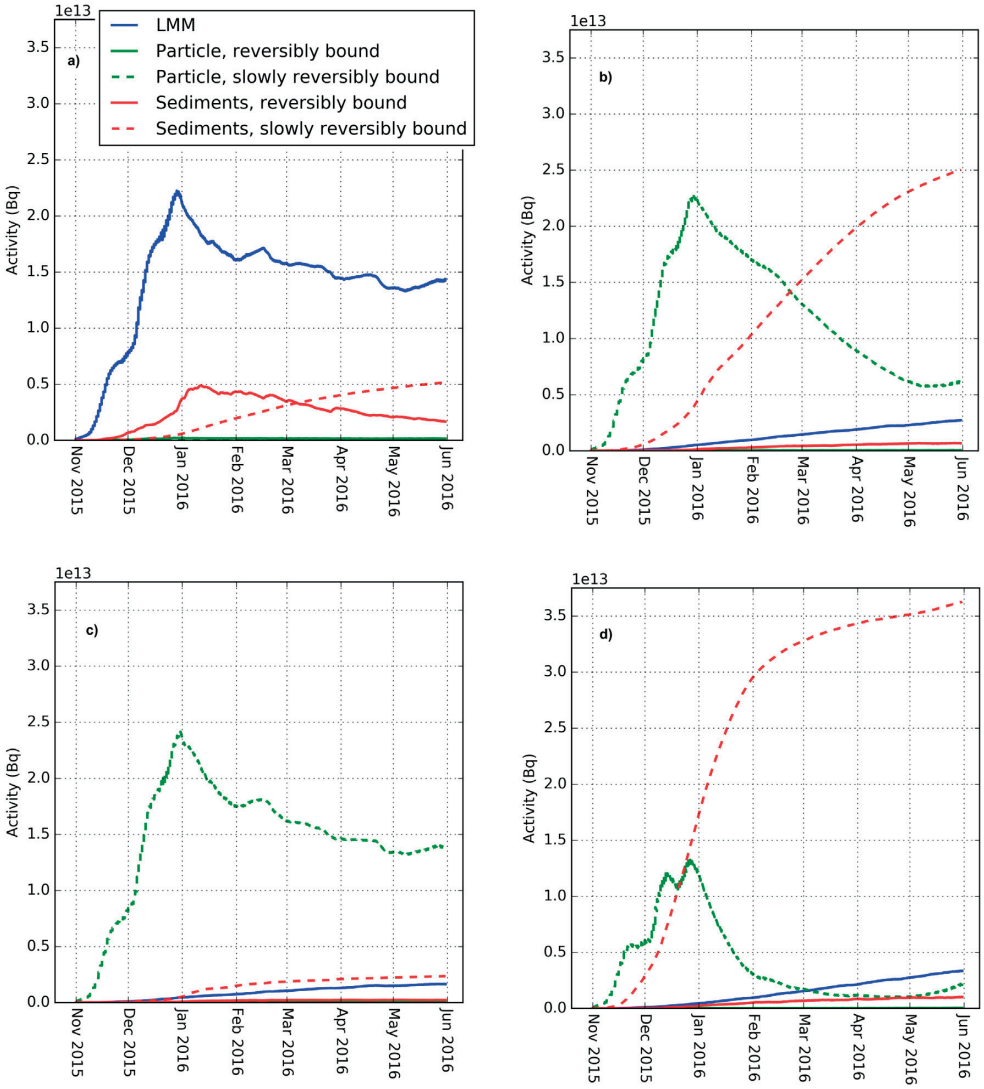

Fig. 5. Time series of the total radioactivity in the whole domain in each of the species from the simulation where the ^{137}Cs radionuclides were discharged as reactive LMM species (ph1, a), as species slowly reversibly bound to medium-size particles (ph5, b), as species slowly reversibly bound to small-size particles (ph5-S, c) and as species slowly reversibly bound to large-size particles (ph5-L, d).

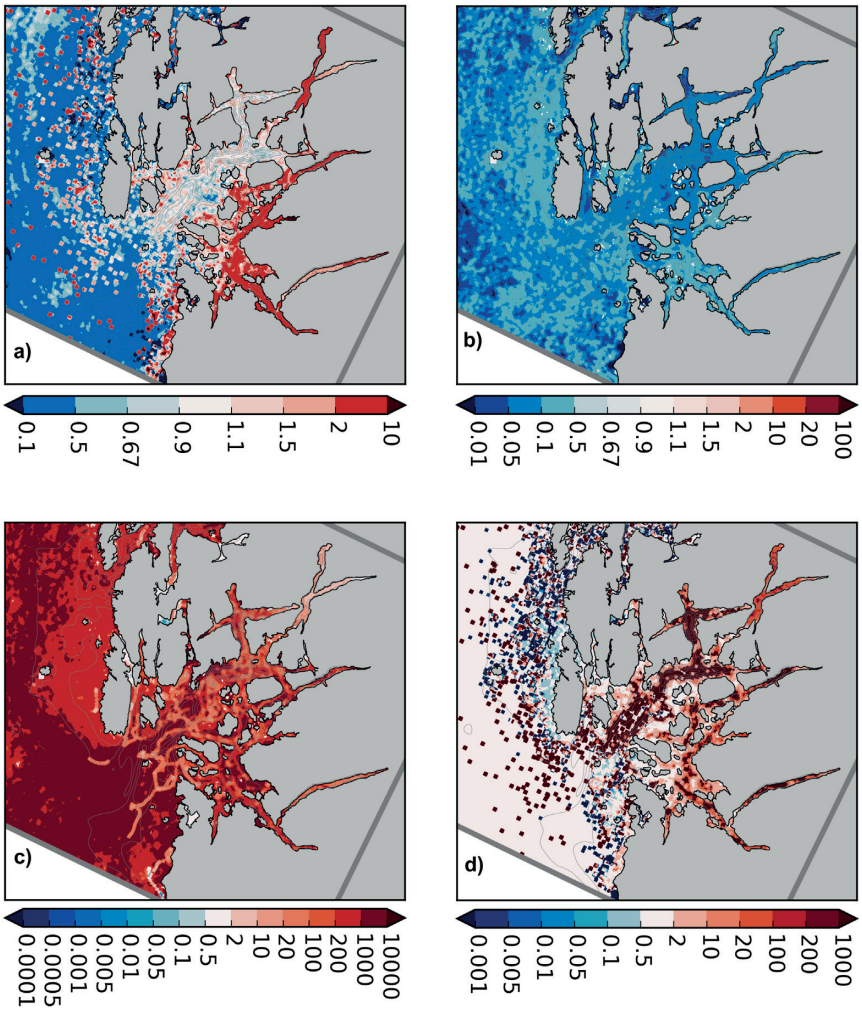

Fig. 6. Ratio of predicted May 2016 averaged total depth-integrated activity concentration (a), the upper 50 m LMM fraction (b), the upper 50 m particle-associated fraction (c) and the sediment-bound fraction (d) between simulation ph5 (^{137}Cs radionuclides discharged as slowly reversibly bound to particles) and simulation ph1 (discharges as LMM species). Note different color scales for each panel. (For interpretation of the references to color in this figure legend, the reader is referred to the web version of this article.)

ph1 at locations far away from the river outlets (Fig. 6c). In fact, as an artificial consequence of the finite number of trajectories used in our Lagrangian calculations, the ratio went towards infinity where the activity concentration in ph1 was close to zero.

In simulation ph1, the transfer to sediments was mainly driven by chemi-sorption of LMM species to the surface of the bottom sediments, which favored shallow regions (Fig. 4). In contrast, the dominating process for transfer of radionuclides to seabed sediments in simulation ph5 was mechanical settling and sedimentation of particles, which generally was more uniformly distributed over the domain, independent of depth, however with enhanced settling near the river outlets. Hence, compared with simulation ph1, the activity concentration of the sediment fraction of ^{137}Cs in simulation ph5 was more than two orders of magnitude higher in the deeper parts of the fjord and near the river outlets (Fig. 6d). In the shallow areas around Karmøy where the adsorption to sediments was high in simulation ph1, the activity concentration of the sediment fraction was slightly lower in simulation ph5 than in ph1 (less than one order of magnitude). The sum of the depth-integrated activity concentration in all species (Fig. 6a) reveals that the increased sedimentation in simulation ph5 increased the exposure in the inner part of Boknafjorden with up to a factor 10, while there was a factor 10 lower total activity concentration in the outer part of the fjord and in the open ocean, compared with simulation ph1, in which the radionuclides were more mobile.

This last result can be explained by the vertical shear in the currents in Sandsfjorden, having the largest radionuclide discharges in the region, which are characterized by strong currents out of the fjord in the surface layer, a return current into the fjord in the mid-layer and weaker currents towards the bottom (Staalstrøm et al., 2013). This was also clearly reproduced by the ocean model, illustrated in depth profiles of time-averaged current components along and across the main orientation of the narrow sound out of Sandsfjorden in Fig. S.4. Hence, radionuclides in the surface layer, such as the LMM species in simulation ph1, were quickly transported out to the central part of Boknafjorden, while radionuclides in deeper

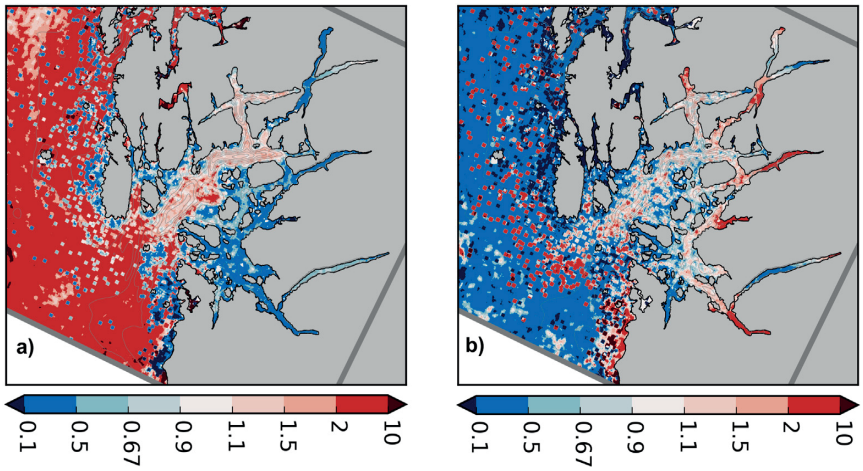

Fig. 7. Ratio of May 2016 total depth-integrated activity concentration between simulation ph5-S (^{137}Cs radionuclides discharged as slowly reversibly bound to small particles) and simulation ph5 (discharges as intermediate size particles) (a), and ratio of predicted total depth-integrated activity concentration between simulation ph5-L (^{137}Cs radionuclides discharged as slowly reversibly bound to large particles) and simulation ph5 (discharges as intermediate size particles) (b).

water masses, such as the particle-associated species in ph5, remained longer near the sources.

3.2.2. Particle size

For the above calculations, we have used constant diameter for all particles, for which the settling velocity determined by Stoke's law (Eq. (2)) is identical for all particle-bound radionuclides. To qualitatively study the impact of different particle sizes, the simulation using default parameters (d = 5 μm, ph5) was compared with simulations with smaller (1 μm, ph5-S) and larger (10 μm, ph5-L) (Table 2) particles, respectively.

The impact of the particle size on the settling can be illustrated by the time it will take for a particle to sink 200 m, a typical depth in Boknafjorden, according to Stoke's law (Eq. (2)). Of course, other factors such as horizontal and vertical advection and turbulent mixing will also affect the predicted sedimentation independently for each individual trajectory. But Stoke's settling is a systematic process affecting the statistical mean behavior. The largest and the intermediate particles can be expected to use 27 and 108 days to settle to the seabed, respectively, which both are within the simulation time period. On the other hand, the smaller particles will never reach bottom during our simulation period with a settling time of 2700 days.

The time series of the speciation in Fig. 5 reveal that the particle size clearly affected the distribution of the radionuclides between the fractions associated with suspended particles and sediments in the whole domain. In the simulation with the smaller particles (Fig. 5c), the majority of the radionuclides remained slowly reversibly bound to suspended particles throughout the whole simulation, with only a small fraction (<15 %) transferred to the sediments. In the simulation with intermediate and large particle size (Fig. 5b and d, respectively), there was an extensive sedimentation and the fraction of radionuclides which were slowly reversibly bound to the seabed sediments increased to ~ 70 % and ~ 80 % in the two simulations, respectively. Furthermore, as expected from the time scales of the transfer rates, the fraction of radionuclides present as LMM species was minor (<10 %) in all simulations.

As a result of the changed settling obtained by changing the particle size, the vertical distribution of the radionuclides was also changed. As expected, smaller particles increased the radionuclide concentration near the surface, while the larger particles sank into the deeper water masses. Since the strongest currents out of Sandsfjorden generally are located near the surface (Fig. S.4), the radionuclides in the simulation with small particles were characterized by high mobility and were therefore flushed more efficiently away from the river outlets towards the far-field regions. This effect can clearly be seen in Fig. 7, where the near-shore activity concentration was lower (> factor 10) in the simulation with small particles (ph5-S) than in the simulation with intermediate particles (ph5), while the activity concentration in the far-field was higher (< factor 10, Fig. 7a). In contrast, the larger particles in simulation ph5-L sank rapidly into the less energetic currents and became immobile as they settled in the sediments near the sources. This resulted in higher near-shore radionuclide exposure (<factor 10) and lower far-field activity concentration (Fig. 7b).

3.2.3. The slowly reversible interaction parameter

The above presented results in Section 3.2 showed that because of the long time scales of the mobilization from the slowly reversibly bound fractions, there were few transformations between the model compartments, except for sedimentation. Therefore, a new simulation was performed, in which the slowly reversible interaction coefficient D_R was increased with almost a factor 30 to a value derived from laboratory experiments for cesium (Børretzen and Salbu, 2002) (simulation ph5-iDR, see Table 2).

Comparison of the simulation with increased D_R (ph5-iDR) with the simulation using default parameter values (ph5) is shown in Fig. 8 as time series of depth-integrated activity concentration from Sandsfjorden and Karmøy. With a time scale of 33 days for transfer of radionuclides which were slowly reversibly bound to particles (k_{53} and k_{64}), the mobilization of slowly reversible species increased in simulation ph5-iDR. The time scale of the reverse transformation (k_{35} and k_{46}; 3.3 days) was still longer than the time scale of the remobilization of reversibly particle-bound species to LMM species (1 day). So radionuclides which were reversibly bound to particles would prefer continuing to LMM species rather than returning to the slowly reversibly bound species. Therefore, as could be expected, the fraction of radionuclides associated with the LLM species increased at Sandsfjorden (factor 5), while the particle- and sediment associated species decreased (factor 2 and factor 3, respectively). A similar pattern could be seen in the entire domain (figure not shown), where the activity concentration in the LMM species was around a factor 10 higher in simulation ph5-iDR than in simulation ph5. Since more radionuclides remobilized to the LMM species before they reached bottom, the sedimentation was

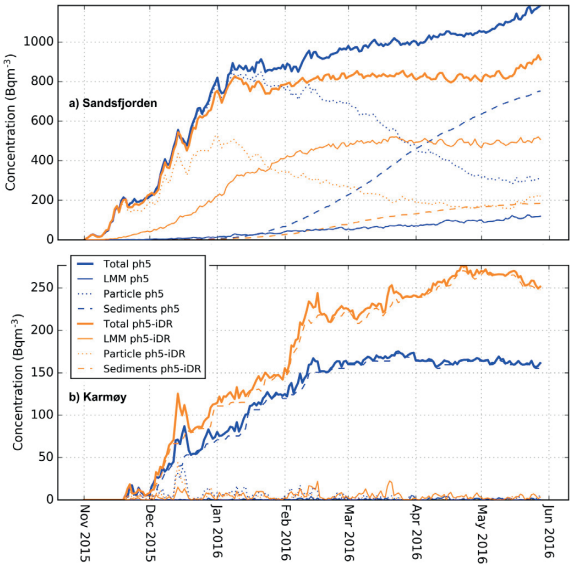

Fig. 8. Time series from Sandsfjorden (a) and Karmøy (b) (see locations in Fig. 1) of the LMM fraction (thin solid lines), the particle-bound fraction (dotted lines) and the sediment-bound fraction (dashed lines) of the total ^{137}Cs activity concentration (thick solid lines), from simulation ph5 (default D_R value, blue), and simulation ph5-iDR (increased D_R value, orange), integrated over the full water depth, computed from boxes at 2.1 km× 2.1 km around each location. In both simulations, the ^{137}Cs radionulcides were released as slowly reversibly bound to particles. (For interpretation of the references to color in this figure legend, the reader is referred to the web version of this article.)

reduced, mostly in the deepest areas, but it was still extensive, which also can be seen from the time series from Sandsfjorden.

With increased D_R, the total activity concentration at Sandsfjorden decreased with roughly 10 %, compared with simulation ph5. This is consistent with the higher mobility of the LMM species. Due to more radionuclides remaining in the strong surface currents, there was a higher transport away from the river outlets. At the same time, the increased activity in the LMM fraction increased the sorption to the sediments in shallow areas, as illustrated by the time series from Karmøy (Fig. 8b) where the sediment inventory increased with 50 %. Therefore, in addition to increased remobilization from the particle-associated species, increasing the slowly reversible interaction parameter D_R also resulted in lateral redistribution of the sediment-bound ^{137}Cs radionuclides, which moved from large depths to shallower areas.

3.3. Sensitivity to the sorption parameters

The results presented in Section 3.2 showed that due to the rapid desorption of the radionuclides reversibly bound to particles while using the default parameters (Table 1), the results were quite insensitive to the initial distribution between radionuclides reversibly bound to particles and LMM species. This picture was radically changed when the ^{137}Cs radionuclides were released as slowly reversibly bound species in simulation ph5, in which the radionuclides essentially remained slowly reversibly bound to particles and sediments throughout the simulation period. Even though increasing the slowly reversible parameter (Section 3.2.3) enhanced the fraction of mobilized LMM species, the reversibly bound species were less impacted. Many factors such as non-equilibrium conditions, mixing of reversibly and slowly reversibly bound species and changing environmental factors (pH and salinity) affect the K_d measurements (Periáñez et al., 2018). To investigate if it is at all possible to end up with a higher fraction of reversibly bound species, we increased the adsorption (increased K_d with a factor 75) and reduced the desorption (decreased D_C with a factor 20) to values derived from laboratory experiments by Børretzen and Salbu (2000, 2002) (simulation ph1-Sorp, Table 2). These new values are in the high range for Cs in water with low salinity, but can represent other more particle-reactive elements such as cobalt, plutonium and americium in marine environment (IAEA, 2004).

Comparison of this new simulation with increased sorption (ph1-Sorp) with the simulation using default parameters (ph1) is shown in Fig. 9 as time series of depth-integrated activity concentration from Sandsfjorden. As expected, the particle-associated fraction is high in simulation ph1-Sorp (increasing to around 70 % of the total activity in February), in contrast to the simulation with low K_d (ph1), in which only a few percent was particle-bound. With longer residence time in the reversibly bound fraction before remobilization, the transport of radionuclides which were reversibly bound to particles played a more important role for the marine dispersion of radioactive contaminants than was the case in the previous simulations.

The LMM fraction, which was dominating (steady above 90 %) in the simulation with low K_d (ph1) was now reduced to less than 20 % in the end of simulation ph1-Sorp. Due to the increased affinity to particles, the mechanical settling and sedimentation process was extensive in simulation ph1-Sorp, while it was basically non-existing in the simulation with low K_d. This can be seen from the time series of the sediment-bound fraction (Fig. 9), which increased monotonically from less than 10 % in February until around 50 % in the end of May. The increased sorption in simulation ph1-Sorp had minor impact on the adsorption to seabed sediments, since the time scale of this process already was very short. Most of the radionuclides in the LMM fraction that entered the seabed interaction layer would adsorb to the sediments anyway, and the increase in the sediment-bound fraction can be explained by enhanced sedimentation rather than higher adsorption.

Again, since the strongest currents are located near the surface (Fig. S.4), the increased settling and deeper distribution of the radionuclides reduced the horizontal transport away from the river outlets. The total activity concentration at Sandsfjorden was thus higher in ph1-Sorp than in ph1 (thick solid lines in Fig. 9), increasing from 20 % higher in January to around 70 % higher in the end of the simulation period. Hence, the increased K_d did not only redistribute the radionuclides between the different species and increased the settling, but also shifted

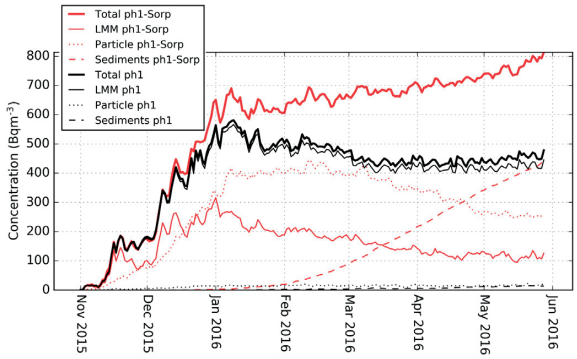

Fig. 9. Time series from Sandsfjorden (see location in Fig. 1) of the LMM fraction (thin solid lines), the particle-bound fraction (dotted lines) and the sediment-bound fraction (dashed lines) of the total ^{137}Cs activity concentration (thick solid lines), from simulation ph1 (default parameters, black), and simulation ph1-Sorp (adjusted sorption coefficients, red), integrated over the full water depth, computed from boxes at 2.1 km × 2.1 km around the location. In both simulations, the ^{137}Cs radionuclides were released as LMM species. (For interpretation of the references to color in this figure legend, the reader is referred to the web version of this article.)

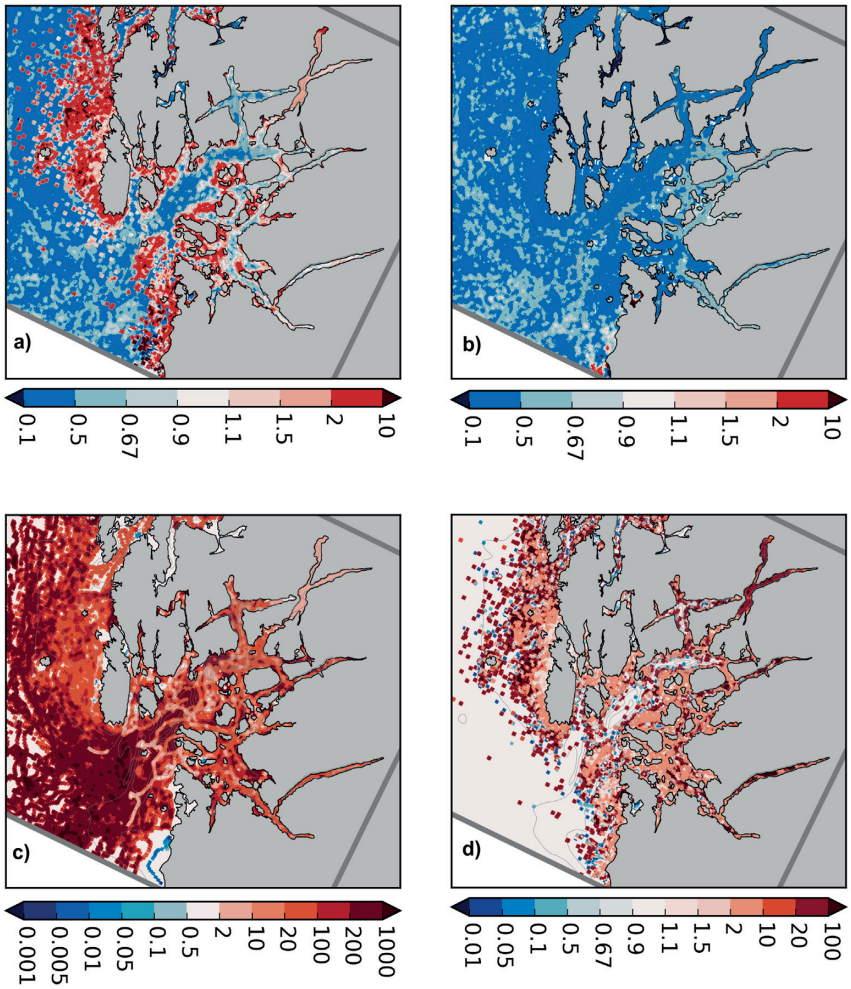

Fig. 10. Ratio of predicted May 2016 total depth-integrated activity concentration (a), the upper 50 m LMM fraction (b), the upper 50 m particle-associated fraction (c) and sediment-bound fraction (d) between simulation ph1-Sorp (adjusted sorption coefficients) and simulation ph1 (default parameters). Note different color scales for each panel. (For interpretation of the references to color in this figure legend, the reader is referred to the web version of this article.)

the lateral distribution of the contamination as shown in Fig. 10. As seen from Fig. 10a, the total depth-integrated activity concentration in ph1-Sorp increased mostly in the shallow water and near the largest river outlets compared to simulation ph1, while it decreased at more remote locations and in the deeper parts of the region, with variations within a factor 10 in each direction. In agreement with the changed speciation in the predictions at Sandsfjorden, there was up to one order of magnitude decrease in the LMM fraction (Fig. 10b), and up to two orders of magnitude increase in the sediments (Fig. 10d). For the particle-bound fraction, which was close to zero in the remote locations in the simulation with low K_d, the ratio increased towards infinity (Fig. 10c).

To identify the individual impact from each of the two parameters, another two simulations were performed, one only with increased distribution coefficient (ph1-iKd) and one only with reduced desorption coefficient (ph1-rDc). The latter value was taken from laboratory experiments obtained for Cs by Børretzen and Salbu (2002). Except for around 20 % higher fraction of sediment-bound species than in ph1 in the end of the simulation period due to the decreased desorption, exclusively decreasing the desorption coefficient had minor impact on the activity concentration levels in Boknafjorden (figure not shown). The results from the simulation with high K_d (ph1-iKd) were basically similar to the results from the simulation ph1-Sorp (increased K_d and reduced D_C). However, due to the relatively higher D_C, the retention time was shorter for species reversibly bound to solid matter, resulting in less activity in the slowly reversibly bound fractions.

3.4. Comparative assessment of the impact on horizontal transport and specie distribution

Table 4 summarizes the largest impacts obtained by enabling or changing selected processes in the model configuration. From the comparison of simulations, we have considered the effect of each process on changes in the specie distribution, near-source and far-field activity concentration as well as the amount of activity remaining in Boknafjorden. The latter was quantified from the difference between the total discharge and the total amount of radioactivity crossing a section from Kårstø to Tungeneset (the green line in

Table 4
Impact of the processes.

Process/key factor	Total activity concentration near river outlets	Total activity concentration in far-field	Activity remaining in fjord system	Specie distribution
Solid-sea water interactions	Low impact (<10 %)	Increased with factor 100	Increased with 20 %	Higher activity in sediments
Discharges as reversibly particle-bound radionuclides	Slightly increased (<10 %)	Low impact (<10 %)	Low impact (increased with 2 %)	Low impact
Discharges as slowly reversibly particle-bound radionuclides	Increased with factor 10	Decreased with factor 10	Increased with 100 %	Higher activity in particles (factor > 1000) and sediments (factor 100), lower in LMM (factor 10)
Reduced particle size	Decreased with factor 2	Increased with factor 2–10	Decreased with 50 %	Higher activity in particles, lower in sediments
Increased particle size	Increased with factor 2	Decreased with factor 2–10	Increased with 33 %	Higher activity in sediments, lower in particles
Increased K_d and reduced D_C	Increased with less than factor 2	Increased with factor 2–10	Increased with 50 %	Higher activity in particles and sediments, lower in LMM
Increased slowly reversible interaction coefficient	Decreased with 10 %	Increased with 65 %	Decreased with 10 %	Factor 10 higher activity in LMM, lower in particles

Fig. 1) in the entire simulation period. Histograms and cumulative histograms of the transport time from all simulations are plotted in Fig. S.5.

First of all, including reactive radionuclides and transformation processes in the simulations, as discussed in Section 3.1, locally increased the total activity concentration with more than two orders of magnitude at some far-field shallow locations. Essentially, accumulation of radionuclides in the sediments reduced the transport away from the sources, potentially affecting the activity concentration levels for all species both at short time scales and at time scales beyond the length of our simulations.

Secondly, the discussions in Section 3.2 identified the gravitational settling of particles to be one of the major contributors to overall uncertainty. The highest transport out of the fjord was attributed to the simulation of non-reactive LMM species (ph1-nr), in which there was no settling nor adsorption to sediments, and only 30 % of the discharged radionuclides remained in the fjord at the very end of the simulation (Fig. S.5). In contrast, the highest impact of increased settling was found in the simulation in which the ^{137}Cs discharges were slowly reversibly bound to large particles (simulation ph5-L), giving more than three times higher remaining activity the fjord system than in simulation ph1-nr.

While only minor impacts were found by changing the radionuclide releases from LMM species to species reversibly bound to particles, releasing them as slowly reversibly bound species changed the results considerably. In these simulations, the particle size was found to be crucial for the horizontal distribution, since small particles remained suspended in the water masses for a long time, giving rise to increased far-field activity concentration levels, while large particles sedimented earlier and the activity concentration increased near the river outlets and decreased at longer distances. However, increasing the slowly reversible interaction coefficient D_R in simulation ph5-iDR transformed more of the slowly reversibly bound particle-associated radionuclides to the reversibly bound fraction. Subsequently, more LMM species were remobilized before the particles reached bottom, and the transport flux out of the fjord increased.

Finally, increased settling was obtained not only by considering speciation changes in the discharges, but also by choosing different values for the parameters in the equations for the interactions with solid matter as discussed in Section 3.3. In the simulation with increased sorption (ph1-Sorp), a higher fraction of the radiocesium was associated with particles, causing increased settling and sedimentation, both near the river outlets but also at far-field locations. This, in turn, reduced the horizontal transport and increased the exposure of the fjord system at the end of the simulation.

4. Conclusions

In the present study, we have studied the impact of key physicochemical processes and particle-sediment dynamics on the estimated activity concentration levels from relatively high resolution numerical simulations of marine radionuclide dispersion. The study was based on a hypothetical accident scenario where radiocesium was introduced to a complex fjord system via rivers. Our results confirmed that enabling radionuclide speciation and dynamic transformation of species and changing the initial composition of species in the model simulations can change the transport estimates, the activity concentration as well as the specie distribution considerably. In particular:

- Inclusion of particle interactions caused local variations in total activity concentration that spanned two orders of magnitude
- Assuming that the radionuclides were released as slowly reversibly bound to particles caused local variations in activity concentration spanning three orders of magnitude for particle-associated species and two orders of magnitude for sediment-associated species
- Increasing the particle size caused increased gravitational settling and strongly reduced horizontal transport out of the fjord system

In summary, we found the gravitational settling of particles towards the seabed to cause the largest discrepancies between the simulation results. The settling and sedimentation was enhanced either by increasing the sorption of LMM species to suspended particles, by increasing the particle size or by increasing the fraction of radiocesium initially discharged as slowly reversibly bound to particles. Since the current speed generally is higher near the surface, more settling into the deeper water masses reduced the transport of radionuclides out of the fjord system while the contamination of sediments as well as the total exposure of the fjord system increased.

Thus, the recommendations provided here, based on our scenario with ^{137}Cs radionuclides, are to include speciation and kinetics of transformation processes also in predictions of elements with relatively low particle affinity. The initial composition of radionuclides in the discharges appears to be crucial for the estimates, especially the fraction of radionuclides slowly reversibly bound to particles. And as expected, particle size impacts the gravitational settling considerably. Since the model estimates are also sensitive to the parameterization of the dynamic speciation, further improvement of the model prediction skill would benefit from more accurate description of the transfer rates. Hence, for validation purposes as well as for calibration of the model system, more applicable measurements and laboratory experiments will be beneficial in future work to improve the model skill. This

includes more detailed description of local environmental conditions such as heterogeneous seabed properties, temporal and vertical variability in suspended matter concentration and particle size distributions as well as salinity dependence of the sorption properties.

It is worth mentioning that even for elements with relatively low affinity to suspended matter and sediments, such as cesium in the marine environment, the relative distribution of the radionuclide species will affect the uptake of radionuclides in filtering benthic organisms, such as mussels and bottom-feeding fish. Complex speciation predictions should therefore be considered in impact, risk and dose assessment in the marine ecosystems. Our study aimed at highlighting the complex interplay between the high spatio-temporal variability of currents in complex coastal fjord systems and key physico-chemical processes affecting radionuclide speciation. Since the focus here was on a whole fjord system and its connection to the open ocean, details of transformation processes including fate of colloidal radionuclides in the immediate proximity to river mouths, where waters are brackish, have not been resolved. This will be the focus of upcoming work.

Supplementary data to this article can be found online at https://doi.org/10.1016/j.scitotenv.2019.01.434.

Acknowledgments

This study has been funded by the The Research Councilof Norway through its Centre of Excellence (CoE) funding scheme (Project No. 223268/F50).

References

Aarkrog, A., 2003. Input of anthropogenic radionuclides into the World Ocean. Deep Sea Research Part II: Topical Studies in Oceanography (ISSN: 0967-0645) 50 (17), 2597–2606. https://doi.org/10.1016/S0967-0645(03)00137-1.

Albretsen, J., Sperrevik, A.K., Staalstrøm , A., Sandvik, A.D., Vikeø , F., Asplin, L., 2011. NorKyst-800 report no. 1: user manual and technical descriptions. Fisken og havet.

Aldridge, J., Kershaw, P., Brown, J., McCubbin, D., Leonard, K., Young, E., 2003. Transport of plutonium (239/240Pu) and caesium (137Cs) in the Irish Sea: comparison between observations and results from sediment and contaminant transport modelling. Continental Shelf Research (ISSN: 0278-4343) 23 (9), 869–899. https://doi.org/10.1016/S0278-4343(03)00047-5.

AMAP, 2004. AMAP assessment 2002. Radioactivity in the Arctic. Arctic Monitoring and Assessment Programme. Oslo. Norway.

Aure, J., Rey, F., 1992, 02. Oceanographic conditions in the Sandsfjord system, western Norway, after a bloom of the toxic prymnesiophyte *Prymnesium parvum* Carter in August 1990. Sarsia 76, 247–254. https://doi.org/10.1080/00364827.1992.10413480.

Beldring, S., Engeland, K., Roald, L.A., Sælthun, N.R., Voksø, A., 2003. Estimation of parameters in a distributed precipitation-runoff model for Norway. Hydrology and Earth System Sciences 7 (3), 304–316. https://doi.org/10.5194/hess-7-304-2003.

Black, E.E., Buesseler, K.O., 2014. Spatial variability and the fate of cesium in coastal sediments near Fukushima, Japan. Biogeosciences 11 (18), 5123–5137. https://doi.org/10.5194/bg-11-5123-2014.

Bogen, J., Bønsnes, T., 2004. Sedimenttransport og substratforhold i Suldalslågen, sluttrapport, 1998-2003. Suldalslågen - Miljørapport nr 39. Norges vassdrags- og energidirektorat.

Brekke, E., Johnsen, G.H., 2006. Overvåkning av vannkvalitet ved utfylling av tunnelmasser i sjø ved Husnes. Rådgivende Biologer AS Rapport nr 957.

Børretzen, P., Salbu, B., 2000. Estimation of apparent rate coefficients for radionuclides interacting with marine sediments from Novaya Zemlya. Science of The Total Environment (ISSN: 0048-9697) 262 (1), 91–102. https://doi.org/10.1016/S0048-9697(00)00575-1.

Børretzen, P., Salbu, B., 2002. Fixation of Cs to marine sediments estimated by a stochastic modelling approach. Journal of Environmental Radioactivity (ISSN: 0265-931X) 61 (1), 1–20. https://doi.org/10.1016/S0265-931X(01)00107-2.

Børretzen, P., Salbu, B., 2009. Bioavailability of sediment-associated and low-molecular-mass species of radionuclides/trace metals to the mussel *Mytilus edulis*. Journal of Environmental Radioactivity (ISSN: 0265-931X) 100 (4), 333–341. https://doi.org/10.1016/j.jenvrad.2008.12.020.

Chapman, D.C., 1985. Numerical treatment of cross-shelf open boundaries in a barotropic coastal ocean model. Journal of Physical Oceanography 15 (8), 1060–1075. https://doi.org/10.1175/1520-0485(1985)015<1060:NTOCSO>2.0.CO;2.

Choi, Y., Kida, S., Takahashi, K., 2013. The impact of oceanic circulation and phase transfer on the dispersion of radionuclides released from the Fukushima Dai-ichi Nuclear Power Plant. Biogeosciences 10 (7), 4911–4925. https://doi.org/10.5194/bg-10-4911-2013.

Döös, K., Jönsson, B., Kjellsson, J., 2017. Evaluation of oceanic and atmospheric trajectory schemes in the TRACMASS trajectory model v6.0. Geoscientific Model Development 10 (4), 1733–1749. https://doi.org/10.5194/gmd-10-1733-2017.

Duffa, C., du Bois, P.B., Caillaud, M., Charmasson, S., Couvez, C., Didier, D., Dumas, F., Fievet, B., Morillon, M., Renaud, P., Thébault, H., 2016. Development of emergency response tools for accidental radiological contamination of French coastal areas. Journal of Environmental Radioactivity (ISSN: 0265-931X) 151, 487–494. https://doi.org/10.1016/j.jenvrad.2015.04.019.

Döös, K., Engqvist, A., 2007. Assessment of water exchange between a discharge region and the open sea — a comparison of different methodological concepts. Estuarine, Coastal and Shelf Science (ISSN: 0272-7714) 74 (4), 709–721. https://doi.org/10.1016/j.ecss.2007.05.022.

Döös, K., Rupolo, V., Brodeau, L., 2011. Dispersion of surface drifters and model-simulated trajectories. Ocean Modelling (ISSN: 1463-5003) 39 (3-4), 301–310. https://doi.org/10.1016/j.ocemod.2011.05.005.

Egbert, G.D., Erofeeva, S.Y., 2002. Efficient inverse modeling of barotropic ocean tides. Journal of Atmospheric and Oceanic Technology 19 (2), 183–204. https://doi.org/10.1175/1520-0426(2002)019<0183:EIMOBO>2.0.CO;2.

Eyrolle, F., Charmasson, S., 2004. Importance of colloids in the transport within the dissolved phase (< 450 nm) of artificial radionuclides from the Rhne River towards the Gulf of Lions (Mediterranean Sea). Journal of Environmental Radioactivity (ISSN: 0265-931X) 72 (3), 273–286. https://doi.org/10.1016/S0265-931X(03)00178-4.

Flather, R., 1976. A tidal model of the north-west European continental shelf. Mem. Soc. R. Sci. Liege. 10, 141–164.

Haidvogel, D., Arango, H., Budgell, W., Cornuelle, B., Curchitser, E., Lorenzo, E.D., Fennel, K., Geyer, W., Hermann, A., Lanerolle, L., Levin, J., McWilliams, J., Miller, A., Moore, A., Powell, T., Shchepetkin, A., Sherwood, C., Signell, R., Warner, J., Wilkin, J., 2008. Ocean forecasting in terrain-following coordinates: formulation and skill assessment of the Regional Ocean Modeling System. Journal of Computational Physics (ISSN: 0021-9991) 227 (7), 3595–3624. https://doi.org/10.1016/j.jcp.2007.06.016 Predicting weather, climate and extreme events.

Hunt, J., Leonard, K., Hughes, L., 2013. Artificial radionuclides in the Irish Sea from Sellafield: remobilisation revisited. Journal of Radiological Protection 33 (2), 261. https://doi.org/10.1088/0952-4746/33/2/261.

IAEA, 2004. Sediment Distribution Coefficients and Concentration Factors for Biota in the Marine Environment. Technical report series, No. 422International Atomic Energy Agency.

Johnsen, T.M., Dale, T., 2009. Partikkelforurensning i Vatsfjorden. Norsk institutt for vannforskning Rapport L. nr 5823-2009.

Karcher, M.J., Gerland, S., Harms, I.H., Iosjpe, M., Heldal, H.E., Kershaw, P.J., Sickel, M., 2004. The dispersion of 99Tc in the Nordic Seas and the Arctic Ocean: a comparison of model results and observations. Journal of Environmental Radioactivity (ISSN: 0265-931X) 74 (1-3), 185–198. https://doi.org/10.1016/j.jenvrad.2004.01.026 Papers from the International Conference on Radioactivity in the Environment, Monaco, 1–5 September 2002.

Kersting, A.B., Efurd, D.W., Finnegan, D.L., Rokop, D.J., Smith, D.K., Thompson, J.L., 1999. Migration of plutonium in ground water at the Nevada Test Site. Nature 397, 56–59. https://doi.org/10.1038/16231.

Klein, H., Bartnicki, J., 2018. Worst case meteorological scenario for Norway in case of an accident in Sellafield Nuclear Site. In: Mensink, C., Kallos, G. (Eds.), Air Pollution Modeling and its Application XXV. Springer International Publishing, Cham, pp. 457–462.

Kobayashi, T., Otosaka, S., Togawa, O., Hayashi, K., 2007. Development of a non-conservative radionuclides dispersion model in the ocean and its application to surface cesium-137 dispersion in the Irish Sea. Journal of Nuclear Science and Technology 44 (2), 238–247. https://doi.org/10.1080/18811248.2007.9711278.

Lin, Y., Couture, R.-M., Klein, H., Ytre-Eide, M. A., Dyve, J. E., Lind,O. C., Bartnicki, J., Nizzetto, L., Butterfield, D., Larssen, T., Salbu, B., Unpublished results. Modelling Environmental Impacts of Cesium-137 under a Hypothetical Release of Radioactive Waste. Submitted to Bulletin of Environmental Contamination and Toxicology.

Lind, O.C., Oughton, D.H., Salbu, B., Skipperud, L., Sickel, M.A., Brown, J.E., Fifield, L.K., Tims, S.G., 2006. Transport of low 240Pu/239Pu atom ratio plutonium-species in the Ob and Yenisey Rivers to the Kara Sea. Earth and Planetary Science Letters (ISSN: 0012-821X) 251 (1), 33–43. https://doi.org/10.1016/j.epsl.2006.08.023.

Maderich, V., Jung, K.T., Brovchenko, I., Kim, K.O., 2017, Decc. Migration of radioactivity in multi-fraction sediments. Environmental Fluid Mechanics (ISSN: 1573-1510) 17 (6), 1207–1231. https://doi.org/10.1007/s10652-017-9545-9.

Marchesiello, P., McWilliams, J.C., Shchepetkin, A., 2001. Open boundary conditions for long-term integration of regional oceanic models. Ocean Modelling (ISSN: 1463-5003) 3 (1), 1–20. https://doi.org/10.1016/S1463-5003(00)00013-5.

McCubbin, D., Leonard, K.S., McDonald, P., Bonfield, R., Boust, D., 2006. Distribution of Technetium-99 in sub-tidal sediments of the Irish Sea. Continental Shelf Research (ISSN: 0278-4343) 26 (4), 458–473. https://doi.org/10.1016/j.csr.2005.12.010.

Min, B.-I., Periáñez, R., Kim, I.-G., Suh, K.-S., 2013. Marine dispersion assessment of 137Cs released from the Fukushima nuclear accident. Marine Pollution Bulletin (ISSN: 0025-326X) 72 (1), 22–33. https://doi.org/10.1016/j.marpolbul.2013.05.008.

Mitchell, P., Condren, O., Vintró, L., McMahon, C., 1999. Trends in plutonium, americium and radiocaesium accumulation and long-term bioavailability in the western Irish Sea mud basin. Journal of Environmental Radioactivity (ISSN: 0265-931X) 44 (2-3), 223–251. https://doi.org/10.1016/S0265-931X(98)00135-0.

Müller, M., Homleid, M., Ivarsson, K.-I., Køltzow, M.A.Ø., Lindskog, M., Midtbø, K.H., Andrae, U., Aspelien, T., Berggren, L., Bjørge, D., Dahlgren, P., Kristiansen, J., Randriamampianina, R., Ridal, M., Vignes, O., 2017. AROME-MetCoOp: a Nordic convective-scale operational weather prediction model. Weather and Forecasting 32 (2), 609–627. https://doi.org/10.1175/WAF-D-16-0099.1.

Nilsson, J.A.U., Döös, K., Ruti, P.M., Artale, V., Coward, A., Brodeau, L., 2013. Observed and modeled global ocean turbulence regimes as deduced from surface trajectory data.

Journal of Physical Oceanography 43 (11), 2249–2269. https://doi.org/10.1175/JPO-D-12-0193.1.
Novikov, A.P., Kalmykov, S.N., Utsunomiya, S., Ewing, R.C., Horreard, F., Merkulov, A., Clark, S.B., Tkachev, V.V., Myasoedov, B.F., 2006. Colloid transport of plutonium in the far-field of the Mayak Production Association, Russia. Science (ISSN: 0036-8075) 314 (5799), 638–641. https://doi.org/10.1126/science.1131307.
Nyffeler, U.P., Li, Y.-H., Santschi, P.H., 1984. A kinetic approach to describe trace-element distribution between particles and solution in natural aquatic systems. Geochimica et Cosmochimica Acta (ISSN: 0016-7037) 48 (7), 1513–1522. https://doi.org/10.1016/0016-7037(84)90407-1.
Orre, S., Smith, J.N., Alfimov, V., Bentsen, M., 2010, Aprr. Simulating transport of 129I and idealized tracers in the northern North Atlantic Ocean. Environmental Fluid Mechanics (ISSN: 1573-1510) 10 (1), 213–233. https://doi.org/10.1007/s10652-009-9138-3.
Peráñez, R., 2003. Kinetic modelling of the dispersion of plutonium in the eastern Irish Sea: two approaches. Journal of Marine Systems (ISSN: 0924-7963) 38 (3-4), 259–275. https://doi.org/10.1016/S0924-7963(02)00242-7.
Periáñez, R., 2004a. On the sensitivity of a marine dispersion model to parameters describing the transfers of radionuclides between the liquid and solid phases. Journal of Environmental Radioactivity (ISSN: 0265-931X) 73 (1), 101–115. https://doi.org/10.1016/j.jenvrad.2003.07.003.
Periáñez, R., 2004b. Testing the behaviour of different kinetic models for uptake/release of radionuclides between water and sediments when implemented in a marine dispersion model. Journal of Environmental Radioactivity (ISSN: 0265-931X) 71 (3), 243–259. https://doi.org/10.1016/S0265-931X(03)00172-3.
Periáñez, R., 2005. Modelling the dispersion of radionuclides by a river plume: application to the Rhone River. Continental Shelf Research (ISSN: 0278-4343) 25 (12), 1583–1603. https://doi.org/10.1016/j.csr.2005.04.001.
Periáñez, R., 2008. A modelling study on 137Cs and 239,240Pu behaviour in the Alboran Sea, western Mediterranean. Journal of Environmental Radioactivity (ISSN: 0265-931X) 99 (4), 694–715. https://doi.org/10.1016/j.jenvrad.2007.09.011.
Periáñez, R., 2009. Environmental modelling in the Gulf of Cadiz: heavy metal distributions in water and sediments. Science of The Total Environment (ISSN: 0048-9697) 407 (10), 3392–3406. https://doi.org/10.1016/j.scitotenv.2009.01.023.
Periáñez, R., 2012. Modelling the environmental behaviour of pollutants in Algeciras Bay (south Spain). Marine Pollution Bulletin (ISSN: 0025-326X) 64 (2), 221–232. https://doi.org/10.1016/j.marpolbul.2011.11.030.
Periáñez, R., Bezhenar, R., Brovchenko, I., Duffa, C., Iosjpe, M., Jung, K., Kobayashi, T., Lamego, F., Maderich, V., Min, B., Nies, H., Osvath, I., Outola, I., Psaltaki, M., Suh, K., de With, G., 2016a. Modelling of marine radionuclide dispersion in IAEA MODARIA program: lessons learnt from the Baltic Sea and Fukushima scenarios. Science of The Total Environment (ISSN: 0048-9697) 569-570 (Supplement C), 594–602. https://doi.org/10.1016/j.scitotenv.2016.06.131.
Periáñez, R., Brovchenko, I., Jung, K., Kim, K., Maderich, V., 2018. The marine Kd and water/sediment interaction problem. Journal of Environmental Radioactivity (ISSN: 0265-931X) 192, 635–647. https://doi.org/10.1016/j.jenvrad.2018.02.014.
Periáñez, R., Elliott, A., 2002. A particle-tracking method for simulating the dispersion of non-conservative radionuclides in coastal waters. Journal of Environmental Radioactivity (ISSN: 0265-931X) 58 (1), 13–33. https://doi.org/10.1016/S0265-931X(01)00028-5.
Periáñez, R., Hierro, A., Bolívar, J.P., Vaca, F., 2013. The geochemical behavior of natural radionuclides in coastal waters: a modeling study for the Huelva estuary. Journal of Marine Systems (ISSN: 0924-7963) 126 (Supplement C), 82–93. https://doi.org/10.1016/j.jmarsys.2012.08.001.
Periáñez, R., Suh, K.-S., Min, B.-I., 2012. Local scale marine modelling of Fukushima releases. Assessment of water and sediment contamination and sensitivity to water circulation description. Marine Pollution Bulletin (ISSN: 0025-326X) 64 (11), 2333–2339. https://doi.org/10.1016/j.marpolbul.2012.08.030.
Periáñez, R., Suh, K.-S., Min, B.-I., 2016b. The behaviour of 137Cs in the North Atlantic Ocean assessed from numerical modelling: releases from nuclear fuel reprocessing factories, redissolution from contaminated sediments and leakage from dumped nuclear wastes. Marine Pollution Bulletin (ISSN: 0025-326X) 113 (1), 343–361. https://doi.org/10.1016/j.marpolbul.2016.10.021.
Salbu, B., 2000. Speciation of Radionuclides in the Environment. In: Meyers, R.A. (Ed.), Encyclopedia of Analytical Chemistry. John Wiley & Sons Ltd., Chichester, pp. 12993–13016.
Salbu, B., 2009. Fractionation of radionuclide species in the environment. Journal of Environmental Radioactivity (ISSN: 0265-931X) 100 (4), 283–289. https://doi.org/10.1016/j.jenvrad.2008.12.013.
Salbu, B., Lind, O., Skipperud, L., 2004. Radionuclide speciation and its relevance in environmental impact assessments. Journal of Environmental Radioactivity (ISSN: 0265-931X) 74 (1), 233–242. https://doi.org/10.1016/j.jenvrad.2004.01.008 Papers from the International Conference on Radioactivity in the Environment, Monaco, 1-5 September 2002.
Sanial, V., Buesseler, K.O., Charette, M.A., Nagao, S., 2017. Unexpected source of Fukushima-derived radiocesium to the coastal ocean of Japan. Proceedings of the National Academy of Sciences 114 (42), 11092–11096. https://doi.org/10.1073/pnas.1708659114.
Shchepetkin, A.F., McWilliams, J.C., 2005. The regional oceanic modeling system (ROMS): a split-explicit, free-surface, topography-following-coordinate oceanic model. Ocean Modelling (ISSN: 1463-5003) 9 (4), 347–404. https://doi.org/10.1016/j.ocemod.2004.08.002.
Simonsen, M., Saetra, Ø., Isachsen, P.E., Lind, O.C., Skjerdal, H.K., Salbu, B., Heldal, H.E., Gwynn, J.P., 2017. The impact of tidal and mesoscale eddy advection on the long term dispersion of 99Tc from Sellafield. Journal of Environmental Radioactivity (ISSN: 0265-931X) 177, 100–112. https://doi.org/10.1016/j.jenvrad.2017.06.002.
Smith, C., Goshawk, J., Charles, K., McDonald, P., Leonard, K., McCubbin, D., 2003. MEAD (part II)—predictions of radioactivity concentrations in the Irish Sea. Journal of Environmental Radioactivity (ISSN: 0265-931X) 68 (3), 193–214. https://doi.org/10.1016/S0265-931X(03)00041-9.
Staalstrøm, A., Borgersen, G., Tjomsland, T., Kempa, M., Brkljacic, M., 2013. Resipientundersøkelse i Sandsfjorden i Rogaland og modellering av partikkelspredning fra Norsk Stein sitt anlegg. Norsk institutt for vannforskning NIVA-Rapport 6523-2013.
Stokes, G.G., 1851. On the effect of the internal friction of fluids on the motion of pendulums. Transactions of the Cambridge Philosophical Society 9, 8.
Sundfjord, A., Bjerkeng, B., 2008. Strøm, turbiditet og hydrografi i fjordbassenget utenfor Engebø, Førdefjorden. Målinger utført for konsekvensutredning for deponi av gruvegang. Norsk institutt for vannforskning Rapport L.nr 5662-2008.
Thornton, B., Ohnishi, S., Ura, T., Odano, N., Sasaki, S., Fujita, T., Watanabe, T., Nakata, K., Ono, T., Ambe, D., 2013. Distribution of local 137Cs anomalies on the seafloor near the Fukushima Dai-ichi Nuclear Power Plant. Marine Pollution Bulletin (ISSN: 0025-326X) 74 (1), 344–350. https://doi.org/10.1016/j.marpolbul.2013.06.031.
Tsumune, D., Tsubono, T., Aoyama, M., Uematsu, M., Misumi, K., Maeda, Y., Yoshida, Y., Hayami, H., 2013. One-year, regional-scale simulation of ^{137}Cs radioactivity in the ocean following the Fukushima Dai-ichi Nuclear Power Plant accident. Biogeosciences 10 (8), 5601–5617. https://doi.org/10.5194/bg-10-5601-2013.
Umlauf, L., Burchard, H., 2003. A generic length-scale equation for geophysical turbulence models. Journal of Marine Research 61, 235–265. https://doi.org/10.1357/002224003322005087.
Viikmäe, B., Torsvik, T., Soomere, T., 2013. Impact of horizontal eddy diffusivity on Lagrangian statistics for coastal pollution from a major marine fairway. Ocean Dynamics (ISSN: 1616-7341) 63 (5), 589–597. https://doi.org/10.1007/s10236-013-0615-3.
Vives i Batlle, J., Aoyama, M., Bradshaw, C., Brown, J., Buesseler, K., Casacuberta, N., Christl, M., Duffa, C., Impens, N., Iosjpe, M., MasquÃÏ, P., Nishikawa, J., 2018. Marine radioecology after the Fukushima Dai-ichi nuclear accident: are we better positioned to understand the impact of radionuclides in marine ecosystems? Science of The Total Environment (ISSN: 0048-9697) 618 (Supplement C), 80–92. https://doi.org/10.1016/j.scitotenv.2017.11.005.
Yamagata, N., Matsuda, S., Kodaira, K., 1963, 11. Run-off of caesium-137 and strontium-90 from rivers. Nature 200. https://doi.org/10.1038/200668b0.
Yamasaki, S., Imoto, J., Furuki, G., Ochiai, A., Ohnuki, T., Sueki, K., Nanba, K., Ewing, R.C., Utsunomiya, S., 2016. Radioactive Cs in the estuary sediments near Fukushima Daiichi Nuclear Power Plant. Science of The Total Environment (ISSN: 0048-9697) 551-552 (Supplement C), 155–162. https://doi.org/10.1016/j.scitotenv.2016.01.155.
Ytre-Eide, M.A., Standring, W.J., Amundsen, I., Sickel, M., Liland, A., Saltbones, J., Bartnicki, J., Haakenstad, H., Salbu, B., 2009. Consequences in Norway of a hypothetical accident at Sellafield: potential release-transport and fallout. Statens Straalevern.

Paper II: Supplementary Material

Suppelmentary material 1: Validation of the ocean circulation model

For validation of the hydrodynamic model, the model results were compared with 61 hydrographical profiles where 14 were taken inshore and the rest were measured in the coastal and more offshore zone. Some of the profiles were repeated at the same location, while others were only measured once within the time period from Nov. 2015 to May 2016. The hydrographical data were either obtained by a Seabird SBE 911plus CTD or a SAIV STD/CTD SD204 instrument, both holding a high degree of accuracy. The position of the measurements are shown in Fig S.1 along with the mean model error of salinity and temperature in 5 m depth. While the model reproduced the temperatures well, it was slightly too saline, both inshore and offshore. Further, we separated the model error between inshore and coastal/offshore profiles and between depths (Fig S.1). The average model temperature error was less than 0.5 °C in all depths between 1 and 100 m, but the model salinity was about two units too high in 1 m to 10 m depth. The salinity error then decreased to about zero at 50 m depth and remained low down to 100 m depth. Both the inner fjords and the coastal area in this region had relatively low surface salinities (20-33) and a correspondingly large variability (standard deviation about 2), and to relate the model error to the observed standard deviation, we have collected longer time series of salinity measurements from a coastal station (Outer Utsira, 4.733E, 59.317N) and a fjord station (Hidlefjorden, 5.8E, 59.067N) with 12-24 samples per year between 2009 and 2016. The model salinity error was standardized and can then be compared between depths (Fig. S.1 bottom, mid panel). Still, we found the

largest salinity errors in the upper 50 m for the fjord locations, while the normalized error was more uniform with depth for the coastal stations with an equal size between the model error and the standard deviation. Summarized, our model salinity error was, in general and for all depths, not exceeding the variability found from observations, and the model temperature was very close to unbiased.

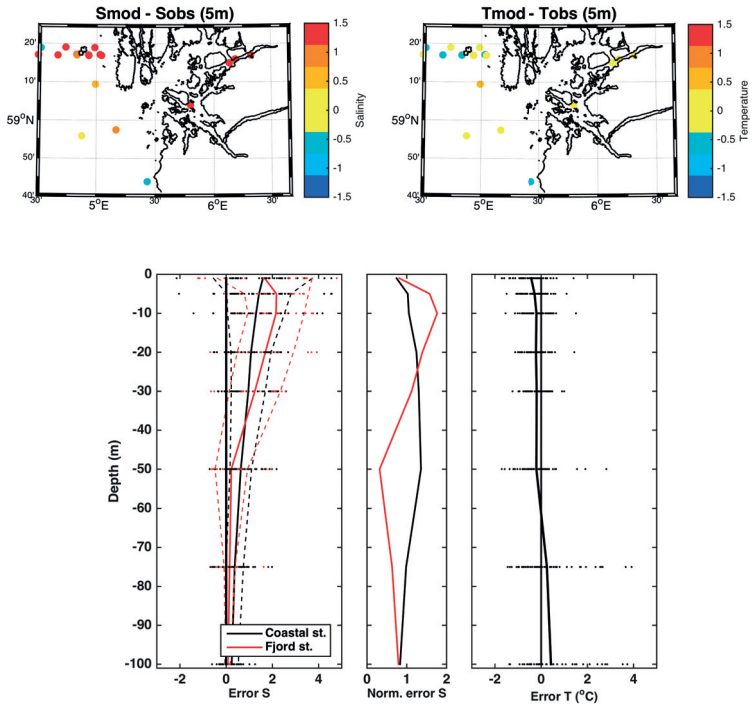

Figure S.1: Position and error from comparison of the hydrodynamic model and observations.

Table S.1: Time scales of the transfer between the species in days. To illustrate the spatially variable k_{13} transfer, a typical suspended matter concentration of $m = 1 \times 10^{-3}\,\mathrm{kg\,m^{-3}}$ is used, but this value can vary with more than one order of magnitude (Fig. S.2). Phase numbers indicate radionuclides in the different model compartments: 1: LMM species, 3: reversibly bound to particles, 4: reversibly bound to sediments, 5: slowly reversibly bound to particles, 6: slowly reversibly bound to sediments.

From phase	To phase	ph1, ph3, ph5 ph5-S, ph5-L	ph5-iDR	ph1-Sorp	ph1-iKd	ph1-rDc
1	3	499	499	133	6,7	2516
3	1	1	1	20	1	5
1	4	0,05	0.05	0.01	0.0007	0.3
4	1	10	10	200	10	50
3	5	97	3.3	97	97	97
5	3	965	33	965	965	965
4	6	97	3.3	97	97	97
6	4	965	33	965	965	965

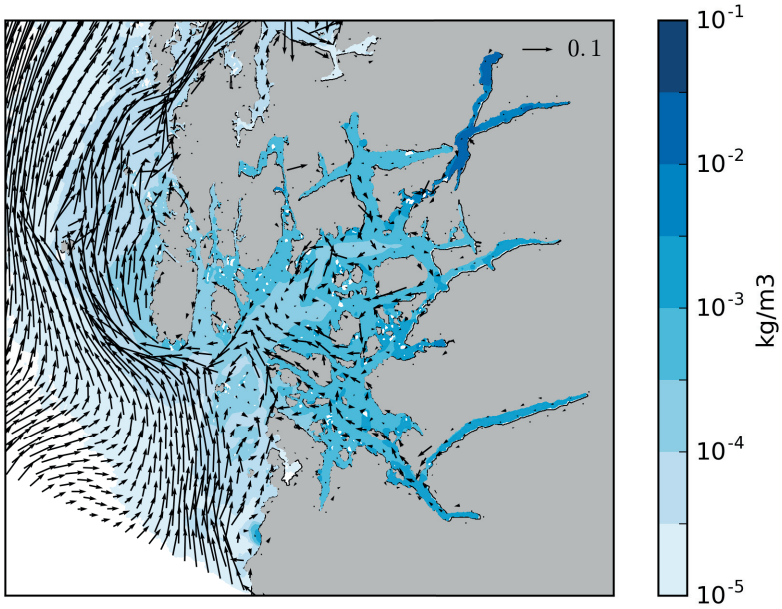

Figure S.2: Estimated concentration of available suspended particulate matter. Arrows show the mean surface currents from the hydrodynamic model.

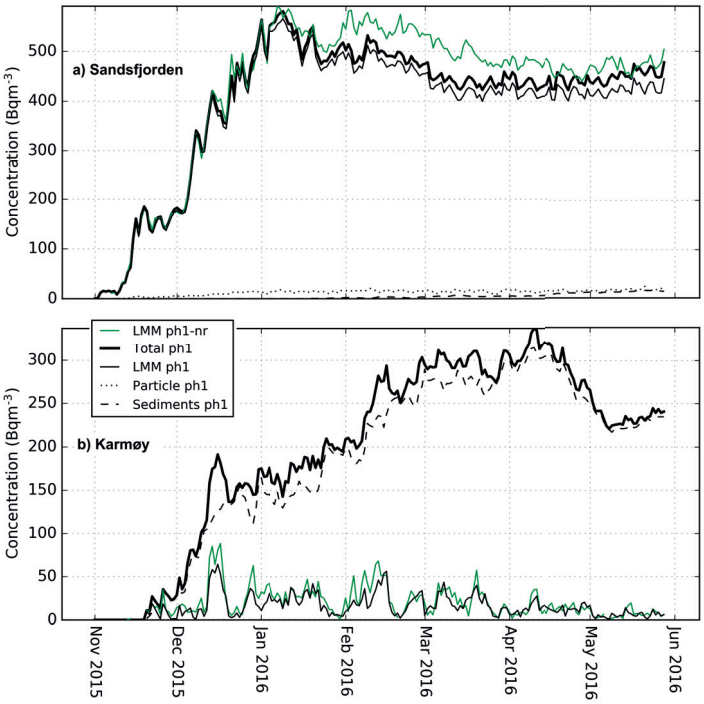

Figure S.3: Time series from Sandsfjorden (a) and Karmøy (b) of the LMM fraction (thin solid line), particle-bound fraction (dotted line) and sediment-bound fraction (dashed line) of the total ^{137}Cs activity concentration (thick solid line) from simulation ph1 (reactive, black), as well as the LMM fraction from the simplified simulation (ph1-nr, non-reactive, green), integrated over the full water depth, computed from boxes at 2.1 km × 2.1 km around each location.

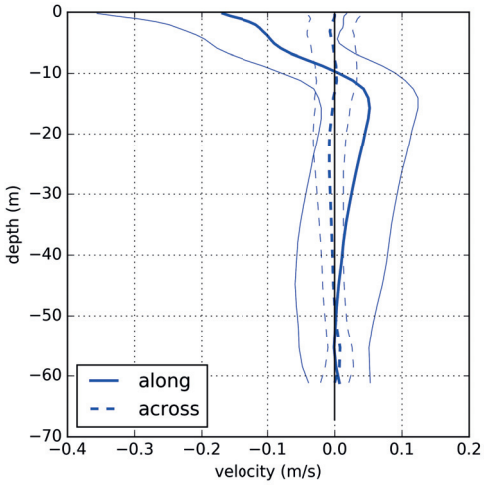

Figure S.4: Time-averaged vertical profiles of the current components from the hydrodynamic model along (solid lines) and across (dashed lines) the orientation of Sandsfjorden in the position marked with red square in Fig 1. Thick lines are mean values, while thin lines indicate one standard deviation.

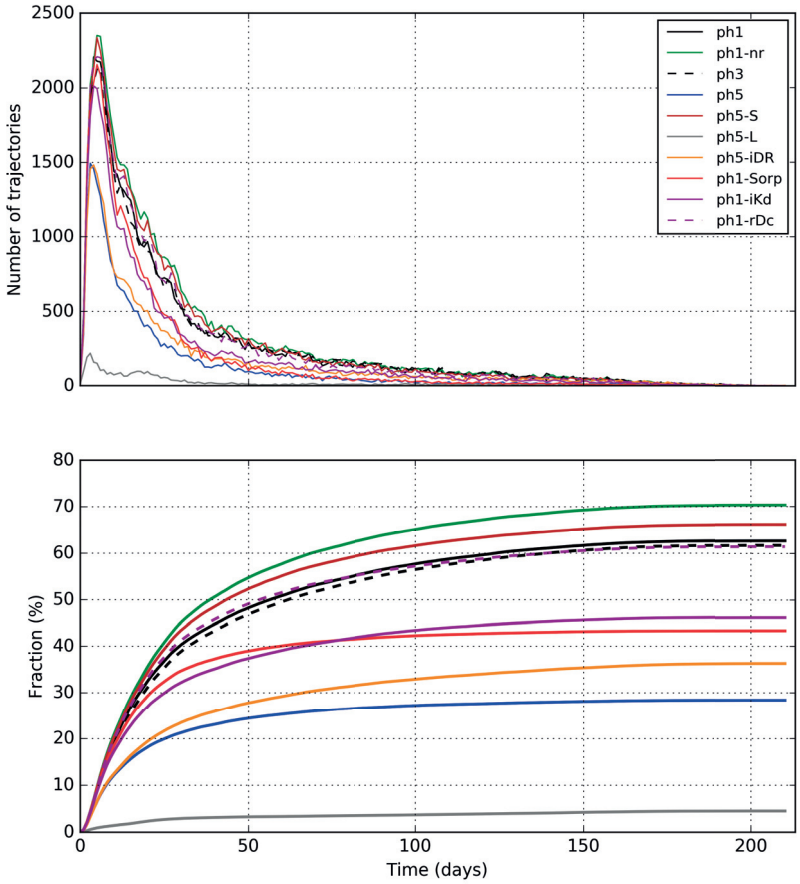

Figure S.5: Histogram of transport time to the opening of the fjord system (crossing the green line in Fig 1) (a) and cumulative sum of the percent of the total number of trajectories leaving the fjord per day after initialization (b).

Paper III

Modeling key processes affecting Al speciation and transport in estuaries

Magne Simonsen[a,b,*], Hans-Christian Teien[b], Ole Christian Lind[b], Øyvind Saetra[a], Jon Albretsen[c], Brit Salbu[b]

[a] *Norwegian Meteorological Institute, P.O. Box 43, Blindern, NO-0313 Oslo, Norway*
[b] *Centre of Environmental Radioactivity CoE, Faculty of Environmental Sciences and Natural Resource Management, Norwegian University of Life Sciences (NMBU), P.O. Box 5003, NO-1433 Ås, Norway*
[c] *Institute of Marine Research, P.O. Box 1870 Nordnes, NO-5817 Bergen, Norway*

Abstract

Assessments of the impacts of aluminium (Al) to aquatic organisms in estuarine waters have suffered from the lack of available models that can accurately predict the presence of toxic physico-chemical forms (species) of Al at adequate spatial and temporal resolution. In the present work, transport and distribution of river-discharged Al species through changing environmental conditions in the Sandnesfjorden estuary, South-Eastern Norway, was predicted using a numerical model system at relatively high spatial ($32\,\mathrm{m} \times 32\,\mathrm{m}$ in horizontal) and temporal (1 h) resolution. New model code was implemented, including dynamic, salinity-dependent speciation and transformation processes, based on *in situ* measurements from several Norwegian estuaries as well as experimental data. This is the first time such elemental speciation code including LMM, colloidal, particle and sediment species is utilized in an estuary case in combination with high resolution hydrodynam-

*Corresponding author
Email address: magnes@met.no (Magne Simonsen)

ics and compared to an extensive observational dataset. Good agreement was obtained between modeled and observed total and fractionated Al concentration at several stations along the fjord transect. Without including background contribution of Al from the coastal water, the model predicted too low Al concentrations (by up to approximately a factor 4) near the fjord mouth. The surface Al concentrations were also underestimated due to overestimated near-surface vertical mixing in the hydrodynamic model. The observed correlation between salinity and total Al concentration was well reproduced by the model in situations with low upper layer volume flux, typical under low river flow conditions. In contrast, the predicted surface salinity and total Al concentration were less correlated under high-flux conditions. As the general trends of Al concentrations and speciation were well reproduced, this study demonstrated that by including carefully chosen transfer rates, the model can be used to predict spatio-temporal distribution of total contamination as well as concentration levels of the elemental species.
Keywords: Aluminium speciation, River discharge, Trace element, Lagrangian estuarine dispersion model, Dynamic specie transformation, Estuarine dynamics

---

1. Introduction

The input of trace elements and radionuclides to the marine environment is largely attributed to river transport via estuaries to the coastal zone. In estuaries, here defined as water bodies with riverine fresh water input and free connection to the open ocean, the environmental conditions are continuously changing when the fresh river water mixes with the saline coastal wa-

ter. Along the estuarine transport pathways, river-discharged trace elements such as aluminium (Al) can appear in a series of physico-chemical forms (species), ranging from single ions and low molecular mass species (LMM) to larger colloids and particles (Salbu, 2009). The exact borderlines between the specie categories are difficult to distinguish as fractionation techniques are needed to separate species according to size, and thereby are operationally defined. Here, particles are defined as entities with nominal diameter greater than 0.45 µm, colloidal species are within the range from 10 kDa (few nm) to 0.45 µm and LMM species are less than 10 kDa (Salbu, 2009).

In most rivers in the southern part of Norway, pH is around 6 or less, and Al is predominantly present as positively charged LMM cation species. To improve the water quality and then reduce the loss of aquatic biodiversity, for instance to avoid depletion of the wild salmon populations, most acidic rivers are limed (pH close to 7), so that Al in the river water discharging into estuaries is predominantly present as neutral species, colloids and particles. During low flow, LMM and colloidal species would be predominant, while during flooding, especially the fraction of particles will increase significantly due to erosion.

The concentration levels as well as the specie distribution and the transport properties of trace elements in estuaries are affected by a number of complex dynamic and biogeochemical processes, initiated by shifting environmental conditions such as pH, salinity and temperature, as previously observed in dynamic mixing zones (Rosseland et al., 1992; Teien et al., 2004, 2006b). The six most important processes considered here are:

Dilution: Once the river water enters the estuary, dilution due to disper-

sion and mixing with coastal water masses gradually reduce the concentration levels of all river input species of trace elements being typically low in seawater. A linear negative correlation between concentration level and salinity is commonly referred to as 'conservative behavior' (Machado et al., 2016), reflecting that dilution is the predominant process influencing the concentration levels. In most cases, however, deviations from this pattern are observed due to additional processes taking place (Machado et al., 2016).

Hydrolysis and polymerization: In contact with sea water, pH increases and LMM cationic species of Al will hydrolyze, polymerize and form transient colloidal positively charged polymer species being highly reactive towards available surfaces (Lydersen et al., 1992; Teien et al., 2004). The colloidal fraction has been shown to contribute significantly to the estuarine transport of metals (Sañudo-Wilhelmy et al., 1996).

Aggregation and sedimentation: Colloids are kept in solution due to Brownian movements, but due to increasing conductivity/salinity in estuaries, aggregation of colloids occurs. In addition, aggregates and river transported particles can settle in the estuarine sediments as the current speed decreases. Thus, the trace element concentrations of species suspended in the water column will decrease while the concentration levels in sediments will increase.

Sorption, desorption and remobilization: In fresh water, a large fraction of trace elements are sorbed to surfaces of colloids and particles, i.e., associated reversibly to surfaces due to physisorption (van der Waals forces), due to electrostatic sorption (Coulomb attraction) or irreversibly due to chemisorption (covalent bonding). Upon contact with sea water, the salinity and hence the concentrations of monovalent and divalent element species will increase.

Therefore, trace elements reversibly associated to colloidal and particle surfaces will be remobilized due to ion exchange processes (Teien et al., 2006b), and subsequently remobilized LMM species will be subject to hydrolysis, polymerization and formation of colloids. Remobilization of trace elements from surfaces of riverine colloids and particles as well as sediments may locally increase the total concentration and especially the LMM fraction despite high dilution effects present in estuaries (Teien et al., 2006b; Machado et al., 2016; Sanial et al., 2017).

Resuspension: Particle surfaces in the sediments can act as sink for trace elements due to sorption and sedimentation. Under events with high water flow in the bottom layer and enhanced bottom stress, such as storms or high river flow rates, the particles can be mechanically resuspended and return to the water column.

Formation of anions such as aluminate: Alternatively, when pH exceeds 7, LMM Al species can hydrolyze stepwise and transform to aluminate, i.e., LMM anions which is the predominant form of Al in alkaline water (pH > 7.5) such as sea water (Lydersen, 1990).

Among the above-mentioned processes, the hydrolysis, polymerization, sorption/desorption and aluminate formation processes are salinity-, time- and temperature dependent, slow during winter (snow-melt episodes) and rapid during summer (Lydersen et al., 1990). Furthermore, these processes and the following speciation are also of major relevance for organisms living in the estuarine zone, as transient Al polymers formed are toxic to fish (Teien et al., 2006b). Thus, dynamic models are needed for describing the mixing zone system and processes taking place.

In numerical transport estimations, where a simplified description of the real environment is required, each defined model phase (compartment) usually contains a range of species with different properties (Periáñez et al., 2018). The 'dissolved fraction' commonly includes both the LMM fraction and the colloidal fraction (Machado et al., 2016). In cases where the transport properties are different for each model compartment, such simplifications may introduce uncertainty in the model predictions (Simonsen et al., 2019). Most models applied for estuaries have focused on dilution and sedimentation, while most often processes affecting element speciation have been ignored. In addition, most experiments on trace elements or radionuclides in estuaries are based on the determination of total concentrations of filtered samples. Data sets from estuary expeditions, providing information on trace elements in different physico-chemical forms, such as LMM, colloidal and particles are scarce (Lind et al., 2006).

Therefore, in the present study, the overall goal was to establish a generic model system for estuaries, including LMM, colloidal and particle species and being applicable for prediction of the transport of contaminants such as radionuclides and trace element species from rivers via estuaries to the ocean, serving as input in environmental impact and risk assessments. Using the ROMS-TRACMASS numerical dispersion model system, the first objective was to implement codes describing predominant elemental species such as LMM, colloid and particles as well as key processes influencing the specie distribution in estuaries in more detail than has been done in previous literature. Secondly, the kinetics of the transformation processes were estimated based on experimental data of the behavior of aluminium species in estuaries,

taking impact from factors such as salinity into account. Finally, a case study of the Sandnesfjorden estuary in south-eastern Norway was performed, where the model output was validated against field experimental data of aluminium species obtained from the river outlet and through the estuary.

2. Methods

2.1. Model description

The marine transport simulations in the present study were computed with the Lagrangian trajectory model TRACMASS (Döös et al., 2017), which previously has been used in a number of studies of ocean transport (e.g., Döös and Engqvist, 2007; Döös et al., 2011; Nilsson et al., 2013; Simonsen et al., 2017, 2019). The three-dimensional pathways of a finite number of Lagrangian units (hereafter called trajectories) were computed 'off-line', i.e., using pre-stored input fields from an ocean circulation model. Additional horizontal diffusion was parameterized using a random walk method with constant diffusivity.

Pre-stored three-dimensional ocean circulation fields from Sandnesfjorden were used from a hydrodynamical model simulation using ROMS (Regional Ocean Modeling System, http://myroms.org) with 32 m × 32 m horizontal resolution and one hour temporal resolution in the output. A similar model system was applied and described by Serra-Llinares et al. (2018), consisting of a fourfold nested model system where the horizontal grid was refined from 4 km (Lien et al., 2014) to 800 m (Albretsen et al., 2011) and 160 m, all model systems using ROMS. All these coastal and fjord models applied high-resolution atmospheric forcing from a 3 km simulation using the Weather

Research and Forecasting model (WRF), developed by the National Center of Atmospheric Research (NCAR) (e.g., Skamarock et al., 2008).

Daily estimates of volume fluxes for six rivers (where River Storelva is the largest) in the domain were based on estimates from a distributed version of the HBV model (Beldring et al., 2003) provided by the Norwegian Water Resources and Energy Directorate. The freshwater discharges from River Storelva were supplied at Laget downstream of Lagstrømmen (the narrow strait between Nævestadfjorden and Sandnesfjorden, Fig 1).

In the TRACMASS configuration used in the simulations in the present study, each trajectory is associated with one out of six model compartments, representing different physico-chemical forms of Al species. Aiming to represent and model the real marine behavior of metals, the model compartments and transformations were implemented as sketched in Fig 2, where the interactions between the model compartments are implemented according to the stochastic method described by Periáñez and Elliott (2002), with transfer rates controlling the probability to shift to each of the other compartments during a time step. The trajectories can appear as two different LMM species (cations and anions) representing species with diameter less than 10 kDa, two colloidal species (humic colloids and polymers) as well as two forms of metal species reversibly bound to solid matter; seabed sediments and suspended particulate matter (SPM). The colloidal compartments represent Al species with diameter ranging from 10 kDa to 0.45 µm, either as reversibly adsorbed to the surface of suspended organic material (humic colloids) or as polymers originating from hydrolysis of the LMM species. The size fractions were selected based on operationally defined nominal sizes using fractiona-

tion techniques.

While the LMM and colloidal species flow passively with the water masses, the particle compartment represents species with diameter larger than 0.45 µm that are sufficiently large to be affected by gravity and small enough to stay suspended in the water column for significant time. In addition to the advection and turbulent mixing with the water masses, the particle-associated trajectories will experience an additional settling velocity w_s towards the seabed, determined by Stoke's law (Stokes, 1851);

$$w_s = -\frac{(\rho_s - \rho_w) g d^2}{18\nu} \tag{1}$$

where ρ_s is the particle density, ρ_w is the density of the water, g is the gravitational acceleration, d is the particle diameter and ν is the water viscosity. In the model, the applied particle diameter is one single value, assumed to be representative for the average particle size. When particle-associated trajectories reach the bottom of the deepest water layer, they are transferred to the sediment compartment where they are preliminary deactivated from further advection. Due to mechanical stress from near-bottom currents, Al in the seabed sediments may also resuspend when the current speed in the deepest model layer exceeds a critical threshold value. In such case, the trajectory is reactivated as a particle-associated specie located in the deepest model layer.

The concentration levels in each of the element species are computed and displayed either as time series of the sum of trajectories present within a box around the stations within a representative time interval, or as smoothed two-dimensional fields of the surface (upper 1 m) concentration.

2.2. Sandnesfjorden case study

The present study considers estuarine transport of river-discharged Al from River Storelva using the ROMS-TRACMASS marine numerical dispersion model system during a period with extensive Al monitoring surveys, utilizing realistic time series of river input and three dimensional hydrodynamic currents and salinity fields from April 20, 2008 to May 31, 2008. The model domain covers Sandnesfjorden, an 8 km long, relatively shallow and narrow fjord located at the southeastern coast of Norway (Fig 1). The tides are minor with maximum amplitude less than 50 cm (`www.sehavniva.no`). Upstream of Sandnesfjorden, River Storelva enters Songevann and Nævestadfjorden, two closed basins connected to Sandnesfjorden by Lagstrømmen, a canal which is 20–100 m wide and 3 m deep at the shallowest. Under low flow conditions, the salt wedge penetrates beyond Laget into Songevann and Nævestadfjorden basins, with salinities above 25 psu, while the surface water is relatively fresh and dominated by river water, especially at high flow (Tjomsland and Kroglund, 2010). The hydrography in Sandnesfjorden depends therefore both on the river flow and the mixing conditions. The largest depth in Sandnesfjorden is 65–70 m, while the threshold around Store Furuøy in the outer part of the fjord is around 30 m deep. Outside Store Furuøy, Sandnesfjorden is connected to the Skagerrak, a marginal sea to the North Sea, where the Norwegian Coastal Current runs predominantly southwestward along the coast. The water masses in Skagerrak are a mixture of relatively salt water from the North Sea and relatively fresh water from the Baltic Sea and adjacent coastal regions and estuaries along the Skagerrak.

The dispersion simulations were performed with relevant parameters as

listed in Table 1 and shown in Fig 2b, considered to be the best possible estimates for the actual scenario.

2.2.1. Estimation of the transfer rates

In TRACMASS, key processes for Al speciation were computed as dynamic processes with specie interactions based on kinetic transfer rates, as sketched in Fig 2. Since pH, ion composition and temperature in the estuary depend on the mixture between fresh water and salt water, we use salinity as the key controlling factor in this study, and the representation of the different environmental conditions from the river outlet to the open ocean was simplified by defining four discrete salinity intervals; 0-1 psu, 1-10 psu, 10-20 psu and above 20 psu. First, a set of transfer rates was suggested for each of the four salinity intervals. These suggested values were based on observed Al specie distribution from 2007 data from water samples and controlled mixing experiments at a broad range of salinities and pH values from Sandnesfjorden as well as from other estuaries such as River Lona (Teien et al., 2006b; Skalsbakken, 2009; Kroglund et al., 2011a,b). The rates were estimated aiming to obtain reasonable element specie distributions after short time ($<$ 1 day) of mixtures and after assumed equilibrium conditions after 10 days of mixing. The time evolution of concentration levels in each specie in an idealized closed system was obtained by numerical integration of the differential equations involving the interactions between the LMM, colloidal and particulate species. Interactions with seabed (sorption/desorption and sedimentation/resuspension) were neglected during estimation of the transfer rates since the sorption processes are limited to the bottom layer and the sedimentation rates depend on inhomogeneously distributed external condi-

tions such as flow properties, settling velocity and water depth. Finally, the different rates were evaluated and adjusted against each other to obtain reasonable time scales for each process, based on the current understanding of estuarine transformation kinetics obtained from experience from numerous field studies and experimental field work (e.g. Teien et al., 2004, 2006b).

These estimated transfer rates were utilized in the Al transport simulation, and predicted concentration levels were compared to observed surface concentration of the LMM, colloidal and particle Al fractions obtained at four stations in Sandnesfjorden (Hope, Skåttholmen, Hopestranda and Store Furuøy, see Fig 1) at different times during the simulation period.

2.2.2. Source term description

In the model simulations in the present work, the flow through Lagstrømmen was considered to be the input of Al trajectories, released in a single grid cell at Laget in position 58.682°N, 9.071°E, distributed between the LMM cations, humic colloids and particle species (consistent with the observed distributions at Laget, Table 2). It was assumed that the Al concentration in River Storelva depends on the flow rate similarly to that of River Lona (Teien et al., 2006b), and hence the number of trajectories released in particle compartment (N_p) increased exponentially with increasing river flow (Q);

$$N_p = (Qf_p)^{\lambda}\psi \tag{2}$$

where λ is a constant and the scale factor ψ ensures that the total number of trajectories released in the simulation is reasonable. As an approximation of the real discharges, the input concentrations of the LMM and colloidal species were assumed to be constant, i.e., the number of released numeri-

cal trajectories in these model compartments (N_{lmm} and N_c, respectively) was linearly proportional to the daily river flow, described by the following equations:

$$N_c = Q f_c \psi \tag{3}$$

$$N_{lmm} = Q f_{lmm} \psi \tag{4}$$

The factors f_p, f_c and f_{lmm} control the distribution within each compartment.

The constants were set to $f_p = 0.2$, $f_c = 0.5$, $f_{lmm} = 0.3$, $\psi = 50$ and $\lambda = 1.6$. Time series of the number of input trajectories, concentration levels and specie distribution in the simulation period are shown in Fig S.1. The magnitude of the total discharge ranged from 110 to 140 $\mu g\,L^{-1}$ which is comparable to the measured surface concentration at Laget (Table 2). In total, 251 874 trajectories were released with 4 hour time intervals.

2.2.3. Observational data for model validation

For the purpose of validating the hydrodynamic model, measurements from 51 repeated CTD casts from Sandnesfjorden taken within the simulation period (Kroglund et al., 2011c) were used to evaluate the corresponding model output directly by calculating differences.

Surface Al concentration levels from the dispersion model predictions were validated against observational data based on surface water samples collected at stations Hope, Skåttholmen, Hopestranda and Store Furuøy (see Fig 1 for locations), at May 10, 12 and 21, 2008, described by Kroglund et al. (2011c) and here presented in Table 2. The samples were fractioned *in situ* and the results are presented as concentration distribution between LMM, colloid and particle fractions after total Al concentration was determined using ICP-OES

according to the method described by Teien et al. (2006b).

3. Results and discussion

3.1. Kinetics of the transformation processes

To represent the natural behavior of Al in estuarine environments, our estimated rates for transformation of species (Fig 2b, Table S.1, with corresponding time scales in Table 3) were assumed to change with salinity according to the methods described in Section 2.2.1. Estuaries are in most cases in non-steady state and *in situ* observations therefore reflect unstable water qualities. Unfortunately, field measurements of transfer rates are not available, but experimental data from controlled mixing experiments can be utilized, demonstrating the changes in element speciation as function of pH, salinity and time (Teien et al., 2004, 2006b; Kroglund et al., 2011b,c). As the model simulations were performed during spring, the transfer rates were calibrated according to intermediate temperatures ($\sim 10\,^{\circ}$C). At higher temperatures, during summer and fall, we can expect faster transformations, while at lower temperatures during winter, the transfer rates will be lower (Lydersen, 1991).

The model input of Al from River Storelva was assumed to be distributed between LMM cations, humic colloids and particle fractions (Kroglund et al., 2011b). Therefore, in the lowest salinity interval (0 psu to 1 psu), of which the purpose was to represent the distribution in the river water, we assumed that the LMM anion and polymer fractions were negligible and hence the transfer rates for the interactions including these species were set to 0. In the alkaline brackish water, mobilized LMM cations from river transported

colloids and particles will polymerize rapidly to polymer-associated species when the salinity exceed 1 psu (Teien et al., 2004, 2006b). Since the pH in alkaline sea water is above pH 8 (Table 2), the polymerization of LMM cation was assumed irreversible and was described by the transfer rate k_{16} which was set to 0 in the lowest salinity interval, while it was high and slightly increasing with increasing salinity.

LMM cations can also sorb to the available surface of solid matter present as humic colloids and SPM, controlled by the transfer rates k_{12} and k_{13}, respectively. These sorption rates were lower than the polymerization rates (k_{16}) and were assumed to decrease with increasing salinity due to stronger competing effects of ions in salt water and reduced available sorption surfaces of aggregated particles. Sorption of LMM cation to seabed sediments (k_{14}) was assumed to be negligible and was set to 0. Electrostatic sorption processes are reversible, and the corresponding remobilization was described by the rates k_{21} (desorption from colloids), k_{31} (desorption from SPM) and k_{41} (desorption from seabed), respectively, which all were assumed to increase with increasing salinity. While a significant fraction of Al is assumed fixed to slowly reversible or irreversible sites at mineral particles, a large fraction of the colloidal fraction is reversibly associated to colloids in river water that easily remobilize in sea water. Hence, the rate k_{21} (desorption of LMM cations from humic colloids) was relatively large and higher than the desorption rates from particles (k_{31}). The desorption rates from seabed (k_{41}) was reduced with a factor ϕ compared to k_{31} since the interaction surface is smaller for seabed particles than for suspended matter (Periáñez et al., 2018). Due to the combination of relatively high fraction of humic colloids

in the river input and that desorption from humic colloids (k_{21}) was higher than desorption from SPM and seabed sediments (k_{31} and k_{41}, respectively), the input to the LMM cations was mainly controlled by the humic colloid concentration. This in turn controlled the fraction available for the rapid polymerization (k_{16}).

The polymers can dissolve as LMM anions or aggregate to SPM, which both are rapid processes. Polymerization and remobilization of LMM anions from the polymer species were described by the rates k_{56} and k_{65}, respectively, the latter was around 30 times higher than the first one. As these rates are sensitive to pH, they were both assumed to be unchanged with respect to salinity, as the pH was reported to increase only from 7.3 to 8.3 (Table 2).

The rate of particle formation by aggregation of humic colloids (k_{23}) is substantial, but assumed to be lower than that of remobilization (k_{21}). Due to aggregation of colloids and sedimentation of particles, lower concentration is observed in estuarine water than predicted by dilution (Hydes and Liss, 1977), and the aggregation was assumed to increase with increasing salinity due to suppression of the electrical double-layers of particles (Lebovka, 2012). Similarly, the rate describing aggregation of polymers (k_{63}) was assumed to increase with increasing salinity. The effect of mechanical stress on the particles resulting in decomposition (weathering) to smaller species (k_{32} and k_{36}) was considered negligible and hence these rates were set to 0.

The interactions between LMM and the solid matter (SPM or seabed sediments) have in some ocean transport studies successfully been simulated as two-step functions, with one compartment where the trace element is reversibly bound (adsorbed) to the surface and one with slowly re-

versible/irreversible bindings (e.g. Periáñez, 2003, 2004). These processes are however expected to play a minor role in short-term and near-shore simulations (Periáñez et al., 2018) and were therefore ignored here.

3.2. Model assessments

To validate the model hydrography and predicted Al concentration in the present study, data obtained from a number of CTD records and water samples have been used. With high spatial and temporal resolution, the current model configuration provides high detail levels in the results with obvious advantages, especially when local small-scale processes with rapid fluctuations are investigated. Validation of model results with *in situ* measurements may, however, be challenging. Due to the fundamental underlying differences between the concentration levels achieved from numerical models and from *in situ* observations, some discrepancies are expected when comparing model results with observations (Sandvik et al., 2016). While models compute average values in a finite volume and time period, observation samples are snap-shot values attributed to a certain point. In regions with non-uniform distribution, this representation error associated to the samples may therefore be considerable (Janjić et al., 2018). Although the resolution in our model is considered to be high in most contexts, small-scale natural processes at sub-grid scales, that cannot be properly resolved by the model, may be significant here as well, especially close to the river outlets, and need therefore to be parameterized. Other factors that may affect the model performance are smoothing of the coastline and topography in the model, response time in the model and negligence of background concentration of Al in inflowing coastal water.

However, our study is aiming to describe the Al speciation and transport through the whole fjord, at relatively high spatial and temporal resolution, utilizing a suggested set of estimated transfer rates. Based on transformation kinetics (Section 3.1), the transfer rates were chosen aiming to achieve reasonable distributions at relatively short as well as long time scales utilizing local measurements where applicable. Hence, to resolve the details of the speciation and transformation processes accurately, high resolution was required. Although the very rapid transformation processes (e.g., minutes) were omitted, this makes the model able to provide concentration levels in the complex speciation setup through the estuary from the river outlet to the open ocean.

3.2.1. Validation of hydrography in the hydrodynamic model

The comparison between the measured CTD-profiles and corresponding values from the hydrodynamic model revealed that the model in general reproduced the observed salinity and temperature relatively well. However, the model predicted too high salinities (7 psu in average) in the surface layer (Fig S.3). The salinity error decreased linearly with depth and was close to zero at about 13 m below surface, indicating that the offshore salinities were realistic. The temperatures in the model were around 2 °C too low in the surface layer and around 1.5 °C too high at depths below 11 m.

The model bias in near-surface salinities was not evenly distributed along the fjord. Comparison between the measured surface salinities and the corresponding model predictions show large variability and a relatively small bias at the stations in the inner part of the fjord, while the model overestimated the salinities closer to the fjord mouth (Fig S.4). The first indicates that

the applied freshwater discharges were realistic, although there may be deviations according to timing of the run-off pulses. The latter indicates that the modeled near-surface salinity exaggerated the along-fjord gradient, and this may be attributed to too weak vertical stratification and deficiencies in the vertical mixing in the ocean model.

3.2.2. Strong wind event May 12, 2008

Strong winds will have a huge effect on the vertical positioning of the pychnoclines along the shore, either by elevating the pychnoclines during offshore winds (upwelling) or lowering during onshore winds (downwelling). The distribution of the water masses may then be altered for hours or days. Fig 3 shows predicted along-fjord transects[1] of modeled salinity for the upper 20 m before, during and after a strong wind-driven overturning of the water masses occurred in the morning of May 12, 2008. The on-shore winds reached gale force from the north-east[2]. In the model, this event induced inflow of coastal water masses into Sandnesfjorden and subsequent deep mechanical mixing with downwelling of the near-shore water masses, then resulting in an increased near-surface salinity in the outer part of the fjord. Before the event (May 11, 2008 at 21 UTC, Fig 3a), the isohalines were mostly organized horizontally with a thin low salinity surface layer. The freshwater input from River Storelva is clearly seen as low salinity water in the inner part of the

[1]Transects from the hydrodynamic model were computed using routines from the 'roppy' library (`https://github.com/bjornraa/roppy.git`)

[2]At Lyngør Lighthouse, the nearest meteorological station, the wind speed exceeded $9\,\mathrm{m\,s^{-1}}$ between May 12 at 04 UTC and May 12 at 09 UTC (Data from Norwegian Meteorological Institute, `www.eklima.no`).

fjord. At the end of the strong wind period (May 12, 2008 at 09 UTC, Fig 3b), the outer part of the fjord became more vertically well-mixed, with weaker stratification and higher surface salinity. At the same time, the model shows that due to the strong wind-driven surface currents pushing coastal water into the fjord, the discharged river water was blocked in the inner part of the fjord, and thereby reducing the salinity through the whole water column near the river outlet. The isohalines became more vertically aligned than before the wind increased. In the afternoon, when the wind had ceased (May 12, 2008 at 15 UTC, Fig 3c), the accumulated river water flushed out of the fjord, resulting in a low salinity layer near the surface as the water masses returned towards the original state.

These rapid exchanges of water masses suggest that the exact location, timing and sampling depth will have large impact on the measured values. With strong gradients, the representation uncertainty in the observations is considerable, and similarly, small displacements of physical features will affect the model results significantly. Model-observation comparison under such circumstances has to be done carefully, since small spatial or temporal displacement of a local phenomena can lead to large deviations in the comparisons.

3.2.3. Trajectory age at the stations

In order to demonstrate how fast the trace elements were transported away from the release point at Laget to different locations in Sandnesfjorden, histograms of the modeled age of trajectories present in the surface water at the four stations are shown in Fig 4. Most of the trajectories arrived at Hope less than six hours after they were released, with the peak value between 2

and 3 hours. The age increases with distance from the source, and at Store Furuøy, near the fjord mouth, the peak was between 24 and 36 hours. Hence, as the time resolution in the hydrodynamic fields as well as the phase shift was 1 hour, there were few possibilities for the model trajectories to obtain the correct phase distribution already at Hope, even with high transfer rates. A better agreement with observed distribution of Al species could therefore be expected at the stations at the greatest distance from the source.

3.3. Total concentrations

Horizontal distribution of modeled total Al concentration (sum of all Al species) is shown in Fig 5, for a date with high river flow early in the simulation period (Fig 5a) and for dates later in the period, when the observation samples were taken (Fig 5b–d). Due to dilution of river water, the estimated concentration levels generally decreased with distance from the river outlet, with occasional accumulation of Al in near-shore bays and coves along both shores. While neglecting background level of Al in the coastal water, the modeled concentration levels decreased towards zero in the far-field regions. Due to generally decreasing Al discharges through the time period, the Al inventory in the fjord also decreased with time. A clear effect of the strong wind event is seen at May 12 (Fig 5c), with remarkably higher surface Al concentration in the inner part of the fjord and reduced Al concentration levels in the outer part compared to the other dates.

Included in the figure are also surface observations of total Al concentration from Hope, Hopestranda and Store Furuøy at May 10, May 12 and May 21, as well as from Skåttholmen at May 12 (Table 2). In general, the model results agreed well with measured data, although the Al concentrations were

underestimated in the outer part of the fjord at all times, primary attributed to the negligence of background contamination in the coastal water. This is confirmed by the time series in Fig 6, showing time series of estimated surface total concentration and salinity from the model simulation as well as surface samples of observed total Al concentration and salinity (Table 2) and the surface values (upper 1 m mean) of salinity from the CTD casts taken at the stations. As previously shown (Section 3.2.1), the modeled surface salinity was systematically overestimated at all stations (7 psu in average), mostly near the fjord mouth and in the beginning of the period. Later in the simulation period, the agreement with observed surface salinity was pretty good (<5 psu) at all stations.

At least in the outer part of the fjord, the dilution of river water, causing increased salinity and decreased surface concentration as the riverine water propagate through the fjord, was overestimated by the model. This points to a too weak stratification and too strong vertical mixing of the water masses in the hydrodynamic model. This is a well-known feature related to coastal modeling, especially under stable stratified conditions (Zilitinkevich et al., 2007). Numerical models tend to smooth out such strong gradients due to discretized model layers and imperfect parameterizations of turbulent flow features. Such large gradients caused by small-scale processes can therefore not always be expected to be properly resolved by the models. It appears that in this particular case, the water masses were strongly stratified with a thin surface layer consisting of almost pure river-water. This layer was only slightly diluted by the coastal water, and hence high Al concentration and low salinity was observed even in the outer part of the fjord. This was

supported by the observed Al concentrations which hardly decreased from Hopestranda to Store Furuøy. The water masses in the model were, however, more effectively diluted due to a combination of too strong upwelling of uncontaminated deep water and too strong vertical turbulent mixing, and the concentration levels decreased with around a factor 5 between Hopestranda and Store Furuøy (Fig 5). This resulted in overestimated salinity (>10 psu) and underestimated Al concentration (up to factor 4), especially in the outer part of the fjord.

In our discharge scenario, only Al releases from River Storelva were considered. Generally, other potential sources that in reality may contribute to the observed metal contamination are releases from nearby rivers, diffuse surface run-off such as agriculture and roads, atmospheric deposition and discharges through the groundwater (Machado et al., 2016). Particularly in our case, output from nearby rivers mixing Al into the coastal current upstream (north) of Sandnesfjorden were expected to contribute to some extent. Assuming constant Al concentration in the coastal water, the contribution of background concentration should be linearly correlated with the salinity. Hence, to account for Al concentration in surrounding Skagerrak water, a background term was added to the model predicted concentration (C), with the relation:

$$\hat{C} = C + \frac{C_0}{S_0} S, \tag{5}$$

where $\hat{C}$ was the background corrected concentration. C_0 and S_0 were set according to data taken at approximately 20 m depth in Flødevigen at May 22, 2008 (Table 2), considered to be representative for the background levels in surrounding coastal water. Time series of estimated concentration levels

inclusive this background term are shown with the black lines in Fig 6. As intended, the Al concentrations increased mainly in the outer part of the fjord, while it was almost unchanged in the inner part. Although this background correction could not completely account for the deviation between the model results and observations at Store Furuøy, the inclusion of the background level of Al improved the model output.

Looking at the other available background data (Table 2), the variability in observed Al concentration was disproportionately high, despite small variations in salinity. Hence, according to our limited dataset, the deep water cannot be assumed to keep constant background concentration, and other additional, and presently unknown, important factors were causing the variability. Even though there are reasons to believe that a substantial fraction of the Al contamination in the outer part of Sandnesfjorden came from other sources than River Storelva, applying a salinity-dependent background term as in Equation (5) will introduce large uncertainties associated with both algorithms and input data. Therefore, the results in the rest of this paper will be presented exclusive the background term, although the reader should be aware that the results should principally be corrected for this term.

Single occasional episodes such as the strong wind event at May 12 (discussed in section 3.2.2) also affected the model results heavily at all stations, with increased mixing of deep-water in the outer part of the fjord. In the inner part of the fjord, a notable difference between model results and observations is seen. While the model predicted accumulation of river water with decreasing surface salinity and increasing Al concentration, this was not evident in the observations. Actually, at all stations, even at Hope and Laget

(Table 2), the observed surface salinity increased considerably (> 5 psu) between May 10 and May 12, while the Al concentration decreased with more than 30 %. This indicate that in this particular situation, the entrainment of deep-water to the surface was stronger in reality than predicted by the model, even in the inner part of the fjord, close to Laget. Neither was the predicted accumulation of river water seen in the observations. In addition, processes taking part upstream of Laget, outside the model domain and hence not captured by the model, might also have contributed to disagreements between model and observations.

Numerous other factors could also have contributed to discrepancies between model and observations. As discussed above, a slightly temporal or spatial displacement of the dynamical structures may result in large errors when comparing to a few *in situ* samples. From the model results, we have identified large spatial gradients as well as rapid exchanges of the water masses. Therefore, the representation errors may be considerable, and we cannot assume all the estuarine dynamics and variabilities to be captured by the observation samples. Due to strong vertical stratification and near-surface gradients, the measurements were affected by the exact depth of the sample equipment, where small perturbations in the sampling depth, caused by waves and motions in the vessel, might have affected the results. The measured salinity can thus be expected to be slightly underestimated. In addition to the factors regarding the flow field from the hydrodynamic model, model errors can also be attributed to uncertainties in parameterizations and assumptions in the configuration of the transport model such as uncertainties in the discharges.

3.4. Conservative behavior

Due to dilution in estuaries, river-discharged contaminants with low sea water concentration are expected to show so-called 'conservative behavior' with a negative linear correlation between concentration and salinity (Machado et al., 2016). Such a relationship was observed in Sandnesfjorden (Fig 7a), where the field experimental Al concentration and salinity data taken during our simulation period were strongly negatively correlated (Pearson $r = -0.97$, Table 4). Despite these correlated observational data, when extracting model estimated time series from fixed positions, the temporal variability of Al concentration and salinity were only slightly correlated. The correlation was low at all stations (Table 4), highest at the stations near the river outlet (Hope and Skåttholmen), and close to zero at Hopestranda and Store Furuøy. As expected, the model variability was higher than the observed, due to a higher number of 'sample pairs' from the model (n=1004) than in the observations (n=10), covering a broader range of conditions. The salinity bias and negligence of background concentration were both expected to affect the results as discussed in Section 3.3, but due to the large uncertainties involved, these corrections were not included in the model results shown in the present subsection.

In contrast to the low correlation at each station, the correlation in total for all stations was relatively high (Pearson $r = -0.80$, Table 4). This indicate that the model predicted a general trend of conservative behavior when considering Sandnesfjorden as a whole. However, some deviations from this conservative behavior occurred, especially in the results from Hopestranda (Fig 7a). Although the Al concentration in general decreased and the salinity

increased with increasing distance from the river outlet, occasionally, both the Al concentration and the salinity increased from Hope to Hopestranda. As seen in the maps in Fig 5, Al was accumulated with high concentration gradients close to the shore near the location of Hopestranda. Only a gentle displacement of these fronts in the model could have large impacts on the results. Hence, the high Al concentrations predicted at Hopestranda might have been attributed to such small gradient disagreement between model and reality. Deviations from the conservative behavior are also expected to be caused by uncertainties in the model representation of current flow and mixing properties, variabilities in salinity in the coastal water and uncertainties in the Al concentration and freshwater flow rate in the river. In addition, transformation of Al species will complicate the transport due to sorption/desorption processes as well as aggregation, precipitation and resuspension of of colloidal and particle species.

With wind forcing, freshwater input, tides and baroclinic pressure gradients being the most important contributors for controlling the surface currents in the fjord, we expected the surface flow pattern to be a major contributor for the deviation from conservative behavior. Therefore, to identify times when the model predicted conservative behavior, in contrast to situations in which the results were non-conservative, the model results were divided into two groups depending on the upper layer volume flux[3] through

[3]The upper layer volume flux from the hydrodynamic model (between surface and 1 m depth) was computed with routines from the 'roppy' library (`https://github.com/bjornaa/roppy.git`). Instead of using instantaneous values, a weighted running mean of the previous 36 h volume flux was used, filtering out the signal of the high frequent

a cross section between Hope and Skåttholmen, marked with a blue line in Fig 1. The first group consisted of situations at low flux conditions, while the high flux conditions were in the second group, shown as time series in Fig 8a. The figure also shows the bias in the surface salinity (comparison of corresponding model and CTD data) computed in each of the four stations.

While the magnitudes of both the flux and the surface salinity bias were highest in the first days of May, there was a general decreasing trend through the remaining time period for both variables. The surface salinity bias and the flux were slightly correlated ($r = 0.5$) with lowest bias under low flow conditions, thereafter increasing bias with increasing volume flux (Fig S.5). The first group, consisting of times with low volume flux (below average, $33\,\mathrm{m^3\,s^{-1}}$), is indicated with green colors in Fig 8a, while times with high volume flux (above average, $33\,\mathrm{m^3\,s^{-1}}$) were in the second group, indicated with red colors.

These two groups were recognized as different regimes in the water masses, affected by river flow rates and wind forcing, as shown by the Hovmöller plot of the salinity field from Skåttholmen site in Fig 8b. Situations in the low flux regime were characterized by relatively low river flow rates (Fig S.1) and prevailing northeasterly winds (not shown), accumulating freshwater in the inner part of the fjord. In the period between April 29 and May 2, the thickness of the surface freshwater layer exceeded 2 m depth (Fig 8b). In the period after May 12, there were moderate winds from shifting directions and weaker stratification of the water column. The high flux events appeared

variability.

in time periods with weak winds from changing directions (but mostly from southwest) and high river flow rates. The salinity increased rapidly between the surface and the well-mixed saline water below the halocline which was located closer to the surface than it was during low flow. Thus, the strong flux may be responsible for upwelling of saline deep water to relatively shallow depths.

Although variations in the flux cannot fully explain the occasional non-conservative behavior in the model, the two different flux regimes (Fig 7b–c) were clearly distinguishable. The low flux events (Fig 7b) appeared to be in good qualitative agreement with the observed pattern, with a clear conservative trend, i.e., high negative correlation between salinity and Al concentration (Table 4). In contrast, the high flux events (Fig 7c) were characterized by increasing Al concentration between Hope and Hopestranda and lower correlation (non-conservative behavior).

This behavior may also partially be explained by assumptions related to the model configuration, such as resolution. Although horizontal resolution of 32 m is considered to be relatively high in most oceanographic contexts, the results were most likely affected by factors such as un-resolved sub-grid scale dynamics, transformation of species and by the model displacement of the river outlet. The non-conservative behavior could also have been caused by local near-shore features at Hopestranda, and by imperfect model descriptions of vertical mixing and upwelling processes. Combining these factors, the model might have overestimated the surface current velocities, especially in the inner part of the fjord. Too strong currents near the discharge point would have overestimated the flushing of Al away from the river outlets.

Further out, where the current speed became lower, the Al contaminants would accumulate, giving rise to increasing Al concentration between Hope and Hopestranda.

However, due to a limited number of field experimental results, (samples were only collected from three days during the simulation period), it is not clear if the occasions of non-conservative behavior shown by the model under high flow events were a part of the natural variability or if they were caused by artificial or numerical mis-predictions introduced by the model system. But what is clear is that these occasional events where the model estimated increasing Al concentration from Hope to Hopestranda appeared almost exclusively during high flow events. Hence, according to the available observations, the model performed best during low flow.

3.5. Distribution of Al species

Contour plots of modeled surface concentrations in each of the elemental species are shown in Fig 9, for a date early in the simulation period with high river flow (May 2, 2008, Fig 9a–c) and a date later in the simulation period with lower river flow (May 21, 2008, Fig 9d–f). At the May 21 plot, the model results are compared with observed surface concentration of Al species. The pattern of the LMM species (Fig 9a and d) was quite homogeneously distributed through the fjord with relatively high concentration levels (40–50 $\mu g\,L^{-1}$) reaching almost out to the mouth of the fjord. In the inner part of the fjord, the LMM fraction consisted mainly of cations, while the outer part was dominated by anions which were dissolved from polymers (not distinguished in figure). The colloidal (Fig 9b and e) and particle species (Fig 9c and f), in contrast, had the highest surface concentration levels in

the inner part of the fjord, which decreased towards the fjord opening and thus had stronger gradients along a fjord transect than the LMM fraction. Since the particles settled towards the bottom, they were effectively removed from the surface water layer, especially during low flow (Fig 9f). Under high flow, the surface particle concentration was relatively high also in the outer part of the fjord (Fig 9c).

Scatter plot of estimated Al concentration and salinity for each specie in Fig 10 was in good agreement with our intended behavior of the transformation processes (Section 3.1). With river discharges distributed between LMM cation, humic colloids and particles, the highest concentrations of these species appeared at low salinity at Hope, near the river outlet. Affected by dilution, the concentration of these species decreased with increasing salinity. However, due to rapid remobilization of Al reversibly associated to humic colloids and subsequent polymerization of LMM cations, the concentration of these species decayed faster than the linear dilution, dependent on the time of the reactions. The polymers were formed from the LMM cations at high transfer rates (k_{16}), and were assumed to be unstable with short life time. Hence, the pattern of the polymer species was similar to that of the LMM cation species, except at the very lowest salinities. The concentration of LMM cations and polymers of Al decreased rapidly with increasing salinity, and both were highest near the river outlet. Predicting these species is essential since they are assumed to be the most toxic to biota (Teien et al., 2006a). As the remobilization of polymers was fast (k_{65}), while the polymerization of LMM anions was slower (k_{56}), the life time for the LMM anions became relatively long. Therefore, as a consequence of higher mobilization

rate than dilution close to the river outlet, the concentration of LMM anion species increased with increasing salinity from Hope to Hopestranda, reaching a maximum at around 15 psu. By correcting for the salinity bias (Section 3.2.1), the modeled LMM anion concentration would have reached maximum at around 5–10 psu, in agreement with Kroglund et al. (2011c). Further out in the fjord, from Hopestranda to Store Furuøy, the LMM anion concentration decreased due to dilution. The prediction of LMM anions is also of interest as these species are known to be reactive towards fish gills (Teien et al., 2011).

Time series of estimated and observed Al specie distribution at the stations are shown in Fig 11. The observed colloidal fraction was close to zero and was overestimated by the model at all stations, especially at Hope and Skåttholmen where the model predicted $\sim 30\,\%$ colloids. At the same time, the LMM fraction was underestimated by the model, also this mostly at the innermost stations. At Hope, the model predicted $\sim 40\,\%$ LMM species, while the observed fraction was $\sim 75\,\%$ (Fig 11). This may be explained by the negligence of background Al in coastal water (mainly present as LMM species, Section 3.3), the assumptions regarding specie distribution in the discharges (Section 2.2.2) and the relative short distance between the river outlet and the first stations (Section 3.2.3). With only a few hours travel time after release, and hence only a few possibilities for transformation of species, the trajectories did not have sufficient time to obtain the expected specie distribution. This issue was however improved in the model results at Hopestranda and Store Furuøy, the stations located most far away from the source as well as in the late time period at all stations.

Comparison with observed fractions shows that the particle fraction was relatively well predicted by the model at all stations. The response of the river flow is clearly seen in the time series for the predicted particle fraction at Hopestranda, as it increased at high flow and decreased under low flow conditions. Higher concentration of Al particles further out in the fjord under high flow conditions was also seen in the maps in Fig 9. An opposite pattern can be seen for the LMM fraction. Hence, at locations around Hopestranda, it can be assumed that the particle species mainly originated directly from river discharges, requiring high river flow rates and strong surface currents out of the fjord to reach that station. In addition, there are large uncertainties related to the role of interactions with the sediments. Sedimented particle-bound Al can be remobilized to become LMM cation species or be subject to resuspension to become particle species. Both processes will increase the transport time compared to the fraction that had not interacted with the seabed.

The combination of the results presented above indicate that to capture all the physico-chemical processes near the river outlet, the applied transfer rates might have been too slow. Alternatively, it may indicate that the travel time from river discharge to the trajectories reached the first stations was too short in the model simulations. In addition, the Al discharges were in reality most likely affected by transformation processes during the transit through the basins upstream of Lagstrømmen (Songevann and Nævestadfjorden, Fig 1), and by sub-grid scale processes in the mixing zone which were not explicitly resolved by our model. Hence, increasing the model resolution may be expected to improve the model skill in the inner part of the fjord.

However, these model-observations comparisons demonstrate that the model in general was capable to reproduce the observed concentration levels of Al species further out in the fjord. Although some weaknesses related to the above-mentioned issues in the current model setup limit the prediction skill somewhat with respect to toxicity, especially directly outside the river outlets, the model can be used to predict distribution of Al species at locations and times of interest within the model domain. Regarding the toxicity for living organisms, the speciation of the trace elements and radionuclides is essential (Teien et al., 2006b). Hence, utilization of such model transport simulations including dynamic transformation of species are highly needed and relevant for evaluation of the elemental specie distribution and other conditions in different parts of an estuary. By utilizing the link between elemental speciation, bioavailability, uptake in organisms and toxicity, such a model can be used for risk assessments.

4. Conclusions

Numerical transport models are useful and applicable tools for predictions of total concentration and metal speciation in the marine environment over large areas and over continuous time periods. The results provided here are unique as this is the first time transport and dynamic transformation kinetics involving colloidal species of a trace element in a fjord system has been predicted over a considerable time period, utilizing high resolution three-dimensional hydrodynamic model fields (32 m horizontal resolution). The present study is also unique as it compares predicted distribution of Al species to real observations at several locations and times during the simulation

period.

In general, results from the simulations validate relatively well with observed data of Al fractions taken in Sandnesfjorden in 2008. However, the quality of the results are affected by a number of more or less uncertain assumptions and input data involved in the model configuration. The observed correlation between salinity and total Al concentration (conservative behavior) appeared to be best predicted by the model under low flux conditions. Although the Al concentrations in the study area were densely monitored, with fractionation data taken at a several times and at a number of stations through the Storelva-Sandnesfjorden estuary, large uncertainties are still related to the description of the transformation processes. In the present case, imperfect hydrography predictions might have affected the transport estimates, and discrepancies between modeled and observed total Al concentration in the fjord mouth indicate significant contribution of Al from the coastal water, probably discharged from rivers through adjacent fjords and coastal areas. To reduce the uncertainties associated to the background levels in future monitoring fieldwork, we suggest that the Al concentration in coastal waters upstream of the key area are properly assessed, ideally by taking samples at different depths in surrounding waters during the whole monitoring period. The model predicted too weak vertical hydrography gradients, and hence, too strong mixing of fresh river water with the more saline coastal water was assumed to affect the model performance as the large near-surface gradients appeared to be smoothed out by the model. Other factors that were assumed to affect the results are imperfect implementation of the river discharges and parameterization of sub-grid scale processes. Hence, we sug-

gest even higher temporal and spatial resolution for further improvement of the model system, as well as a better description of the processes involved during transit through the river basins upstream of Lagstrømmen.

However, despite these issues, as the general trends of Al concentration and speciation were well reproduced, the results obtained by present work demonstrates the potential of high resolution models with dynamic speciation to predict exposure of contaminants such as metals and radionuclides for risk assessments in the marine environment. This is especially relevant for models that are able to provide predictions of the bioavailable species at high detail level in the full water column, not only in the surface. As the tool we have developed and applied in the present study is generic, it can easily be extended for application of other metals and radionuclides.

Acknowledgements

This study has been funded by The Research Council of Norway through its Centre of Excellence (CoE) funding scheme (Project No. 223268/F50). Thanks to Frode Kroglund for kindly sharing the CTD data.

References

Albretsen, J., Sperrevik, A. K., Staalstrøm, A., Sandvik, A. D., Vikebø, F., Asplin, L., 2011. NorKyst-800 report no. 1: User manual and technical descriptions. Fisken og havet.

Beldring, S., Engeland, K., Roald, L. A., Sælthun, N. R., Voksø, A., 2003. Estimation of parameters in a distributed precipitation-runoff model for

Norway. Hydrology and Earth System Sciences 7 (3), 304–316.
URL 10.5194/hess-7-304-2003

Döös, K., Engqvist, A., 2007. Assessment of water exchange between a discharge region and the open sea – A comparison of different methodological concepts. Estuarine, Coastal and Shelf Science 74 (4), 709 – 721.
URL https://doi.org/10.1016/j.ecss.2007.05.022

Döös, K., Jönsson, B., Kjellsson, J., 2017. Evaluation of oceanic and atmospheric trajectory schemes in the TRACMASS trajectory model v6.0. Geoscientific Model Development 10 (4), 1733–1749.
URL https://doi.org/10.5194/gmd-10-1733-2017

Döös, K., Rupolo, V., Brodeau, L., 2011. Dispersion of surface drifters and model-simulated trajectories. Ocean Modelling 39 (3–4), 301 – 310.
URL https://doi.org/10.1016/j.ocemod.2011.05.005

Hydes, D., Liss, P., 1977. The behaviour of dissolved aluminium in estuarine and coastal waters. Estuarine and Coastal Marine Science 5 (6), 755 – 769.

Janjić, T., Bormann, N., Bocquet, M., Carton, J. A., Cohn, S. E., Dance, S. L., Losa, S. N., Nichols, N. K., Potthast, R., Waller, J. A., Weston, P., 2018. On the representation error in data assimilation. Quarterly Journal of the Royal Meteorological Society 144 (713), 1257–1278.
URL https://doi.org/10.1002/qj.3130

Kroglund, F., Haraldstad, T., Teien, H.-C., Salbu, B., Rosseland, B., Gütturp, J., 2011a. Påvirkes laksesmolt av aluminium i brakkvann? Storelva i Holt, Aust-Agder og Audna, Vest-Agder, 2006. Niva-rapport

6244-2011, Norsk institutt for vannforskning, in Norwegian with English summary.

Kroglund, F., Høgberget, R., Haraldstad, T., Økland, F., Thorstad, E. B., Teien, H.-C., Rosseland, B. O., Salbu, B., Nilsen, T. O., Stefansson, S. O., Guttrup, J., 2011b. Are salmon smolts affected by aluminium in estuaries? Results from River Storelva, 2007. Niva-report 6245-2011, Norsk institutt for vannforskning, in Norwegian with English summary.

Kroglund, F., Høgberget, R., Haraldstad, T., Økland, F., Thorstad, E. B., Teien, H.-C., Rosseland, B. O., Salbu, B., Nilsen, T. O., Stefansson, S. O., Guttrup, J., 2011c. Are salmon smolts affected by aluminium in estuaries? Results from River Storelva, 2008. Niva-report 6246-2011, Norsk institutt for vannforskning, in Norwegian with English summary.

Lebovka, N. I., 2012. Aggregation of charged colloidal particles. In: Müller, M. (Ed.), Polyelectrolyte Complexes in the Dispersed and Solid State I: Principles and Theory. Springer Berlin Heidelberg, Berlin, Heidelberg, pp. 57–96.
URL https://doi.org/10.1007/12_2012_171

Lien, V. S., Gusdal, Y., Vikebø, F. B., 2014. Along-shelf hydrographic anomalies in the Nordic Seas (1960–2011): locally generated or advective signals? Ocean Dynamics 64 (7), 1047–1059.
URL https://doi.org/10.1007/s10236-014-0736-3

Lind, O. C., Oughton, D. H., Salbu, B., Skipperud, L., Sickel, M. A., Brown, J. E., Fifield, L. K., Tims, S. G., 2006. Transport of low 240Pu/239Pu

atom ratio plutonium-species in the Ob and Yenisey Rivers to the Kara Sea. Earth and Planetary Science Letters 251 (1), 33 – 43.
URL https://doi.org/10.1016/j.epsl.2006.08.023

Lydersen, E., 1990. The solubility and hydrolysis of aqueous aluminium hydroxides in dilute fresh waters at different temperatures. Hydrology Research 21 (3), 195–204.
URL https://doi.org/10.2166/nh.1990.0015

Lydersen, E., 1991. Aluminium in Dilute Acidic Freshwaters: Chemical, Analytical and Biological Relevance. University of Oslo, Department of Biology.
URL https://books.google.no/books?id=HEeSPQAACAAJ

Lydersen, E., Salbu, B., Poleo, A. B., Muniz, W. P., 1990. The influences of temperature on aqueous aluminium chemistry. Water, Air, and Soil Pollution 51 (3-4), 203–215.

Lydersen, E., Salbu, B., Polèo, A. B. S., 1992. Size and charge fractionation of aqueous aluminium in dilute acidic waters: effects of changes in pH and temperature. Analyst 117, 613–617.
URL 10.1039/AN9921700613

Machado, A. A. d. S., Spencer, K., Kloas, W., Toffolon, M., Zarfl, C., 2016. Metal fate and effects in estuaries: A review and conceptual model for better understanding of toxicity. Science of The Total Environment 541, 268 – 281.
URL https://doi.org/10.1016/j.scitotenv.2015.09.045

Nilsson, J. A. U., Döös, K., Ruti, P. M., Artale, V., Coward, A., Brodeau, L., 2013. Observed and modeled global ocean turbulence regimes as deduced from surface trajectory data. Journal of Physical Oceanography 43 (11), 2249–2269.
URL http://dx.doi.org/10.1175/JPO-D-12-0193.1

Nyffeler, U. P., Li, Y.-H., Santschi, P. H., 1984. A kinetic approach to describe trace-element distribution between particles and solution in natural aquatic systems. Geochimica et Cosmochimica Acta 48 (7), 1513 – 1522.
URL http://dx.doi.org/10.1016/0016-7037(84)90407-1

Periáñez, R., 2003. Kinetic modelling of the dispersion of plutonium in the eastern Irish Sea: two approaches. Journal of Marine Systems 38 (3–4), 259 – 275.
URL http://dx.doi.org/10.1016/S0924-7963(02)00242-7

Periáñez, R., 2004. Testing the behaviour of different kinetic models for uptake/release of radionuclides between water and sediments when implemented in a marine dispersion model. Journal of Environmental Radioactivity 71 (3), 243 – 259.
URL 10.1016/S0265-931X(03)00172-3

Periáñez, R., Brovchenko, I., Jung, K., Kim, K., Maderich, V., 2018. The marine kd and water/sediment interaction problem. Journal of Environmental Radioactivity 192, 635 – 647.
URL https://doi.org/10.1016/j.jenvrad.2018.02.014

Periáñez, R., Elliott, A., 2002. A particle-tracking method for simulating the

dispersion of non-conservative radionuclides in coastal waters. Journal of Environmental Radioactivity 58 (1), 13 – 33.
URL http://dx.doi.org/10.1016/S0265-931X(01)00028-5

Rosseland, B., Blakar, I., Bulger, A., Kroglund, F., Kvellstad, A., Lydersen, E., Oughton, D., Salbu, B., Staurnes, M., Vogt, R., 1992. The mixing zone between limed and acidic river waters: Complex aluminium chemistry and extreme toxicity for salmonids. Environmental Pollution 78 (1), 3 – 8.
URL https://doi.org/10.1016/0269-7491(92)90003-S

Salbu, B., 2009. Fractionation of radionuclide species in the environment. Journal of Environmental Radioactivity 100 (4), 283 – 289.
URL https://doi.org/10.1016/j.jenvrad.2008.12.013

Sandvik, A. D., Øystein Skagseth, Skogen, M. D., 2016. Model validation: Issues regarding comparisons of point measurements and high-resolution modeling results. Ocean Modelling 106, 68 – 73.
URL https://doi.org/10.1016/j.ocemod.2016.09.007

Sanial, V., Buesseler, K. O., Charette, M. A., Nagao, S., 2017. Unexpected source of Fukushima-derived radiocesium to the coastal ocean of Japan. Proceedings of the National Academy of Sciences 114 (42), 11092–11096.
URL https://doi.org/10.1073/pnas.1708659114

Sañudo-Wilhelmy, S. A., Rivera-Duarte, I., Flegal, A. R., 1996. Distribution of colloidal trace metals in the San Francisco Bay estuary. Geochimica et Cosmochimica Acta 60 (24), 4933 – 4944.
URL https://doi.org/10.1016/S0016-7037(96)00284-0

Serra-Llinares, R. M., Freitas, C., Nilsen, R., Elvik, K. M. S., Albretsen, J., Bøhn, T., Karlsen, Ø., Bjørn, P. A., 2018. Towards direct evidence of the effects of salmon lice (Lepeophtheirus salmonis Krøyer) on sea trout (Salmo trutta L.) in their natural habitat: proof of concept for a new combination of methods. Environmental Biology of Fishes 101 (12), 1677–1692. URL https://doi.org/10.1007/s10641-018-0816-1

Simonsen, M., Lind, O. C., Øyvind Saetra, Isachsen, P. E., Teien, H.-C., Albretsen, J., Salbu, B., 2019. Coastal transport of river-discharged radionuclides: Impact of speciation and transformation processes in numerical model simulations. Science of The Total Environment 669, 856 – 871. URL https://doi.org/10.1016/j.scitotenv.2019.01.434

Simonsen, M., Øyvind Saetra, Isachsen, P. E., Lind, O. C., Skjerdal, H. K., Salbu, B., Heldal, H. E., Gwynn, J. P., 2017. The impact of tidal and mesoscale eddy advection on the long term dispersion of 99Tc from Sellafield. Journal of Environmental Radioactivity 177, 100 – 112. URL https://doi.org/10.1016/j.jenvrad.2017.06.002

Skalsbakken, M. L., 2009. Aluminium (Al) in freshwater and estuarine water, and use of sodium silicate as countermeasure for detoxification of Al in water from River Storelva.

Skamarock, W. C., Klemp, J. B., Dudhia, J., Gill, D. O., Barker, D. M., Duda, M. G., Huang, X.-Y., Wang, W., Powers, J. G., 2008. A Description of the Advanced Research WRF Version 3. Ncar technical note ncar/tn-475+str, NCAR, doi:10.5065/D68S4MVH.

Stokes, G. G., 1851. On the Effect of the Internal Friction of Fluids on the Motion of Pendulums. Transactions of the Cambridge Philosophical Society 9, 8.

Teien, H.-C., Kroglund, F., Salbu, B., Rosseland, B. O., 2006a. Gill reactivity of aluminium-species following liming. Science of the Total Environment 358 (1-3), 206—220.
URL https://doi.org/10.1016/j.scitotenv.2005.04.023

Teien, H.-C., Kroglund, F., Salbu, B., Åtland, A., Rosseland, B. O., 2011. Aluminium in alkaline and acid water – accumulation on gills and effects in fish. The ninth Keele meeting on Aluminium Niagara-on-the-Lake, Ontario, Canada, 19-23 February 2011.

Teien, H. C., Salbu, B., Kroglund, F., Rosseland, B. O., 2004. Transformation of positively charged aluminium-species in unstable mixing zones following liming. Science of The Total Environment 330 (1), 217 – 232.
URL https://doi.org/10.1016/j.scitotenv.2004.03.040

Teien, H.-C., Standring, W. J., Salbu, B., 2006b. Mobilization of river transported colloidal aluminium upon mixing with seawater and subsequent deposition in fish gills. Science of The Total Environment 364 (1), 149 – 164.
URL https://doi.org/10.1016/j.scitotenv.2006.01.005

Tjomsland, T., Kroglund, F., 2010. Modellering av strøm og saltholdighet i Sandnesfjorden ved Risør. Niva-rapport 6049-2010, Norsk institutt for vannforskning.

Zilitinkevich, S. S., Elperin, T., Kleeorin, N., Rogachevskii, I., 2007. Energy- and flux-budget (EFB) turbulence closure model for stably stratified flows. Part I: steady-state, homogeneous regimes. Boundary-Layer Meteorology 125 (2), 167–191.
URL https://doi.org/10.1007/s10546-007-9189-2

Table 1: Configuration of the dispersion simulations.

Parameter	Symbol	Value
Vertical diffusivity	A_v	$0\,\mathrm{m^2\,s^{-1}}$
Horizontal diffusivity	A_h	$10\,\mathrm{m^2\,s^{-1}}$
Particle diameter	d	$5\,\mu\mathrm{m}$
Particle density	ρ	$2600\,\mathrm{kg\,m^{-3}}$
Critical velocity for resuspension	v_{crit}	$0.05\,\mathrm{m\,s^{-1}}$
Sediment correction factor	ϕ	0.1
Total Al discharged in simulation	-	7556 kg
Number of trajectories in simulation	-	251874
Total Al concentration in river water	-	110-140 $\mu\mathrm{g\,L^{-1}}$
Discharge depth	-	0 m
Simulation period	-	2008.04.20 - 2008.05.31

Table 2: Observations of Al concentrations and salinity from Sandnesfjorden and surrounding areas obtained in May 2007 and 2008.

Date	Location	Position	Total Al ($\mu g\,L^{-1}$)	LMM ($\mu g\,L^{-1}$)	Colloid ($\mu g\,L^{-1}$)	Particles ($\mu g\,L^{-1}$)	Salinity (psu)	pH
2008.05.10	Laget	58.6788°N 9.0570°E	164	61	58	45	1.1	7.3
2008.05.10	Hope	58.6844°N 9.076 92°E	128	98	3	27	4.8	7.84
2008.05.10	Hopestranda	58.691 68°N 9.121 25°E	76	68	0	14	9.7	8.24
2008.05.10	Store Furuøy	58.702 42°N 9.212 87°E	93	-	-	-	9	8.12
2008.05.12	Laget	58.6788°N 9.0570°E	95	82	0	13	8.7	8.03
2008.05.12	Hope	58.6844°N 9.076 92°E	85	65	0	20	10	8.08
2008.05.12	Skåttholmen	58.687 93°N 9.094 77°E	41	37	0	4	14.6	8.20
2008.05.12	Hopestranda	58.691 68°N 9.121 25°E	21	17	0	4	17.2	8.22
2008.05.12	Store Furuøy	58.702 42°N 9.212 87°E	18	14	0	4	16.9	8.18
2008.05.21	Innløp Laget	58.6786°N 9.0478°E	140	35	58	47	1.1	7.50
2008.05.21	Hope	58.6844°N 9.076 92°E	81	60	2	19	7.9	8.24
2008.05.21	Hopestranda	58.691 68°N 9.121 25°E	78	61	0	17	10.4	8.13
2008.05.21	Store Furuøy	58.702 42°N 9.212 87°E	68	43	0	25	12.9	8.24
2008.05.22	Flødevigen	58.4248°N 8.7547°E	36	29	0	7	31.2	-
2008.05.11	Flødevigen	58.4248°N 8.7547°E	72	43	0	29	34.2	-
2007.05.08	Tvedestrand	58.5693°N 8.9999°E	19	15	0	4	28.9	-

Table 3: Time scales of the transfer rates in hours at different ranges of salinity.

	Process	0–1 psu	1–10 psu	10–20 psu	> 20 psu
k_{12}	LMM cation → Humic colloid	23	28	35	46
k_{13}	LMM cation → Particle	69	93	139	154
k_{16}	LMM cation → Polymer	-	2.3	2.0	1.9
k_{21}	Humic colloid → LMM cation	80	3	3	3
k_{23}	Humic colloid → Particle	139	70	46	28
k_{31}	Particle → LMM cation	80	48	40	30
k_{41}	Sediments → LMM cation	798	479	399	299
k_{56}	LMM anion → Polymer	-	56	56	56
k_{65}	Polymer → LMM anion	-	2	2	2
k_{63}	Polymer → Particle	-	12	4.6	3.5

Table 4: Correlation coefficients for modeled and observed salinity and total Al concentration (sum of all species) at the stations, for all times, times with low flux and times with high flux.

	Pearson	Spearman	n
Obs data	-0.97	-0.90	10
Total (All stations)	-0.80	-0.75	1004
Hope	-0.72	-0.69	251
Skåttholmen	-0.31	-0.23	251
Hopestranda	0.12	0.18	251
Store Furuøy	0.04	0.12	251
Total Low Flux	-0.89	-0.89	488
Total High Flux	-0.84	-0.73	480
Hope Low Flux	-0.78	-0.84	122
Hope High Flux	-0.70	-0.59	120
Skåttholmen Low Flux	-0.56	-0.53	122
Skåttholmen High Flux	-0.48	-0.40	120
Hopestranda Low Flux	-0.31	-0.26	122
Hopestranda High Flux	-0.20	-0.17	120
Store Furuøy Low Flux	-0.35	-0.38	122
Store Furuøy High Flux	-0.45	-0.27	120

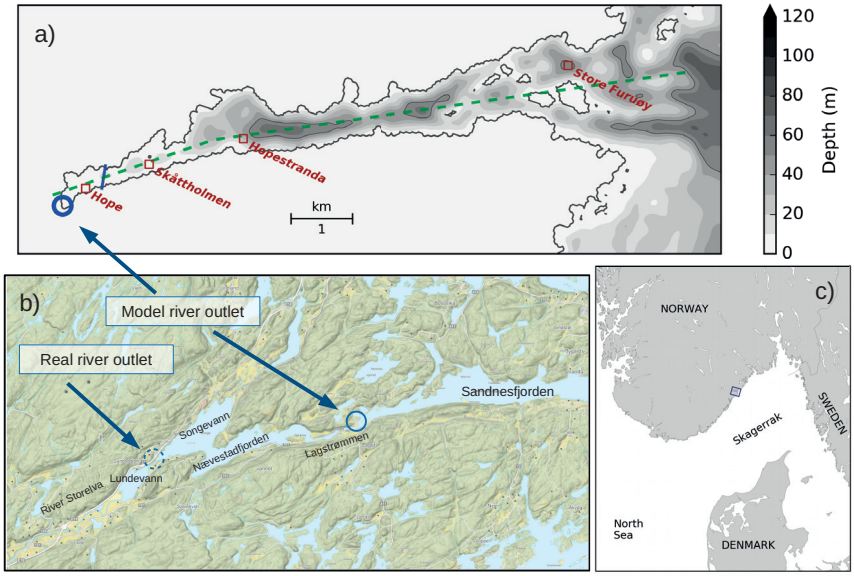

Figure 1: a: Subset of the model domain, showing the model coastline of the Sandnesfjorden area. The blue circle is the position of the discharge point, the red squares are the positions of the observation stations. Grey shading is depth contours. Blue solid line is the cross section for computation of the transport flux. Green dashed line is the transect shown in Fig 3. b: The waterways upstream of the model river outlet. Dashed blue circle is the real river outlet, solid blue circle is the model river outlet. Map from www.norgeskart.no. c: Overview of the Skagerrak region, the blue square indicates the model domain.

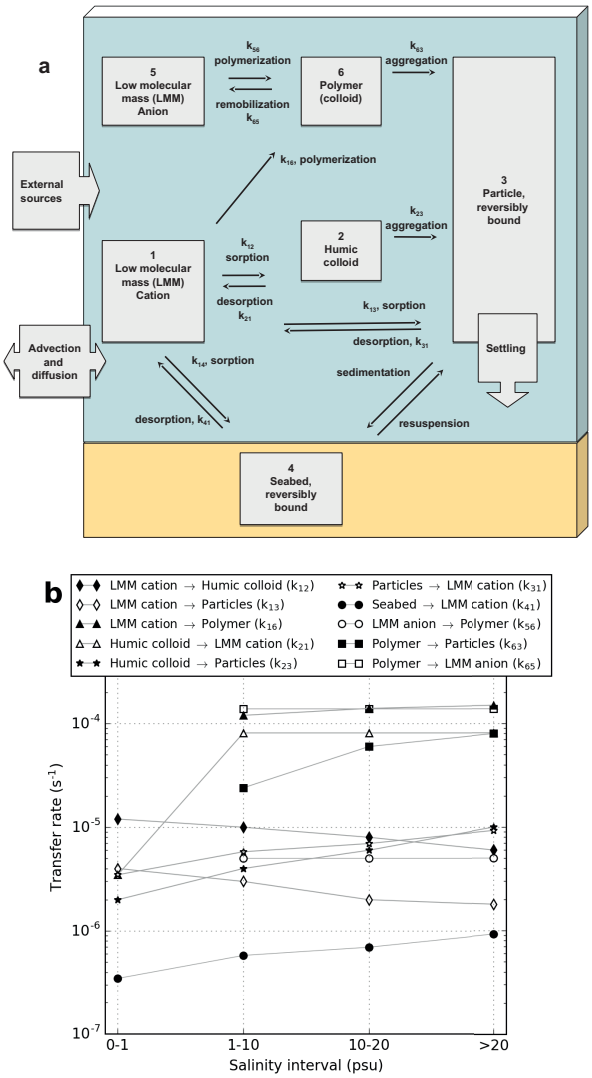

Figure 2: a: Model compartments based on Al species categories and interaction pathways. The external sources can introduce Al into any of the model compartments and may vary in time and space. It is not included any threshold limit for aluminate (LMM anion). Interaction between LMM and seabed is limited to the seabed interaction layer. Advection and diffusion determine the horizontal and vertical transport of Al in the water column. b: The estimated transfer rates.

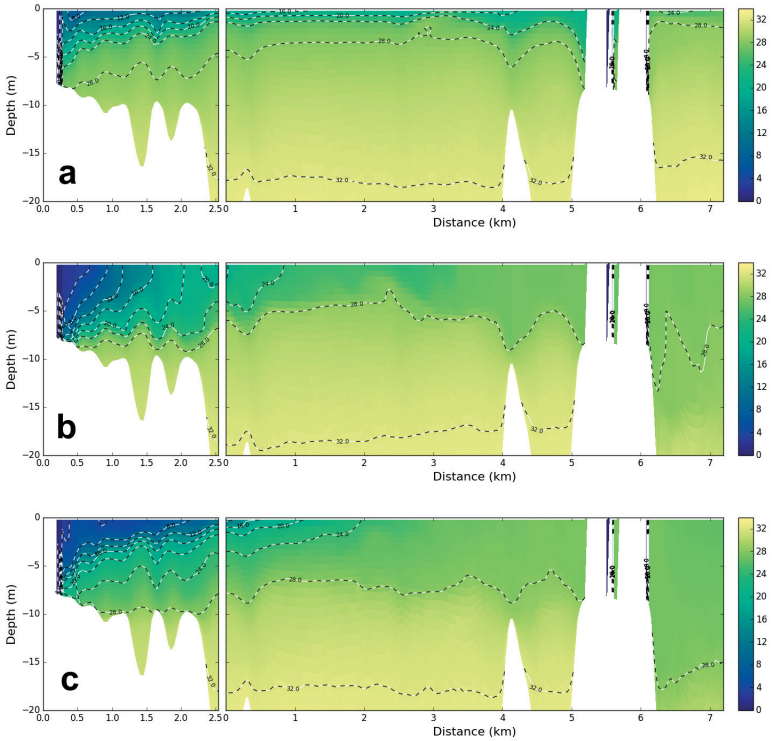

Figure 3: Salinity transects along the green dashed line in Fig 1 from the hydrodynamic model (ROMS), a: before the strong wind event (May 11 at 2100), b: during the strong wind event (May 12 at 0900) and c: after the strong wind event (May 12 at 1500).

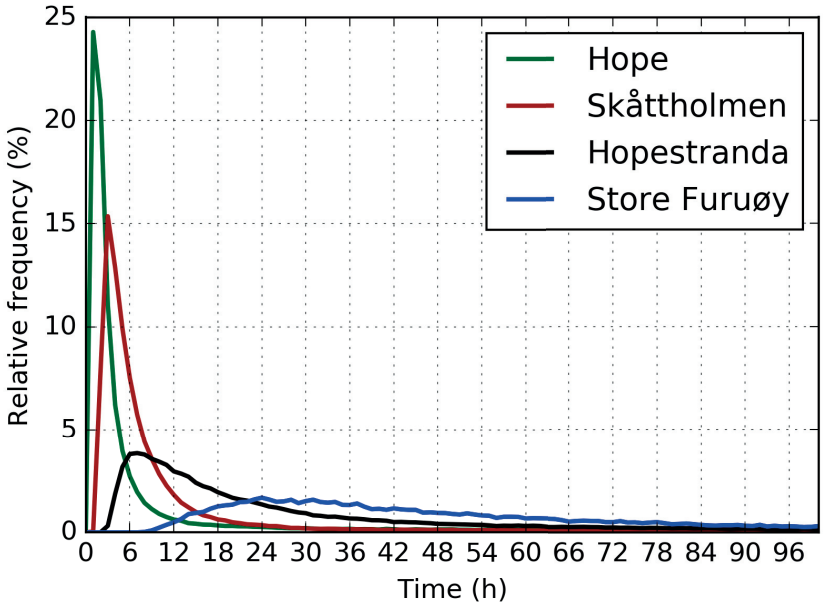

Figure 4: Relative distribution of modeled age for the trajectories at the four stations. For better visualization, the graphs are limited to the first 100 hours.

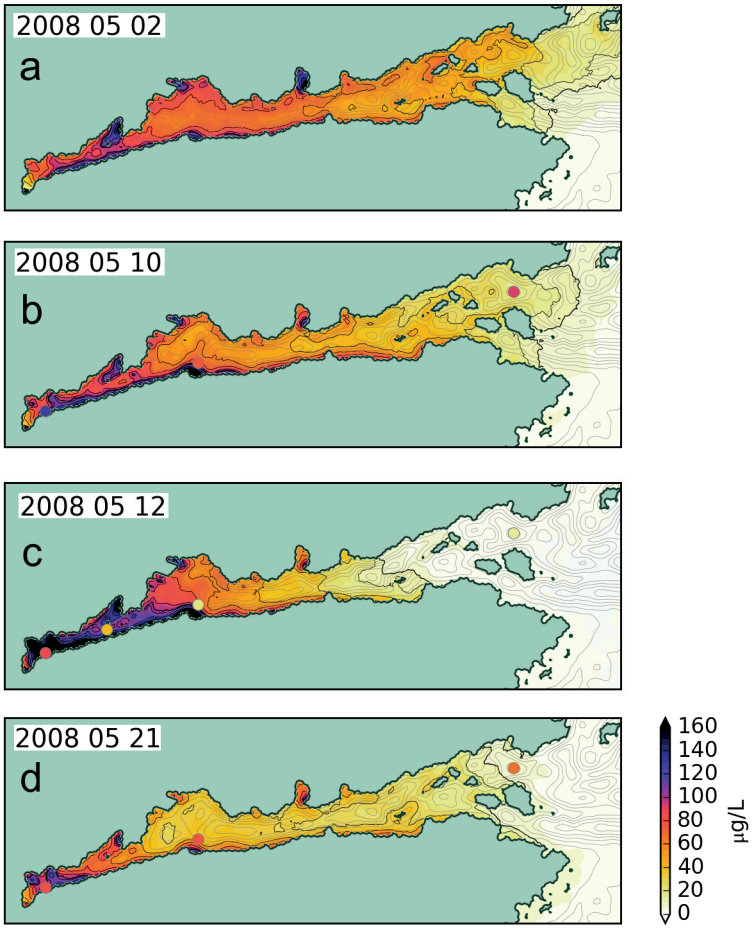

Figure 5: Contours of total surface (0–1 m average) Al concentration from the model at a: May 2, 2008, b: May 10, 2008, c: May 12, 2008 and d: May 21, 2008. Colored circles in panels b, c and d indicate observed surface total Al concentration.

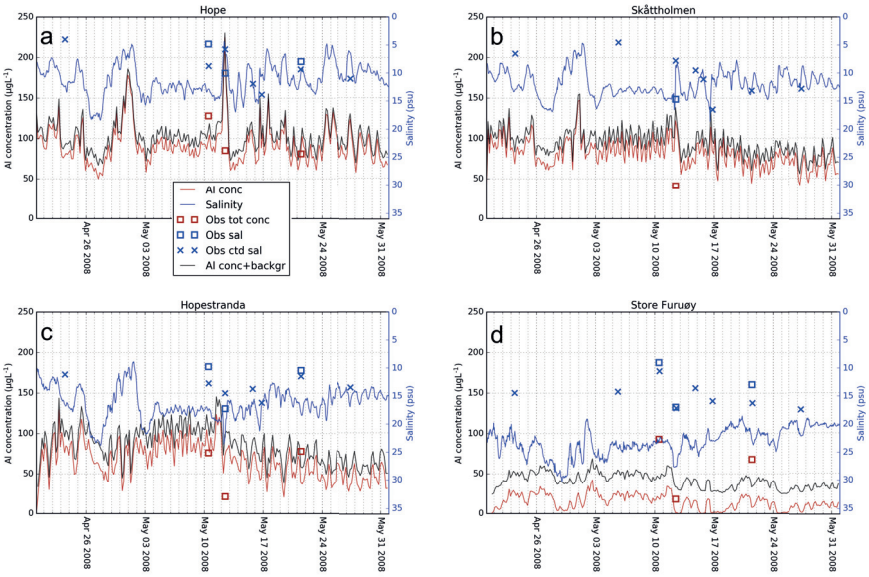

Figure 6: Time series of total surface (0–1 m average) Al concentration (red lines) and salinity (blue lines) from the model and observed surface samples taken at 1 m depth of total Al concentration (red squares) and salinity (blue squares) from a: Hope, b: Skåtholmen, c: Hopestranda and d: Store Furuøy. Blue crosses are mean salinity of the upper 1 m of the CTD casts. Black lines are Al concentration including additional background levels.

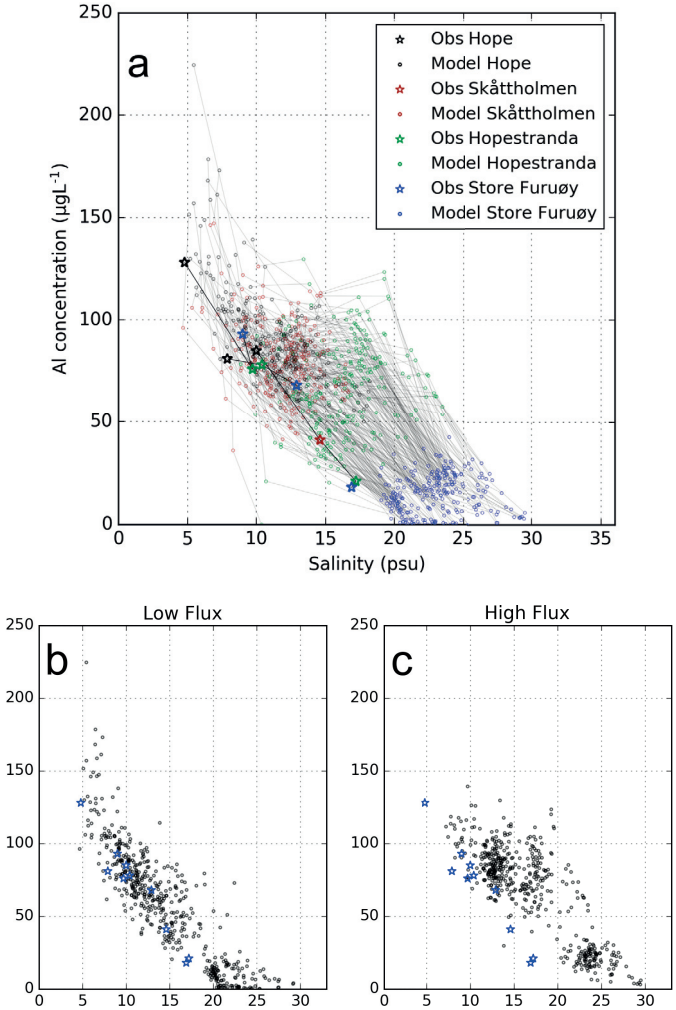

Figure 7: The estimated surface Al concentration and salinity from all stations. a: Model results (circles) from the four stations at equal time are connected with gray lines. Observations (stars) taken at equal dates are connected with black lines. b: Model results (circles) and observations (stars) from low flux events. c: Model results (circles) and observations (stars) from high flux events.

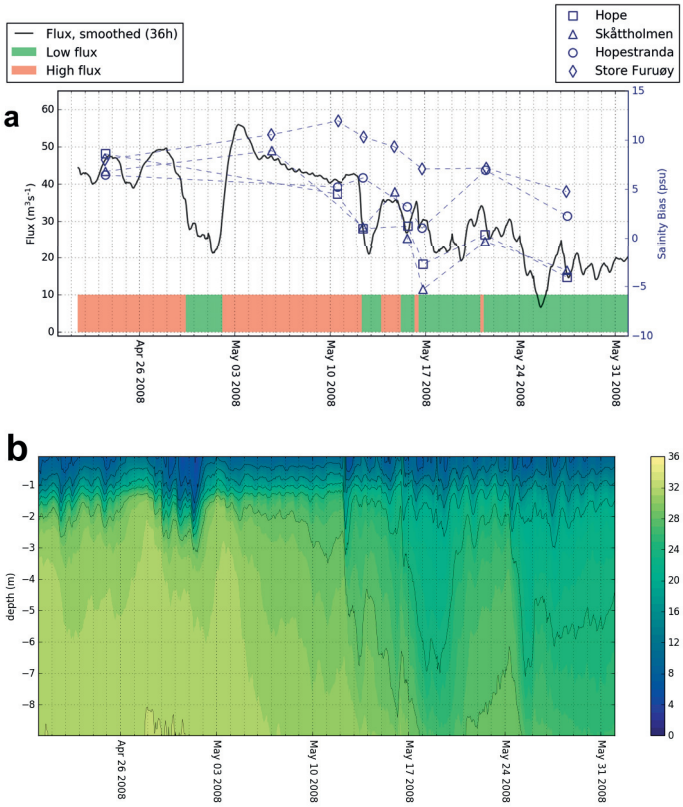

Figure 8: a: Time series of 36 h weighted running mean of upper layer volume flux through the cross section (black line) marked with blue line in Fig 1. Green color indicate periods with low flux (below average), while red colors indicate periods with high flow (above average). Blue markers indicate the bias in model surface salinity compared to surface CTD data (upper 1 m mean) from the four stations. b: Hovmöller plot of salinity (psu) from the hydrodynamic model at Skåtholmen site.

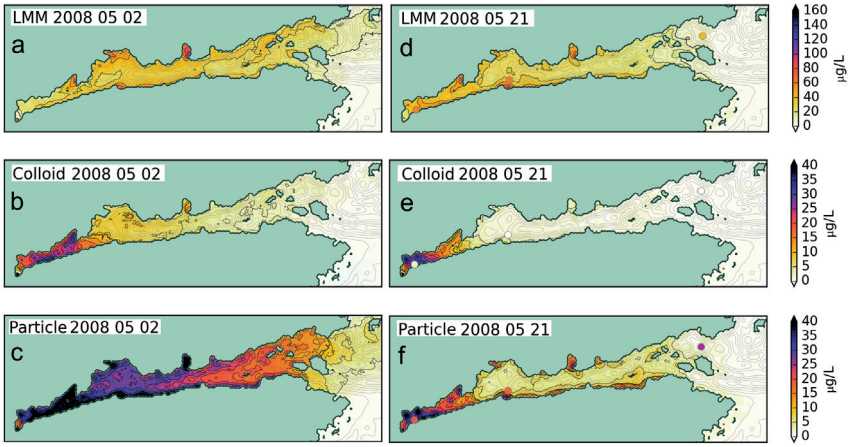

Figure 9: Contours of fractions of surface Al concentration in LMM (top), colloidal (middle) and particle phases (bottom) from the model at May 2, 2008 (left) and May 21, 2008 (right). Colored circles indicate observed surface Al concentration from May 21, 2008.

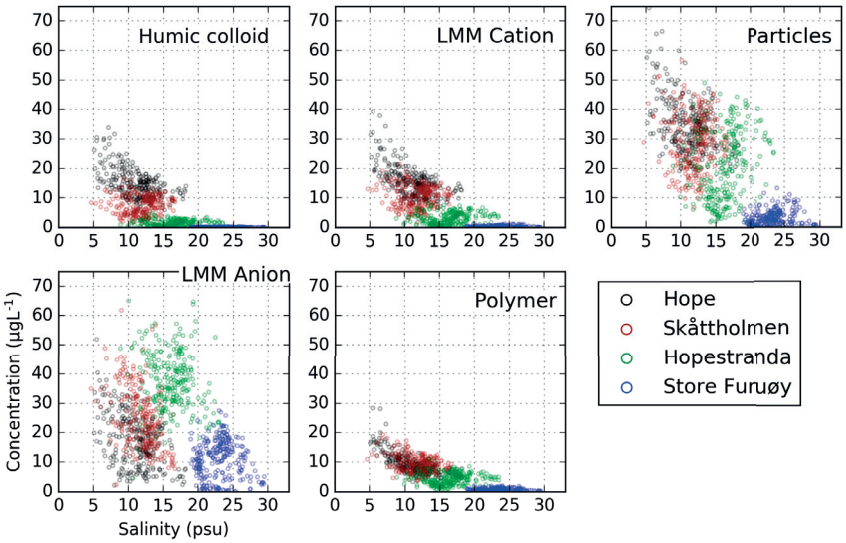

Figure 10: Scatter plot of estimated surface Al concentration in each specie vs salinity. Each circle represent one model 'sample pair', obtained at 4 h time intervals, from the four stations marked in Fig 1a.

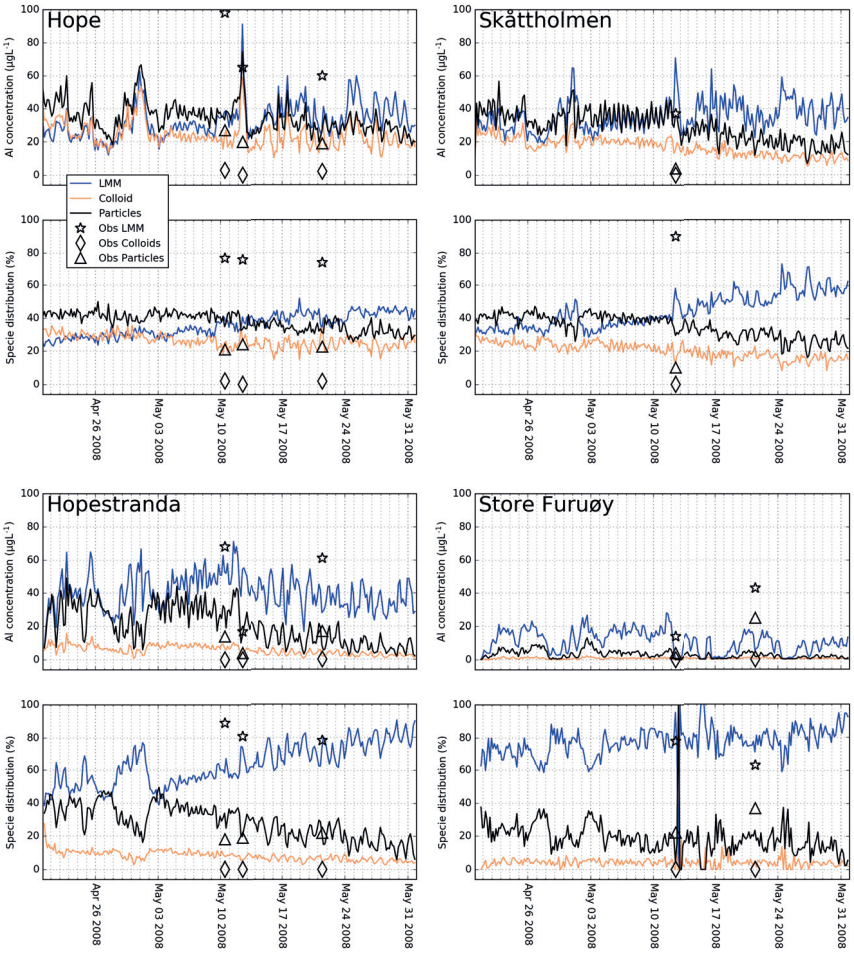

Figure 11: Time series of estimated and observed Al specie concentration and Al specie fractions in surface water (upper 1 m mean) at the four stations marked in Fig 1a.

Paper III: Supplementary Material

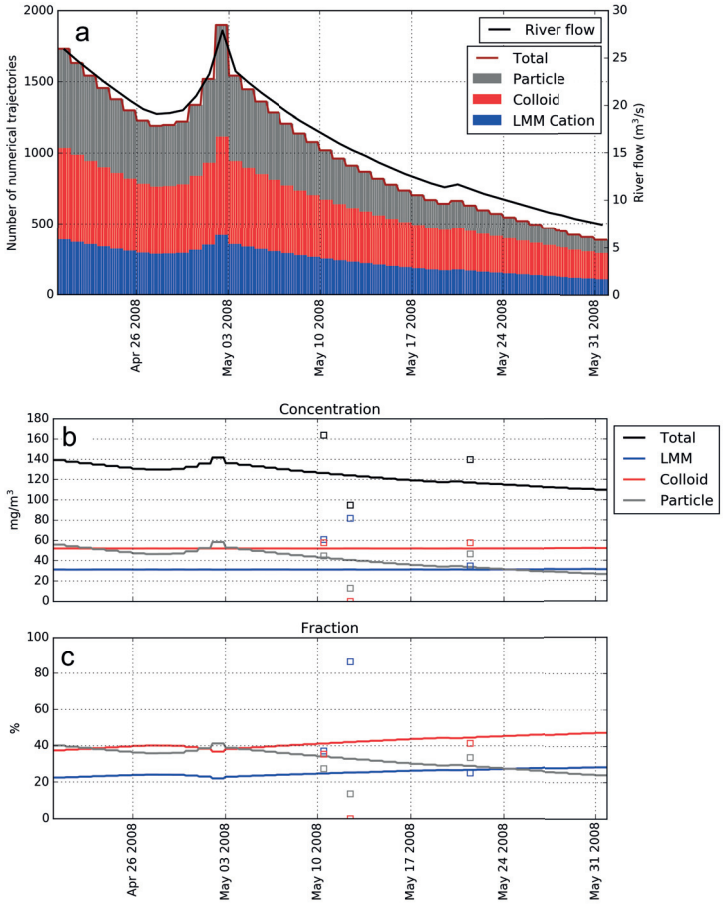

Figure S.1: Time series of model discharges. a: Daily river flow rate from the HBV model (black line), number of numerical trajectories released with 4 hours intervals in total (red line) and in LMM, colloidal and particle species (blue, red and gray bars, respectively). b: Al concentration in the discharged river water. Squares are observations at Laget. c: Fraction in % in each of the species in the discharged river water. Squares are observations at Laget.

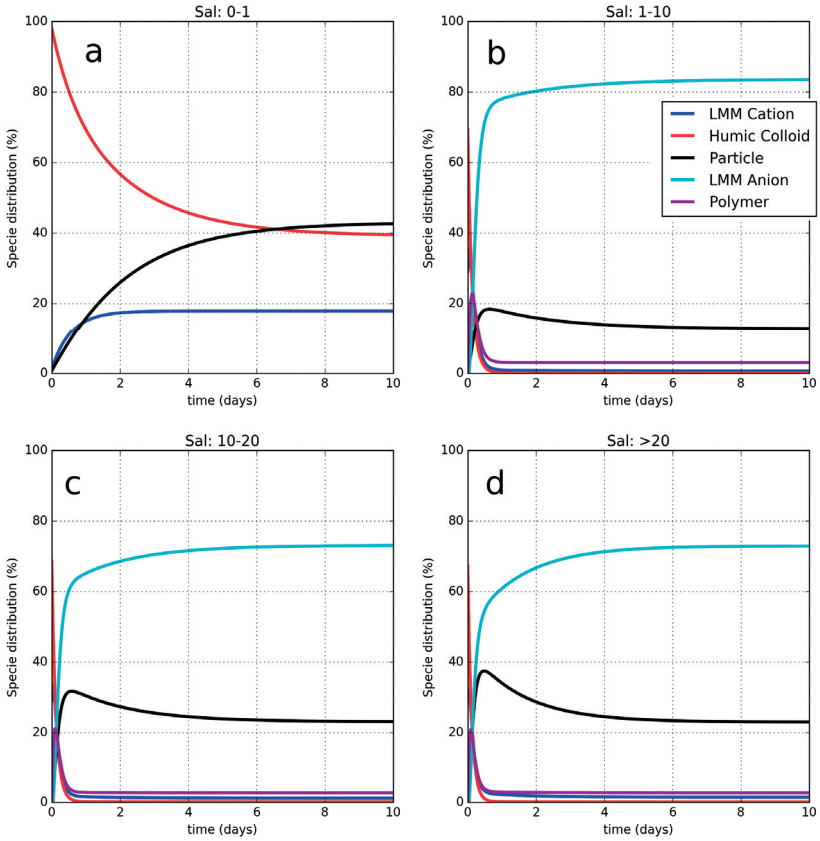

Figure S.2: Time series of specie distribution in an idealized system, where an initial fraction of 100 % humic colloids is assumed and the transfer rates from Table S.1 are applied, for salinity intervals a: 0-1 psu, b: 1-10 psu, c: 10-20 psu and d: > 20 psu.

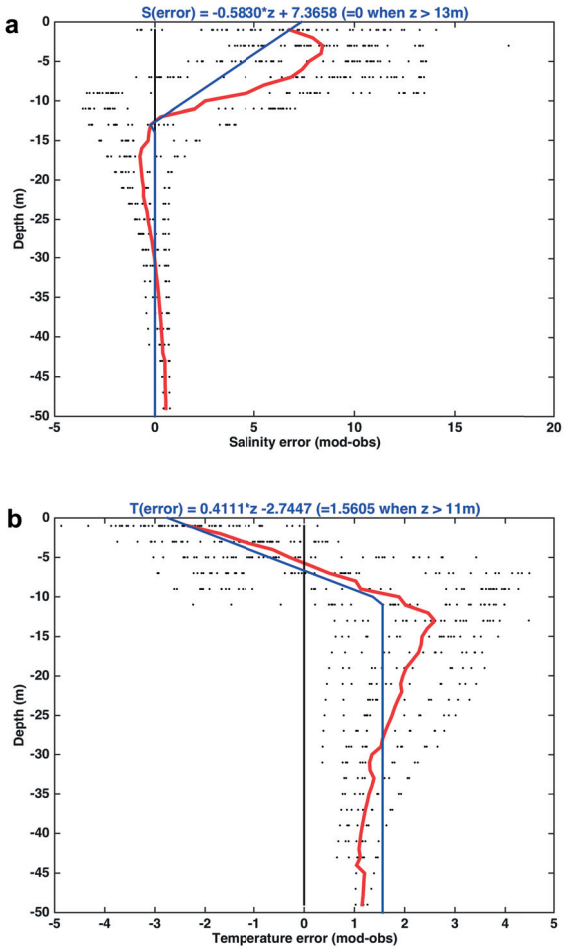

Figure S.3: Error in salinity (a) and temperature (b) from the hydrodynamic model (ROMS) as function of depth based on all CTD-casts taken during the simulation period. Every data point is shown with small black dots, the red lines denote the average error and the blue lines are the simplified, linear error lines.

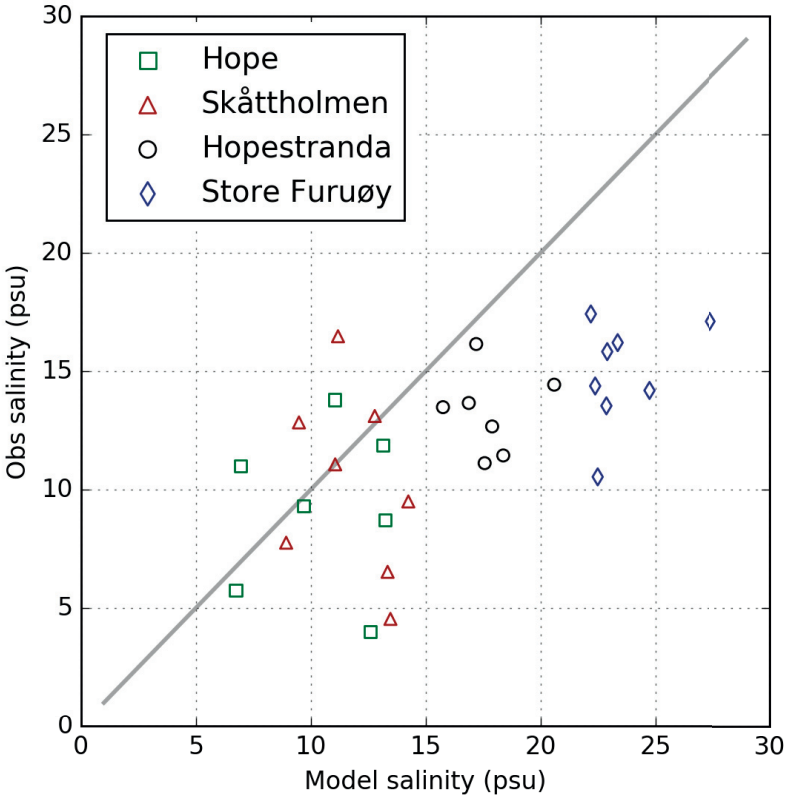

Figure S.4: Surface salinity from hydrodynamic model (ROMS) and observed salinity based on CTD-casts taken at the stations during the simulation period.

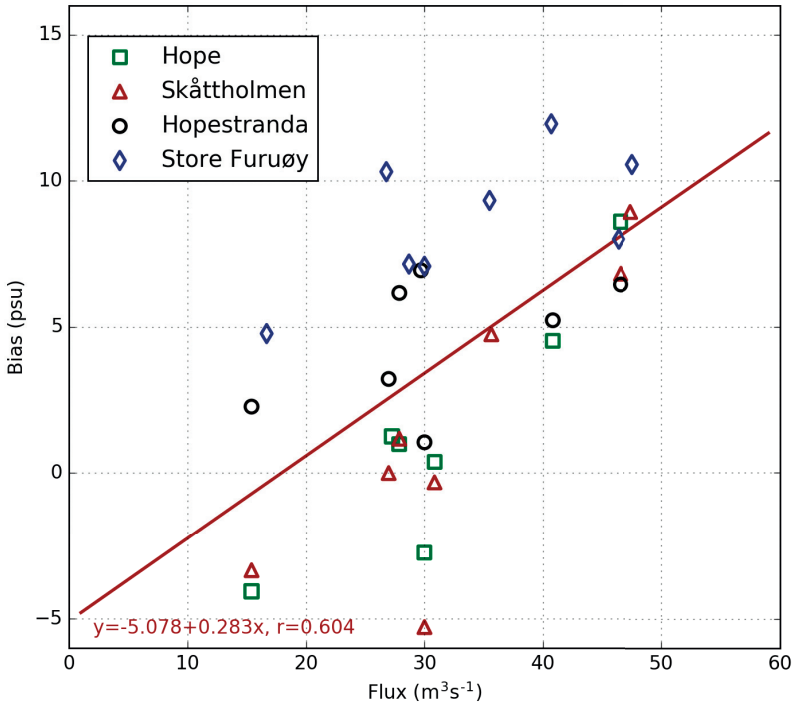

Figure S.5: Error in surface salinity (1 m) from the hydrodynamic model (ROMS) validated with CTD data from the four stations as a function of upper layer volume flux (1 m) through the cross section marked with the blue solid line in Fig 1, computed as weighted mean over the last 36 hours. Red line is the best fit linear regression.

Table S.1: Transfer rates in s^{-1}, where $D_C = 1.16 \times 10^{-5}$ is the desorption coefficient (Nyffeler et al., 1984).

	Process	0–1 psu	1–10 psu	10–20 psu	> 20 psu
k_{12}	LMM cation → Humic colloid	1.2×10^{-5}	1.0×10^{-5}	8.0×10^{-6}	6.0×10^{-6}
k_{13}	LMM cation → Particle	4.0×10^{-6}	3.0×10^{-6}	2.0×10^{-6}	1.8×10^{-6}
k_{16}	LMM cation → Polymer	0.0	1.2×10^{-4}	1.4×10^{-4}	1.5×10^{-4}
k_{21}	Humic colloid → LMM cation	$0.3 \times D_C$	$7.0 \times D_C$	$7.0 \times D_C$	$7.0 \times D_C$
k_{23}	Humic colloid → Particle	2.0×10^{-6}	4.0×10^{-6}	6.0×10^{-6}	1.0×10^{-5}
k_{31}	Particle → LMM cation	$0.3 \times D_C$	$0.5 \times D_C$	$0.6 \times D_C$	$0.8 \times D_C$
k_{41}	Sediments → LMM cation	$0.03 \times D_C$	$0.05 \times D_C$	$0.06 \times D_C$	$0.08 \times D_C$
k_{56}	LMM anion → Polymer	0.0	5.0×10^{-6}	5.0×10^{-6}	5.0×10^{-6}
k_{65}	Polymer → LMM anion	0.0	$12.0 \times D_C$	$12.0 \times D_C$	$12.0 \times D_C$
k_{63}	Polymer → Particle	0.0	2.4×10^{-5}	6.0×10^{-5}	8.0×10^{-5}

ISBN: 978-82-575-1602-4
ISSN: 1894-6402

Norwegian University
of Life Sciences

Postboks 5003
NO-1432 Ås, Norway
+47 67 23 00 00
www.nmbu.no

102974 / ANDVORDGRAFISK.NO